Universidade do Minho
Escola de Engenharia

Nuno Miguel Ribeiro De Oliveira

Biomedical Devices Engineered Based on the Control of the Surface Wettability

maio de 2017

Biomedical Devices Engineered Based on the Control of the Surface Wettability
Nuno Miguel Ribeiro De Oliveira

UMinho | 2017

FCT
Fundação para a Ciência e a Tecnologia
MINISTÉRIO DA EDUCAÇÃO E CIÊNCIA

POPH
QUALIFICAR É CRESCER.

QREN
QUADRO DE REFERÊNCIA ESTRATÉGICO NACIONAL
PORTUGAL 2007.2013

Governo da República Portuguesa

UNIÃO EUROPEIA
Fundo Social Europeu

Universidade do Minho
Escola de Engenharia

Nuno Miguel Ribeiro De Oliveira

Biomedical Devices Engineered Based on the Control of the Surface Wettability

Tese de Doutoramento em Engenharia de Tecidos,
Medicina Regenerativa e Células Estaminais

Trabalho efetuado sob a orientação do
Professor Doutor João Filipe Colardelle da Luz Mano
e do
Professor Doutor Rui Luís Gonçalves dos Reis

maio de 2017

STATEMENT OF INTEGRITY

I hereby declare having conducted my thesis with integrity. I confirm that I have not used plagiarism or any form of falsification of results in the process of the thesis elaboration.

I further declare that I have fully acknowledged the Code of Ethical Conduct of the University of Minho.

University of Minho, 23 de Maio de 2017

Full name: Nuno Miguel Ribeiro de Oliveira

Signature: Nuno Miguel Ribeiro de Oliveira

Acknowledgements

I believe that my thesis would not have been completed without the support and concern of many people. After this arduous work, it is the moment to express my gratitude to the people who supported me throughout this PhD.

Em primeiro lugar, agradeço à minha família pois não seria possível chegar ao fim desta jornada sem as suas palavras de motivação e todo o apoio emocional e financeiro. À minha mãe *Luísa*, ao meu pai *António*, ao meu irmão *Filipe* e à minha cara-metade *Alberta:* O meu Muito Obrigado!

To my supervisor, *Professor João F. Mano*, for all the discussions, for all the suggestions to improve my work, and for encourage me to participate in wide range of activities which allowed me to grow significantly at professional and personal level, thank you very much.

To my co-supervisor, *Professor Rui L. Reis*, for all the support and for the opportunity of working in such a renowned group as well as for the using of the facilities at AvePark, thank you very much.

I want to deliver a word of appreciation and admiration to *Professor Ali Khademhosseini*, for the opportunity of integrating and using of the facilities of the prestigious institution BIRC with filiation to MIT and Harvard Medical School, thank you very much.

During my PhD, I have been very privileged to meet and to collaborate with many other great people, namely Ana I. Neto, Ana M.S. Costa, Clara C. Correira, Jie Ju, Diana Sequeira, Joana M. Silva, Lara L. Reys, Manuel Alatorre-Meda, Mariana B. Oliveira, M. Isabel Rial-Hermida, Simone S. Silva, Sofia G. Caridade, and Yu Shrike Zhang. Thank you all.

During these years, I had the opportunity to meet fantastic people. A very special thanks to Álvaro Leite, Ester Ferreira, Rui Costa, Sílvia Vieira, Ana Catarina Lima, Albino Martins, Sofia Caridade, Mahwish Bakht, Shahid Naseer, Tugba Kiliç, Isa Rial, Pathomthat Srisuk, Sílvia Oliveira, Mônica Thürmer, Nelson Monteiro, Pedro Costa, Mariana Oliveira, Clara Correia, Joana Marques, Simone Silva, Lara Reys, João Requicha, Ana Dias, Sara Gil, Ana Marques, Marta Ondrésik, Praveen Sher, Emanuel Fernandes, Paula Sol, Raquel Almeida, and I am pretty sure that it is missing a lot of names on this list. Thank you all.

I would like to acknowledge all the 3B's Research Group team and show my appreciation for all colleagues that helped me professionally and personally. Thank you all.

I would like to show my gratitude for all the BIRC team that helped me a lot professionally and personally during all the time in Boston. Thank you all.

I acknowledge the financial support from Fundação para a Ciência e Tecnologia (FCT) – PhD grant SFRH / BD / 73172 / 2010 – Programa Operacional Potencial Humano (POPH) no Quadro de Referência Estratégica Nacional (QREN) e co-financiado pelo Fundo Social Europeu (FSE).

Abstract

The wettability control has been showed as an important parameter for several systems and applications on the biomedical field. Once the surface wettability has crucial influence in protein adsorption and cell adhesion. Here, the focus was on the technology development based on the advanced control of wettability in surfaces, tuning directly the surface characteristics or modifying surfaces by coating with hydrophobic microparticles (HmP). Superhydrophobic (SH) surfaces can be achieved combining low surface energy and hierarchical topography at nano/microscale. A simple method was developed to prepare SH surfaces, using diatomaceous earth (DE) that was able to confer the desired hierarchical topography. SH surfaces were obtained by further fluorosilanization of surfaces that decreased surface energy. The wettability of surfaces could be modified by plasma treatment in a controlled way. Using masks only specific areas were exposed to plasma, allowing to perform hydrophilic/superhydrophobic patterning on surfaces. Planar SHS of polystyrene (PS) with hydrophilic paths or square spots were developed to engineer devices for cellular studies. Paths worked as channels to drive cell culture medium flows without using walls for liquid confinement. Controlling liquid flows on planar surfaces, a cell culture flow system was developed based on the open fluidics concept. The pertinence of the system was showed by studying the effect of shear stress stimuli combined with bone morphogenic protein (specifically BMP-2) stimulation in the osteogenic differentiation of C2C12 myoblast cells. A synergistic effect of these stimuli combination was found on the osteoblast differentiation. Using similar SH surafces of PS but with hydrophilic squared spots, a hanging drop system (HDS) for the production and culturing of human adipose-derived stem cell (hASC) spheroids under co-culture conditions with different cell types was engineered. The co-culture with Saos-2 cells indicated that the spheroid production and hASC differentiation into an early osteogenic phenotype can be obtained in a one-step procedure.

By coating liquid droplets with HmP, which were produced by the fluorosilanization of DE, liquid marbles (LM) were produced. Here, the use of LM was showed for high-throughput drug screening on anchorage-dependent cells. To provide the required cell adhesion sites inside the liquid environment of LM, surface-modified poly(L-lactic acid) microparticles are used. By injecting the chemical agent in study and monitoring color changes inside of LM, cytotoxic screening tests were performed. The presence of viable cells was assessed by injecting AlamarBlue reagent, which changed its color from blue to red in presence of viable cells. The developed method was validated

by directly comparing with a standardized method used for cytotoxicity assessment. Inspired by LM, a novel class of hydrophobic hydrogels, which can free-float on the surface of different aqueous media, was created by coating conventional hydrogels with a layer of HmP. It was demonstrated that floating hydrogel-based devices could be developed for pH sensing on liquid surfaces. Such as the floating systems preserved the intrinsic biocompatibility of the core hydrogels, floating tissue constructs were also microengineered.

On this work, different biomedical devices could be engineered just based on the control of the surface wettability. These devices have high potential to achieve widespread use, namely for applications in sensing, drug screening, fabrication of 3D microtissues for tissue engineering, and biomedicine.

Resumo

O controlo da molhabilidade mostra-se como um importante parâmetro em vários sistemas e aplicações na área biomédica. Uma vez que a molhabilidade de superfícies tem grande influência na adsorção de proteínas e adesão celular. Aqui, o foco caiu sobre o desenvolvimento de tecnologia baseada no controlo da molhabilidade de superfícies, manipulando diretamente as características da superfície ou cobrindo superfícies com micropartículas hidrofóbicas (mPH). Superfícies superhidrofóbicas (SSH) podem ser obtidas combinando baixa energia de superfície com topografia à escala nano/micrométrica. Foi desenvolvido um método simples para preparação de SSH, usando terra de diatomáceas (TD) para conferir a topografia desejada e posterior reação química na superfície com um fluorosilano que diminuiu a energia de superfície. A molhabilidade destas superfícies pôde ser alterada de uma forma controlada e seletiva por tratamento de plasma e usando máscaras, permitindo a criação de padrões hidrófilicos/superhidrofóbicos nas superfícies. SSH de poliestireno com padrões hidrófilicos com a forma de tiras ou quadrados foram desenvolvidas para a construção de dispositivos para uso em estudos celulares. As tiras hidrófilicas funcionaram como canais capazes de conduzir o escoamento do meio de cultura sem o uso de paredes físicas. Tendo o controlo do escoamento de fluidos em superfícies planas, um sistema para cultura celular foi desenvolvido sob o conceito de fluídica aberta. A pertinência deste sistema foi mostrada pelo estudo do efeito combinado, da tensão de corte do escoamento com a presença de uma proteína morfogénica do osso (BMP-2), na diferenciação osteogénica de mioblastos C2C12. Tendo sido encontrado um efeito de sinergia entre os dois estímulos na diferenciação. Usando SSH mas com quadrados hidrófilicos, um sistema de gota suspensa foi desenvolvido para a produção e cultura de esferoides de células estaminais humanas extraídas de gordura (hASC) em condições de co-cultura com diferentes tipos de células. A co-cultura com células Saos-2 indicou que se pode, num só passo, produzir e diferenciar esferoides de hASC numa fase inicial do fenótipo osteogénico.

Cobrindo uma gota de líquido com mPH – produzidas através de reação química à superfície da TD com um fluorosilano – produziram-se “berlindes líquidos” (BL). Aqui, foi mostrado o uso destes BL para a análise do efeito de fármacos sobre células aderentes. Para fornecer os pontos de adesão essenciais às células usaram-se micropartículas de ácido poliláctico no interior dos BL. Injetando os agentes químicos em análise e monitorizando a mudança de cor no interior dos BL foram realizados testes de rastreio de citotoxicidade. A existência de células viáveis foi determinada

através do uso do reagente AlamarBlue, que muda a sua cor de azul para vermelho na presença de células viáveis. O método desenvolvido foi validado por comparação com um método padronizado usado em análises de citotoxicidade. Inspirado nos BL, uma nova classe de hidrogéis hidrofóbicos foi criada cobrindo hidrogéis convencionais com uma camada de mPH, mostrando estes a capacidade de flutuar sobre meio aquoso. Com base neste hidrogéis foram criados dispositivos flutuantes para monitorizar o pH na superfície de um líquido. Como a biocompatibilidade intrínseca do hidrogel base usado se manteve, construções de tecidos celulares flutuantes foram também criadas.

Neste trabalho, diferentes dispositivos biomédicos foram construídos apenas com base no controlo da molhabilidade de superfícies. Os dispositivos mostraram um elevado potencial para várias aplicações como monitorização, análise de fármacos e construção de tecidos celulares para engenharia de tecidos.

Table of Contents

List of Abbreviations and Acronymes

A

ALP - Alkaline phosphatase

ATCC - Human dermal fibroblasts

B

BMSC - Mesenchymal bone marrow stem cells

C

COC - Cyclic olefin copolymer

CAE - Constant Analyzer Energy mode

CCF - Cell culture flow

CCS - Cancer cell spheroids

CNC – Computer Numerical Control

D

DMEM - Dulbecco's Modified Eagle's Medium

DE - Diatomaceous Earth

E

EB - Embryoid bodies

EC - Endothelial cells

ERI - Effective red intensity

ECGM - Endothelial Cell Growth Medium

EDS - Energy-dispersive X-ray spectroscopy

F

F-SH - Fluorinated superhydrophobic

FBS - Fetal bovine serum

FACS - Fuorescence-activated cell sorting

G

GelMA - Gelatin methacryloyl

GFPs - Green fluorescent proteins

H

HUVECs - Human umbilical vein endothelial cells

L

LM - Liquid marbles

M

MTS - 3- (4,5-dimethylthiazol-2-yl) -5- (3-carboxymethoxyphenyl) -2- (4-sulfophenyl) -2H- tetrazolium)

N

NIR - Near-infrared

P

PDMS - Poly-dimethylsiloxane

PFDTS - 1H,1H,2H,2H-Perfluorodecyltriethoxysilane

PS - Polystyrene

PPFC - Parallel plate flow chambers

PS-SH - PS superhydrophobic

PLLA - Poly(L-lactic acid)

PFDTS – Perfluorodecyltriethoxysilane

PVA - Polyvinyl alcohol

PBS - Phosphate buffer saline

PMMA - Poly(methyl methacrylate)

PVC - Poly(vinyl) carbonate

PC - Polycarbonate

R

Ra - Average roughness

RMS - Root-mean-squared

Rq – Roughness

RCV - Relative cell viability

S

SEM - Scanning Electron Microscope

SH – Superhydrophobic

U

UV - Ultraviolet

W

WCA - Water contact angle

Others

μ

μPTFE- Hydrophobic polytetrafluoroethylene microparticles

List of Figures

List of Tables

List of Publications

The work developed under the scope of this PhD thesis resulted in the publications listed below:

Papers in international scientific journals with referees

1. **Nuno M. Oliveira**, Rui L. Reis; João F. Mano; Recent Advances on Open Fluidic Systems for Biomedical Applications: A Review. *Submitted*.
2. **Nuno M. Oliveira**, Rui L. Reis; João F. Mano; The Potential of Liquid Marbles for Biomedical Applications: A Critical Review. *Submitted*.
3. **Nuno M. Oliveira**; Rui L. Reis; João F. Mano; Open Fluidics: A Cell Culture Flow System Developed Over Wettability Contrast-Based Chips. *Submitted.*
4. **Nuno M. Oliveira**, Mariana B. Oliveira, Rui L. Reis; João F. Mano; Hanging Drop Platform for Stem Cell 3D Spheroids Production and Characterization under Co-Culture Conditions. *Submitted*.
5. **Nuno M. Oliveira**; Yu S. Zhang; Jie Ju; Ai-Zheng Chen; Yu Chen; Sameer R. Sonkusale; Mehmet R. Dokmeci; Rui L. Reis; João F. Mano; Ali Khademhosseini; Hydrophobic Hydrogels: Toward Construction of Floating (Bio)microdevices. *Chemistry of Materials* **2016**, 28, 3641–3648.
6. **Nuno M. Oliveira**; Clara R. Correia; Rui L. Reis; João F. Mano; Liquid Marbles for High-Throughput Biological Screening of Anchorage-Dependent Cells. *Advanced Healthcare Materials* **2015**, 4, 264–270.
7. **Nuno M. Oliveira**; Rui L. Reis; João F. Mano; Superhydrophobic Surfaces Engineered Using Diatomaceous Earth. *ACS Applied Materials & Interfaces* **2013**, 5, 4202–4208.

Publications resulting from collaborative work

1. Lara L. Reys; Simone S. Silva; Diana Soares da Costa; **Nuno M. Oliveira**; João F. Mano; Rui L. Reis; Tiago H. Silva; Fucoidan Hydrogels Photo-Cross-Linked with Visible Radiation As Matrices for Cell Culture. *ACS Biomaterials Science & Engineering* **2016**, 2, 1151–1161.
2. Simone S. Silva; **Nuno M. Oliveira**; Mariana B. Oliveira; Diana P. Soares da Costa; Deboki Naskar; João F. Mano; Subhas C. Kundu; Rui L. Reis; Fabrication and characterization of Eri silk fibers-based sponges for biomedical application. *Acta Biomaterialia* **2016**, 32, 178-189.
3. Joana M. Silva; Sofia G. Caridade; **Nuno M. Oliveira**; Rui L. Reis; João F. Mano; Chitosan–alginate multilayered films with gradients of physicochemical cues. *Journal of Materials Chemistry B* **2015**, 3, 4555-4568.
4. M. Isabel Rial-Hermida; **Nuno M. Oliveira**; Angel Concheiro; Carmen Alvarez-Lorenzo; João F. Mano; Bioinspired superamphiphobic surfaces as a tool for polymer- and solvent-independent preparation of drug-loaded spherical particles. *Acta Biomaterialia* **2014**, 10, 4314–4322.
5. Ana M. S. Costa; Manuel Alatorre-Meda; **Nuno M. Oliveira**; João F. Mano; Biocompatible Polymeric Microparticles Produced by a Simple Biomimetic Approach. *Langmuir* **2014**, 30, 4535–4539.

Conference abstracts published in international scientific journals

1. **Nuno M. Oliveira**; Clara R. Correia; Rui L. Reis; João F. Mano; Liquid marbles to culture adherent cells for high-throughput drug screening. *Journal of Tissue Engineering and Regenerative Medicine* **2014**, 8(S1), 376-376.
2. **Nuno M. Oliveira**; Rui L. Reis; João F. Mano; Superhydrophobic surfaces produced using natural silica-based structures with potential for biomedical applications. *Journal of Tissue Engineering and Regenerative Medicine* **2013**, 7(S1), TS41.

Conference posters

1. **Nuno M. Oliveira**; Clara R. Correia; Rui L. Reis; João F. Mano; Liquid marbles to culture adherent cells for high-throughput drug screening. European Chapter of the Tissue Engineering and Regenerative Medicine International Society (TERMIS-EU), Genova-Italy, **2014**.
2. **Nuno M. Oliveira**; Rui L. Reis; João F. Mano; Superhydrophobic surfaces produced using natural silica-based structures with potential for biomedical applications. Term Stem 2013, Porto-Portugal, **2013**.

Introduction to the Thesis Format

This thesis is organized in 4 sections that include a total of 9 chapters. The first section provides the general introduction to the thesis. The second section corresponds to the experimental methods and materials used. The third section shows the experimental results obtained in the context of this thesis and their discussion, focusing on the development of biomedical devices based on the advanced control of the wettability of different surfaces. The fourth section finalizes this thesis with concluding remarks.

The chapters of this thesis are all based on peer-reviewed papers published or submitted for publication. Each thesis chapter is presented in manuscript form containing: abstract, introduction, materials and methods, results and discussion, conclusions and acknowledgements. A list of relevant references is also provided as a subsection within each chapter. The contents of each chapter is described below in more detail.

Section I. General Introduction

Chapter 1 – Recent Advances on Open Fluidic Systems for Biomedical Applications: A Review

This chapter reviews the recent advances on open fluidics field, highlighting the specific characteristics of this technology comparing with traditional microfluidics. Additionally, the description of several applications on the biomedical field using open fluidic devices is provided.

Chapter 2 – The Potential of Liquid Marbles for Biomedical Applications: A Critical Review

On this chapter, the liquid marble characteristics and manipulation methods to handle with these structures are reviewed. Then, the reported applications for the liquid marbles on the biomedical field are described. Finalizing, a critical discussion on the potential of liquid marbles for new biomedical applications is performed based on published information about this topic.

Section II. Experimental Section

Chapter 3 – Materials and Methods

A list of the materials used and methods applied to obtain the results described further on is provided.

Section III. Development of Biomedical Devices Based on the Advanced Control of Wettability in Different Surfaces

Chapter 4 – Superhydrophobic Surfaces Engineered Using Diatomaceous Earth

This chapter aims to demonstrate that superhydrophobic surfaces can be engineered: using diatomaceous earth to achieve a micro/nanoscale hierarchical topography on the surface; and performing a fluorosilanization process to obtain a surface with low surface energy. Additionally, it was showed that the wettability of the superhydrophobic surface can be modified by plasma treatment in a controlled way, allowing to pattern hydrophilic features with different geometries.

Chapter 5 – Open Fluidics: A Cell Culture Flow System Developed Over Wettability Contrast-Based Chips

In this chapter, an original cell culture flow system based on the open fluidics concept was proposed. The system was developed using a planar superhydrophobic platform with hydrophilic paths on its surface. The paths worked as channels to drive cell culture medium flows without using physical walls for liquid confinement. The validation of the proposed concept was performed by studying the effect of the shear stress stimulus in the osteogenic differentiation of C2C12 myoblast cells.

Chapter 6 – Hanging Drop Platform for Stem Cell 3D Spheroids Production and Characterization under Co-Culture Conditions

Using a similar platform to chapter 5 by with hydrophilic square shapes on its surface, a hanging drop system based on a superhydrophobic (SH) platform was proposed for the production and culturing of human adipose-derived stem cell (hASC) spheroids under co-culture conditions.

Chapter 7 – Liquid Marbles for High-Throughput Biological Screening of Anchorage-Dependent Cells

In this chapter, stable liquid marbles produced by coating liquid droplets with hydrophobic powder were presented. The hydrophobic powder consisted in diatomaceous earth modified by a fluorosilanization process and it was obtained during the development of the work reported on chapter 4. The use of liquid marbles for high-throughput drug screening on anchorage-dependent cells was proposed.

Chapter 8 – Hydrophobic Hydrogels: Toward Construction of Floating (Bio)microdevices

Inspired by the liquid marbles of chapter 7, a novel class of hydrophobic hydrogels that can free-float on the surface of different aqueous media by coating conventional hydrogels with a layer of

hydrophobic microparticles. These floating hydrogel-based devices were developed for pH sensing applications on liquid surfaces and to engineering of floating tissue constructs.

Section IV. Concluding Remarks

Chapter 9 – Conclusions and Future Perspectives

This chapter finalizes the thesis by summarizing its major conclusions.

SECTION I – GENERAL INTRODUCTION

Chapter 1

Recent Advances on Open Fluidic Systems for Biomedical Applications: A Review

This chapter is based on the following publication:

Nuno M. Oliveira, Rui L. Reis, João F. Mano. Recent Advances on Open Fluidic Systems for Biomedical Applications: A Review. *Submitted*.

1.1. Abstract

Microfluidics has become an important tool to engineer microenvironments with high precision. Once, microfluidics comprises devices and methods for controlling and manipulating fluids at submillimeter scale. This type of technologies has shown significant impact in several scientific fields, namely chemistry, biotechnology, engineering or cell biology. Here, we reviewed an emergent topic in the microfluidics field that is the open fluidics.

Open fluidic systems are characterized for present a higher air/liquid interface comparing with traditional microfluidics, presenting at least one area of the device open to air. Unique advantages are offered by open fluidic devices due to its singular architectures, such as simplicity of fabrication, easy to clean, and enhanced functionality and accessibility for liquid handling. Furthermore, these systems do not present the typical issues of traditional microfluidics, such as the risk of channel clogging and the occurrence of flow perturbation due to bubbles. Open fluidic platforms can assume different designs that were allocated in two groups, physical confinement and wettability-contrast confinement. Physical confinement group comprises: platforms combining both open and traditional microfluidics; open channels with rectangular and triangular cross-section; suspended microfluidics; and the use of narrow edge of a solid surface for fluid confinement. Second group covers: (super)hydrophilic/(super)hydrophobic patterned surfaces; paper-based microfluidics; and microfluidic devices based on textiles. Related with these different platforms, device characteristics, manufacturing techniques and fluid transport/manipulation methods were reviewed.

Finalizing this work, several recent applications on the biomedical field that were developed based on open fluidics were revised.

1.2. Introduction

The precise control of volume and manipulation of fluids is very important for several scientific fields, for example in chemistry, biotechnology, engineering or cell biology.[1-3] Microfluidic technology has become an important tool to engineer environments with high control of the studying conditions.[3, 4] Generally, microfluidics alludes to devices and methods for controlling and manipulating fluids at submillimeter scale.[2, 4] This technology has been presented as an attractive candidate to replace traditional experimental approaches, especially in the biomedical field.[5]

The most popular approach for manufacturing microfluidic devices consisted in using "soft lithography" of poly-dimethylsiloxane (PDMS), contributing largely for the technological development of this field.[3, 5] Using this technique, structures with a micrometer resolution are easily molded from a hard master into PDMS.[6] Additionally, PDMS present valuable characteristics such as low cost, optical transparency, elasticity, permeability to gasses and ease of use, presenting high fidelity reproducing molds.[5, 7] This combination allowed both the miniaturization and the parallelization of processes in compact devices, saving reagents and consequently costs.[3, 8] Owing to the ease fabrication and flexibility of these devices, several kinds of functional microfluidic elements were described on literature, namely sensors, mixers, separators, dispensers, pumps, valves, etc.[1, 6, 7] Furthermore, different techniques for both fluids and particles manipulation in microfluidics have been developed, using electrical, magnetic, optical, capillary and mechanical force.[1, 2]

However for biomedical research, some concerns about the use of PDMS were raised. It was found the leaching of uncrosslinked oligomers from PDMS that can be toxic for cells.[9, 10] Due to the hydrophobic properties and permeability of this material, the absorption of hydrophobic small molecules by the PDMS was showed.[11, 12] Additionally, the permeability to water vapor can

result in rapid evaporation, being this issue more relevant in static no-flow experiments.[10, 13] Nevertheless, these drawbacks of PDMS can be mitigated, demanding additional device preparation.[7] Recently, alternative materials to PDMS were been explored, namely thermoplastics (polystyrene – PS, cyclic olefin copolymer – COC, polymethyl methacrylate – PMMA, and polycarbonate – PC), paper, wax and textiles.[5]

Associated to the microfluidic technology arose new concepts such as the lab-on-a-chip and organ-on-a-chip concept. Lab-on-a-chip concept postulates the fully integration in a single chip of several microfluidic components and procedures with a goal of miniaturizing chemical and biological processes.[1, 14] While, organ-on-a-chip refers to complex microengineered systems aiming to mimic physiological key features of specific human organs and tissues and their interactions.[15] [16] Other concept that emerged on the microfluidics field was the open microfluidics. Here, we reviewed the technological advances on this topic, namely device characteristics, manufacturing techniques and recent applications on the biomedical field. On this review, for a matter of accuracy, we use the expression “open fluidics”, once we included also devices at the millimeter scale.

1.3. Open fluidics

Open fluidic systems are characterized for present at least one area of the device open to air, comprising systems such as droplets on surfaces or open fluidic channels.[17, 18] Unique advantages are offered by the open fluidics, such as simplicity of fabrication, easy to clean, enhanced functionality and accessibility for liquid handling.[19-21] These systems can also overcome typical issues of traditional microfluidics, such as the risk of channel clogging and the occurrence of flow perturbation due to bubbles.[20, 22] Open fluidic platforms can assume different geometries that we divided in two groups, physical confinement and wettability-contrast confinement. In the first group, the fluid is confined and manipulated using channels with

rectangular or triangular shape without one side; channels formed by opposing two vertical walls; or using the narrow edge of a solid surface. The wettability-contrast confinement comprises (super)hydrophilic areas patterned on (super)hydrophobic surfaces, using flat solid surfaces. On this group, we also included paper-based microfluidics and systems in which fluid flows were driven by hydrophilic textile fibers on a supporting (super)hydrophobic surface.

1.3.1. Physical confinement

Some platforms combining both traditional and open microfluidics were developed, aiming to take advantage of a synergistic effect from the combination of both technologies in a single device.[23-28] This combination brought benefits to the systems, for example the accessibility was increased and gas bubbles were eliminated due to the open section, and the impact of evaporation was minimized for the use of the closed section.[24, 27] These closed-open platforms consisted in parallel microchannels of PDMS that the ceiling was partially removed in the middle[24] or in the end of the channels – Figure 1.1A and B.[23] Simpler, an open access microfluidic platform where the parallel channels culminated in an open reservoir instead a tubing system was also reported, allowing to directly manipulate the fluid in the system with a micropipette.[27] In the channel sections without ceiling, the fluid flow remained confined to the open-microchannels due to the high surface tension of the liquid-air interface and to the hydrophobicity of the top surface of the walls.[23, 24] On this topic of closed-open microfluidics, Keenan *et al.* reported the construction of a microfluidic gradient generator.[25] The system was able to produce soluble gradients by injecting picoliter amounts of fluid, from a closed microchannel system, into an open reservoir. Further on, we present the application of this gradient generator in neutrophil desensitization studies.[26]

Regarding to microfluidic systems fully open based on a physical fluid confinement, the most common geometry of the channels is a rectangular cross-section with one open side.[29-37]

Several reports studying the wetting phenomenon and the fluid transport dynamics on this open rectangular microchannels can be found for different materials, namely silicon,[29, 30, 33] SU-8,[31] quartz,[32] and PDMS.[37] It was found that a large variety of wetting morphologies can be observed.[29, 30] Generally, the wetting behavior was dependent of both the ratio between width and depth of the channel[29, 31, 32, 37] and the wetting properties of the underlying material.[29, 33] Similarly, various wetting morphologies were also observed in open triangular cross-section channels, being dependent of the wedge angle of the channel and the liquid contact angle with the substrate.[38] Berthier *et al.* presented the open triangular cross-section such as an interesting solution for capillary actuation of whole blood in the point-of-care systems domain.[39] These studies aimed to determine the appropriate parameters to accomplish spontaneous capillary flows, avoiding the use of costly actuation systems.[20, 32, 39, 40]

Other promising type of open channels are channels devoid of floor and ceiling, being the liquid supported by two opposite vertical walls, that were named "suspended microfluidics" – Figure 1.1C.[19, 21, 41] These systems showed the ability to generate spontaneous capillary flows in a precise, simple and robust way. The suspended channels were easily constructed using PDMS through soft lithography[19] and thermoplastics such as COC and PMMA using milling.[21, 41] Based on this technology, Casavant *et al.* created arrays of suspended microdots for the study of cell growth and cell invasion toward a source chemoattractant.[19] It was highlighted the potential of these suspended microfluidic devices for high-throughput multiplexed screening applications with cells in 3D matrices.

Davey and Neild reported an innovative open fluidic channel that consisted in a straight open channel defined by a narrow strip of a solid surface – Figure 1.1D.[17] They used the edge of a glass slide to confine the fluid, achieving a similar effect to the liquid confinement provided by a (super)hydrophilic pattern on a (super)hydrophobic flat surface – topic developed ahead.[17] The

flow on the channel was induced by a syringe pump in push–pull mode, such as often used in traditional microfluidics. It was observed that the use of hydrophobic needles on the input and hydrophilic needles on the output increased the stability of the systems.[17, 42] Additionally, it was possible to produce a stable fluid flow with a flow rate of 500 $\mu L.min^{-1}$ in channels of 1 mm width and 30 mm length.[17] The channel length showed to be important for the stability of the system, occurring channel dewetting for a length of 40 mm.[42] Using the same strategy for liquid confinement, Tan and Neild created a Y-junction open fluidic channel – Figure 1.1E.[43] A system with two branches with 1 mm width merging into a main channel with also 1 mm width was constructed by 3D printing. Using this system, it was studied the mixing of two fluids and for high flow rates (>300 $\mu L.min^{-1}$) the fluid mixing occurred faster than expected for molecular diffusion.[43] However, taking advantage from the air/fluid interface be exposed, a rapid mixing of the fluids could be induced by simply blowing an air jet horizontally to the Y-junction. Being the developed device proposed as an efficient mixer able to integrate complex systems, combining open and closed microfluidics.[43]

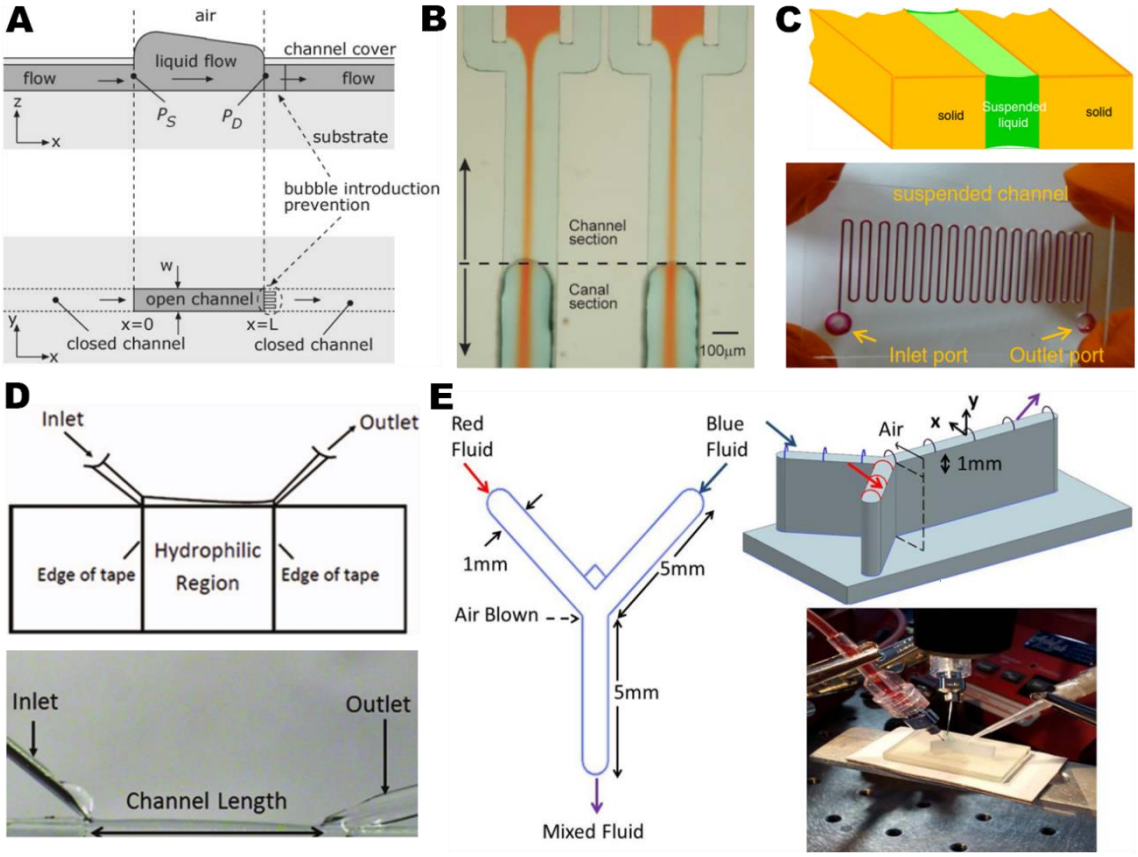

Figure 1.1: (A) Cross-sectional lengthways and upper view of closed-open-closed channel. Adapted from Ref. [24] with permission of the Royal Society of Chemistry. (B) Open fluidic device combining both traditional and open microfluidics, named as channel section and canal section in the image, respectively. Adapted from Ref. [23] with permission of the Royal Society of Chemistry. (C) Suspended flow between two vertical and parallel walls and an example of a suspended channel in a PMMA plate. Adapted from Ref. [21] with permission of Springer. (D) Schematic representation of a straight open channel defined by a narrow strip of a solid surface. The flow was produced by the pressure difference between inlet and outlet in the open fluidic channel. Flow was confined to the exposed hydrophilic region and by the thickness of the glass slide. Adapted from Ref. [42] with permission of AIP Publishing. (E) Schematic representation of the Y-junction open microchannel manufactured with two 1 mm wide branches merging into a 1 mm main channel. Fluid was infused and mixed where the branches met and then the flow was extracted at the end of the main channel. Air was blown horizontally to the Y-junction channel to help in cases where passive mixing cannot be achieved. Adapted from Ref. [43] with permission of AIP Publishing.

1.3.2. Wettability-contrast confinement

Flat surfaces can be used as platforms to engineer open fluidic systems, where the fluid confinement is made by chemical barriers, acting like virtual walls.[44] These non-physical walls consist in chemical patterns created on the top of a substrate, originating (super)hydrophilic areas bounded by the (super)hydrophobic substrate. Similarly to the effect of the edge of a solid surface, a fluid on a flat surface can be retained due to the large contact angle hysteresis at the (super)hydrophilic/(super)hydrophobic boundary.

By definition hydrophilic surfaces present a water contact angle (WCA) lower than 90° and the hydrophobic surfaces present a higher WCA. Concerning to extreme water repellency phenomena, superhydrophilic surfaces are completely wettable by water, presenting a WCA lower than 5° and a high surface energy. Superhydrophobic surfaces are characterized for totally repel water, presenting a static WCA greater than 150° and low surface energy.[45, 46] These extreme phenomena are only possible by combining both surface chemistry (surface free energy) and roughness. Increasing the roughness of a substrate with high surface energy typically increases the apparent hydrophilicity of the surface, whereas increasing the roughness of a substrate with low surface energy usually increases the apparent hydrophobicity of the surface.[47, 48] Additionally, air trapping that may occur on surface roughness is also essential to reach superhydrophobicity.[47]

There are several methods for the production of superhydrophobic surfaces that were compiled in different reviews.[46, 48-53] Referring just some of these methods, superhydrophobic surfaces can be produced by covalent layer-by-layer assembly of amine-reactive polymers;[54, 55] by UV-initiated radical polymerization of a hydrophobic monomer;[56-58] by the deposition of self-assembled monolayers of hydrophobic molecules in micro/nanostructured surfaces;[59-62] by polymer precipitation through a phase separation method in a smooth surface;[63-65] by drop-

casting onto a sandpaper using a fluoroacrylic copolymer solution;[66] by vapor deposition of fluorosilane molecules in micro/nanostructured surfaces or by immersion within the fluorosilane solution.[67-71]

Regarding to the fabrication of surfaces with (super)hydrophobic/(super)hydrophilic patterning, there are also several methods of production.[45, 72, 73] Some examples of the patterning strategies are: protect the wettable areas that should remain untreated using an adhesive mask or an inkjet-printed sacrificial layer prior to the hydrophobization process;[71, 74-78] using a photomask or a stencil mask or a sacrificial protective coating, perform the selective exposing of the (super)hydrophobic surface to a surface treatment such as UV[79, 80] or UV/ozone[81, 82] or plasma treatment;[67, 83] direct writing of the desired pattern by laser on the (super)hydrophobic surface;[84, 85] using printing techniques, perform the deposition of molecules that suffer oxidative self-polymerization or lipid solutions onto (super)hydrophobic surfaces originating the desired (super)hydrophilic patterns.[56, 69]

Based on the control of the wettability contrast on surfaces, it was showed the possibility to hold fluids[58, 67, 79, 86-89] and direct liquid flows on flat surfaces.[59, 64, 65, 90-92] By studying water condensation on hydrophilic stripes bounded by a hydrophobic substrate, it was showed that water could assume a cylindrical shape highly defined.[86] For small volumes, these water stripes were characterized for to be stable and homogenous. However, for an apparent contact angle on the substrate higher than 90°, the fluid stripes become unstable and a single bulge per stripe arose. Then, increasing the water volume the bulges in neighboring channels coalesced.[83, 86, 93] Working below these critical volume in order to avoid instability, gradients of different materials could be produced in an easy and fast way by capillary flow in a fluid stripe, promising for diagnosis, cell study and drug screening applications.[67, 74, 75] Similar path designs and also non-straight paths have been used such as channels to drive continuous fluid streams, but using

superhydrophobic delimitations instead hydrophobic.[64, 65, 91] Particularly, Dong *et al.* showed to precisely control the separation of a liquid flow from a solid edge, by simultaneously regulating the position of wettability boundary and the flow inertia – Figure 1.2E.[92] In detail, the separation was achieved in different positions by moving the (super)hydrophilic/superhydrophobic dividing line at the solid edge. Interestingly, tit was suggested that this strategy can be very useful for firefighting or irrigation applications.[92]

Besides the stripe shape, other geometric shapes such as squares, circles, triangles or hexagons can be patterned on surfaces – Figure 1.2A. These platforms revealed high potential for droplet-array production for high-throughput assessments.[80, 81, 89] High-density of arrays of single droplets can be produced and assessed independently, due to the extreme wettability contrast that ensures the physical separation between very close droplets.[58, 87] Additionally, it was showed that arrays of thousands of droplets can be produced in a single step by rolling a droplet across the patterned surface or dipping this surface into an aqueous solution.[58, 77, 87] Owing to the high contrast in the wettability created on substrate, the water was naturally removed from the superhydrophobic delimitations and filled the superhydrophilic spots, being this phenomena called discontinuous dewetting – Figure 1.2B.[58, 87]

Remarkably, using customized shapes for surface patterning, Hancock *et al.* showed to be able to create tailored 3D droplets at the macro- and microscales – Figure 1.2C.[88] Being suggested that the use of this technology to pattern surfaces with microparticles and cells, controlling spatial differences in surface concentration, such as sine waves, linear and spiral gradients.[88]

A technology that may include in the open fluidic category, specifically in the wettability-contrast confinement group, is the paper-based microfluidics. We will not develop on this topic, once several review papers can be found in literature.[94-100] Some hydrophobization and patterning methods described before are also used on paper-based microfluidics and liquid confinement is based on

wettability contrast. However on the majority of the paper-based platforms, the fluid is not on the top of the substrate surface but absorbed in the porous structure of paper.

Other interesting category of devices, which may include in open fluidics, are the microfluidic devices based on textiles. These devices can assume a completely flat architecture with (super)hydrophilic patterns printed on a (super)hydrophobic textile background, similarly to paper-based microfluidics, or fabricated using hydrophilic yarn on the top of a non-wettable support.[96, 101-106] For example, Xing et al. reported a microfluidic platform able to drive liquid flows using a hydrophilic cotton yarn sewn into a superhydrophobic textile platform – Figure 1.2D .[106] With this device, continuous flows easily controllable were achieved, by the combination of surface tension-induced Laplace pressure and capillarity presented in the fibrous structure. Similarly, Yildirim et al. engineered fiber surfaces to produce microfluidic devices using superhydrophilic polymeric fibers.[107] However, the liquid spread spontaneously on the exterior of the fibers, contrary to textile hydrophilic fibers. These fiber surfaces showed suitable for the construction of mechanically robust and flexible, lightweight and inexpensive microfluidic devices.[107]

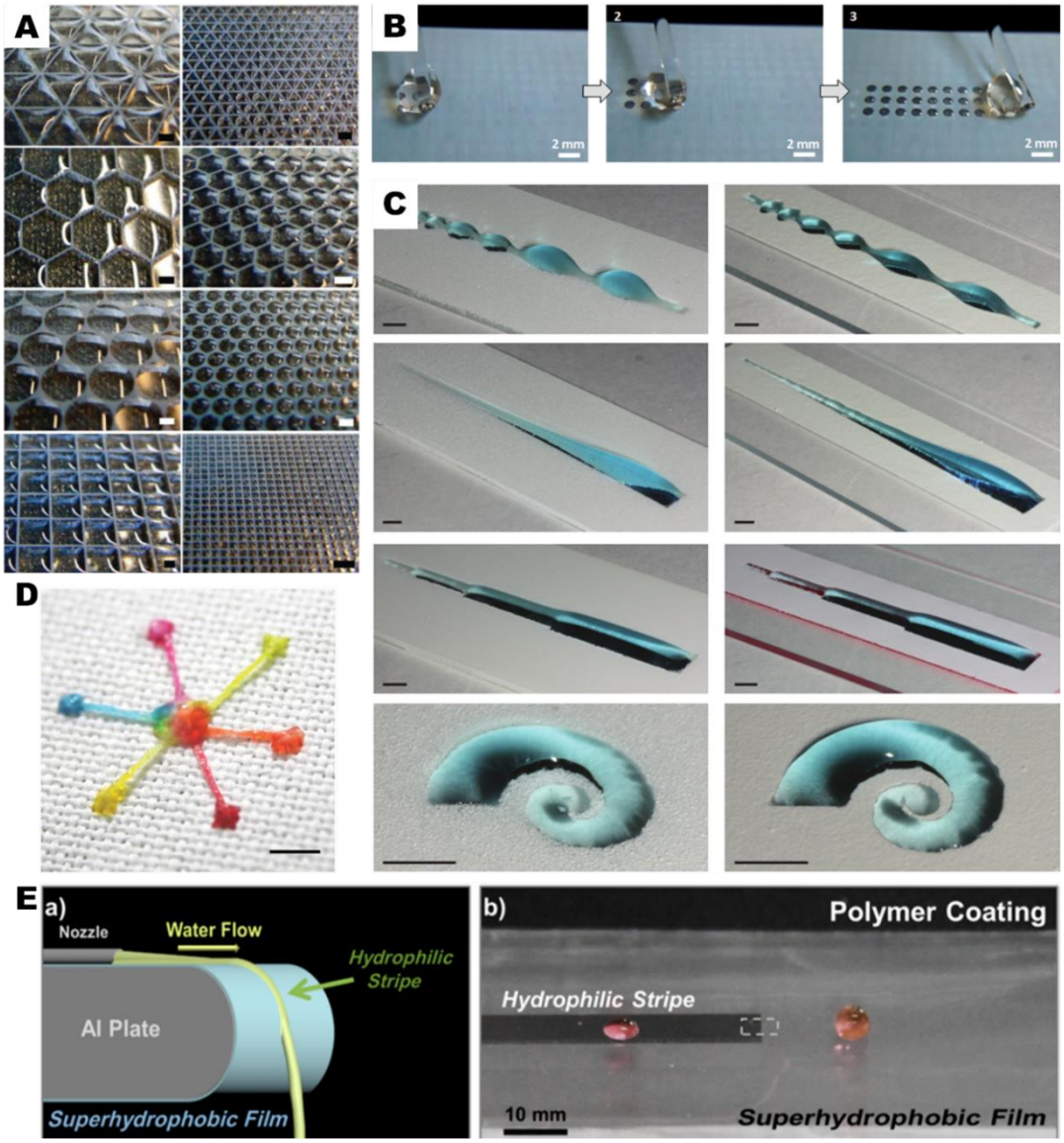

Figure 1.2: (A) Microarrays of water droplets with different geometries formed on superhydrophilic/superhydrophobic patterned surfaces. Scale bars: 1 mm. Adapted from Ref. [87] with permission of the Royal Society of Chemistry. (B) Representation of the discontinuous dewetting method used for the formation of arrays of microdroplets. Adapted from Ref. [58] with permission of John Wiley & Sons. (C) Droplets formed by pipetting fluid onto sine wave, wedge, staircase, and spiral hydrophilic areas previously created by patterning. Scale bars: 3 mm. Adapted from Ref. [88] with permission of John Wiley & Sons. (D) A multi-inlet–single-outlet design on a textile platform using a hydrophilic cotton yarn sewn into the platform. Scale bars: 5 mm. Adapted from Ref. [106] with permission of the Royal Society of Chemistry. (E) Schematic representation of a nozzle mounted on the top surface of an aluminum plate with a superhydrophobic/ (super)hydrophilic stripe patterning. The water pumped though the nozzle was able to travel along the (super)hydrophilic stripe until separation from the solid edge at the (super)hydrophilic/superhydrophobic dividing line. Adapted with permission from Ref. [92]. Copyright 2015 American Chemical Society.

1.3.3. Fluid transport/manipulation in open fluidics

Different methods had been reported for transport/manipulation of fluids in open fluidic systems, which can be done passively (using capillary action) and actively (providing energy to the system). Passive approaches for actuation and control of fluids have aroused great interest, since they allow fully automated operation with low-cost. Yang *et al.* studied the dynamics of capillary-driven liquid flow in grooved channels with two different geometries: rectangular and curved cross-section.[32] The hydrophilic channels were created in a hydrophobic substrate and water/glycerol mixtures presenting different surface tension and viscosity were tested. It was found that the flow velocity of the tested fluids increased with decreasing the channel width, being independent from cross-section geometry.[32] On the other hand, Feng and Rothstein showed to be possible to construct open microchannels that just allow fluid flow in one direction.[108] The unidirectional spontaneous flow was achieved by decorating the interior of linear channels with an array of angled fin-like-structures in both side walls – Figure 1.3C. This behavior was explained by the direction-dependent Laplace pressure induced by these structures on the channel, allowing the capillary spreading of the fluid only in the predefined direction.[108] Regarding to open fluidic devices based on wettability-contrast confinement, Ghosh *et al.* presented a wettability patterning method to produce open microfluidic paths that were able to induce on-chip liquid movement, by overcoming viscous and gravity forces – Figure 1.3A.[79] Wedge-shaped patterns were used to produce superhydrophilic paths embedded on a superhydrophobic background. Driving capillary forces were responsible for the liquid movement and increased linearly with the wedge angle along of the paths.[79] Complex liquid manipulations such as liquid metering, merging, dispensing, and droplet splitting were achieved by patterning complex designs using the wedge-shaped patterns as the basic building blocks. For example, using a planar superhydrophobic surface with superhydrophilic

wedge paths arranged radially and dispensing droplets on the central spot, the droplets were rapidly and equally split amongst the different paths.[79]

There are some methods used for liquid manipulation in closed microchannels that can also be applied to open fluidics, namely electrowetting[28, 30, 38] and pressure driven flow.[17, 42, 43, 65, 92] Using electrowetting actuation, the advancing and receding of liquid stripes in both rectangular and triangular grooved microchannels were actively controlled – Figure 1.3B.[30, 38] Owing to the electrowetting effect, the apparent contact angle of liquid could be reversibly tuned and consequently the liquid movement induced. These movements were controlled by adjusting the frequency and amplitude of the applied voltage. This liquid activity showed to be capillarity driven and dependent of apparent contact angle, liquid viscosity and groove geometry.[30, 38] Using a platform combining both closed and open microfluidics, Wang and Jones have showed that water droplets can also be manipulated by electrowetting actuation.[28]

Similarly to the traditional microfluidics, the pressure driven flows in open fluidic systems are usually induced by mechanical pumps.[17, 42, 43, 65, 92] However, Vourdas *et al.* presented an innovative toll for actuation and valving in open fluidics using pressure – Figure 1.3D.[36] By applying pressure at the rear face (backpressure) of porous and hydrophobic fluidic walls, that initially were sticky, the walls became slippery. Thus, controlling the backpressure, the gas pockets at the liquid-solid interface that influence wall stickiness were controlled. Consequently, the manipulation of liquid volumes became possible in an open channel with rectangular cross-section, but may applicable to other cross-section geometries.[36]

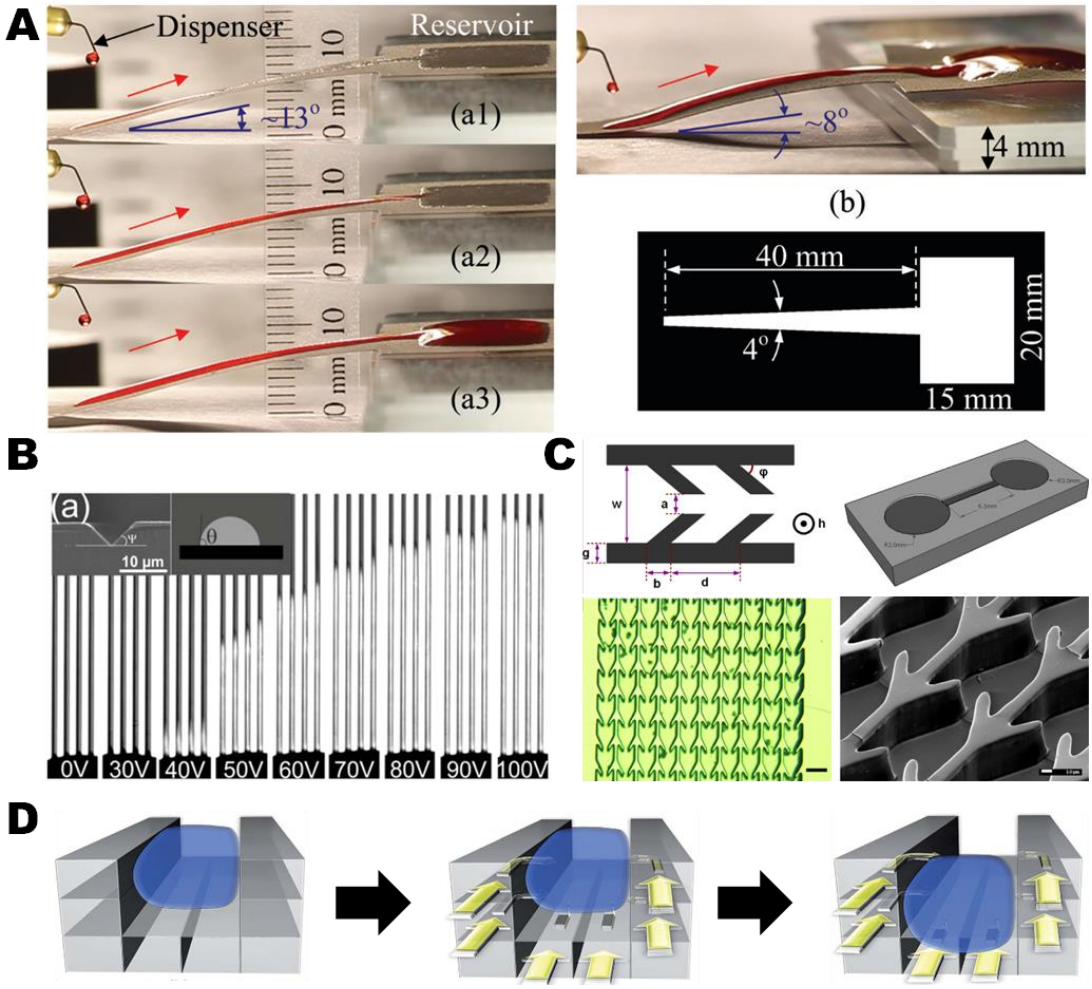

Figure 1.3: (A) Transport of liquid up along an inclined superhydrophilic wedge-shaped path. Water was able to move up along to an elevation of 9 mm. Deign of the photomasking template used for path patterning. Adapted from Ref. [79] with permission of the Royal Society of Chemistry. (B) Image of liquid stripes in triangular grooves during electrowetting. The corresponding applied voltage is given at the bottom of each stripe. Adapted with permission from Ref. [38]. Copyright 2015 American Chemical Society. (C) Schematic illustrations and images of an open channel that allowed only unidirectional spontaneous flow by decorating the interior of the channel with an array of angled fin-like-structures in both side walls. Adapted from Ref. [108] with permission from Elsevier. (D) Schematic illustration of the valve architecture and operation. The channel with porous and hydrophobic walls accommodated the liquid and then a gas flow was applied at the adjacent channels. The backpressure increases and consequently the gas pockets at the liquid-solid interface, inducing the wall slippery and inciting the liquid movement. Adapted from Ref. [36] with permission of the Royal Society of Chemistry.

1.4. Open fluidic platforms for biomedical applications

The high functionality and flexibility typical of open fluidics have been translated on the development of several applications using these platforms, focusing on the biomedical field applications here.

1.4.1. Metabolite extraction

Open fluidic platforms have been reported for metabolite extraction applications using different architectures. Barkal *et al.* created an open platform that allowed microbial culture and posteriorly the solvent extraction of the metabolites in a single device.[109] Teardrop-shaped open microfluidic channels were micromilled in PS using a CNC micromilling machine. On the larger area of the channel a grooved circular well was used for cell culture and the opposite end of the channel was used to dispense the extraction solvent using a micropipette. With this design the flow of organic solvent were directed over the aqueous culture area by spontaneous capillarity (analogous to wedge-shaped paths presented by Ghosh *et al.*),[79] originating a stable biphasic interface. Additionally, it was showed that the efficiency of processes was enhanced once the devices allowed the production of arrays and also compatibility with the use of a multichannel pipette. Taking advantage from the features of these teardrop-shaped open channels, it was suggested their applicability for screening analysis of biological samples such as blood, saliva, mucus, extracellular matrix components, etc.[109]

Based on suspended microfluidics, Casavant *et al.* created an alternative metabolite extraction platform using a multilayer biphasic system to recover metabolites from cell culture.[19] As the capillarity flow method can also generate flow in open systems with immiscible liquid interfaces, the ability of an immiscible solvent to flow in a suspended microfluidic system over an aqueous liquid was showed. A two level microsystem was developed for contacting extraction solvents with cell culture medium from cells in culture and performing the extraction of molecules secreted by cells.[19]

1.4.2. Hydrogel production

Such as described before, it was possible to create tailored 3D droplets at the macro- and microscales using hydrophilic patterns with customized shapes on hydrophobic substrates.[88] Taking this technology as the base, hydrogels with controlled 3D topography at the macro- and microscale were synthesized by photocrosslinking shaped droplets of prepolymer solution, using UV light. It was confirmed that the created hydrogels retained with high fidelity the 3D shape imposed to the prepolymer droplets.[88]

Patel *et al*. presented a simple approach to micro-manufacture arrays of bio-adhesive hydrogels using a sandwiching method to achieve the ionic gelation of a prepolymer solution.[110] First, a gelatin-based solution was poured onto a PDMS microwell mold. Then, using a hydrophobic glass slide as carrier, a hanging droplet of silicate nanoparticle solution was formed. Finally, by precise alignment between PDMS platform and glass slide carrier and sandwiching both, the diffusion between two solutions occurred and the microgels formed, may containing encapsulated cells.[110] By a similar sandwiching method but using flat surfaces with superhydrophobic-hydrophilic micropatterns, alginate hydrogels with defined sizes and shapes were quickly produced.[111] The size and shape were defined by specific patterns on the flat surfaces, likewise to the tailored 3D hydrogels. The droplet formation on micropatterns was performed through discontinuous dewetting (described before), decreasing the time required for the microarray platform preparation. Arrays of adhered hydrogels were obtained by performing the sandwiching step with the carrier of alginate droplets over the carrier of calcium chloride droplets. On the other hand, using the carrier of calcium chloride droplets on top position, freestanding hydrogel particles were produced.[111] Additionally, these hydrogel particles showed potential for tissue engineering applications, once they were able to encapsulate live cells and present magnetic properties, by incorporating magnetic beads.

1.4.3. Gradients generation

Methods for generating gradients of chemicals, materials, biological molecules or cells have showed high importance in biotechnology, materials science and cell biology.[112] Several applications have been reported, namely in diagnostics, material screening and fundamental biological studies, for example mimicking cellular and tissue microenvironments.[74, 89, 112, 113] Open fluidic devices revealed to be very useful to generate soluble and microparticle concentration gradients, gradient hydrogels or molecular gradient for chemotaxis studies.

Simple gradient generation methods based on (super)hydrophilic/(super)hydrophobic patterned surfaces were engineered. Hancock *et al.* developed a gradient technique employing an inexpensive hydrophilic/hydrophobic-patterned platform and passive mechanisms (surface tension and diffusion) – Figure 1.4A.[74] This platform was created by coating a glass slide using a hydrophobic spray commercially available and protecting with an adhesive mask the desired area that should remain untreated and hydrophilic. After removing the rectangular-shaped mask, a fluid stripe confined to the hydrophilic area was produced. In one end of this stripe, a droplet of a second solution was dispensed using a micropipette. On this step, a concentration gradient of the second fluid into the first fluid was generated by diffusion – Figure 1.4A. The developed method allowed to generate both soluble and microparticle gradients.[74] Additionally, using this bench-top technique, gradient biomaterials were produced by crosslinking gradients of prepolymer solutions. As proof-of-concept, concentration gradients of encapsulated cells and with a 3D spatial distribution in the biomaterials were produced.[75] Other example of an open fluidic platform, using wettability-contrast confinement, able to generate gradients was developed by Efremov *et al.*.[89] In detail, an array platform of hydrophilic spots was created and operated in one of two modes of use: arrays of droplets with one droplet per hydrophilic spot; or liquid paths formed by neighboring droplets

that were merged over the hydrophobic boundaries using a pipette tip. By injecting a solution on these liquid paths, concentration gradients of chemicals or cells were generated – Figure 1.4C.[89] Other interesting concept for gradient generation in hydrogels is the multi-gradient hydrogels.[34] These multi-gradient hydrogels were manufactured layer by layer, using a rectangular grooved open channel – Figure 1.4B. Each layer could present a different gradient of particles, soluble factors, materials properties or polymer concentrations. It was proposed that the multiple gradients in biomaterials can create more relevant microenvironments for cellular studies, for example mimicking simple systems for studying co-cultures.[34]

Using an open access microfluidic device, briefly described before, concentration gradients were produced for the study of cell migration during chemotaxis.[27] Taking advantage from the direct access to the open reservoir where the parallel microchannels culminated, stable gradients were generated by passive diffusion using a micropipette – Figure 1.4D. After dispensing the chemoattractant molecules in the reservoir, the gradient equilibration in the channels occurred fast due to the small dimensions of channels. Then, the cellular response of cells seeded on the opposite end of the microchannels was monitored. As gradients were generated by a passive method, shear forces usually present in traditional microfluidic devices were avoided. This feature was important to prevent cell damage and confounding cellular response originated by shear forces.[27]

By combining closed and open microfluidics, other microfluidic gradient generator was also engineered.[26] The gradient was created by injecting the chemoattractant in precise amounts into an open reservoir, in which human neutrophils were previously seeded and allowed to settle and attach – Figure 1.4E. Then, parameters such as cell migration and morphology were quantitatively examined. Besides the study of human neutrophils, the developed gradient generator could have potential application for assays with neurons, immune cells or embryonic stem cells.[26]

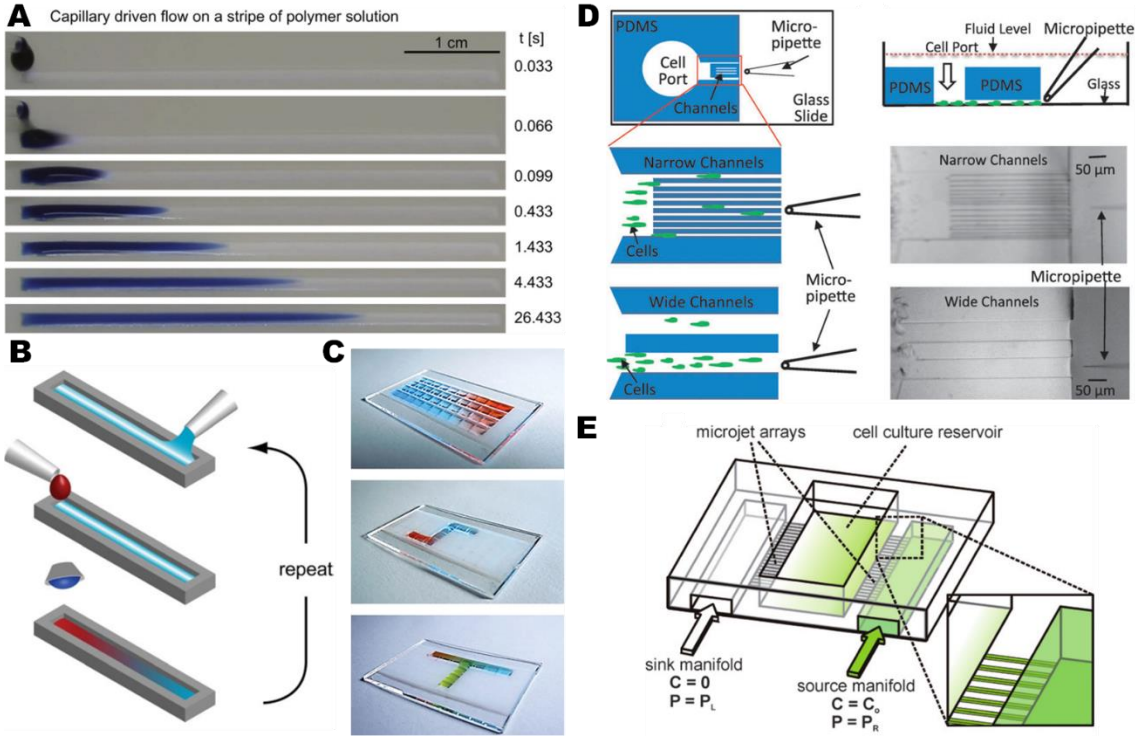

Figure 1.4: (A) Images of the droplet coalescence with a fluid stripe and gradient generation of the second fluid into the first fluid over time. Adapted from Ref. [75] with permission from Elsevier. (B) Protocol for production of multi-gradient hydrogels through a layer by layer methodology, using a rectangular grooved open channel. Channel was prewet and a droplet of a second fluid was added, generating a gradient. The solutions were left to achieve the desired uniformity and this gradient precursor solutions were photocrosslinked. The process was repeated several times until obtain the multi-gradient and layered hydrogel. Adapted from Ref. [34] with permission of the Royal Society of Chemistry. (C) Concentration gradients in liquid channels with different geometries produced using an array of hydrophilic spots. Adapted from Ref. [89] with permission of John Wiley & Sons. (D) The open microfluidic device for studying gradient sensing and cell migration. Owing to the direct access to the open reservoir where the parallel microchannels culminated, stable gradients were generated by passive diffusion using a micropipette. Then, the cellular response of cells seeded on the cell port in the opposite end of the microchannels was monitored. Adapted from Ref. [27] with permission of the Royal Society of Chemistry. (E) 3D schematic of the device showing the open architecture of the cell culture/gradient chamber, where soluble gradients were generated by injecting picoliter amounts of fluid, from a closed microchannel system, into an open reservoir. Adapted from Ref. [26] with permission of the Royal Society of Chemistry.

1.4.4. Cell culture on chip

One of the major advantages that open fluidics brings to cell culture is the direct accessibility, allowing for example single-cell manipulation and probing using a micropipette.[23] Open fluidic platforms have given a high contribution on the development of array production using materials, molecules and cells for high-throughput screening application, namely using platforms based on the wettability-contrast confinement.[58, 78, 81, 85, 114] The usage of superhydrophilic/superhydrophobic patterned surfaces made possible the development of simplistic methods, for example, for producing ultrahigh-density cell microarrays.[114] The ability to control the arrangement and geometry of surface patterning allowed to create patterns of several different cell types on the same substrate to study cell-cell communication.[115] The method was based on a parallel formation of several cell-containing microreservoirs on the cell seeding/adhesion step that were confined by the wettability contrast between hydrophilic regions and superhydrophobic boundaries. Then, with the several cell types adhered to the platform, the platform was submerged in cell culture medium and cell response to the neighboring cells monitored.[115]

On a single platform, several different conditions can be tested simultaneously and separately in a tiny space, which allows saving time, materials and costs. It was showed that different combinations of nanostructured multilayered films were produced using layer by layer methodology in a single chip for fast high-throughput screening. In situ examination of the morphological, physicochemical, and biological properties of the multilayered films was performed on the developed microarray chip.[78] The opposite can also be done: first, to perform cell seeding into the hydrophilic spots and then add the reagents in study to the cell droplet array. The reagent addition can be done one by one using a micropipette or simultaneously using the sandwiching method described before.[58, 85] The carrier of the reagents in study, such as drugs or transfection

mixtures, can be prepared using a noncontact ultralow volume dispenser with the equivalent geometry to the geometry of cell carrier.[58]

These new tools, which some are virtually accessible to anyone, showed high potential to be used in fields such as regenerative medicine/tissue engineering, diagnosis, cellular biology and drug discovery.

1.4.5. Hanging-drop systems

There is high interest for 3D cell spheroids, owing to their great potential for cell therapy, drug discovery and tissue engineering applications. Thus, the interest for developing new tools for cell spheroid production has been increasing. Some reported platforms for the production of these 3D cellular structures are based on open fluidics, namely using hydrophilic/superhydrophobic patterned surfaces.[77, 116-119] Generally, droplets with cells in suspension were placed on the hydrophilic spots – Figure 1.5A. Then, the platform was immediately turned upside-down, taking advantage of the high adhesiveness between droplets and spots for maintaining the droplets on the platform surface. Due to the gravity effect, the cells in suspension on the droplets aggregated to create cell spheroids. The spheroid size and morphology were precisely controlled by adjusting the droplet size and cellular density.[116, 118, 119] Additionally, it was showed that these same hanging droplet platforms allowed to produce arrays of cell spheroids for high-throughput drug screening tests.[77, 117, 119] This category of platforms presented several advantages over the conventional hanging droplet methods, namely the use of reduced volume for cell growth, direct accessibility that allowed easy cell culture medium change and the addition of drugs or other molecules, and both suitability and robustness for combinatorial high-throughput drug screening analysis.[77, 117]

Alternatively, other open fluidic platforms for hanging droplet cell culture were developed based on the suspended microfluidics concept. One example is a two-well hanging droplet platform,

consisting in a larger well for cell culture and a smaller well for liquid manipulation by pipette that were interconnected – Figure 1.5B.[18] The device was produced using PS by CNC milling. As the liquid manipulation was performed in an adjacent well to cell culture well, lower shear stress was experienced by cells during fluid exchange. This asymmetric two-well droplet system opened the possibility for performing long-term culture with minimal disturbance to the cell culture conditions, using shear-sensitive or non-adherent cells. In order to demonstrate the platform versatility, co-culture experiments were also performed, testing both direct and indirect co-culture conditions.[18] Other example of a suspended microfluidic system for hanging droplet cell culture was presented by Birchler et *al.*.[22] This system consisted in a PDMS platform with circular areas for hanging droplets and interconnected thought channels for liquid circulation – Figure 1.5C. Combining the developed open fluidic platform with a fluorescence-activated cell sorting (FACS) device, specific single cells could be directly loaded into defined culturing compartments of the platform in an automatic and precise way. Through this combination, cells were directly sorted into a ready-to-use platform without unnecessary manipulation.[22]

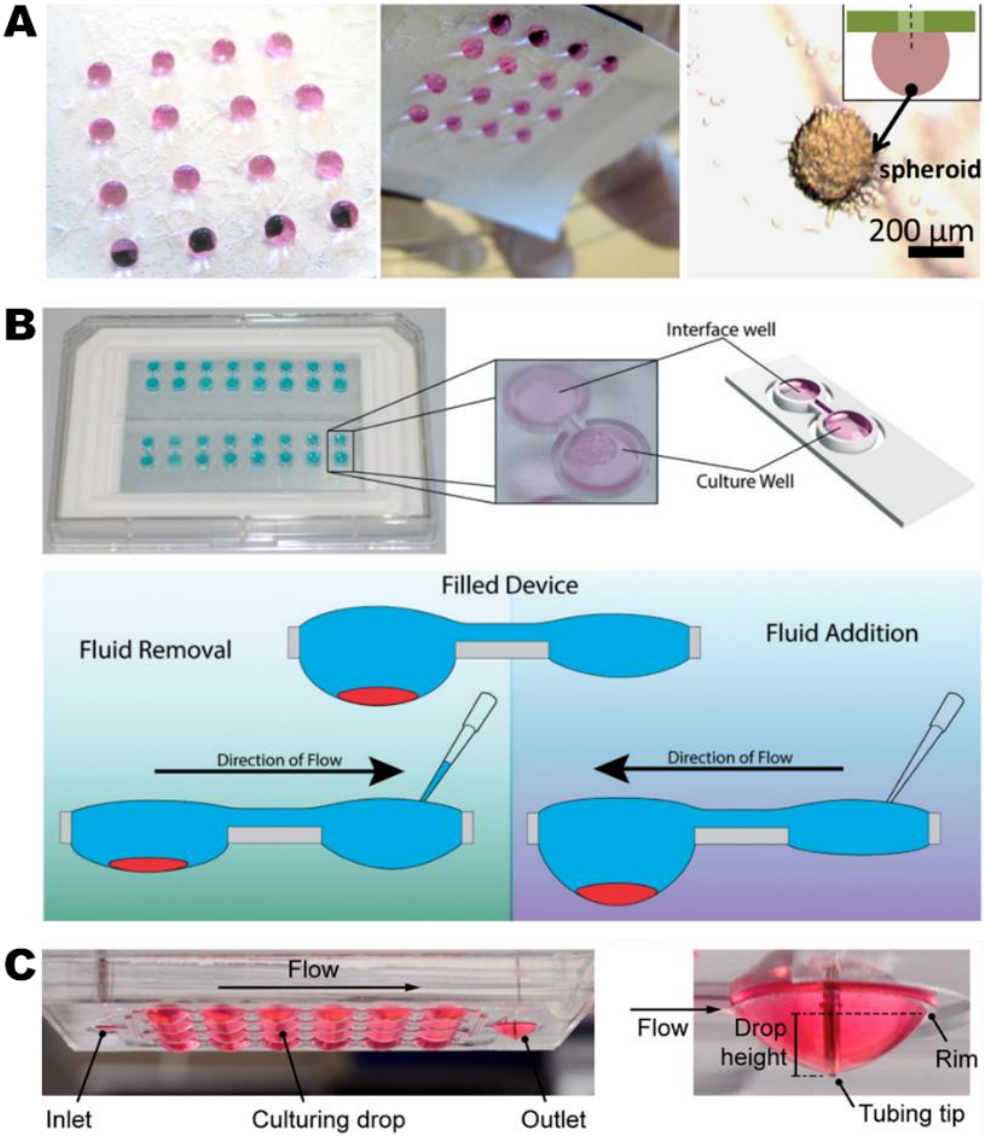

Figure 1.5: (A) Images of the chips with the cell suspensions and then immediately turned upside-down. By the gravity effect, the cells in suspension aggregated, originating cell spheroids. Adapted with permission from Ref. [77]. Copyright 2014 American Chemical Society. (B) Schematic illustration of the two-well hanging droplet device and operation of a filled device containing cells (in red), when fluid is removed or added through the adjacent well to cell culture well with minimal disturbance to the culture. . Adapted from Ref. [18] with permission of the Royal Society of Chemistry. (C) Image of the hanging-drop PDMS platform with circular areas for containing cell droplets and interconnected thought channels for liquid circulation. Adapted with permission from Ref. [22]. Copyright 2016 American Chemical Society.

1.4.6. Perfusion system for cell culture

Applying the open fluidic concept, a fluidic system was created to improve long-term *in vitro* culturing and monitoring of organotypic brain slices.[120] The platform was built using PC by micromilling and was constituted of two levels. The bottom level contained fluidic structures with channels and a circular chamber aligned with the culturing area, where the culture medium was perfused. Medium perfusion was controlled through a syringe pump connected to the channels, allowing a constant supply of nutrients and waste removal to the system. The upper level consisted in a hole to accommodate a porous membrane insert in the culturing area, where the slices of tissue were placed. Due to the continuous perfusion of cell culture medium, the brain slices were cultured for longer periods with reduced handling of the tissues during culturing and the *in vivo*-like environment could be better mimicked.[120]

1.5. Summary

This review deals with an emerging topic related with microfluidics, specifically the open fluidics. The recent advanced on the field and the several applications associated to the biomedical field were described here.

Open fluidic systems are characterized for present a higher air/liquid interface comparing with traditional microfluidics. Open fluidics offer intrinsic advantages to its architecture, such as simplicity of fabrication, easy to clean, enhanced functionality and accessibility for liquid handling. Additionally, these systems overcame usual problems of traditional microfluidics, namely the risk of channel clogging and the occurrence of flow perturbation due to bubbles. Open fluidic platforms can assume different architecture that were divided in two groups: physical confinement and wettability-contrast confinement.

In the first group, platforms combining both open and traditional microfluidics and open channels with rectangular and triangular cross-section were presented. The suspended microfluidic concept, a promising technology in open fluidics topic, was described and valuable applications of this type of platforms were reviewed. Finalizing this group, other innovative concept was advanced, the liquid flows confined and controlled for a narrow strip of a solid surface.

Regarding to wettability-contrast confinement, platforms with (super)hydrophilic patterns bounded by a (super)hydrophobic substrate, paper-based microfluidics and microfluidic devices based on textiles were included on this topic. A briefly description of basic concepts related with surface wettability was performed. Several techniques to produce superhydrophobic surfaces and (super)hydrophobic/(super)hydrophilic patterning were listed. Hydrodynamic conditions and phenomena to reach stable flows or precise fluid manipulation on these patterned platforms were discussed. On paper-based microfluidics, we did not develop the topic what concern production and applications, once several specialized review can be found. Lastly, some microfluidic devices based on textiles were presented. Then, several methods for fluid transport and manipulation in open fluids devices were also reviewed here, namely capillary-driven liquid flow, unidirectional spontaneous flow, electrowetting actuation and pressure driven flow.

Finalizing this review, we revised the several applications on the biomedical field that were developed based on open fluidic platforms. These reported applications included: metabolite extraction, hydrogel production, gradient generation, microarray systems, hanging-drop systems and perfusion systems for cell culture.

1.6. Acknowledgements

The authors acknowledge funding from the European Research Council grant agreement ERC-2012-ADG 20120216-321266 for project ComplexiTE. N. M. Oliveira acknowledges the financial support from Portuguese Foundation for Science and Technology – FCT (Grant SFRH/BD/73172/2010), from the financial program POPH/FSE from QREN.

1.7. References

1. Stone, H. A.; Stroock, A. D.; Ajdari, A., Engineering flows in small devices: Microfluidics toward a lab-on-a-chip. *Annual Review of Fluid Mechanics* **2004,** *36*, 381-411.

2. Yun, H.; Kim, K.; Lee, W. G., Cell manipulation in microfluidics. *Biofabrication* **2013,** *5*.

3. Mehling, M.; Tay, S., Microfluidic cell culture. *Current Opinion in Biotechnology* **2014,** *25*, 95-102.

4. Hyun, K. A.; Jung, H. I., Advances and critical concerns with the microfluidic enrichments of circulating tumor cells. *Lab on a Chip* **2014,** *14*, 45-56.

5. Sackmann, E. K.; Fulton, A. L.; Beebe, D. J., The present and future role of microfluidics in biomedical research. *Nature* **2014,** *507*, 181-189.

6. McDonald, J. C.; Duffy, D. C.; Anderson, J. R.; Chiu, D. T.; Wu, H. K.; Schueller, O. J. A.; Whitesides, G. M., Fabrication of microfluidic systems in poly(dimethylsiloxane). *Electrophoresis* **2000,** *21*, 27-40.

7. Berthier, E.; Young, E. W. K.; Beebe, D., Engineers are from pdms-land, biologists are from polystyrenia. *Lab on a Chip* **2012,** *12*, 1224-1237.

8. Vyawahare, S.; Griffiths, A. D.; Merten, C. A., Miniaturization and parallelization of biological and chemical assays in microfluidic devices. *Chemistry & Biology* **2010,** *17*, 1052-1065.

9. Lee, J. N.; Park, C.; Whitesides, G. M., Solvent compatibility of poly(dimethylsiloxane)-based microfluidic devices. *Analytical Chemistry* **2003,** *75*, 6544-6554.

10. Regehr, K. J.; Domenech, M.; Koepsel, J. T.; Carver, K. C.; Ellison-Zelski, S. J.; Murphy, W. L.; Schuler, L. A.; Alarid, E. T.; Beebe, D. J., Biological implications of polydimethylsiloxane-based microfluidic cell culture. *Lab on a Chip* **2009,** *9*, 2132-2139.

11. Toepke, M. W.; Beebe, D. J., Pdms absorption of small molecules and consequences in microfluidic applications. *Lab on a Chip* **2006,** *6*, 1484-1486.

12. Ren, K. N.; Zhao, Y. H.; Su, J.; Ryan, D.; Wu, H. K., Convenient method for modifying poly(dimethylsiloxane) to be airtight and resistive against absorption of small molecules. *Analytical Chemistry* **2010,** *82*, 5965-5971.

13. Heo, Y. S.; Cabrera, L. M.; Song, J. W.; Futai, N.; Tung, Y. C.; Smith, G. D.; Takayama, S., Characterization and resolution of evaporation-mediated osmolality shifts that constrain microfluidic cell culture in poly(dimethylsiloxane) devices. *Analytical Chemistry* **2007,** *79*, 1126-1134.

14. Dittrich, P. S.; Manz, A., Lab-on-a-chip: Microfluidics in drug discovery. *Nature Reviews Drug Discovery* **2006,** *5*, 210-218.

15. Bhatia, S. N.; Ingber, D. E., Microfluidic organs-on-chips. *Nature Biotechnology* **2014,** *32*, 760-772.

16. Zheng, F. Y.; Fu, F. F.; Cheng, Y.; Wang, C. Y.; Zhao, Y. J.; Gu, Z. Z., Organ-on-a-chip systems: Microengineering to biomimic living systems. *Small* **2016,** *12*, 2253-2282.

17. Davey, N.; Neild, A., Pressure-driven flow in open fluidic channels. *Journal of Colloid and Interface Science* **2011,** *357*, 534-540.

18. de Groot, T. E.; Veserat, K. S.; Berthier, E.; Beebe, D. J.; Theberge, A. B., Surface-tension driven open microfluidic platform for hanging droplet culture. *Lab on a Chip* **2016,** *16*, 334-344.

19. Casavant, B. P.; Berthier, E.; Theberge, A. B.; Berthier, J.; Montanez-Sauri, S. I.; Bischel, L. L.; Brakke, K.; Hedman, C. J.; Bushman, W.; Keller, N. P.; Beebe, D. J., Suspended microfluidics. *Proceedings of the National Academy of Sciences of the United States of America* **2013,** *110*, 10111-10116.

20. Yang, D.; Krasowska, M.; Priesta, C.; Ralston, J., Dynamics of capillary-driven liquid-liquid displacement in open microchannels. *Physical Chemistry Chemical Physics* **2014,** *16*, 24473-24478.

21. Berthier, J.; Brakke, K. A.; Gosselin, D.; Bourdat, A. G.; Nonglaton, G.; Villard, N.; Laffite, G.; Boizot, F.; Costa, G.; Delapierre, G., Suspended microflows between vertical parallel walls. *Microfluidics and Nanofluidics* **2015,** *18*, 919-929.

22. Birchler, A.; Berger, M.; Jaggin, V.; Lopes, T.; Etzrod, M.; Misun, P. M.; Pena-Francesch, M.; Schroeder, T.; Hierlemann, A.; Frey, O., Seamless combination of fluorescence-activated cell sorting and hanging-drop networks for individual handling and culturing of stem cells and microtissue spheroids. *Analytical Chemistry* **2016,** *88*, 1222-1229.

23. Hsu, C. H.; Chen, C. C.; Folch, A., "Microcanals" for micropipette access to single cells in microfluidic environments. *Lab on a Chip* **2004,** *4*, 420-424.

24. Melin, J.; van der Wijngaart, W.; Stemme, G., Behaviour and design considerations for continuous flow closed-open-closed liquid microchannels. *Lab on a Chip* **2005,** *5*, 682-686.

25. Keenan, T. M.; Hsu, C. H.; Folch, A., Microfluidic "jets" for generating steady-state gradients of soluble molecules on open surfaces. *Applied Physics Letters* **2006,** *89*.

26. Keenan, T. M.; Frevert, C. W.; Wu, A.; Wong, V.; Folch, A., A new method for studying gradient-induced neutrophil desensitization based on an open microfluidic chamber. *Lab on a Chip* **2010,** *10*, 116-122.

27. Jowhar, D.; Wright, G.; Samson, P. C.; Wikswo, J. P.; Janetopoulos, C., Open access microfluidic device for the study of cell migration during chemotaxis. *Integrative Biology* **2010,** *2*, 648-658.

28. Wang, W. Q.; Jones, T. B., Moving droplets between closed and open microfluidic systems. *Lab on a Chip* **2015,** *15*, 2201-2212.

29. Seemann, R.; Brinkmann, M.; Kramer, E. J.; Lange, F. F.; Lipowsky, R., Wetting morphologies at microstructured surfaces. *Proceedings of the National Academy of Sciences of the United States of America* **2005,** *102*, 1848-1852.

30. Baret, J. C.; Decre, M. M. J.; Herminghaus, S.; Seemann, R., Transport dynamics in open microfluidic grooves. *Langmuir* **2007,** *23*, 5200-5204.

31. Chen, Y. F.; Tseng, F. G.; ChangChien, S. Y.; Chen, M. H.; Yu, R. J.; Chieng, C. C., Surface tension driven flow for open microchannels with different turning angles. *Microfluidics and Nanofluidics* **2008,** *5*, 193-203.

32. Yang, D.; Krasowska, M.; Priest, C.; Popescu, M. N.; Ralston, J., Dynamics of capillary-driven flow in open microchannels. *Journal of Physical Chemistry C* **2011,** *115*, 18761-18769.

33. Zhou, M.; Yu, J.; Li, J.; Wu, B.; Zhang, W., Wetting induced fluid spread on structured surfaces at micro scale. *Applied Surface Science* **2012,** *258*, 7596-7600.

34. Piraino, F.; Camci-Unal, G.; Hancock, M. J.; Rasponi, M.; Khademhosseini, A., Multi-gradient hydrogels produced layer by layer with capillary flow and crosslinking in open microchannels. *Lab on a Chip* **2012,** *12*, 659-661.

35. Ouali, F. F.; McHale, G.; Javed, H.; Trabi, C.; Shirtcliffe, N. J.; Newton, M. I., Wetting considerations in capillary rise and imbibition in closed square tubes and open rectangular cross-section channels. *Microfluidics and Nanofluidics* **2013,** *15*, 309-326.

36. Vourdas, N.; Dalamagkidis, K.; Stathopoulos, V. N., Active porous valves for plug actuation and plug flow manipulation in open channel fluidics. *Rsc Advances* **2015,** *5*, 104594-104600.

37. Sowers, T. W.; Sarkar, R.; Prameela, S. E.; Izadi, E.; Rajagopalan, J., Capillary driven flow of polydimethylsiloxane in open rectangular microchannels. *Soft Matter* **2016,** *12*, 5818-5823.

38. Barman, J.; Swain, D.; Law, B. M.; Seemann, R.; Herminghaus, S.; Khare, K., Electrowetting actuated microfluidic transport in surface grooves with triangular cross section. *Langmuir* **2015,** *31*, 1231-1236.

39. Berthier, J.; Brakke, K. A.; Furlani, E. P.; Karampelas, I. H.; Poher, V.; Gosselin, D.; Cubizolles, M.; Pouteau, P., Whole blood spontaneous capillary flow in narrow v-groove microchannels. *Sensors and Actuators B-Chemical* **2015,** *206*, 258-267.

40. Berthier, J.; Brakke, K. A.; Berthier, E., A general condition for spontaneous capillary flow in uniform cross-section microchannels. *Microfluidics and Nanofluidics* **2014,** *16*, 779-785.

41. Berthier, J.; Brakke, K. A.; Gosselin, D.; Navarro, F.; Belgacem, N.; Chaussy, D., Spontaneous capillary flow in curved, open microchannels. *Microfluidics and Nanofluidics* **2016,** *20*.

42. Tan, J. N.; Alan, T.; Neild, A., Stability of flowing open fluidic channels. *Aip Advances* **2013,** *3*.

43. Tan, J. N.; Neild, A., Microfluidic mixing in a y-junction open channel. *Aip Advances* **2012,** *2*.

44. Dietrich, S.; Popescu, M. N.; Rauscher, M., Wetting on structured substrates. *Journal of Physics-Condensed Matter* **2005,** *17*, S577-S593.

45. Ueda, E.; Levkin, P. A., Emerging applications of superhydrophilic-superhydrophobic micropatterns. *Advanced Materials* **2013,** *25*, 1234-1247.

46. Lima, A. C.; Mano, J. F., Micro/nano-structured superhydrophobic surfaces in the biomedical field: Part i: Basic concepts and biomimetic approaches. *Nanomedicine* **2015,** *10*, 103-119.

47. Sun, T. L.; Feng, L.; Gao, X. F.; Jiang, L., Bioinspired surfaces with special wettability. *Accounts of Chemical Research* **2005,** *38*, 644-652.

48. Roach, P.; Shirtcliffe, N. J.; Newton, M. I., Progess in superhydrophobic surface development. *Soft Matter* **2008,** *4*, 224-240.

49. Feng, X. J.; Jiang, L., Design and creation of superwetting/antiwetting surfaces. *Advanced Materials* **2006,** *18*, 3063-3078.

50. Li, X. M.; Reinhoudt, D.; Crego-Calama, M., What do we need for a superhydrophobic surface? A review on the recent progress in the preparation of superhydrophobic surfaces. *Chemical Society Reviews* **2007,** *36*, 1350-1368.

51. Yan, Y. Y.; Gao, N.; Barthlott, W., Mimicking natural superhydrophobic surfaces and grasping the wetting process: A review on recent progress in preparing superhydrophobic surfaces. *Advances in Colloid and Interface Science* **2011,** *169*, 80-105.

52. Sahoo, B. N.; Kandasubramanian, B., Recent progress in fabrication and characterisation of hierarchical biomimetic superhydrophobic structures. *Rsc Advances* **2014,** *4*, 22053-22093.

53. Wang, S. T.; Liu, K. S.; Yao, X.; Jiang, L., Bioinspired surfaces with superwettability: New insight on theory, design, and applications. *Chemical Reviews* **2015,** *115*, 8230-8293.

54. Manna, U.; Broderick, A. H.; Lynn, D. M., Chemical patterning and physical refinement of reactive superhydrophobic surfaces. *Advanced Materials* **2012,** *24*, 4291-+.

55. Manna, U.; Lynn, D. M., Patterning and impregnation of superhydrophobic surfaces using aqueous solutions. *Acs Applied Materials & Interfaces* **2013,** *5*, 7731-7736.

56. Li, J. S. S.; Ueda, E.; Nallapaneni, A.; Li, L. X. X.; Levkin, P. A., Printable superhydrophilic-superhydrophobic micropatterns based on supported lipid layers. *Langmuir* **2012,** *28*, 8286-8291.

57. Auad, P.; Ueda, E.; Levkin, P. A., Facile and multiple replication of superhydrophilic-superhydrophobic patterns using adhesive tape. *Acs Applied Materials & Interfaces* **2013,** *5*, 8053-8057.

58. Popova, A. A.; Schillo, S. M.; Demir, K.; Ueda, E.; Nesterov-Mueller, A.; Levkin, P. A., Droplet-array (da) sandwich chip: A versatile platform for high-throughput cell screening based on superhydrophobic-superhydrophilic micropatterning. *Advanced Materials* **2015,** *27*, 5217-5222.

59. Burriel, P.; Ignes-Mullol, J.; Claret, J.; Sagues, F., Two-dimensional microfluidics using circuits of wettability contrast. *Langmuir* **2010,** *26*, 4613-4615.

60. Nishimoto, S.; Becchaku, M.; Kameshima, Y.; Shirosaki, Y.; Hayakawa, S.; Osaka, A.; Miyake, M., Tio2-based superhydrophobic-superhydrophilic pattern with an extremely high wettability contrast. *Thin Solid Films* **2014,** *558*, 221-226.

61. Lee, C.; Cho, H.; Kim, D.; Hwang, W., Fabrication of patterned surfaces that exhibit variable wettability ranging from superhydrophobicity to high hydrophilicity by laser irradiation. *Applied Surface Science* **2014,** *288*, 619-624.

62. Huang, J. Y.; Lai, Y. K.; Pan, F.; Yang, L.; Wang, H.; Zhang, K. Q.; Fuchs, H.; Chi, L. F., Multifunctional superamphiphobic tio2 nanostructure surfaces with facile wettability and adhesion engineering. *Small* **2014,** *10*, 4865-4873.

63. Song, W. L.; Veiga, D. D.; Custodio, C. A.; Mano, J. F., Bioinspired degradable substrates with extreme wettability properties. *Advanced Materials* **2009,** *21*, 1830-+.

64. Oliveira, N. M.; Neto, A. I.; Song, W. L.; Mano, J. F., Two-dimensional open microfluidic devices by tuning the wettability on patterned superhydrophobic polymeric surface. *Applied Physics Express* **2010,** *3*.

65. Sousa, M. P.; Mano, J. F., Patterned superhydrophobic paper for microfluidic devices obtained by writing and printing. *Cellulose* **2013,** *20*, 2185-2190.

66. Elsharkawy, M.; Schutzius, T. M.; Megaridis, C. M., Inkjet patterned superhydrophobic paper for open-air surface microfluidic devices. *Lab on a Chip* **2014,** *14*, 1168-1175.

67. Oliveira, N. M.; Reis, R. L.; Mano, J. F., Superhydrophobic surfaces engineered using diatomaceous earth. *Acs Applied Materials & Interfaces* **2013,** *5*, 4202-4208.

68. Rial-Hermida, M. I.; Oliveira, N. M.; Concheiro, A.; Alvarez-Lorenzo, C.; Mano, J. F., Bioinspired superamphiphobic surfaces as a tool for polymer- and solvent-independent preparation of drug-loaded spherical particles. *Acta Biomaterialia* **2014,** *10*, 4314-4322.

69. Zhang, L. B.; Wu, J. B.; Hedhili, M. N.; Yang, X. L.; Wang, P., Inkjet printing for direct micropatterning of a superhydrophobic surface: Toward biomimetic fog harvesting surfaces. *Journal of Materials Chemistry A* **2015,** *3*, 2844-2852.

70. Reys, L. L.; Silva, S. S.; da Costa, D. S.; Oliveira, N. M.; Mano, J. F.; Reis, R. L.; Silva, T. H., Fucoidan hydrogels photo-cross-linked with visible radiation as matrices for cell culture. *Acs Biomaterials Science & Engineering* **2016,** *2*, 1151-1161.

71. Sun, J. Z.; Bao, B.; Jiang, J. K.; He, M.; Zhang, X. Y.; Song, Y. L., Facile fabrication of a superhydrophilic-superhydrophobic patterned surface by inkjet printing a sacrificial layer on a superhydrophilic surface. *Rsc Advances* **2016,** *6*, 31470-31475.

72. Tian, D. L.; Song, Y. L.; Jiang, L., Patterning of controllable surface wettability for printing techniques. *Chemical Society Reviews* **2013,** *42*, 5184-5209.

73. Yamada, K.; Henares, T. G.; Suzuki, K.; Citterio, D., Paper-based inkjet-printed microfluidic analytical devices. *Angewandte Chemie-International Edition* **2015,** *54*, 5294-5310.

74. Hancock, M. J.; He, J. K.; Mano, J. F.; Khademhosseini, A., Surface-tension-driven gradient generation in a fluid stripe for bench-top and microwell applications. *Small* **2011,** *7*, 892-901.

75. Hancock, M. J.; Piraino, F.; Camci-Unal, G.; Rasponi, M.; Khademhosseini, A., Anisotropic material synthesis by capillary flow in a fluid stripe. *Biomaterials* **2011,** *32*, 6493-6504.

76. Oliveira, M. B.; Mano, J. F., On-chip assessment of the protein-release profile from 3d hydrogel arrays. *Analytical Chemistry* **2013,** *85*, 2391-2396.

77. Oliveira, M. B.; Neto, A. I.; Correia, C. R.; Rial-Hermida, M. I.; Alvarez-Lorenzo, C.; Mano, J. F., Superhydrophobic chips for cell spheroids high-throughput generation and drug screening. *Acs Applied Materials & Interfaces* **2014,** *6*, 9488-9495.

78. Neto, A. I.; Vasconcelos, N. L.; Oliveira, S. M.; Ruiz-Molina, D.; Mano, J. F., High-throughput topographic, mechanical, and biological screening of multilayer films containing mussel-inspired biopolymers. *Advanced Functional Materials* **2016,** *26*, 2745-2755.

79. Ghosh, A.; Ganguly, R.; Schutzius, T. M.; Megaridis, C. M., Wettability patterning for high-rate, pumpless fluid transport on open, non-planar microfluidic platforms. *Lab on a Chip* **2014,** *14*, 1538-1550.

80. Feng, W. Q.; Li, L. X.; Du, X.; Welle, A.; Levkin, P. A., Single-step fabrication of high-density microdroplet arrays of low-surface-tension liquids. *Advanced Materials* **2016,** *28*, 3202-3208.

81. Neto, A. I.; Custodio, C. A.; Song, W. L.; Mano, J. F., High-throughput evaluation of interactions between biomaterials, proteins and cells using patterned superhydrophobic substrates. *Soft Matter* **2011,** *7*, 4147-4151.

82. Neto, A. I.; Meredith, H. J.; Jenkins, C. L.; Wilker, J. J.; Mano, J. F., Combining biomimetic principles from the lotus leaf and mussel adhesive: Polystyrene films with superhydrophobic and adhesive layers. *Rsc Advances* **2013,** *3*, 9352-9356.

83. Boreyko, J. B.; Hansen, R. R.; Murphy, K. R.; Nath, S.; Retterer, S. T.; Collier, C. P., Controlling condensation and frost growth with chemical micropatterns. *Scientific Reports* **2016,** *6*.

84. Paradisanos, I.; Fotakis, C.; Anastasiadis, S. H.; Stratakis, E., Gradient induced liquid motion on laser structured black si surfaces. *Applied Physics Letters* **2015,** *107*.

85. Xu, K. R.; Wang, X. P.; Ford, R. M.; Landeres, J. P., Self-partitioned droplet array on laser-patterned superhydrophilic glass surface for wall-less cell arrays. *Analytical Chemistry* **2016,** *88*, 2652-2658.

86. Gau, H.; Herminghaus, S.; Lenz, P.; Lipowsky, R., Liquid morphologies on structured surfaces: From microchannels to microchips. *Science* **1999,** *283*, 46-49.

87. Ueda, E.; Geyer, F. L.; Nedashkivska, V.; Levkin, P. A., Droplet microarray: Facile formation of arrays of microdroplets and hydrogel micropads for cell screening applications. *Lab on a Chip* **2012,** *12*, 5218-5224.

88. Hancock, M. J.; Yanagawa, F.; Jang, Y. H.; He, J. K.; Kachouie, N. N.; Kaji, H.; Khademhosseini, A., Designer hydrophilic regions regulate droplet shape for controlled surface patterning and 3d microgel synthesis. *Small* **2012,** *8*, 393-403.

89. Efremov, A. N.; Grunze, M.; Levkin, P. A., Digital liquid patterning: A versatile method for maskless generation of liquid patterns and gradients. *Advanced Materials Interfaces* **2014,** *1*.

90. Xing, S. Y.; Harake, R. S.; Pan, T. R., Droplet-driven transports on superhydrophobic-patterned surface microfluidics. *Lab on a Chip* **2011,** *11*, 3642-3648.

91. Obeso, C. G.; Sousa, M. P.; Song, W. L.; Rodriguez-Perez, M. A.; Bhushan, B.; Mano, J. F., Modification of paper using polyhydroxybutyrate to obtain biomimetic superhydrophobic substrates. *Colloids and Surfaces a-Physicochemical and Engineering Aspects* **2013,** *416*, 51-55.

92. Dong, Z. C.; Wu, L.; Li, N.; Ma, J.; Jiang, L., Manipulating overflow separation directions by wettability boundary positions. *Acs Nano* **2015,** *9*, 6595-6602.

93. Speth, R. L.; Lauga, E., Capillary instability on a hydrophilic stripe. *New Journal of Physics* **2009,** *11*.

94. Yetisen, A. K.; Akram, M. S.; Lowe, C. R., Paper-based microfluidic point-of-care diagnostic devices. *Lab on a Chip* **2013,** *13*, 2210-2251.

95. Nery, E. W.; Kubota, L. T., Sensing approaches on paper-based devices: A review. *Analytical and Bioanalytical Chemistry* **2013,** *405*, 7573-7595.

96. Coltro, W. K. T.; Cheng, C. M.; Carrilho, E.; de Jesus, D. P., Recent advances in low-cost microfluidic platforms for diagnostic applications. *Electrophoresis* **2014,** *35*, 2309-2324.

97. Hu, J.; Wang, S. Q.; Wang, L.; Li, F.; Pingguan-Murphy, B.; Lu, T. J.; Xu, F., Advances in paper-based point-of-care diagnostics. *Biosensors & Bioelectronics* **2014,** *54*, 585-597.

98. Chen, Y. H.; Kuo, Z. K.; Cheng, C. M., Paper - a potential platform in pharmaceutical development. *Trends in Biotechnology* **2015,** *33*, 4-9.

99. Cate, D. M.; Adkins, J. A.; Mettakoonpitak, J.; Henry, C. S., Recent developments in paper-based microfluidic devices. *Analytical Chemistry* **2015,** *87*, 19-41.

100. Meredith, N. A.; Quinn, C.; Cate, D. M.; Reilly, T. H.; Volckens, J.; Henry, C. S., Paper-based analytical devices for environmental analysis. *Analyst* **2016,** *141*, 1874-1887.

101. Li, X.; Tian, J. F.; Shen, W., Thread as a versatile material for low-cost microfluidic diagnostics. *Acs Applied Materials & Interfaces* **2010,** *2*, 1-6.

102. Reches, M.; Mirica, K. A.; Dasgupta, R.; Dickey, M. D.; Butte, M. J.; Whitesides, G. M., Thread as a matrix for biomedical assays. *Acs Applied Materials & Interfaces* **2010,** *2*, 1722-1728.

103. Ballerini, D. R.; Li, X.; Shen, W., Flow control concepts for thread-based microfluidic devices. *Biomicrofluidics* **2011,** *5*.

104. Nilghaz, A.; Wicaksono, D. H. B.; Gustiono, D.; Majid, F. A. A.; Supriyanto, E.; Kadir, M. R. A., Flexible microfluidic cloth-based analytical devices using a low-cost wax patterning technique. *Lab on a Chip* **2012,** *12*, 209-218.

105. Nilghaz, A.; Ballerini, D. R.; Shen, W., Exploration of microfluidic devices based on multi-filament threads and textiles: A review. *Biomicrofluidics* **2013,** *7*.

106. Xing, S. Y.; Jiang, J.; Pan, T. R., Interfacial microfluidic transport on micropatterned superhydrophobic textile. *Lab on a Chip* **2013,** *13*, 1937-1947.

107. Yildirim, A.; Yunusa, M.; Ozturk, F. E.; Kanik, M.; Bayindir, M., Surface textured polymer fibers for microfluidics. *Advanced Functional Materials* **2014,** *24*, 4569-4576.

108. Feng, J. S.; Rothstein, J. P., One-way wicking in open micro-channels controlled by channel topography. *Journal of Colloid and Interface Science* **2013,** *404*, 169-178.

109. Barkal, L. J.; Theberge, A. B.; Guo, C. J.; Spraker, J.; Rappert, L.; Berthier, J.; Brakke, K. A.; Wang, C. C. C.; Beebe, D. J.; Keller, N. P.; Berthier, E., Microbial metabolomics in open microscale platforms. *Nature Communications* **2016,** *7*.

110. Patel, R. G.; Purwada, A.; Cerchietti, L.; Inghirami, G.; Melnick, A.; Gaharwar, A. K.; Singh, A., Microscale bioadhesive hydrogel arrays for cell engineering applications. *Cellular and Molecular Bioengineering* **2014,** *7*, 394-408.

111. Neto, A. I.; Demir, K.; Popova, A. A.; Oliveira, M. B.; Mano, J. F.; Levkin, P. A., Fabrication of hydrogel particles of defined shapes using superhydrophobic-hydrophilic micropatterns. *Advanced Materials* **2016**, n/a-n/a.

112. Kim, S.; Kim, H. J.; Jeon, N. L., Biological applications of microfluidic gradient devices. *Integrative Biology* **2010,** *2*, 584-603.

113. Kim, C.; Kreppenhofer, K.; Kashef, J.; Gradl, D.; Herrmann, D.; Schneider, M.; Ahrens, R.; Guber, A.; Wedlich, D., Diffusion- and convection-based activation of wnt/beta-catenin signaling in a gradient generating microfluidic chip. *Lab on a Chip* **2012,** *12*, 5186-5194.

114. Geyer, F. L.; Ueda, E.; Liebel, U.; Grau, N.; Levkin, P. A., Superhydrophobic-superhydrophilic micropatterning: Towards genome-on-a-chip cell microarrays. *Angewandte Chemie-International Edition* **2011,** *50*, 8424-8427.

115. Efremov, A. N.; Stanganello, E.; Welle, A.; Scholpp, S.; Levkin, P. A., Micropatterned superhydrophobic structures for the simultaneous culture of multiple cell types and the study of cell-cell communication. *Biomaterials* **2013,** *34*, 1757-1763.

116. Seo, J.; Lee, J. S.; Lee, K.; Kim, D.; Yang, K.; Shin, S.; Mahata, C.; Jung, H. B.; Lee, W.; Cho, S. W.; Lee, T., Switchable water-adhesive, superhydrophobic palladium-layered silicon nanowires potentiate the angiogenic efficacy of human stem cell spheroids. *Advanced Materials* **2014,** *26*, 7043-+.

117. Neto, A. I.; Correia, C. R.; Custodio, C. A.; Mano, J. F., Biomimetic miniaturized platform able to sustain arrays of liquid droplets for high-throughput combinatorial tests. *Advanced Functional Materials* **2014,** *24*, 5096-5103.

118. Lee, M.; Yang, K.; Hwang, Y. H.; Byun, Y.; Lee, D. Y.; Cho, S. W.; Lee, H., Spheroform: Therapeutic spheroid-forming nanotextured surfaces inspired by desert beetle physosterna cribripes. *Advanced Healthcare Materials* **2015,** *4*, 511-515.

119. Neto, A. I.; Correia, C. R.; Oliveira, M. B.; Rial-Hermida, M. I.; Alvarez-Lorenzo, C.; Reis, R. L.; Mano, J. F., A novel hanging spherical drop system for the generation of cellular spheroids and high throughput combinatorial drug screening. *Biomaterials Science* **2015,** *3*, 581-585.

120. Bakmand, T.; Troels-Smith, A. R.; Dimaki, M.; Nissen, J. D.; Andersen, K. B.; Sasso, L.; Waagepetersen, H. S.; Gramsbergen, J. B.; Svendsen, W. E., Fluidic system for long-term in vitro culturing and monitoring of organotypic brain slices. *Biomedical Microdevices* **2015,** *17*.

Chapter 2

The Potential of Liquid Marbles for Biomedical Applications: A Critical Review

This chapter is based on the following publication:

Nuno M. Oliveira, Rui L. Reis, João F. Mano. The Potential of Liquid Marbles for Biomedical Applications: A Critical Review. *Submitted*.

2.1. Abstract

Liquid marbles (LM) are freestanding droplets covered by micro/nanoparticles with hydrophobic/hydrophilic properties which enable to manipulate the marbles like a soft solid. This soft solid has being presented as an alternative approach to conventional superhydrophobicity. Widely range of applications were found for LM in different scientific fields, but just very recently in the biomedical field.

Here, we reviewed the LM properties, namely shell structure, LM shape, evaporation, floatability and robustness. Additionally, we also described the several methods for LM manipulation that allow remote control of marbles, using magnetic, electrostatic and gravitational forces, ultraviolet and infrared radiation, and LM self-propulsion. Then, we described the biomedical applications found for the LM. Very distinctive applications have being reported, namely diagnostic assays, cell culture, drug screening and cryopreservation of mammalian cells. Finally, a critical view of the LM potential for biomedical applications was presented, suggesting some possible advances on this emergent field.

2.2. Introduction

Liquid marbles (LM) consist in liquid droplets coated with a hydrophobic powder, according Aussillous and Quéré that reported for the first time this concept.[1] LM production is achieved by simply rolling a liquid droplet over hydrophobic micro or nanoparticles. Being the encapsulated material protected by the hydrophobic shell, thus preventing the physical contact between the liquid and the external environment.[1-4] However, it was also reported that hydrophilic particles can be used on LM production, specifically graphite and carbon black.[5, 6] LM make easy the manipulation of liquids that combined with other intrinsic properties justify the growing interest of the scientific community.

Widely range of applications were found for LM, such as oil adsorption and separation,[7, 8] pH and gas sensing,[9-13] chemical reactions,[14, 15] synthesizing microparticles,[16] revealing water pollution on the water/vapor interface[17] and manipulation of small amounts of liquids (micro-reactors, micro-pumps).[14, 18, 19] The LM use in cosmetics has been also suggested, due to the non-oily feel imparted to skin by marbles.[20] Several studies and applications for LM have been published in different scientific fields, but just very recently in the biomedical field.

Some excellent reviews on LM field exist in literature. The scopes of these reviews cover general properties, manipulation and applications of LM.[2-4, 21-25] However on this review, the aim was to focus on the emerging field of LM in biomedical applications. Based on the most recent progress, we intended to show how the properties and manipulation of LM were explored in applications development on the biomedical field. This review is finalized with a critical view of the latent potential of LM for new applications on the referred field. Therefore, this paper is composed by three sections: (a) compilation of the LM properties and the developed methodologies for LM manipulation, (b) illustration of the most recent progress in the biomedical applications for the LM,

and (c) discussion of the LM potential for new biomedical applications based on the recent progress on the LM field.

2.3. Liquid marbles

2.3.1. Properties

2.3.1.1. Shell structure

LM are non-stick droplets covered by micro and/or nanometrically scale particles with hydrophobic (and few hydrophilic) properties which enable to manipulate the marbles like a soft solid – Figure 2.1A. This soft solid is regarded as an alternative approach to superhydrophobicity, once also inhibits the wetting of liquid droplets on solid surfaces. The original superhydrophobicity concept postulated that the anti-wetting properties were achieved by physical and/or chemical modification of a solid surface.[26-28] In the case of LM the approach is opposite, the modification is performed on the liquid droplet interface with the external environment instead of the supporting surface. Due to the non-wetting/non-sticking property, LM present very low friction with a wide diversity of solid and liquid supports. This low-friction characteristic allows LM to move easily and reveals to be crucial on both manipulation and development of numerous LM applications.[14, 24, 29, 30]

Hydrophobic particles can be loosely fixed over flat surfaces to prepare moldable superhydrophobic surfaces.[31] For the case of LM, it was reported that the encapsulating layer of particles can present a structure from a loosely packed monolayer to a multilayer structure. Generally, LM coating has a non-uniform thickness, consisting in an arrangement of mono- and multilayers of particles – Figure 2.1D.[32, 33] Morphologically, LM wall presents significant roughness and porosity in appearance and is composed by particle aggregates separated by liquid region spacing (liquid clearings) – Figure 2.1D.[33-35] Due to these features the air is entrapped on LM shell creating “air pockets”, providing an analogous outcome to the “lotus effect” on rough surfaces.[3,

36] The air pockets give also to the LM the interesting ability to float in liquids – Figure 2.1B.[30, 34, 37] The absence of direct contact between the encapsulated fluid and both solid and liquid supports was experimentally confirmed.[34] However, it was clearly demonstrated that the powder shell coating LM is permeable for gases, allowing their use in gas sensing and biological applications (reviewed ahead).[12, 13, 38-41]

2.3.1.2. Liquid marble shape: static, rolling and floating conditions

The shape of LM is determined by the equilibrium between the effects of gravity and surface tension.[2, 3] As marbles are soft, they deform in a way to minimize their potential energy. Increasing their size, LM tend to lower their center of mass and consequently increase the contact area with the supporting surface.[42] Wherein, small LM present a quasi-spherical shape, due to the negligible effect of gravity. However, in large LM the gravity force predominates on the shape formation, originating marbles with flattened puddle shapes.[1, 33] The classification of small and large is performed by comparison to the capillary length, being classified small marbles the ones that present a height significantly less than the double of the capillary length.[4, 21]

Due to the very low friction between the LM and the supporting surface, LM can easily move down a tilted substrate.[1] On this movement LM do not slide but roll, and larger marbles roll more slowly comparing with smaller LM.[42, 43] Moreover, it was shown that rotating marbles can deform into doughnut and peanut shapes, due to the centrifugal force influence combined with LM coating flexibility – Figure 2.1E.[1, 2]

Recently, Ooi et al. proposed a model to characterize the deformation of LM floating in a liquid surface.[44] A floating oblate spheroid model was developed from the floating solid sphere model.[45] Additionally, they reported that the developed model is different than the model proposed by Whyman and Bormashenko, for a sessile droplet resting on a solid surface.[46] This was justified by the fact that for the floating LM case a deformation occurs in both the marble and

the liquid surface. These models may important for improve the models of LM evaporation, since the exposed surface area to air may change for the different cases.

2.3.1.3. Evaporation phenomenon

The evaporation of LM is one of the most important parameters for long term applications, because with the evaporation LM lose their shape and collapse.[23, 24, 47] Several works have been reported studying the evaporation in LM, analyzing the effect of different types and layer organization of coating particles.[5, 48-54] The encapsulated liquid is also important, and as expected for more volatile liquids the evaporation rate is higher.[54]

Dandan and Erbil reported that graphite-coated LM presented lower evaporation rates comparing with bare water droplets in the same conditions, presenting the LM a lifetime twice longer than the water droplets.[5] However using hydrophobic polytetrafluoroethylene microparticles (μPTFE) on the water-air interface of LM, the water marbles just presented 5 to 35% more of lifetime than of the pure water droplets.[49] Bhosale et al. compared μPTFE with fumed silica nanoparticles chemically modified with two different hydrophobic molecules: hexamethyldisilazane and dimethyldichlorosilane.[50] The obtained results showed that the water diffusion through LM shell was not related with the particle size. Instead, the authors suggested that the higher resistance to water loss of LM coated with hexamethyldisilazane-modified nanoparticles may be attributed to the lower aggregation of this particles. Recently, Laborie et al. also suggested that the rate of water evaporation is independent of the particle size.[52] However, unlike Bhosale et al., they associated the slower drying of LM with the presence of multilayer coatings and they suggested that the multilayers may be formed by aggregates of nanoparticles. This work indicated that LM covered with a monolayer of hydrophobic particles dried faster than bare liquid droplets. On the other hand, multilayer coated LM dried slower than water droplets. Being the evaporation rate of LM dependent

of the ratio between shell thickness and the LM diameter.[52] Ooi et al. also suggested that the coating density could be the main factor driving the liquid evaporation process in LM.[54]

Despite the several studies on this subject, it seems necessary more studies to fully understand the relationship between the evaporation behavior in LM and the coating structure.

2.3.1.4. Floating ability

In literature several works studying and exploring the ability of LM to float can be found – Figure 2.1B. [9, 11, 17, 34, 37, 44, 49, 55-63] Taking advantage from this LM property, applications were developed on sensors field for pH-sensing[9-11, 56-58] and to reveal water pollution,[17] and also on development of floating self-propelling devices.[59, 60] Generally, pH-sensing LM were coated with pH-responsive particles that change their wettability from hydrophobic to hydrophilic with pH variations. These LM usually exhibit long-term stability floating in solutions with a pH above or below a defined value. With the addition of an acid[56, 57] or a base[9, 11, 58, 63] to the supporting liquid, the LM immediately disintegrate due to the increase of the coating hydrophilicity. The pH changes can be visually detected by LM destruction and/or by colorant release. For the detection of water pollution the mechanism is similar, but instead of a change on LM shell the alteration occurs on the supporting liquid. As an example of this application, LM were able to successfully recognize the water contamination by organic compounds.[17] With these contaminants, the water surface tension decreased and the floating LM lost their integrity, revealing the water contamination without water sampling. On the same area of responsive floating LM to external stimuli, Nakai et al. reported a thermoresponsive LM that lost their integrity when the temperature increased and reached 46.5 °C.[64] This temperature corresponded to the melting point of the material used for the LM coating. The authors suggested that these marbles can be used for chemical reactions between the LM interior and the supporting liquid, being the reaction triggered by heating.

2.3.1.5. Robustness/Elasticity

Understanding the mechanical robustness of LM is very important for designing of applications that involve the transportation and manipulation of LM. This robustness comprise the capability of marbles to resist to deformation, pressure and impact.

In static conditions, the resistance to deformation and pressure could be assessed by quasi-static compression methods, showing the LM high elasticity – Figure 2.1C.[65, 66] For small mechanical compression, Asare-Asher et al. reported that LM could sustain a purely elastic deformation of up to 30% of their original size, using potassium chloride solution encapsulated by polyethylene microparticles (53-75 μm) – Figure 2.1C.[66] The elastic properties of LM are attributed to interfacial forces, namely to the capillary interactions between the colloidal particles coating the marbles.[67, 68] The same elastic behavior was found with LM under compression conditions and during the noncoalescent collisions of LM.[67, 68] Using high mechanical compression, Liu et al. studied the critical pressure before LM rupture, attributing this rupture to the poor coverage of particles on marble surface when highly stretched.[69] They found that the mechanical robustness of marbles was influenced by the hydrophobicity and size of the coating particles.

Regarding to particles hydrophobicity, Liu et al. found that particles with a water contact angle (WCA) of 118° created more robust LM comparing with particles presenting 145°.[69] They attributed this result to the fact that the WCA of particles was closer to 90°, because at this WCA particles are more strongly bound to the liquid surface.[4, 69] This explanation was corroborated from other works that demonstrated experimentally the higher mechanical robustness of a particle layer at the liquid-air interface with a WCA of 90°.[70] Zang et al. also confirmed this results, showing that a coating using particles with properties in limit of the hydrophobic to hydrophilic regime presented the highest mechanical robustness for LM.[71] For this study, silica-based nanoparticles (~20 nm) with different relative SiOH content and a WCA in the range of 80–135°

were used.[70-72] However, Zhou et al. found higher mechanical stability for the LM produced using particles with a WCA of 132°, from a studied WCA range of 84–132°.[73] For the coating, acetylated cellulose powders (average size of ~40 μm) with different degrees of acetylation were used. This unexpected result may be owing to the very irregular shape of the coating powders.[73] Once the theoretical explanation for the WCA of 90° such as the best for the highest LM robustness is based on particles with smooth and spherical shape,[4] this explanation may do not fit in the specific case of Zhou et al.. More meticulous studies aiming this subject are indispensable.

As previously mentioned, it was reported that the particle size also plays an important role regarding to marble robustness. Several reports stated that smaller particles make more stable LM.[33, 37] [50, 69] It has been found that nanoparticles behave like an "elastic membrane", creating very robust marbles in comparison with microparticle coatings.[50, 69] A possible explanation is that increasing the particles size also increase the liquid clearings on the layer of particles, weakening the LM shell.[33-35, 69] Besides the opposite effect obtained from the use of nanoparticles that enable a more uniform deposition, the nanoparticles can create a better network between particles based on the attraction imposed by lateral capillary forces.[50, 69, 74]

The mechanical robustness of LM surprisingly allow procedures such as inject and extract liquid from the LM core without destroy them.[47, 75, 76] Bajwa et al. reported a deeply study to characterize the behavior and the operational limits of LM upon liquid exchange *via* external inflow and outflow.[75] They reported that with the liquid injection a swirl motion on the marble surface occurred. Increasing injection flow rate the shear forces increased, consequently also the swirl motion and at high swirl rates LM robustness decreased. However, for moderate levels of swirl an enhanced on the robustness was observed. Larger marbles showed to take more liquid before disruption comparing with smaller marbles. It was also reported that the liquid can be removed and re-injected from the LM core and the marbles regained their spherical shape and non-wetting

behavior. With these extraction-injection cycles, the LM were weakening and disrupted after three cycles.[75] Finally, the authors showed be possible simultaneously inject and extract the liquid from the LM, thus being possible to use the marbles for perfusion experiments at low flow rates.

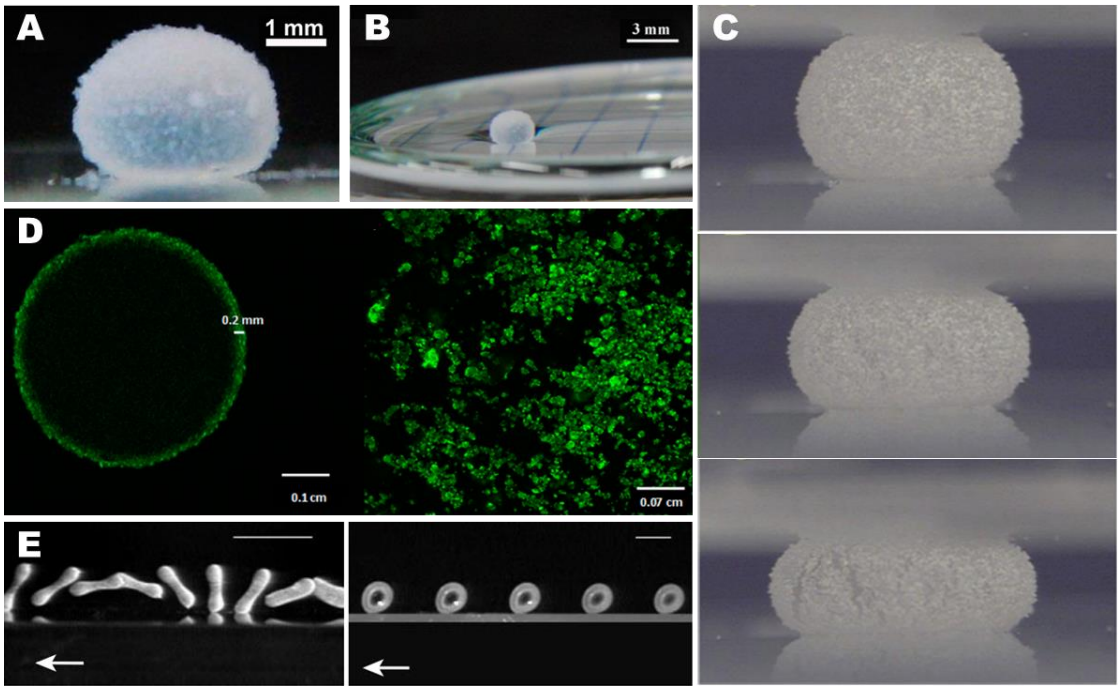

Figure 2.1: (A) A LM resting on a glass slide, and (B) a LM floating on the surface of glycerol. Adapted with permission from Ref. [60]. Copyright 2015 American Chemical Society. (C) LM under compression: small and medium deformation, and breakage point – immediately before LM rupture. Adapted from Ref. [66] with permission from Elsevier. (D) Image of a LM and view of a cross section of the LM coated with a fluorescein O-methacrylate based powder. Adapted with permission from Ref. [33]. Copyright 2015 American Chemical Society. (E) Peanut and doughnut shapes of a rotating marble. Adapted with permission from Macmillan Publishers Ltd: NATURE ref. [1], copyright 2001.

2.4. Liquid marbles manipulation

Due to the removal of the liquid-solid interaction into a solid-solid interface, LM are non-stick droplets presenting an extremely low friction with the supporting surface, and consequently small forces for LM manipulation are required. Several different manipulation strategies have been reported, namely using magnetic, electrostatic and gravitational forces. Recently, the use of ultraviolet and infrared irradiation and self-propelling marbles were also reported.

2.4.1. Magnetic

One of the most common means for manipulation of LM is the use of magnetic forces. Its popularity is owed to the simplicity of use and the remote control (no physical contact required) – Figure 2.2A.[7, 14, 24, 25, 29, 30, 77-84] There is two means for using magnetic response on LM: a magnetic coating[80, 83, 84] or a magnetic content.[77, 82]

For the coating, the used particles are hydrophobic nanoparticles of iron (Fe_3O_4)[29, 80] or synthesized nano/microparticles combining iron and other materials.[7, 83, 84] Fundamentally, the iron is used to confer superparamagnetic properties to the coating particles, making possible the LM manipulation by using an external magnetic field – Figure 2.2A. Since the hydrophobic coating powder can be manipulated, these magnetic marbles allowed the hydrophobic coating to open and to close reversibly and also the controllable merging of two marbles.[14, 29] Marbles with magnetic coating also roll and do not slide on a solid surface, after a moving permanent magnet.[14]

By taking advantage of the LM feature of being opened and closed reversibly, it was possible to have directly access and added a second liquid to the marble core, producing a bicomponent LM suitable for chemical reactions.[14] This LM feature also allowed to perform optical detection with a reflection mode that enabled to probe chemical reactions taking place within marbles.[79] By exploring the easy manipulation of magnetic LM, Zhao et al. proposed to integrate different processes in a single device – Figure 2.3D. Using the magnetism, the LM could be moved along of the proposed device, opening the marble electrochemical measurements were carried out by introducing an electrode probe inside of LM and combined with optical detection.[81] Recently, it was also proposed a device to magnetically actuate in floating LM, aiming the transport of aqueous solution with minimal volume loss for digital microfluidic applications.[82]

2.4.2. Electrostatic

It was showed that LM can also be deformed, moved and change their wettability when exposed to an electric field.[2, 85-91] Aussillous and Quéré showed for the first time that LM can be moved by the effect of an electrostatic field, where this field was reached by simply rubbing a stick of Teflon on a fabric.[2] By using electrostatic interactions, it was also showed that a liquid droplet can be spontaneously coated with hydrophobic particles, resulting in multi-layered LM.[87] By exposing LM to an electric field provided by the plates of a capacitor, LM could be activated being observed LM deformation[88] and performed controlled movement.[89, 90] Similar behavior was also reported for "Janus" marbles, droplets composed of two hemispheres characterized by presenting different physical and/or chemical properties. It was showed that "Janus" marbles could be rotated with an electric field due to the difference in electric properties of the particles used for the coating, in this case Teflon and carbon black that are dielectric and semiconductor particles respectively.[91]

2.4.3. Gravitational

The simplest ways to provide movement to LM is allowing it to roll down an inclined plane, during which gravitational potential energy is transformed into kinetic energy conducting to a descending movement.[24, 92] The speed acquired by the LM is influenced by the inclination angle, surface tension, viscosity and Bond number.[24, 42] Smaller marbles roll more faster comparing with larger LM.[42, 43] Two marbles can be merged in a controlled way under the action of gravity.[93] [94] Based on this method, Castro el al. presented a 3D printed platform for continuous production of "Janus" and composite LM.[94] The marbles were produced through the coalescence of two LM with different coatings and the process control was performed by adjusting the inclination angle of the designed platform. The authors suggested that the developed device has potential application

for surface engineering with innovative functionality for drug therapies, particles-based barcode biomarkers and smart membranes.[94]

2.4.4. Ultraviolet and infrared radiation

Similarly to the pH-responsive coatings of LM reviewed earlier, the wettability of some special LM coatings can be changed by optical irradiation, without any physical contact. Using photoresponsive material as the coating material, it was reported that the LM rupture can be remotely controllable by using ultraviolet (UV) radiation – Figure 2.2B.[30, 95, 96] Smart LM were created using a coating of particles that simultaneously were magnetic and pH-responsive, whose hydrophilicity increases when protonated.[30] A photoacid generator within the coating particles was used and when irradiated with UV light generated high concentration of H^+ that caused the coating particles to become hydrophilic, breaking the LM. Nakai et al. presented a similar photo-responsive LM, but using spiropyran powder to coat water droplets.[95] With UV exposure an isomerization process occurred on the coating material, originating a more hydrophilic coating. The authors reported to obtain LM that were stable for more than a week in dark and humid conditions, but when exposed to UV radiation the LM burst. Another UV-responsive LM was created by Tan et al., by using hydrophobized titanium dioxide as the coating particles – Figure 2.2B.[96] In this case with UV light, hydrophilic hydroxyl groups were formed on coating surface, due to the well-studied photoresponsive behavior of titanium dioxide.

Other way to perform a remote control of LM is by using a near-infrared (NIR) laser– Figure 2.2C.[97-99] For one of the reported examples, the marbles were coated with carbon nanotubes and fullerene, which present high absorbance in the NIR region. Upon NIR irradiation, the LM immediately disintegrated due to the transformation of NIR energy into heat.[97] However, Paven et al. developed a more advanced system that allowed to drive floating LM using simply a NIR laser or sunlight.[98] Comparing with other external stimuli namely pH and temperature, the light-driven

transportation of LM showed advantages such as the control of the timing, position, area, direction and velocity. Important parameters for the use of these NIR-responsive LM suggested by the authors in delivery and release of materials.[98] Chu et al. also reported to have high control manipulating LM with a NIR laser, but using chloroform marbles submerged in water – Figure 2.2C.[99] Due to the conversion of NIR energy into heat, vapor bubbles were formed inside of the LM. Controlling the laser irradiation on the marble surface, marbles were able to ascend, horizontally move and suspend in water. Authors suggested the applicability of this system for constructing smart micro-reactors, micro-engines or micro-robots in aqueous environment.[99]

2.4.5. Self-propulsion

Taking advantage of LM ability to float, manipulations have been proposed to create self-propelling marbles.[59, 60] LM containing aqueous ethanol solutions were placed on the water surface and they revealed autonomous motion. This motion is explained by the Marangoni solutocapillary effect that happen due to the ethanol evaporation and posterior condensation on the water surface. The ethanol diffusion onto the supporting water generates a gradient of surface tension, impelling motion to the floating object.[59, 60] It was found that the lifetime of self-propulsion increased with LM volume and ethanol concentration,[59] but the motion velocity revealed to be independent of the marble volume.[60]

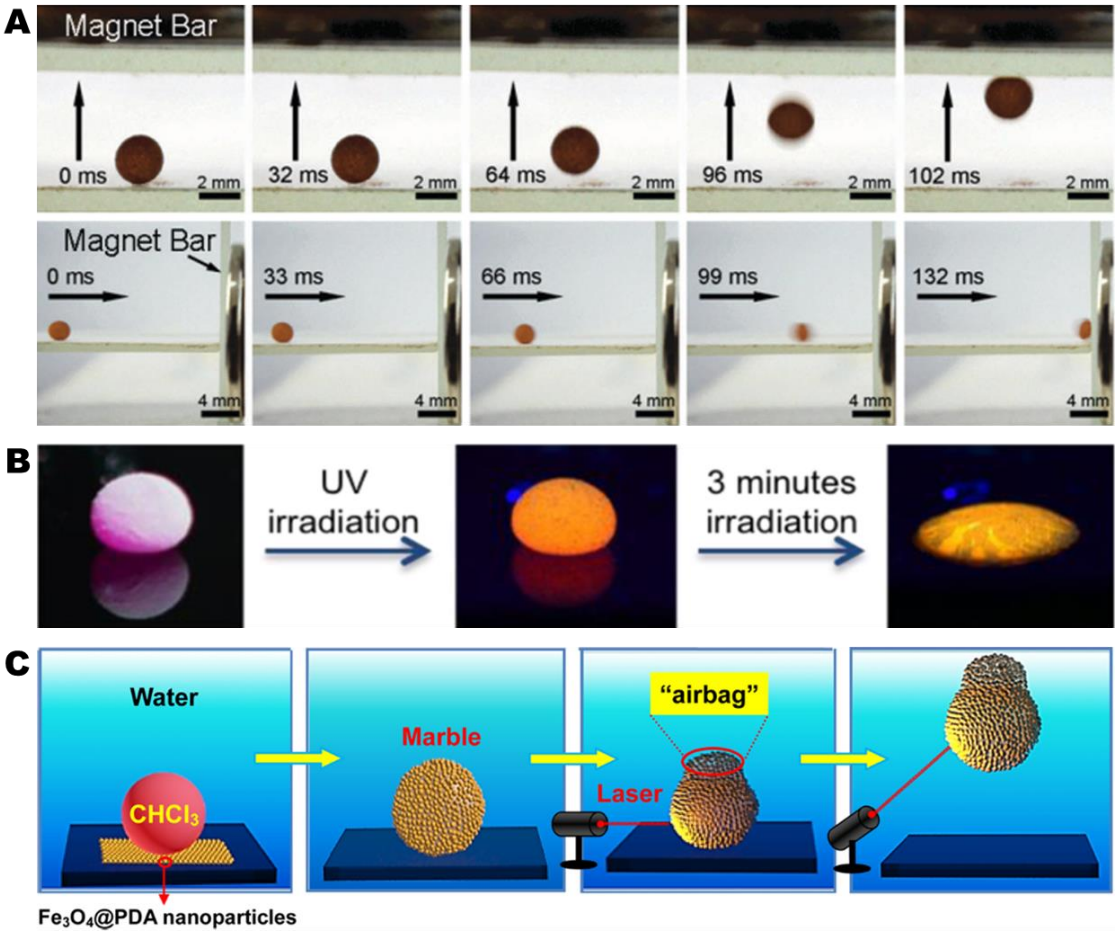

Figure 2.2: (A) Images of a LM moving vertically and horizontally driven by a magnet bar. Adapted from Ref. [84] with permission of the Royal Society of Chemistry. (B) LM exposed to UV radiation and after several minutes of exposition the LM collapsed. Adapted with permission from Ref. [96]. Copyright 2014 American Chemical Society. (C) Schematic illustration of remote manipulation of a chloroform ($CHCl_3$) marble in water using a near-infrared laser. Adapted with permission from Ref. [99]. Copyright 2016 American Chemical Society.

2.5. Biomedical applications

Due to their peculiar properties and versatility in the design, LM are very promising candidates to be valuable in the biomedical field. Very recently, this new direction on LM applications started to be explored, such as demonstrated by some reports that can be found in literature.[47, 61, 76, 81, 100-105] These few works reported very distinctive applications, namely diagnostic assays, cell culture, drug screening and cryopreservation of mammalian cells – Figure 2.3.

2.5.1. Diagnostic assays

Due to their small dimensions, the use of LM as miniature reactors has awakened high interest for the miniaturization of chemical processes. Such micro-reactors offer significant advantages namely in reducing the use of chemical reagents and solvents, providing a well-confined micro-environment and a versatile and cost-effective platform. Taking benefit from these LM characteristics, several potential applications have been successfully exploited for chemiluminescence reactions, acid–base reactions,[14] nanocomposite synthesis,[16] polymerizations,[106] silver mirror reactions,[15] and heterogeneous catalytic reactions.[18] An obvious use of LM in the biological area is also the miniaturization of processes for biological reactions and diagnostic assays.

The use of LM as micro-bioreactors for rapid blood typing was demonstrated – Figure 2.3C.[100] The "blood marbles" were produced by rolling blood droplets over hydrophobic powder of precipitated calcium carbonate. Sets of three marbles were prepared for each single test, one marble for each one of the three antibody solutions (Anti-A, Anti-B and Anti-D). After injecting on the respective LM the antibody solution, the ABO and Rh blood grouping was determined by monitoring the occurrence or not of a haemagglutination reaction. The occurrence of this reaction resulted in a two phase separation inside of the marbles, finding clearly a light-red and a dark-red color zone. The dark zone was consequence of a precipitation of the agglutinated red blood cells to the bottom of the LM, indicating the presence of the respective antigen. In contrast, the detection of no separation indicated the absence of the corresponding antigen. From the combined analysis of the results obtained for each one of the three antibodies, the blood grouping was determined – Figure 2.3C. Blood type assessment is a mandatory step before a blood transfusion to avoid the fatal consequences of incompatibility. Besides the low-cost and disposability of the technique, the authors also claimed that the test can be performed without any special medical facilities and with reduced biohazard due to the encapsulation of the blood samples.[100]

Zhao et al. also reported the applicability of LM as suitable platforms for biological assays.[81] They established a new method for the quantitative detection of dopamine in LM based on electrochemical measurements. The authors proposed that this technique can be useful on the diagnosis of neurological disorders in brain functions.[81] Besides this application, a glucose assay based on a colorimetric method was reported. Using magnetic particles for marbles production, authors took advantage of the magnetic opening feature of magnetic LM to perform both measurements. The dopamine detection was performed by immersing a miniaturized electrode in the liquid of the partially opened marble. For the glucose assay, the measure was achieved through the optical absorbance of the liquid in the fully opened LM by transmission mode. Beyond the measurement methods, an integrated approach was proposed for the LM production and analysis using potentially a single device, introduced briefly before – Figure 2.3D.[81] The magnetic actuation system was envisioned as the way to manipulate (move, open and close) the LM along all of the integrated processes. Complementarily to the electrochemical detection and the transmission-mode optical detection, it was proposed to integrate on the device a reflection-mode optical detection and an encapsulation process performed by infra-red heat-induced. Using wax-based particles in LM preparation, a uniform film surrounding the LM content could be formed by heating. For instance, this encapsulation step allows the samples preservation after analysis for follow-up assessment or biobanking and archiving.[81]

2.5.2. Cell culture

A well-known and explored property of LM are the gas permeable nature of their shell, demonstrate in several reports related with gas sensing and gas reactions.[12, 13, 38-40, 106] The gas permeability is a vital feature for LM application in cell culture, allowing oxygen and carbon dioxide exchange between cell culture medium and surrounding environment. Tian and co-workers demonstrated that LM provided a suitable environment for cell culture by culturing aerobic

microorganisms.[41] Besides this work, other 3D bioreactors based on LM have been reported, namely for formations of cancer cell spheroids (CCS),[47] embryoid bodies (EB),[101, 102] olfactory ensheathing cell spheroids[61] and for in vitro maturation of sheep oocytes.[103]

CCS cultured in vitro are postulated as capable to mimic the in vivo physiology of tumors more realistically than 2D cell cultures.[107-109] These cell spheroids were produced by simply inoculating hepatocellular carcinoma cells in LM.[47] The necessary cell aggregation for CCS formation occurred due to intrinsic characteristics of LM: the confined volume that promoted a higher intercellular interaction; and their non-adhesive shell that discouraged cell adhesion.

Following the same rationale, the use of these 3D bioreactors for EB formation was also reported, since pluripotent embryonic stem cells tend to form aggregates – Figure 2.3A.[101] LM are presented as a facile and highly efficient means for in vitro production of EB. Additionally to EB formation, it was reported that the LM offered a suitable micro-environment to induce spontaneously (without using growth factors) the EB differentiation into functional cardiomyocytes.[102] The authors emphasized that this technology would be highly beneficial to provide a continuous source of cardiomyocytes for regenerative medicine applications, drug discovery and safety testing.[102]

Floating LM may be employed to produce spheroids of olfactory ensheathing cells.[61] The choice for these LM was justified by the fact that floating LM allowed better handling and minimized the effect of evaporation, since the LM were placed over a liquid bath that increased the humidity. Furthermore using floating LM, the effect of gravity that forces cell aggregation at the LM bottom was minimized, due to the motion of the marble over the surface of the supporting liquid improving the mixing process inside the LM. This revealed to be crucial to obtain identical size spheroids. In complementary work, it was shown that LM can also be used for co-culture trials.[61] Olfactory ensheathing cells were co-cultured with Schwann cells or astrocytes cells. On the liquid

environment provided by LM, the olfactory ensheathing cells were able to replicate their normal behavior of surrounding other cells, because the cells could freely associate with the other cell types.[61]

Recently, LM were presented as suitable micro-bioreactors to induce the maturation of oocytes in vitro.[103] Furthermore, it was suggested that LM have high potential for other applications in reproductive biology, such as in oocyte fertilization and individual embryo culture. The reduced reagent consumption and low potential for contamination that LM provide have been pointed as valuable characteristics.[103]

The use of LM was present as a valuable alternative to the hanging drop method that is the most common method used for these reviewed applications.[47, 61, 101-103]

2.5.3. Drug screening

Taking advantage from the fact that LM allow the injection and extraction of controlled volumes of liquid without disrupting their structure, Oliveira et al. showed that LM could be used for high-throughput drug screening – Figure 2.3B.[76] Simultaneously, the liquefied environment in the LM was designed to accommodate the culture of anchorage-dependent cells that require a physical support to adhere and be able to proliferate. To accomplish this goal, microparticles were introduced in the liquid environment, providing the indispensable cell anchorage sites for cell adhesion.[76] After preparing the LM with a mixture of cells and micropaticles followed by an incubation period for cell adaptation, a drug/chemical agent was injected on the produced micro-bioreactors. Through the injection of a reagent that the color change against a specific cellular response, several conditions could be analyzed and compared. Due to the fact that the LM were translucent,[76] the monitoring the color change of the LM was possible. The color monitoring was performed by collecting images of the LM, and then the global information was obtained by image processing – Figure 2.3B. Such technology would have impact in high-throughput drug screening

under 3D cell culture environments, where results can be obtained through colorimetric-based and non-destructive measurements.[76]

2.5.4. Cryopreservation of mammalian cells

One very interesting and promising application for LM is their application in cryopreservation of mammalian cells – Figure 2.3E. Serrano et al. presented LM as a successful alternative tool to the conventional methods for the cryopreservation of a mammalian cell line, without using any cryopreservant agents.[104] Most of these agents cause cytotoxic effects requiring to be use at low concentrations, namely dimethyl sulfoxide and glycerol.[110, 111] Two procedures inspired on the conventional protocols were used: the rapid freezing by immersion in liquid nitrogen and slow cooling up to -80 °C using a standard freezing container. LM were prepared by rolling droplets of highly concentrated cell suspension (prepared on fetal bovine serum) over poly(tetrafluoroethylene) powder.[104] Then LM were maintained in frozen conditions for 15 days. After the thawing procedure, the integrity of the LM was confirmed to be intact and the following cellular parameters were evaluated: viability, morphology, proliferation, size, complexity, and cell cycle – Figure 2.3E. Droplet volume and cell concentration showed to be the critical factors for using the LM successfully on this application. The authors found a safe range of work: 5–30 μL for the droplet volume and (0.5–2) × 10^5 cells μL^{-1} for cell concentration. Accomplishing these limits, LM showed to reach the same level of performance of standard freezing procedures for all the evaluated cellular parameters.[104]

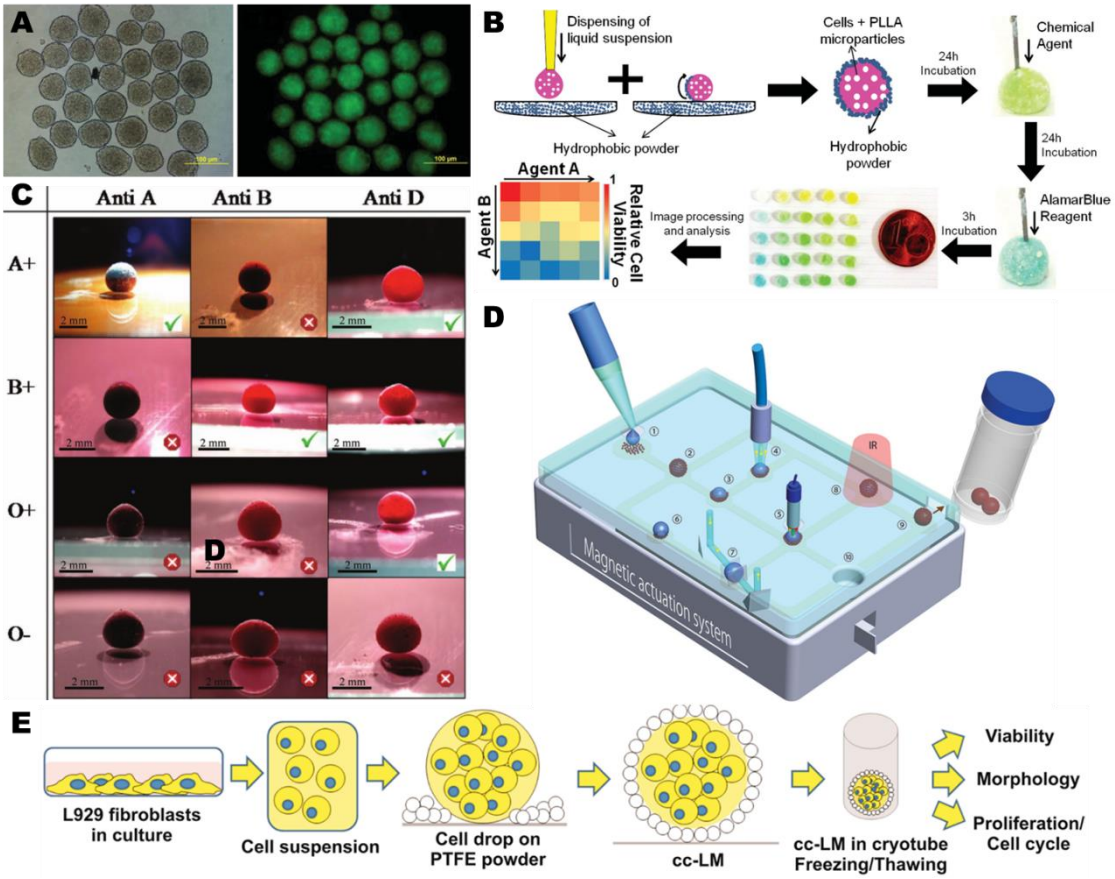

Figure 2.3: (A) Phase-contrast and fluorescence microscopy images presenting the morphology of embryoid bodies produced using LM. (B) Schematic illustration of the method for high-throughput drug screening. (C) Blood typing by injecting antibodies into blood marbles. (D) Illustration of a proposed device for "on-line" detection and for sample encapsulation based on magnetic LM. Adapted from Refs. [102], [76], [100] and [81], respectively, with permission of John Wiley & Sons. (E) Scheme of the developed procedure for cryopreservation of mammalian cells. Adapted with permission from Ref. [104]. Copyright 2015 American Chemical Society.

2.6. Critical analysis: the potential of liquid marbles for biomedical applications

The LM present a high versatility such as shown in the several applications already reported in literature, mainly on the chemistry field. Some of these applications can be just adapted or may inspire new applications for biomedical purposes. The majority of the reported data concerning evaporation, floatability and robustness of LM was obtained using water as the encapsulated liquid.

Similar data should be obtained for cell culture medium and human body fluids, because the surface tension for these fluids is different from water.[100, 112, 113] Being the surface tension of the encapsulated liquid one of the crucial parameters that influence LM behavior,[2, 3] specific studies are required to find the appropriated materials to encapsulate these fluids.

LM present high potential for application in the development of co-culture models to mimic *in vivo* environments, because they can ensure a compartmentalized 3D cell culture environment.[107-109] This application for the LM started to be explored by Vadivelu et al., where they studied the interaction of olfactory ensheathing cells with Schwann cells and with astrocytes. Reporting that olfactory ensheathing cells wrapped the other cells, behavior that was observed for the first time.[61] We believe that other co-culture models can be created using the same method by mixing different cell types in one LM. Alternatively, we also envisage that in the first stage different 3D cell structures (spheroids or cell/microparticle aggregates) can be produced in separated LM. Then, by the coalescence of two or more marbles into a larger one, the produced 3D structures can be co-culture in the same confined environment.[93, 94] Other opportunity is to perform indirect co-culture of cells, using a connecting tube between two LM with different cell types in culture and study the paracrine signaling on cellular response. A similar scheme was reported by Bormashenko et al., where they connected two different LM with a capillary tube to build a micro-pump powered by the differences on the surface tension between two different marbles.[19]

Other more complex and revolutionary co-culture scheme can be to produce capsules with cells inside generated from LM. Specifically the idea is that LM spontaneously become capsules through a chemical or physical process that promotes the merging between the coating particles creating a membrane.[15, 18, 114] Incubating different cell types on these capsules, a kind of “organoid” structures can be produced and the biochemical communication between them can be study, ensuring that the capsule membrane is permeable to both nutrients and cellular metabolites. Such

kind of compartmentalization of cellular microenvironments were performed before using the layer-by-layer technology.[115, 116] "Organoids" produced with LM could be then cultured together in the same culture well or integrated in a fluidic system, following the same rationale of the "organ-on-a-chip".[117, 118] Chin et al. already reported a process to produce stable liquid capsules from LM, promoting an interfacial polymerization by vaporization of ethyl-2cyanoacrylate.[114] Other works showed that the coating particles of LM can be part of chemical reactions happing inside of the marbles, performing a role as catalytic particles[18] or reactive substrates.[15] However, these solutions are not suitable to be used in cell culture, but we believe that similar processes can be found by combining different biocompatible materials.

Having in mind the suggestion of Zhao et al. for the integration of several processes in a single device and using the magnetism for LM manipulation,[81] a similar device can be developed for biomedical applications. We propose the development of an advanced high-throughput system for cytotoxic analysis of drugs and materials. The system may incorporate the several steps for this kind of assessment: production of magnetic LM with cells; incubation of cells for the formation of cell spheroids or 3D cell/microparticle aggregates;[47, 61, 76, 101, 102] optical morphology assessment of the 3D cell structures; drug/material supply by injection or direct access to the LM core;[14, 47, 75, 76] cellular response assessment by colorimetric methods or electrochemical measurements; [76, 81] by on-line analysis of results, a sorting of LM can be performed; then using the selected LM, the cells can be maintained in culture on the same platform or moved for other environment by LM burst; cells from the selected conditions can also be used in more powerful methods of cell evaluation such as flow cytometry.[104] We believe that almost all of these processes can be fully automatized on the proposed device. Besides the application in high-throughput analysis, such proposed platform could also find application in diagnostic assays.

Inspired by the LM, Oliveira et al. created a novel concept termed “hydrophobic hydrogels”, consisting into coat hydrogels with hydrophobic particles.[105] They found that similarly to LM the created hydrogels could float. Based on this ability, floating (bio)microdevices were developed for different applications, namely optical pH sensing, microengineering of self-assembling floating hydrogels and construction of engineered biological tissues.[105] A step forward on this technology can be the use of these floating hydrogels to create *in vitro* skin tissue, once this tissue prefer the air-liquid interface. Possibly, a stratified structure similar to skin tissue can be obtained by encapsulating cells on the hydrogel and other cell type cultured on the hydrogel top at the air-liquid interface. To culture cells on the hydrogel top, the surface should be free of hydrophobic particles and can be achieved by controlling the covered hydrogel surfaces in the coating process.

Based on the published knowledge about LM, we believe that several applications on the biomedical field can be reported soon. Some applications seem more straightforward to reach, for example the development of the LM as a cryopreservation tool directed to especial sensitive cells such as pluripotent stem cells.[104, 119] Other applications should be more difficult to reach, such as some of the suggested applications presented here in this section.

2.7. Summary

This review deals with the recent advanced on LM field and the emerging applications on the biomedical area, showing the natural evolution of some applications from other scientific fields to the biomedical engineering.

The most recent advances on the LM properties and manipulation were reviewed. The interfacial characteristics of LM were largely explained, namely the shell structure that present primordial influence on the LM properties. This relationship between the coating and the LM capabilities was described, specifically for the capability of LM to deform and float. The evaporation phenomenon

and robustness were elucidated, because are features with high importance for long term applications such as occasionally required on the biological and biomedical fields. The manipulation of LM is also a critical issue on this field to avoid contaminations. However, several methods have being reported for LM handling without direct actuation over the marbles. The remote manipulation can be performed by magnetic, electrostatic or gravitational forces and even by using UV or NIR light.

The biomedical applications found for the LM were reviewed, in a perspective how the LM properties and manipulation methods were explored for this aim. Applications on diagnosis, drug screening, cell culture and cryopreservation were described. Finalizing, a critical view of the LM potential for biomedical applications was presented, suggesting some possible advances on this emerging area.

2.8. Acknowledgements

The authors acknowledge funding from the European Research Council grant agreement ERC-2012-ADG 20120216-321266 for project ComplexiTE. N. M. Oliveira acknowledges the financial support from Portuguese Foundation for Science and Technology – FCT (Grant SFRH/BD/73172/2010), from the financial program POPH/FSE from QREN.

2.9. References

1. Aussillous, P.; Quere, D., Liquid marbles. *Nature* **2001,** *411*, 924-927.

2. Aussillous, P.; Quere, D., Properties of liquid marbles. *Proceedings of the Royal Society a-Mathematical Physical and Engineering Sciences* **2006,** *462*, 973-999.

3. Bormashenko, E., Liquid marbles: Properties and applications. *Current Opinion in Colloid & Interface Science* **2011,** *16*, 266-271.

4. McHale, G.; Newton, M. I., Liquid marbles: Topical context within soft matter and recent progress. *Soft Matter* **2015,** *11*, 2530-2546.

5. Dandan, M.; Erbil, H. Y., Evaporation rate of graphite liquid marbles: Comparison with water droplets. *Langmuir* **2009,** *25*, 8362-8367.

6. Bormashenko, E.; Pogreb, R.; Musin, A.; Balter, R.; Whyman, G.; Aurbach, D., Interfacial and conductive properties of liquid marbles coated with carbon black. *Powder Technology* **2010,** *203*, 529-533.

7. Wang, B.; Liu, Y.; Zhang, Y. B.; Guo, Z. G.; Zhang, H.; Xin, J. H.; Zhang, L., Bioinspired superhydrophobic fe3o4@polydopamine@ag hybrid nanoparticles for liquid marble and oil spill. *Advanced Materials Interfaces* **2015,** *2*.

8. Huang, S. Y.; Zhang, Y.; Shi, J. F.; Huang, W. P., Superhydrophobic particles derived from nature-inspired polyphenol chemistry for liquid marble formation and oil spills treatment. *Acs Sustainable Chemistry & Engineering* **2016,** *4*, 676-681.

9. Sun, J. H.; Wei, W.; Zhao, D. H.; Hu, Q.; Liu, X. Y., Liquid marbles prepared from ph-responsive self-assembled micelles. *Soft Matter* **2015,** *11*, 1954-1961.

10. Ueno, K.; Bournival, G.; Wanless, E. J.; Nakayama, S.; Giakoumatos, E. C.; Nakamura, Y.; Fujii, S., Liquid marble and water droplet interactions and stability. *Soft Matter* **2015,** *11*, 7728-7738.

11. Ohno, S.; Tsuda, Y.; Nakai, K.; Fujii, S.; Nakamura, Y.; Yusai, S., Ph-responsive liquid marbles prepared using fluorinated fatty acid. *Chemistry Letters* **2016,** *45*, 547-549.

12. Tian, J. F.; Arbatan, T.; Li, X.; Shen, W., Liquid marble for gas sensing. *Chemical Communications* **2010,** *46*, 4734-4736.

13. Fujii, S.; Aono, K.; Suzaki, M.; Hamasaki, S.; Yusa, S.; Nakamura, Y., Ph-responsive hairy particles synthesized by dispersion polymerization with a macroinitiator as an inistab and their use as a gas-sensitive liquid marble stabilizer. *Macromolecules* **2012,** *45*, 2863-2873.

14. Xue, Y. H.; Wang, H. X.; Zhao, Y.; Dai, L. M.; Feng, L. F.; Wang, X. G.; Lin, T., Magnetic liquid marbles: A "precise" miniature reactor. *Advanced Materials* **2010,** *22*, 4814-+.

15. Sheng, Y. F.; Sun, G. Q.; Wu, J.; Ma, G. H.; Ngai, T., Silica-based liquid marbles as microreactors for the silver mirror reaction. *Angewandte Chemie-International Edition* **2015,** *54*, 7012-7017.

16. Chu, Y.; Wang, Z. K.; Pan, Q. M., Constructing robust liquid marbles for miniaturized synthesis of graphene/ag nanocomposite. *Acs Applied Materials & Interfaces* **2014,** *6*, 8378-8386.

17. Bormashenko, E.; Musin, A., Revealing of water surface pollution with liquid marbles. *Applied Surface Science* **2009,** *255*, 6429-6431.

18. Wei, W.; Lu, R. J.; Ye, W. T.; Sun, J. H.; Zhu, Y.; Luo, J.; Liu, X. Y., Liquid marbles stabilized by fluorine-bearing cyclomatrix polyphosphazene particles and their application as high-efficiency miniature reactors. *Langmuir* **2016,** *32*, 1707-1715.

19. Bormashenko, E.; Balter, R.; Aurbach, D., Micropump based on liquid marbles. *Applied Physics Letters* **2010,** *97*.

20. Yue, S.; Shen, W.; Hapgood, K., Characterisation of liquid marbles in commercial cosmetic products. *Advanced Powder Technology* **2016,** *27*, 33-41.

21. McHale, G.; Newton, M. I., Liquid marbles: Principles and applications. *Soft Matter* **2011,** *7*, 5473-5481.

22. Bormashenko, E., New insights into liquid marbles. *Soft Matter* **2012,** *8*, 11018-11021.

23. Erbil, H. Y., Evaporation of pure liquid sessile and spherical suspended drops: A review. *Advances in Colloid and Interface Science* **2012,** *170*, 67-86.

24. Ooi, C. H.; Nguyen, N. T., Manipulation of liquid marbles. *Microfluidics and Nanofluidics* **2015,** *19*, 483-495.

25. Nagappan, S.; Ha, C. S., Emerging trends in superhydrophobic surface based magnetic materials: Fabrications and their potential applications. *Journal of Materials Chemistry A* **2015,** *3*, 3224-3251.

26. Sun, T. L.; Feng, L.; Gao, X. F.; Jiang, L., Bioinspired surfaces with special wettability. *Accounts of Chemical Research* **2005,** *38*, 644-652.

27. Erbil, H. Y.; Demirel, A. L.; Avci, Y.; Mert, O., Transformation of a simple plastic into a superhydrophobic surface. *Science* **2003,** *299*, 1377-1380.

28. Roach, P.; Shirtcliffe, N. J.; Newton, M. I., Progess in superhydrophobic surface development. *Soft Matter* **2008,** *4*, 224-240.

29. Zhao, Y.; Fang, J.; Wang, H. X.; Wang, X. G.; Lin, T., Magnetic liquid marbles: Manipulation of liquid droplets using highly hydrophobic fe3o4 nanoparticles. *Advanced Materials* **2010,** *22*, 707-+.

30. Zhang, L. B.; Cha, D. K.; Wang, P., Remotely controllable liquid marbles. *Advanced Materials* **2012,** *24*, 4756-4760.

31. Costa, A. M. S.; Dencheva, N. V.; Caridade, S. G.; Denchev, Z. Z.; Mano, J. F., Moldable superhydrophobic surfaces. *Advanced Materials Interfaces* **2016,** *3*, 1600074-n/a.

32. Nguyen, T. H.; Hapgood, K.; Shen, W., Observation of the liquid marble morphology using confocal microscopy. *Chemical Engineering Journal* **2010,** *162*, 396-405.

33. Fernandes, A. M.; Mantione, D.; Gracia, R.; Leiza, J. R.; Paulis, M.; Mecerreyes, D., From polymer latexes to multifunctional liquid marbles. *Acs Applied Materials & Interfaces* **2015,** *7*, 4433-4441.

34. Bormashenko, E.; Bormashenko, Y.; Musin, A.; Barkay, Z., On the mechanism of floating and sliding of liquid marbles. *Chemphyschem* **2009,** *10*, 654-656.

35. Matsukuma, D.; Watanabe, H.; Fujimoto, A.; Uesugi, K.; Takeuchi, A.; Suzuki, Y.; Jinnai, H.; Takahara, A., X-ray computerized tomography observation of the interfacial structure of liquid marbles. *Bulletin of the Chemical Society of Japan* **2015,** *88*, 84-88.

36. Barthlott, W.; Neinhuis, C., Purity of the sacred lotus, or escape from contamination in biological surfaces. *Planta* **1997,** *202*, 1-8.

37. Cengiz, U.; Erbil, H. Y., The lifetime of floating liquid marbles: The influence of particle size and effective surface tension. *Soft Matter* **2013,** *9*, 8980-8991.

38. Tian, J. F.; Arbatan, T.; Li, X.; Shen, W., Porous liquid marble shell offers possibilities for gas detection and gas reactions. *Chemical Engineering Journal* **2010,** *165*, 347-353.

39. Hu, M. M.; Tian, M. J.; He, J.; He, Y. J., Sensing ammonia using dry waters containing cupric chloride solution. *Colloids and Surfaces a-Physicochemical and Engineering Aspects* **2012,** *414*, 216-219.

40. Matsubara, K.; Danno, M.; Inoue, M.; Nishizawa, H.; Honda, Y.; Abe, T., Surface fluorination of polystyrene particles via cf4 plasma irradiation using a barrel-plasma-treatment system. *Surface & Coatings Technology* **2013,** *236*, 269-273.

41. Tian, J. F.; Fu, N.; Chen, X. D.; Shen, W., Respirable liquid marble for the cultivation of microorganisms. *Colloids and Surfaces B-Biointerfaces* **2013,** *106*, 187-190.

42. Mahadevan, L.; Pomeau, Y., Rolling droplets. *Physics of Fluids* **1999,** *11*, 2449-2453.

43. Richard, D.; Quere, D., Viscous drops rolling on a tilted non-wettable solid. *Europhysics Letters* **1999,** *48*, 286-291.

44. Ooi, C. H.; Vadivelu, R. K.; St John, J.; Dao, D. V.; Nguyen, N. T., Deformation of a floating liquid marble. *Soft Matter* **2015,** *11*, 4576-4583.

45. Vella, D.; Lee, D. G.; Kim, H. Y., The load supported by small floating objects. *Langmuir* **2006,** *22*, 5979-5981.

46. Whyman, G.; Bormashenko, E., Oblate spheroid model for calculation of the shape and contact angles of heavy droplets. *Journal of Colloid and Interface Science* **2009,** *331*, 174-177.

47. Arbatan, T.; Al-Abboodi, A.; Sarvi, F.; Chan, P. P. Y.; Shen, W., Tumor inside a pearl drop. *Advanced Healthcare Materials* **2012,** *1*, 467-469.

48. McHale, G.; Shirtcliffe, N. J.; Newton, M. I.; Pyatt, F. B.; Doerr, S. H., Self-organization of hydrophobic soil and granular surfaces. *Applied Physics Letters* **2007,** *90*.

49. Tosun, A.; Erbil, H. Y., Evaporation rate of ptfe liquid marbles. *Applied Surface Science* **2009,** *256*, 1278-1283.

50. Bhosale, P. S.; Panchagnula, M. V.; Stretz, H. A., Mechanically robust nanoparticle stabilized transparent liquid marbles. *Applied Physics Letters* **2008,** *93*.

51. Bhosale, P. S.; Panchagnula, M. V., On synthesizing solid polyelectrolyte microspheres from evaporating liquid marbles. *Langmuir* **2010,** *26*, 10745-10749.

52. Laborie, B.; Lachaussee, F.; Lorenceau, E.; Rouyer, F., How coatings with hydrophobic particles may change the drying of water droplets: Incompressible surface versus porous media effects. *Soft Matter* **2013,** *9*, 4822-4830.

53. Ogawa, S.; Watanabe, H.; Wang, L. M.; Jinnai, H.; McCarthy, T. J.; Takahara, A., Liquid marbles supported by monodisperse poly(methylsilsesquioxane) particles. *Langmuir* **2014,** *30*, 9071-9075.

54. Ooi, C. H.; Bormashenko, E.; Nguyen, A. V.; Evans, G. M.; Dao, D. V.; Nguyen, N. T., Evaporation of ethanol-water binary mixture sessile liquid marbles. *Langmuir* **2016,** *32*, 6097-6104.

55. Gao, L. C.; McCarthy, T. J., Ionic liquid marbles. *Langmuir* **2007,** *23*, 10445-10447.

56. Dupin, D.; Armes, S. P.; Fujii, S., Stimulus-responsive liquid marbles. *Journal of the American Chemical Society* **2009,** *131*, 5386-+.

57. Fujii, S.; Kameyama, S.; Armes, S. P.; Dupin, D.; Suzaki, M.; Nakamura, Y., Ph-responsive liquid marbles stabilized with poly(2-vinylpyridine) particles. *Soft Matter* **2010,** *6*, 635-640.

58. Dupin, D.; Thompson, K. L.; Armes, S. P., Preparation of stimulus-responsive liquid marbles using a polyacid-stabilised polystyrene latex. *Soft Matter* **2011,** *7*, 6797-6800.

59. Ooi, C. H.; Nguyen, A. V.; Evans, G. M.; Gendelman, O.; Bormashenko, E.; Nguyen, N. T., A floating self-propelling liquid marble containing aqueous ethanol solutions. *Rsc Advances* **2015,** *5*, 101006-101012.

60. Bormashenko, E.; Bormashenko, Y.; Grynyov, R.; Aharoni, H.; Whyman, G.; Binks, B. P., Self-propulsion of liquid marbles: Leidenfrost-like levitation driven by marangoni flow. *Journal of Physical Chemistry C* **2015,** *119*, 9910-9915.

61. Vadivelu, R. K.; Ooi, C. H.; Yao, R. Q.; Velasquez, J. T.; Pastrana, E.; Diaz-Nido, J.; Lim, F.; Ekberg, J. A. K.; Nguyen, N. T.; St John, J. A., Generation of three-dimensional multiple spheroid model of olfactory ensheathing cells using floating liquid marbles. *Scientific Reports* **2015,** *5*.

62. Ooi, C. H.; Plackowski, C.; Nguyen, A. V.; Vadivelu, R. K.; John, J. A.; Dao, D. V.; Nguyen, N. T., Floating mechanism of a small liquid marble. *Scientific Reports* **2016,** *6*.

63. Si, Y. F.; Guo, Z. G., Novel ph-responsive liquid marble as microfluidic responder for controlled release. *Chemistry Letters* **2016,** *45*, 779-781.

64. Nakai, K.; Fujii, S.; Nakamura, Y.; Yusa, S., Thermoresponsive liquid marbles prepared with low melting point powder. *Chemistry Letters* **2015,** *44*, 1077-1079.

65. Whyman, G.; Bormashenko, E., Interpretation of elasticity of liquid marbles. *Journal of Colloid and Interface Science* **2015,** *457*, 148-151.

66. Asare-Asher, S.; Connor, J. N.; Sedev, R., Elasticity of liquid marbles. *Journal of Colloid and Interface Science* **2015,** *449*, 341-346.

67. Bormashenko, E.; Whyman, G.; Gendelman, O., Elastic properties of liquid surfaces coated with colloidal particles. *Advances in Condensed Matter Physics* **2015**.

68. Bormashenko, E.; Pogreb, R.; Balter, R.; Aharoni, H.; Bormashenko, Y.; Grynyov, R.; Mashkevych, L.; Aurbach, D.; Gendelman, O., Elastic properties of liquid marbles. *Colloid and Polymer Science* **2015,** *293*, 2157-2164.

69. Liu, Z.; Fu, X. Y.; Binks, B. P.; Shum, H. C., Mechanical compression to characterize the robustness of liquid marbles. *Langmuir* **2015,** *31*, 11236-11242.

70. Zang, D. Y.; Rio, E.; Delon, G.; Langevin, D.; Wei, B.; Binks, B. P., Influence of the contact angle of silica nanoparticles at the air-water interface on the mechanical properties of the layers composed of these particles. *Molecular Physics* **2011,** *109*, 1057-1066.

71. Zang, D. Y.; Chen, Z.; Zhang, Y. J.; Lin, K. J.; Geng, X. G.; Binks, B. P., Effect of particle hydrophobicity on the properties of liquid water marbles. *Soft Matter* **2013,** *9*, 5067-5073.

72. Kostakis, T.; Ettelaie, R.; Murray, B. S., Effect of high salt concentrations on the stabilization of bubbles by silica particles. *Langmuir* **2006,** *22*, 1273-1280.

73. Zhou, X. M.; Lin, X. X.; White, K. L.; Lin, S.; Wu, H.; Cao, S. L.; Huang, L. L.; Chen, L. H., Effect of the degree of substitution on the hydrophobicity of acetylated cellulose for production of liquid marbles. *Cellulose* **2016,** *23*, 811-821.

74. Forny, L.; Pezron, I.; Saleh, K.; Guigon, P.; Komunjer, L., Storing water in powder form by self-assembling hydrophobic silica nanoparticles. *Powder Technology* **2007,** *171*, 15-24.

75. Bajwa, A.; Xu, Y. H.; Hashmi, A.; Leong, M.; Ho, L.; Xu, J., Liquid marbles with in-flows and out-flows: Characteristics and performance limits. *Soft Matter* **2012,** *8*, 11604-11608.

76. Oliveira, N. M.; Correia, C. R.; Reis, R. L.; Mano, J. F., Liquid marbles for high-throughput biological screening of anchorage-dependent cells. *Advanced Healthcare Materials* **2015,** *4*, 264-270.

77. Bormashenko, E.; Pogreb, R.; Bormashenko, Y.; Musin, A.; Stein, T., New investigations on ferrofluidics: Ferrofluidic marbles and magnetic-field-driven drops on superhydrophobic surfaces. *Langmuir* **2008,** *24*, 12119-12122.

78. Nguyen, N. T., Micro-magnetofluidics: Interactions between magnetism and fluid flow on the microscale. *Microfluidics and Nanofluidics* **2012,** *12*, 1-16.

79. Zhao, Y.; Xu, Z. G.; Parhizkar, M.; Fang, J.; Wang, X. G.; Lin, T., Magnetic liquid marbles, their manipulation and application in optical probing. *Microfluidics and Nanofluidics* **2012,** *13*, 555-564.

80. Li, F. G.; Wu, W.; Ning, A. F.; Wang, J., Surface functionalization and magnetic motion of hydrophobic magnetic nanoparticles with different sizes. *International Journal of Chemical Reactor Engineering* **2015,** *13*.

81. Zhao, Y.; Xu, Z. G.; Niu, H. T.; Wang, X. G.; Lin, T., Magnetic liquid marbles: Toward "lab in a droplet". *Advanced Functional Materials* **2015,** *25*, 437-444.

82. Khaw, M. K.; Ooi, C. H.; Mohd-Yasin, F.; Vadivelu, R.; St John, J.; Nguyen, N. T., Digital microfluidics with a magnetically actuated floating liquid marble. *Lab on a Chip* **2016,** *16*, 2211-2218.

83. Li, L. X.; Li, B. C.; Fan, L.; Mu, B.; Wang, A. Q.; Zhang, J. P., Palygorskite@fe3o4@polyperfluoroalkylsilane nanocomposites for superoleophobic coatings and magnetic liquid marbles. *Journal of Materials Chemistry A* **2016,** *4*, 5859-5868.

84. Lin, X. X.; Ma, W.; Wu, H.; Cao, S. L.; Huang, L. L.; Chen, L. H.; Takahara, A., Superhydrophobic magnetic poly(dopam-co-pfoea)/fe3o4/cellulose microspheres for stable liquid marbles. *Chemical Communications* **2016,** *52*, 1895-1898.

85. Newton, M. I.; Herbertson, D. L.; Elliott, S. J.; Shirtcliffe, N. J.; McHale, G., Electrowetting of liquid marbles. *Journal of Physics D-Applied Physics* **2007,** *40*, 20-24.

86. McHale, G.; Herbertson, D. L.; Elliott, S. J.; Shirtcliffe, N. J.; Newton, M. I., Electrowetting of nonwetting liquids and liquid marbles. *Langmuir* **2007,** *23*, 918-924.

87. Liyanaarachchi, K. R.; Ireland, P. M.; Webber, G. B.; Galvin, K. P., Electrostatic formation of liquid marbles and agglomerates. *Applied Physics Letters* **2013,** *103*.

88. Bormashenko, E.; Pogreb, R.; Stein, T.; Whyman, G.; Schiffer, M.; Aurbach, D., Electrically deformable liquid marbles. *Journal of Adhesion Science and Technology* **2011,** *25*, 1371-1377.

89. Bormashenko, E.; Pogreb, R.; Balter, R.; Gendelman, O.; Aurbach, D., Composite non-stick droplets and their actuation with electric field. *Applied Physics Letters* **2012,** *100*.

90. Bormashenko, E.; Pogreb, R.; Balter, R.; Aharoni, H.; Aurbach, D.; Strelnikov, V., Liquid marbles containing petroleum and their properties. *Petroleum Science* **2015,** *12*, 340-344.

91. Bormashenko, E.; Bormashenko, Y.; Pogreb, R.; Gendelman, O., Janus droplets: Liquid marbles coated with dielectric/semiconductor particles. *Langmuir* **2011,** *27*, 7-10.

92. Aussillous, P.; Quere, D., Shapes of rolling liquid drops. *Journal of Fluid Mechanics* **2004,** *512*, 133-151.

93. Planchette, C.; Biance, A. L.; Pitois, O.; Lorenceau, E., Coalescence of armored interface under impact. *Physics of Fluids* **2013,** *25*.

94. Castro, J. O.; Neves, B. M.; Rezk, A. R.; Eshtiaghi, N.; Yeo, L. Y., Continuous production of janus and composite liquid marbles with tunable coverage. *Acs Applied Materials & Interfaces* **2016,** *8*, 17751-17756.

95. Nakai, K.; Fujii, S.; Nakamura, Y.; Yusa, S., Ultraviolet-light-responsive liquid marbles. *Chemistry Letters* **2013,** *42*, 586-588.

96. Tan, T. T. Y.; Ahsan, A.; Reithofer, M. R.; Tay, S. W.; Tan, S. Y.; Hor, T. S. A.; Chin, J. M.; Chew, B. K. J.; Wang, X. B., Photoresponsive liquid marbles and dry water. *Langmuir* **2014,** *30*, 3448-3454.

97. Nakai, K.; Nakagawa, H.; Kuroda, K.; Fujii, S.; Nakamura, Y.; Yusa, S., Near-infrared-responsive liquid marbles stabilized with carbon nanotubes. *Chemistry Letters* **2013,** *42*, 719-721.

98. Paven, M.; Mayama, H.; Sekido, T.; Butt, H. J.; Nakamura, Y.; Fujii, S., Light-driven delivery and release of materials using liquid marbles. *Advanced Functional Materials* **2016,** *26*, 3199-3206.

99. Chu, Y.; Liu, F. T.; Qin, L. M.; Pan, Q. M., Remote manipulation of a microdroplet in water by near-infrared laser. *Acs Applied Materials & Interfaces* **2016,** *8*, 1273-1279.

100. Arbatan, T.; Li, L. Z.; Tian, J. F.; Shen, W., Liquid marbles as micro-bioreactors for rapid blood typing. *Advanced Healthcare Materials* **2012,** *1*, 80-83.

101. Sarvi, F.; Arbatan, T.; Chan, P. P. Y.; Shen, W., A novel technique for the formation of embryoid bodies inside liquid marbles. *Rsc Advances* **2013,** *3*, 14501-14508.

102. Sarvi, F.; Jain, K.; Arbatan, T.; Verma, P. J.; Hourigan, K.; Thompson, M. C.; Shen, W.; Chan, P. P. Y., Cardiogenesis of embryonic stem cells with liquid marble micro-bioreactor. *Advanced Healthcare Materials* **2015,** *4*.

103. Ledda, S.; Idda, A.; Kelly, J.; Ariu, F.; Bogliolo, L.; Bebbere, D., A novel technique for in vitro maturation of sheep oocytes in a liquid marble microbioreactor. *Journal of Assisted Reproduction and Genetics* **2016,** *33*, 513-518.

104. Serrano, M. C.; Nardecchia, S.; Gutierrez, M. C.; Ferrer, M. L.; del Monte, F., Mammalian cell cryopreservation by using liquid marbles. *Acs Applied Materials & Interfaces* **2015,** *7*, 3854-3860.

105. Oliveira, N. M.; Zhang, Y. S.; Ju, J.; Chen, A. Z.; Chen, Y.; Sonkusale, S. R.; Dokmeci, M. R.; Reis, R. L.; Mano, J. F.; Khademhosseini, A., Hydrophobic hydrogels: Toward construction of floating (bio)microdevices. *Chemistry of Materials* **2016,** *28*, 3641-3648.

106. Sato, E.; Yuri, M.; Fujii, S.; Nishiyama, T.; Nakamura, Y.; Horibe, H., Liquid marbles as a micro-reactor for efficient radical alternating copolymerization of diene monomer and oxygen. *Chemical Communications* **2015,** *51*, 17241-17244.

107. MuellerKlieser, W., Three-dimensional cell cultures: From molecular mechanisms to clinical applications. *American Journal of Physiology-Cell Physiology* **1997,** *273*, C1109-C1123.

108. Yamada, K. M.; Cukierman, E., Modeling tissue morphogenesis and cancer in 3d. *Cell* **2007,** *130*, 601-610.

109. Pampaloni, F.; Reynaud, E. G.; Stelzer, E. H. K., The third dimension bridges the gap between cell culture and live tissue. *Nature Reviews Molecular Cell Biology* **2007,** *8*, 839-845.

110. Klebe, R. J.; Mancuso, M. G., Identification of new cryoprotective agents for cultured mammalian-cells. *In Vitro-Journal of the Tissue Culture Association* **1983,** *19*, 167-170.

111. Kim, M. S.; Lee, S. T.; Lim, J. M.; Gong, S. P., Medium composition for effective slow freezing of embryonic cell lines derived from marine medaka (oryzias dancena). *Cytotechnology* **2016,** *68*, 9-17.

112. Vargaftik, N. B.; Volkov, B. N.; Voljak, L. D., International tables of the surface-tension of water. *Journal of Physical and Chemical Reference Data* **1983,** *12*, 817-820.

113. Rosina, J.; Kvasnak, E.; Suta, D.; Kolarova, H.; Malek, J.; Krajci, L., Temperature dependence of blood surface tension. *Physiological Research* **2007,** *56*, S93-S98.

114. Chin, J. M.; Reithofer, M. R.; Tan, T. T. Y.; Menon, A. G.; Chen, E. Y.; Chow, C. A.; Hor, A. T. S.; Xu, J. W., Supergluing mof liquid marbles. *Chemical Communications* **2013,** *49*, 493-495.

115. Correia, C. R.; Pirraco, R. P.; Cerqueira, M. T.; Marques, A. P.; Reis, R. L.; Mano, J. F., Semipermeable capsules wrapping a multifunctional and self-regulated co-culture microenvironment for osteogenic differentiation. *Scientific Reports* **2016,** *6*.

116. Correia, C. R.; Gil, S.; Reis, R. L.; Mano, J. F., A closed chondromimetic environment within magnetic-responsive liquified capsules encapsulating stem cells and collagen ii/tgf-3 microparticles. *Advanced Healthcare Materials* **2016,** *5*, 1346-1355.

117. Moraes, C.; Mehta, G.; Lesher-Perez, S. C.; Takayama, S., Organs-on-a-chip: A focus on compartmentalized microdevices. *Annals of Biomedical Engineering* **2012,** *40*, 1211-1227.

118. Zheng, F. Y.; Fu, F. F.; Cheng, Y.; Wang, C. Y.; Zhao, Y. J.; Gu, Z. Z., Organ-on-a-chip systems: Microengineering to biomimic living systems. *Small* **2016,** *12*, 2253-2282.

119. Cohen, R. I.; Thompson, M. L.; Schryver, B.; Ehrhardt, R. O., Standardized cryopreservation of pluripotent stem cells. In *Current protocols in stem cell biology*, John Wiley & Sons, Inc.: 2007.

SECTION II – EXPERIMENTAL SECTION

Chapter 3. Materials and Methods

Chapter 3

Materials and Methods

This chapter aims to detail and add relevant information that is not present in the experimental sections of the different chapters (chapters 4 to 8) of this thesis, regarding to some critical materials and methods used during the development of such works.

3.1. Production of poly (L-lactic acid) microparticles

Poly (L-lactic acid) (PLLA) microparticles were produced by emulsion solvent evaporation technique.[1-5] 1 g of PLLA (Mw1600–2400, 70% crystallinity, Polysciences, Germany) was dissolved in 20 mL of methylene chloride (CH_2Cl_2) to obtain a 5% w/V transparent solution of PLLA/CH_2Cl_2. This solution was added under agitation to 100 mL of 0.5% w/v polyvinyl alcohol. The resulting solution was stirred for 2 days at room temperature (RT) to evaporate the organic solvent. The produced PLLA microparticles were collected by filtration and washed several times with distilled water. Ultimately, microparticles were subsequently frozen at −80 °C and lyophilize for 3 days. The surface of PLLA microparticles was modified by plasma treatment technique. PLLA microparticles were placed inside the plasma reactor chamber fitted with a radio frequency generator. Air was used as the working atmosphere. After the pressure of the chamber had stabilized to ∼0.2 mbar, a glow discharge plasma was created by controlling the electrical power at 30V of electrical potential difference. Microparticles were treated for 5min. The sample was removed from the chamber and a gentle mixing was employed in order to maximize the PLLA surface exposition to plasma treatment. This procedure was repeated three times to apply a total plasma reaction time of 15 min. A total of 450 mg of PLLA plasma-treated microparticles were sterilized by UV radiation for 30 min and then immersed in 30 mL of 0.02 M acetic acid containing 1200 μg of collagen I for 4 h at RT. A mild shaking was employed every hour. Ultimately, microparticles were collected and washed three times with sterile phosphate buffer saline (PBS).

3.2. Synthesis of gelatin methacryloyl

Gelatin methacryloyl (GelMA) prepolymer was synthesized by reaction of gelatin with methacrylic anhydride (MA) – Figure 3.1(i).[6, 7] Type A porcine skin gelatin was dissolved at 10% (w/v) into Dulbecco's phosphate buffered saline (DPBS; GIBCO) at 60 °C under vigorous stirring. MA was

added at a rate of 0.5 mL/min to the gelatin solution, until the target concentration of 8 % (v/v) was reached and then allowed to react for 2 h. Following a 2× dilution with additional warm (40 °C) DPBS to stop the reaction, the mixture was dialyzed against distilled water using 12–14 kDa cutoff dialysis membrane for 1 week at 40 °C. The solution was lyophilized for 1 week to generate a white porous foam and stored at − 80 °C until further use. GelMA polymer and 1% (w/v) photoinitiator (Irgacure 2959) were dissolved in DPBS at 60 °C, for further use in the preparation of photocrosslinked GelMA hydrogel – Figure 3.1(ii).

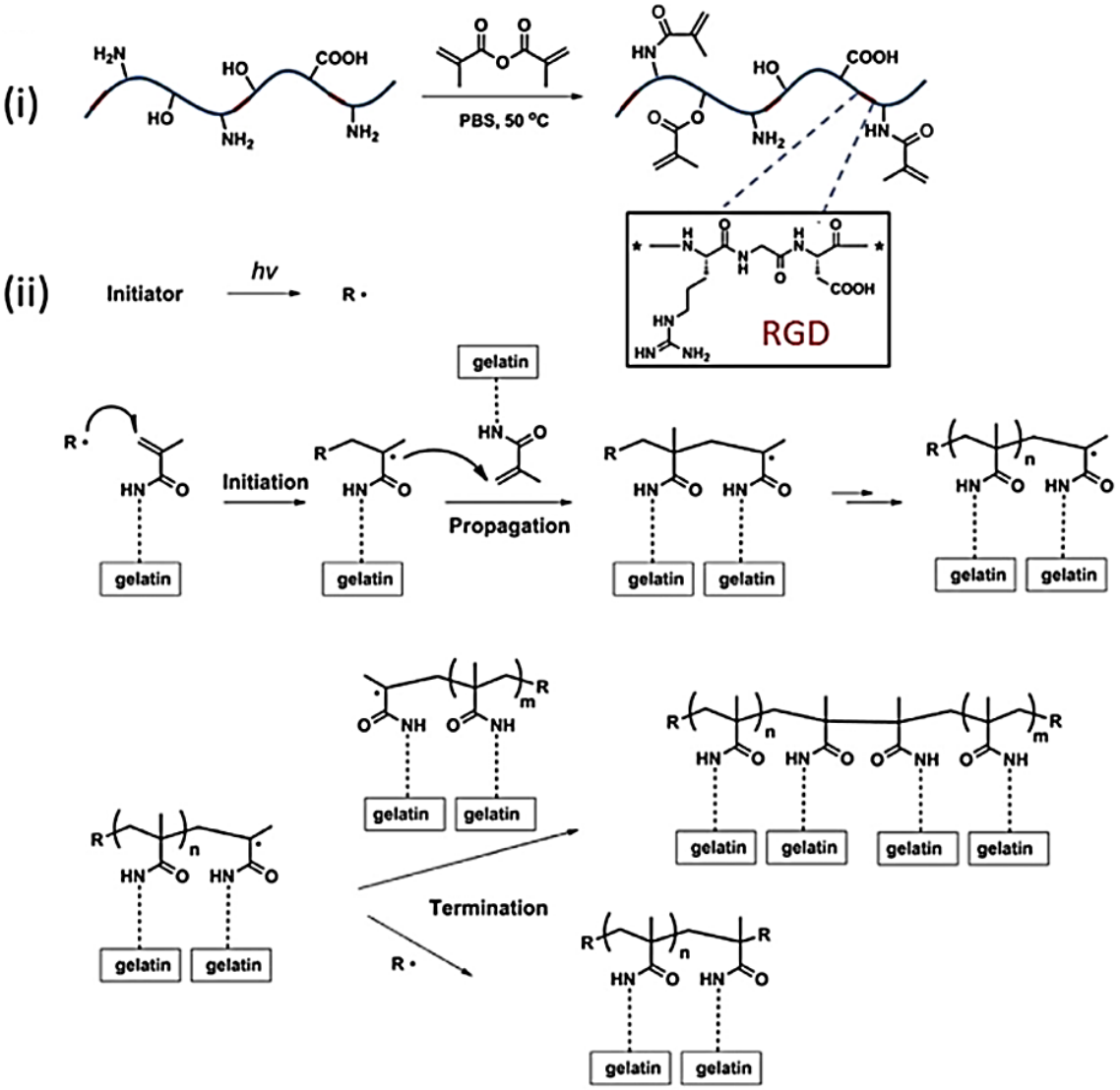

Figure 3.1: Schematic representation for preparation of photocrosslinked GelMA hydrogel. (i) Reaction of gelatin and methacrylic anhydride for grafting of methacryloyl substitution groups. The modification occurs at primary amine and hydroxyl groups. The RGD domains are illustrated along the GelMA chains, and their chemical structure is depicted

within the inset. (ii) Representative reactions during the photocrosslinking of GelMA to form hydrogel networks. Free radicals are generated from photoinitiators, which initiate the chain polymerization of the methacryloyl substitutions. Propagation occurs between methacryloyl groups located on the same chain and on different chains. Termination occurs between two propagating chains or between one propagating chain and a second radical. Chain transfers and many other minor reactions are not shown, for clarity. Adapted from Ref. [8] with permission from Elsevier.

3.3. Production of superhydrophobic (SH) surfaces with hydrophilic patterns

Two different procedures were used to produce SH surfaces in this the thesis: using DE to produce a SH surface over different substrates, namely glass and PS (chapter 4); and using a phase separation methodology to produce SH surfaces of fully constituted of PS (chapters 5 and 6).

In chapter 4, a simple strategy was adopt to produce the SH surfaces: using DE to achieve a micro/nanoscale hierarchical topography on the substrate surface; and, performing a fluorosilanization process to obtain a surface with low surface energy. In the specific case of glass substrate, the following sequence of steps was performed: the substrate was coated with DE; DE was bound to the glass by melting superficially the substrate (the ensemble was heated at 675 °C for 1.5 hours); finally, the fluorosilanization process was performed. However, for the case of PS substrate the employed procedure was: first, the fluorosilanization process was performed in the loosely microparticles of DE; then, the substrate was coated with the fluorinated DE; and finally, the ensemble was heated at 90 °C for 20 minutes and cooled always under pressure, ensuring a strong binding between the fluorinated DE and the PS substrate. Additionally, hydrophilic features with different geometries were patterned on the SH surfaces, using an appropriated stencil mask for the selective exposure of the desired surface areas to plasma treatment.

In chapter 5 and 6, PS superhydrophobic surfaces were produced by a phase separation method, which is a simple, fast and inexpensive method.[9, 10] Using a mixture of a good solvent and a

non-solvent of PS, a controlled precipitation of PS was performed on the smooth surface of PS substrates.[11-13] The PS precipitation on the surface led to the formation of a micro/nanoscale roughness on the surface explained by the following mechanism: the mixture of a solvent and a non-solvent of polystyrene formed both poor and rich polymeric phases. In the poor phase, polymer nuclei were formed by precipitation. The rich phase aggregated around these nuclei in order to decrease surface tension. During polymer precipitation within the rich PS phase, a continuous deposition of spheres on the surface took place.[9, 14-16] The patterning of wettable features on this SH surfaces was performed by protecting the desired areas with adhesive masks before the phase separation procedure. The adhesive masks consisted in stickers of polyvinyl chloride (PVC) that were glued in the pristine PS substrates.[17, 18] In chapter 5, these PVC stickers had the shape of strips with 30 mm x 2 mm and were placed with a spacing of 4 mm. However, in chapter 6, stickers with a square shape with 2 mm x 2 mm separated by 2 mm were used. These PVC stickers were removed using tweezers, immediately before SH surface use and only after all the modification procedures of PS surface being performed.

3.4. Surface modification by plasma treatment

In this work, the plasma treatment was used with three different objectives: (i) to produce hydrophilic patterns on the superhydrophobic surfaces engineered using DE (chapter 4); (ii) to prepare the SH surface of PS for the flurosilanization process (chapter 5)[19-21]; and, (iii) to increase hydrophilicity of wettable paths created on the same SH surfaces (chapter 5).

In chapter 4, Argon plasma treatment was performed over the fluorosilanated surfaces of both glass and PS substrates with entrapped DE. With this treatment, it is believed that the fluorosilanated surfaces experienced a similar process to the one reported for fluoropolymers (specifically, polytetrafluoroethylene (PTFE) and tetrafluoroethylene–perfluoroalkyl vinylether

copolymer (PFA)) treated with Argon plasma.[22-24] In these cases, both defluorination and oxidation occurred on the fluoropolymer surfaces, being showed that CF_2 carbons were changed by CF, CH_2, C=O, and C–O carbons in the PFA surface.[24] It was suggested that oxygen functional groups were formed by the combination of argon plasma irradiation and air exposure. Specifically, radicals were produced by the plasma irradiation on the fluoropolymers surface. Then, these radicals were quickly changed into peroxy radicals by contacting the air.[23] This modification on fluoropolymers surface led to an increase on surface hydrophilicity, confirmed by the decrease in water contact angle (WCA). Here, similar results were observed: by XPS analysis was determined that the relative content of CF carbons decreased and C–H, C–O, and O=C–O carbons increased with plasma treatment; and, the WCA of the fluorosilanated surfaces decreased steadily down to the hydrophilic regime by increasing the exposure time to the Argon plasma treatment (chapter 4). In chapter 5, both superhydrophobic PS and smooth PS surfaces were oxidized by air plasma treatment. On this process, the oxidation is produced by radical reactions between the polymer chain backbones and atomic oxygen in plasma, generating oxygen-based functional groups.[25] Specifically, the –OH groups formed on the superhydrophobic PS surface were important for the covalent binding with the silane molecule in the flurosilanization process.[26] On the smooth PS surface, the aim was to increase the hydrophilicity of the wettable paths that could be reached by the introduction of these oxygen-based functional groups in the surface.[25, 26] The PS hydrophilicity was precisely controlled by adjusting the exposure time to the air plasma treatment. On this step, the plasma treatment was confined to the wettable paths by selective exposure of the desired area to plasma using a stencil mask.

3.5. Surface chemical modification of different materials by flurosilanization

Besides the hydrophobization method used to produce the SH surfaces of PS, the chemical modification of different material surfaces was performed to increase hydrophobicity, using 1H,1H,2H,2H-Perfluorodecyltriethoxysilane (PFDTS, 97%). This chemical modification was performed in the created glass substrates with entrapped DE (chapter 4), in the loosely microparticles of DE (chapters 4, 7 and 8), and in the SH surfaces of PS (chapter 5). In this last case, the aim was to increase hydrophobicity and change the surface chemistry with the objective to increase the surface resistance to protein adsorption.

The preparation of the substrates for the chemical modification was different for each material. For the case of glass substrates with DE and after the sintering process, the samples were washed with ethanol in an ultrasound bath for 15 minutes to remove DE excess. Then, the substrates were immediately immersed in a PDTS solution at 1% in ethanol for up to 48 hours. In the case of the loosely microparticles of DE, two different procedures were used for the preparation of the DE powder. Initially, in chapter 4, the DE microparticles were heated at 600 °C for 1 hour. Then, in chapters 7 and 8, based on literature [27] an alternative procedure was adopted and the DE was dried at 190 °C under vacuum for at least 2 h. In both procedures, the aim was to promote water desorption and expose more silanol groups on the surface of DE microparticles for an efficient flurosilanization process. After this drying step, by mixing DE (1 g) with PFDTS solution (10 mL at 1% v/v) prepared in deionized water a DE suspension was prepared, the mixture was left to react overnight. By filtration it was separated the solid phase from the liquid. For both cases the glass substrates with DE and the loosely microparticles of DE and after the flurosilanization process, the samples were dried in air and heated to 220 °C for 5 min to ensure the complete PFDTS hydrolysis and condensation, thus forming a stable fluorosilanated layer on the silica surface.[28] Additionally,

the chemically modified DE microparticles were washed with 20 mL of ethanol to remove any silane that may not bind to the surface. After drying, a hydrophobic powder was obtained. In the case of the SH surfaces of PS (chapter 5), the preparation of the substrates for the flurosilanization process consisted in to submit the samples to a plasma treatment for 30 seconds at 30W and 0.1-0.2 mbar (Plasma Prep5, Gala Instruments). Then, the substrates were immersed in a PDTS solution at 1% in ethanol for up to 48 hours. These chemically modified substrates were washed with absolute ethanol to remove the unreacted PFDTS. Specifically in this case, the stickers on the surfaces were just removed after all these procedures to ensure that the regions covered by the stickers remained untreated and transparent, crucial to obtain SH surfaces with the wettable paths. Generally, the silanization reaction follows the sequence: hydrolysis of triethoxyl groups into trihydroxyl groups and then polycondensation of the hydroxyl groups with the surface hydroxyls groups from the substrate surface.[29] The general mechanism for this chemical reaction is illustrated in Figure 3.2. However, this reaction is complex and several reaction routes may be involved.[29-31] For example, various interfacial processes may be possible, namely covalent binding to the substrate surface, lateral polymerization of adsorbed silane molecules or three-dimensional polymerization. Overall, the kinetics of the silanization reaction is crucial to manage the layer formation process, being dependent of the type of the reactive group/element bound to Si in the silane molecule (usually an alkoxy group or chloride), their number, and experimental conditions.

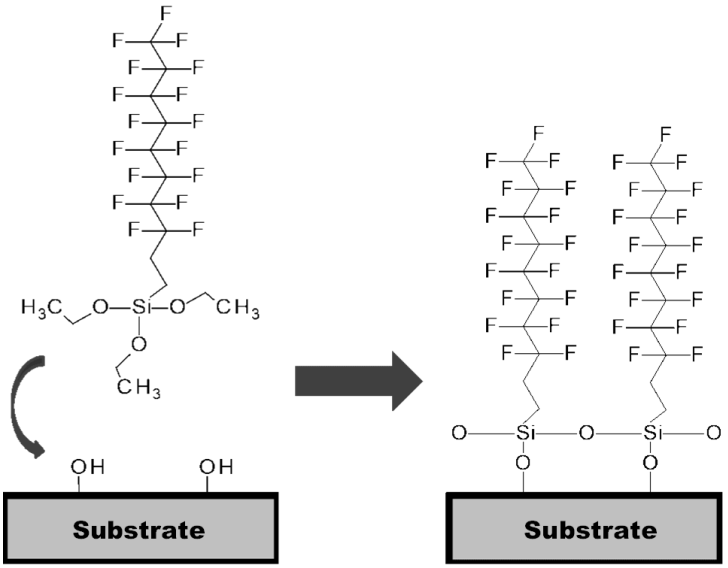

Figure 3.2: Illustration of the possible general route for PFDTS silanization reaction on the different substrate surfaces.

To confirm the chemical modifications on the different substrate surfaces, both energy-dispersive X-ray spectroscopy (EDS) and X-ray photoelectron spectroscopy (XPS) analysis were performed.

3.6. Characterization of the fluid flows on the planar chips with hydrophilic paths

Fluid flow can be classified to three regimes which is laminar, transitional and turbulent regime. Laminar regime is a regime where the flow is characterized by smooth streamlines and highly ordered fluid motion. Turbulent is a regime where flow is characterized by velocity oscillations, highly disordered fluid motion and eddies. Transitional regime prevails between these two limits where the flow oscillates between laminar and turbulent before it becomes completely turbulent. The transitional from laminar to turbulent flow depends on several parameters, namely surface roughness, geometry, surface temperature, flow velocity, and type of fluid, midst others. However, Osborne Reynolds discovered that the flow regime is essentially dependent of the ratio between

inertial forces – which are proportional to the fluid density and the square of the fluid velocity – and viscous forces in the fluid, called as the Reynolds number.[32]

Thus, the laminar flow is characterized by a small or moderate Reynolds numbers, meaning that the viscous forces are large enough to suppress fluctuations and to keep an ordered fluid motion. Regarding the turbulent flow, the inertial forces overlap the viscous force, resulting that the viscous force cannot avoid the spontaneous and rapid oscillations of the fluid. These different flow regimes can be assessed experimentally, such as performed by Osborne Reynolds – Figure 3.3. By injecting dye streaks into the flow in a glass pipe, Reynolds observed that the dye streak forms a straight and smooth line at low velocities when the flow is laminar. However, some dye dispersion may observed due to molecular diffusion. While for turbulent flow, by injecting the dye into the flow, the dye disperses by the rapid mixing of fluid particles from adjacent layers and the dye line breaks into entangled dye filaments throughout the main flow.

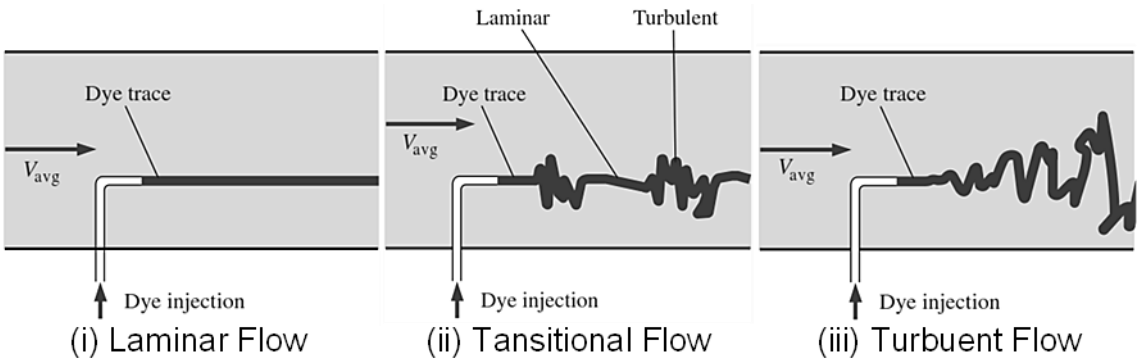

Figure 3.3: The behavior of colored fluid injected into the flow in laminar, transitional and turbulent regimes in a pipe.

Basically, the first step of the experiment consists into establish a laminar flow, by controlling the flow rate. Then, by slowly increase the flow rate, the dye streak is monitored, recording the flow pattern changings and volumetric flow rate. Inspired by the Reynolds experiment, the flow regime for different flow rates was assessed for the liquid streams flowing over the hydrophilic paths patterned on the SH surfaces, in Chapter 5.

3.7. *In vitro* biological studies

In this thesis, several different cell types were used for the different experimental works, namely C2C12 cell line (mouse myoblasts), human stem cells derived from the adipose tissue (hASC), L929 cell line (mouse fibroblasts), Saos-2 cell line (human osteoblast-like cells), human umbilical venous endothelial cells (HUVEC), and human dermal fibroblasts (ATCC). C2C12, L929 and Saos-2 cell lines and ATCC cells were cultured and expanded in Dulbecco's Modified Essential Medium (DMEM) with 10% (v/v) of fetal bovine serum (FBS) and 1% (v/v) of antibiotic/antimycotic (ATB). Human abdominal subcutaneous adipose tissue was used to isolate hASC.[33-36] The undifferentiated cells were cultured and expanded under basal condition, using Minimum Essential alpha Medium (α-MEM) with 10% (v/v) of FBS and 1% (v/v) of ATB, until passages 2 and 3. For experimental assays, the hASCs were used in passages 3 to 5. In chapter 6, the HUVEC cells were cultured and expanded in medium 199 (M199) with 20% (v/v) FBS, 1% (v/v) ATB and 1% (v/v) Glutamax, supplemented with heparin (100 μg/mL) and endothelial cell growth supplement (50 μg/mL; ECGS). In chapter 8, pristine HUVECs were obtained from ATCC whereas GFP-positive HUVECs were obtained in-lab, which were cultured in Endothelial Cell Growth Medium (ECGM, Lonza). For all cell types, the cell culture media were exchanged every 2-3 days.

In chapter 5, 35 μL of cell suspension of C2C12 at a density of $5x10^5$ cells.mL^{-1} were dispensed in each path of the chip, previously coated with fibronectin protein (EMD Millipore). After overnight incubation for cell adhesion, assays were performed to study the effect of mechanical stimulus (flow shear stress) combined with bone morphogenic protein (specifically BMP-2) stimulation on the osteogenic differentiation of C2C12 myoblast cells. In static conditions, cells were culture for 48 hours on the paths of the chip. The dynamic conditions consisted in 24 hours of initial static cell culture followed by 24 hours of cell culture under a constant flow of cell culture medium. In both conditions the cell culture medium was exchanged after 24 hour of culture. The cell culture

medium was supplemented with 200 ng.mL^{-1} of BMP-2 (Invitrogen). Two different times of contact between cells and the supplemented medium were tested, namely 24 or 48 hours.

In chapter 6, cell suspensions of different cell types (L929, Saos-2 and HUVEC cells) were dispensed in each wettable spot of the chips. For each cell type, a cell suspension at a cellular density of 2.5x10^{5} cells.mL^{-1} was prepared with the respective cell culture medium (DMEM for L929 and Saos-2; M199 for HUVEC). Then, a volume of 5 μL of cell suspension was dispensed per spot. To promote cell adhesion, cell suspension droplets were left in the wettable spots for 4 hours. Then, the non-adhered cells were removed by washing the spots with fresh culture medium and the chips with adhered cells were incubated overnight. The wettable spots later used for the formation of cell spheroids without co-culture were left empty during this step. After remove cell culture medium from wettable spots, a 7.5 μL droplet of hASC cell suspension at a cell density of 3.33x10^{5} cells.mL^{-1} was dispensed in each spot of the chips, which were rapidly turned 180°, acquiring a hanging drop configuration for spheroid formation. For the co-cultures with adhered L929 and Saos-2, α-MEM medium with the previously described formulation was used to prepare hASC cell suspension. For the co-culture with adhered HUVEC, the hASC cell suspension was prepared using M119 medium with reduced content of FBS (from 20% to 10% (v/v)), to have comparable conditions between the different tested co-cultures. As control conditions, spheroids were formed and cultured in cell-free wettable spots, using both cell culture media (α-MEM and M199 with 10% (v/v) FBS) separately. Thus, hASC cells were cultured in the hanging drop configuration for 72h, promoting spheroids formation and growth in presence (or absence, in the case of controls) of a layer of cell lines.

Regarding to chapter 7, in the scope of the *in vitro* biocompatibility assessment, indirect cytotoxicity tests using extracts of the hydrophobic powder being studied were performed based on ISO/EN 10993 part 5 guidelines, using L929 cells.[37-39] After sterilization by autoclaving, 4 g of

hydrophobic powder were incubated in 20 mL of DMEM culture medium for 48 hours to extract possible leachable from the hydrophobic powder. After the extraction and filtering, the extraction fluid was used to culture L929 cells for 48 hours, the cells were previously adhered on the wells of a 6-well tissue culture plate. A MTS colorimetric assay was performed to assess cell metabolic activity and consequently the cytotoxicity of the different materials comparing with controls. After confirm that the hydrophobic powder was non-cytotoxicity for cells, droplets of the L929 cell suspension – with Poly(L-lactic acid) (PLLA) microparticles on the same suspension – were dispensed one by one over a hydrophobic powder layer. Thus, by rolling the droplets over the hydrophobic powder, liquid marbles (LM) with encapsulated cells were produced. Additionally, to access the PLLA microparticles effect over cell behavior, LM with or without PLLA microparticles in the cell suspension were produced. Cell metabolic activity and proliferation assessment were performed by MTS colorimetric and DNA quantification assays, respectively.

In chapter 8, cell suspensions of ATCC and HUVEC were prepared at concentration of 1×10^{6} cells.mL^{-1}, using GelMA prepolymer solution in PBS. The photo-cross-linking of these prepolymer solutions was performed by UV light for 60 seconds. The floating hydrogels encapsulating ATCC or HUVEC were produced with a parallelepiped shape, using in-house made poly(methyl methacrylate) (PMMA) stencil masks to control the initial shape of GelMA solution exposed to UV light. Only after to give the desired shape to the hydrogels, the coating with hydrophobic powder was performed. These floating hydrogels encapsulating ATCC or HUVEC were cultured in their respective medium for up to 10 days. Cell viability was monitorized by staining them with the Live/Dead kit at days 0, 3, 7, and 10.

3.8. AlamarBlue assay performed *in situ*

The alamarBlue assay is quantitative with respect to time and dose, assessing the ability of metabolically active cells to convert the reagent into a colorimetric indicator. As the reagent has a nontoxic nature, long-term exposure to cells without negative impact is allowed. These alamarBlue features are valuable for viability and cytotoxicity assays. This assay uses the natural reducing power of living cells to convert resazurin (the active compound in alamarBlue reagent) into the molecule resorufin, being nontoxic and cell permeable compounds. Resazurin presenting a blue color is reduced into resorufin, which produces a very bright red color. Viable cells continuously convert resazurin to resorufin, thereby generating a quantitative measure of viability and cytotoxicity.

In Chapter 6, alamarBlue reagent was directly used on-chip to assess spheroid cell viability, by dispensing the reagent in each spot of the chip. Regarding Chapter 7, the alamarBlue reagent was placed in direct contact with cells, by injecting the reagent in each liquid marble. In both cases and after incubation, color images were took using a digital camera. Using the ImageJ software, the images were split in the three channels: red, green and blue. On the 8 bit red channel, the red intensity was measured manually by defining on the image the area of interest for each testing condition. Conditions without cells were used as background for red intensity determination. By subtracting the red intensity value of background to the red intensity value for each testing condition, the effective red intensity for each studied condition was determined. The red intensity value was measured using the ImageJ software. Then, by dividing the red intensity value of each condition for the reference value (control without cells), the cell viability ratio was determined.

3.9. References

1. Bodmeier, R.; Mcginity, J. W., Solvent selection in the preparation of poly(dl-lactide) microspheres prepared by the solvent evaporation method. *International Journal of Pharmaceutics* **1988,** *43*, 179-186.

2. Correia, C. R.; Sher, P.; Reis, R. L.; Mano, J. F., Liquified chitosan-alginate multilayer capsules incorporating poly(l-lactic acid) microparticles as cell carriers. *Soft Matter* **2013,** *9*, 2125-2130.

3. Correia, C. R.; Reis, R. L.; Mano, J. F., Multilayered hierarchical capsules providing cell adhesion sites. *Biomacromolecules* **2013,** *14*, 743-751.

4. Bodmeier, R.; Mcginity, J. W., Polylactic acid microspheres containing quinidine base and quinidine sulfate prepared by the solvent evaporation method .3. Morphology of the microspheres during dissolution studies. *Journal of Microencapsulation* **1988,** *5*, 325-330.

5. Hamoudeh, M.; Fessi, H.; Salim, H.; Barbos, D., Holmium-loaded plla nanoparticles for intratumoral radiotherapy via the tmt technique: Preparation, characterization, and stability evaluation after neutron irradiation. *Drug Development and Industrial Pharmacy* **2008,** *34*, 796-806.

6. Van den Bulcke, A. I.; Bogdanov, B.; De Rooze, N.; Schacht, E. H.; Cornelissen, M.; Berghmans, H., Structural and rheological properties of methacrylamide modified gelatin hydrogels. *Biomacromolecules* **2000,** *1*, 31-38.

7. Nichol, J. W.; Koshy, S. T.; Bae, H.; Hwang, C. M.; Yamanlar, S.; Khademhosseini, A., Cell-laden microengineered gelatin methacrylate hydrogels. *Biomaterials* **2010,** *31*, 5536-5544.

8. Yue, K.; Trujillo-de Santiago, G.; Alvarez, M. M.; Tamayol, A.; Annabi, N.; Khademhosseini, A., Synthesis, properties, and biomedical applications of gelatin methacryloyl (gelma) hydrogels. *Biomaterials* **2015,** *73*, 254-271.

9. Tan, S. X.; Xie, Q. D.; Lu, X. Y.; Zhao, N.; Zhang, X. L.; Xu, J., One step preparation of superhydrophobic polymeric surface with polystyrene under ambient atmosphere. *Journal of Colloid and Interface Science* **2008,** *322*, 1-5.

10. Fan, Z. P.; Liu, W. L.; Wei, Z. J.; Yao, J. S.; Sun, X. L.; Li, M.; Wang, X. Q., Fabrication of two biomimetic superhydrophobic polymeric surfaces. *Applied Surface Science* **2011,** *257*, 4296-4301.

11. Oliveira, N. M.; Neto, A. I.; Song, W. L.; Mano, J. F., Two-dimensional open microfluidic devices by tuning the wettability on patterned superhydrophobic polymeric surface. *Applied Physics Express* **2010,** *3*.

12. Aruna, S. T.; Binsy, P.; Richard, E.; Basu, B. J., Properties of phase separation method synthesized superhydrophobic polystyrene films. *Applied Surface Science* **2012,** *258*, 3202-3207.

13. Wang, Y.; Liu, Z. M.; Han, B. X.; Sun, Z. Y.; Zhang, J. L.; Sun, D. H., Phase-separation-induced micropatterned polymer surfaces and their applications. *Advanced Functional Materials* **2005,** *15*, 655-663.

14. Erbil, H. Y.; Demirel, A. L.; Avci, Y.; Mert, O., Transformation of a simple plastic into a superhydrophobic surface. *Science* **2003,** *299*, 1377-1380.

15. Yuan, Z. Q.; Chen, H.; Tang, J. X.; Chen, X.; Zhao, D. J.; Wang, Z. X., Facile method to fabricate stable superhydrophobic polystyrene surface by adding ethanol. *Surface & Coatings Technology* **2007,** *201*, 7138-7142.

16. Zhao, N.; Xu, J.; Xie, Q. D.; Weng, L. H.; Guo, X. L.; Zhang, X. L.; Shi, L. H., Fabrication of biomimetic superhydrophobic coating with a micro-nano-binary structure. *Macromolecular Rapid Communications* **2005,** *26*, 1075-1080.

17. Oliveira, M. B.; Neto, A. I.; Correia, C. R.; Rial-Hermida, M. I.; Alvarez-Lorenzo, C.; Mano, J. F., Superhydrophobic chips for cell spheroids high-throughput generation and drug screening. *Acs Applied Materials & Interfaces* **2014,** *6*, 9488-9495.

18. Oliveira, M. B.; Luz, G. M.; Mano, J. F., A combinatorial study of nanocomposite hydrogels: On-chip mechanical/viscoelastic and pre-osteoblast interaction characterization. *Journal of Materials Chemistry B* **2014,** *2*, 5627-5638.

19. Lima, A. C.; Puga, A. M.; Mano, J. F.; Concheiro, A.; Alvarez-Lorenzo, C., Free and copolymerized gamma-cyclodextrins regulate the performance of dexamethasone-loaded dextran microspheres for bone regeneration. *Journal of Materials Chemistry B* **2014,** *2*, 4943-4956.

20. Lima, A. C.; Song, W. L.; Blanco-Fernandez, B.; Alvarez-Lorenzo, C.; Mano, J. F., Synthesis of temperature-responsive dextran-ma/pnipaam particles for controlled drug delivery using superhydrophobic surfaces. *Pharmaceutical Research* **2011,** *28*, 1294-1305.

21. Puga, A. M.; Lima, A. C.; Mano, J. F.; Concheiro, A.; Alvarez-Lorenzo, C., Pectin-coated chitosan microgels crosslinked on superhydrophobic surfaces for 5-fluorouracil encapsulation. *Carbohydrate Polymers* **2013,** *98*, 331-340.

22. Golub, M. A.; Lopata, E. S.; Finney, L. S., X-ray photoelectron-spectroscopy study of argon-plasma-treated fluoropolymers. *Langmuir* **1994,** *10*, 3629-3634.

23. Kim, S. R., Surface modification of poly(tetrafluoroethylene) film by chemical etching, plasma, and ion beam treatments. *Journal of Applied Polymer Science* **2000,** *77*, 1913-1920.

24. Inagaki, N.; Narushima, K.; Yamamoto, T., Surface modification of tetrafluoroethylene-perfluoroalkyl vinylether copolymer (pfa) by plasmas for copper metallization. *Journal of Applied Polymer Science* **2002,** *85*, 1087-1097.

25. Johansson, B. L.; Larsson, A.; Ocklind, A.; Ohrlund, A., Characterization of air plasma-treated polymer surfaces by esca and contact angle measurements for optimization of surface stability and cell growth. *Journal of Applied Polymer Science* **2002,** *86*, 2618-2625.

26. North, S. H.; Lock, E. H.; Cooper, C. J.; Franek, J. B.; Taitt, C. R.; Walton, S. G., Plasma-based surface modification of polystyrene microtiter plates for covalent immobilization of biomolecules. *Acs Applied Materials & Interfaces* **2010,** *2*, 2884-2891.

27. Zhuravlev, L. T., The surface chemistry of amorphous silica. Zhuravlev model. *Colloids and Surfaces a-Physicochemical and Engineering Aspects* **2000,** *173*, 1-38.

28. Xiu, Y. H.; Zhu, L. B.; Hess, D. W.; Wong, C. P., Preparation of superhydrophobic silica thin films for antistiction of mems devices using a novel sol-gel process. *57th Electronic Components & Technology Conference, 2007 Proceedings* **2007**, 1135-1142.

29. Liu, Y.; Li, Y. M.; Li, X. M.; He, T., Kinetics of (3-aminopropyl)triethoxylsilane (aptes) silanization of superparamagnetic iron oxide nanoparticles. *Langmuir* **2013,** *29*, 15275-15282.

30. Gooding, J. J.; Ciampi, S., The molecular level modification of surfaces: From self-assembled monolayers to complex molecular assemblies. *Chemical Society Reviews* **2011,** *40*, 2704-2718.

31. Aissaoui, N.; Bergaoui, L.; Landoulsi, J.; Lambert, J. F.; Boujday, S., Silane layers on silicon surfaces: Mechanism of interaction, stability, and influence on protein adsorption. *Langmuir* **2012,** *28*, 656-665.

32. Reynolds, O., An experimental investigation of the circumstances which determine whether the motion of water shall be direct or sinuous, and of the law of resistance in parallel channels. *Philosophical Transactions of the Royal Society of London* **1883,** *174*, 935-982.

33. Rada, T.; Reis, R. L.; Gomes, M. E., Distinct stem cells subpopulations isolated from human adipose tissue exhibit different chondrogenic and osteogenic differentiation potential. *Stem Cell Reviews and Reports* **2011,** *7*, 64-76.

34. Rada, T.; Gomes, M. E.; Reis, R. L., A novel method for the isolation of subpopulations of rat adipose stem cells with different proliferation and osteogenic differentiation potentials. *Journal of Tissue Engineering and Regenerative Medicine* **2011,** *5*, 655-664.

35. Mihaila, S. M.; Frias, A. M.; Pirraco, R. P.; Rada, T.; Reis, R. L.; Gomes, M. E.; Marques, A. P., Human adipose tissue-derived ssea-4 subpopulation multi-differentiation potential towards the endothelial and osteogenic lineages. *Tissue Engineering Part A* **2013,** *19*, 235-246.

36. Strioga, M.; Viswanathan, S.; Darinskas, A.; Slaby, O.; Michalek, J., Same or not the same? Comparison of adipose tissue-derived versus bone marrow-derived mesenchymal stem and stromal cells. *Stem Cells and Development* **2012,** *21*, 2724-2752.

37. Gomes, M. E.; Reis, R. L.; Cunha, A. M.; Blitterswijk, C. A.; de Bruijn, J. D., Cytocompatibility and response of osteoblastic-like cells to starch-based polymers: Effect of several additives and processing conditions. *Biomaterials* **2001,** *22*, 1911-1917.

38. Salgado, A. J.; Coutinho, O. P.; Reis, R. L., Novel starch-based scaffolds for bone tissue engineering: Cytotoxicity, cell culture, and protein expression. *Tissue Engineering* **2004,** *10*, 465-474.

39. Barile, F. A.; Dierickx, P. J.; Kristen, U., In-vitro cytotoxicity testing for prediction of acute human toxicity. *Cell Biology and Toxicology* **1994,** *10*, 155-162.

SECTION III – DEVELOPMENT OF BIOMEDICAL DEVICES BASED ON THE ADVANCED CONTROL OF WETTABILITY IN DIFFERENT SURFACES

Chapter 4

Superhydrophobic Surfaces Engineered Using Diatomaceous Earth

This chapter is based on the following publication:

Nuno M. Oliveira; Rui L. Reis; João F. Mano; Superhydrophobic Surfaces Engineered Using Diatomaceous Earth.

ACS Applied Materials & Interfaces **2013**, 5, 4202–4208.

4.1. Abstract

We present a simple method to prepare superhydrophobic surfaces using siliceous exoskeleton of diatoms, a widespread group of algae. This makes diatomaceous earth an accessible and cheap natural material. A micro/nanoscale hierarchical topography was achieved by coating a glass surface with diatomaceous earth, giving rise to a superhydrophilic surface. Superhydrophobic surfaces were obtained by a further surface chemical modification through fluorosilanization. The wettability of the superhydrophobic surface can be modified by Argon plasma treatment in a controlled way by exposure time variation. The chemical surface modification by fluorosilanization and posterior fluorinated SH surface modification by plasma treatment was analyzed by X-ray photoelectron spectroscopy. Using appropriated hollowed masks only specific areas on the surface were exposed to plasma permitting to pattern hydrophilic features with different geometries on the superhydrophobic surface. We showed that the present strategy can be also applied in other substrates, including thermoplastics, enlarging the potential applicability of the resulting surfaces.

4.2. Introduction

In general, superhydrophobic (SH) surfaces are defined as surfaces with a static water contact angle (WCA) higher than 150°.[1, 2] These surfaces have attracted much interest in both fundamental and applied research. Different applications for SH surfaces were proposed including in self-cleaning, antifouling, anti-adhesion, microfluidic systems and high-throughput screening devices.[2-7] The inspiration to produce artificial SH surfaces comes from nature. The most well know example of a natural SH surface is the Lotus leaf.[8] Hierarchical surface topographies at micro/nanoscale such as those found on Lotus leaves are critically important for this effect. The superhydrophobicity includes a combination of multiscale roughness and a low surface energy of the materials used.[9] Many techniques and strategies to mimic that hierarchical surface topography were developed, including: lithography, polymer reconformation, template method, sol-gel processing, or layer-by-layer methods.[2] One of these strategies involved the spin-coating of a glass slide with a mixture of micro and nanoparticles of silica prepared by sol-gel.[10] Tsai and coworkers also reported a similar strategy to produce SH surfaces through successive Langmuir-Blodgett depositions of micro/nanoparticles on a glass slide surface;[11] after silica deposition, the silanization of the particulate films decreased the surface energy, allowing to obtain a SH surface. Different sizes and number of layers of micro-silica particles were tested. It was demonstrated that the superhydrophobicity increased with the increase of the silica particle size. Other interesting strategy to produce SH surfaces is using natural structures as templates that exhibit the necessary hierarchical structure. Sun *et al* have developed a method to produce SH surfaces using a natural lotus leaf as template.[12] They were able to replicate the topography of the lotus leaf by polymer casting, using poly(dimethylsiloxane). The resulting lotus-leaf-like substrate has the same superhydrophobic characteristics of the original lotus leaf. Biomimetic SH

polystyrene films were also obtained by replicating the surface pattern of a natural taro leaf, another superhydrophobic natural surface.[13]

These two strategies to produce SH surfaces inspired us to develop a new approach to generate such kind of surfaces. We propose the use of silica-based structures already available in nature to create the necessary hierarchical topography. We hypothesize that these structures can be used directly on the surface and not as templates. The proof-of-principle will be based on the use of Diatomaceous Earth (DE) to produce the SH surfaces. Diatomaceous or diatoms are unicellular algae and widely spread in both fresh water and seawater playing a crucial role in the earth's carbon cycle.[14, 15] Other very appreciated characteristic of diatomaceous is their amazing silica microskeleton and the biomineralization mechanisms associated with its formation. Diatoms are taken as a model for some research works on nanoscacle self-assembly and biomimetics.[16, 17] The sedimented dead diatoms on the bottom of lakes or sea are called DE or diatomite.[15] The exoskeletons of diatoms are microstructures with nanotextures on their surface and are constituted mostly by amorphous silica. The use of these microstructures to coat smooth surfaces should enable to create a hierarchical structure eliciting extreme wettability properties. We will explore the possibility to create superhydrophobic surfaces by treating such substrates with fluorosilanes.

Simpson and D'Urso have a patent with the idea to produce a superhydrophobic powder using DE.[18] They refer the possibility to use the powder to make superhydrophobic surfaces. On this patent it was proposed that to use a polymer in solution as a binder to adhere the DE particles to the surface. The substrate surface can be coated with superhydrophobic DE particles by painting, dipping or spraying. On this work, we propose to use the intrinsic characteristics of the substrate to promote the binding with DE particles. That can be performed by melting superficially the substrate to get a DE layer locked on its surface. Through this method we believe that a more robust SH surface can be obtained, because DE particles will be trapped and not only deposited

on the surface. We explore also the possibility to change the SH surface wettability in a controlled way and to print patterns on the surface. These possibilities make possible to use the patterned substrates both open microfluidic and high-throughput screening applications.[3, 4]

4.3. Materials and Methods

4.3.1. Materials processing

Glass substrates with 2.5 × 2.5 cm were prepared using glass microscope slides. The substrates were cleaned with detergent, acetone, ethanol and deionized water to remove any surface contaminant and dried in air. A DE suspension was prepared by mixing 1 g of DE (Food-Grade Fossil Shell Fluor® from Perma-Guard, Inc; kindly supplied by Agrogreen Canada Inc., Ontario, Canada) in 4 mL of water, followed constant stirring. 500 µL of the DE suspension were dropped on the top of each substrate. Then the substrates with the DE suspension were heated in a furnace under air atmosphere for 1.5 hours at 675 ˚C to obtain a sintered DE film on the surface. The samples were cooled slowly until room temperature and washed with ethanol in an ultrasound bath for 15 minutes to remove DE excess. The washed substrates were immersed in a 1H,1H,2H,2H-Perfluorodecyltriethoxysilane (PFDTS) (from Aldrich Chemistry) solution at 1% in ethanol for 48 hours. Subsequently the samples were dried in air and heated to 220˚C for 5 min to promote silane hydrolysis and condensation, thereby forming a stable fluorosilanated layer on the DE surface.

We also used polystyrene (PS) as the substrate instead of glass, to demonstrate that the proposed methodology can be also used at low temperature. Substrates with 2.5 × 2.5 cm were prepared by cutting PS Petri dishes. The substrates were washed with ethanol in an ultrasound bath for 15 minutes and dried in air. Then over the substrates a 2 millimeter-thick layer of PFDTS modified DE was placed. The substrates with DE were heated at 90 °C for 20 minutes and enforcing a pressure

of 30 × 10^5 $N.m^{-2}$. The ensemble was heated and cooled always under pressure. To perform the process a hydraulic press with heating/cooling platens was used. After cooling the DE excess on PS surface was removed washing the surface with ethanol, which was then dried in air. The used DE to coat PS substrates was previously chemically modified with PFDTS. First, DE was heated at 600 °C for 1 hour to promote water desorption and expose more silanol groups on diatom surface. A DE suspension was prepared by mixing 1 g of DE with 10 mL of a 1% PFDTS solution prepared in deionized water, the mixture was left to react overnight. Both solid and liquid phases were separated by filtration. After dried in air, the solid phase was heated at 220 ˚C for 5 min to promote silane hydrolysis and condensation. The chemically modified DE was washed with 20 mL of ethanol to remove any unreacted silane. After dried the PFDTS modified DE was used to perform surface modification onto the PS substrates.

4.3.2. Surface modification by plasma treatment

Surface treatments using a plasma reactor Plasma Prep 5 (Gala Instrument GmbH, Bad Schwalbach, Germany) were performed in the diatom coated glass samples with fluorine. Argon gas was used and the pressure in the reactor chamber was controlled in the range 0.1-0.2 mbar. The treatment was performed using a radio frequency source (13.56 MHz) and a power of 30 W for different time periods.

4.3.3. Surface morphology characterization

The morphology of the samples was analyzed using a NanoSEM-FEI Nova 200 Scanning Electron Microscope (FEG/SEM; FEI Company, Hillsboro, OR, USA). All specimens were pre-coated with a conductive layer of gold. The surface topography of the samples at lower magnification was assessed by a non-contact optical profiling technique using an interferometer profiler (WYKO-Veeco, model NT1100; Veeco, Tucson, AZ, USA) equipped with the WycoVision®32 analytical software package. The surface of both unmodified glass substrate and DE modified glass substrate was

analyzed. For each sample, five different regions with 0.9 × 1.2 mm^2 were measured to determine topographic roughness parameters, namely average roughness (Ra) and root-mean-squared (RMS) roughness (Rq). 3D images from both surfaces to show roughness distribution were obtained applying a filter for noise reduction. The water contact angle (WCA) was analyzed for the different samples: unmodified glass slides (G1), glass coated with diatoms (G2), diatom coated glass modified by fluorosilane (G3) and after Argon plasma treatment performed on fluorinated samples (G4). WCA was also determined in the produced surfaces using PS substrates. The WCA was measured in a OCA 15+ goniometer from DataPhysics Corporation (San Jose, CA, USA) at room temperature. The static WCA was measured by a sessile drop method with a 6 µl water droplet. Using the same method, the WCA hysteresis was determined using a liquid injection rate of 0.3 $\mu l.s^{-1}$, changing the drop volume between 5 and 8 µl.

4.3.4. Chemical characterization

The chemical composition of the PFDTS modified DE particles was analyzed on a NanoSEM-FEI Nova 200 Scanning Electron Microscope (FEG/SEM; FEI Company, Hillsboro, OR, USA), equipped with an EDAX-Pegasus X4M energy dispersive spectrometer. Energy-dispersive X-ray spectroscopy (EDS) analysis were performed at an accelerating voltage of 15 keV, using conventional ZAF correction procedure integrated on the EDAX- Pegasus software.

The surface chemistry composition of glass samples was analyzed by X-ray photoelectron spectroscopy (XPS) using a Thermo Scientific K-Alpha ESCA instrument (Thermo VG Scientific, East Grinstead, UK) equipped with monochromatic Al (Kα) X-ray source operating at 1486.6 eV. Due to non conductor nature of samples it was necessary to use a low energy flood gun (electrons in the range 0-14 eV) and a low energy Argon ions gun to minimize surface charging. Photoelectrons were collected from a take-off angle of 90° relative to sample surface. The measurements were performed in a Constant Analyzer Energy mode (CAE) with 100 eV pass energy for survey spectra

and 30 eV pass energy for high resolution spectra. Charge referencing was carried out by setting lower binding energy C1s photo peak at 285.0 eV C1s hydrocarbon peak. Using the standard Scofield photoemission cross sections, surface elemental composition was determined.

4.4. Results and Discussion

The wetting behavior of a surface is dependent on both surface topography and surface chemistry. We used DE to generate a rough topography on smooth glass. The initial substrate was glass microscope slide that presents a smooth surface – see Figure 4.1A_1. The glass is hydrophilic, having a WCA of 31.3 ± 2.6˚. The glass was coated by DE suspension and then was heated until 675 ˚C to induce the agglomeration and stabilization of the diatom layer over the glass surface. Substrates were then cleaned in an ultrasound bath to eliminate the non-sintered fraction of DE.

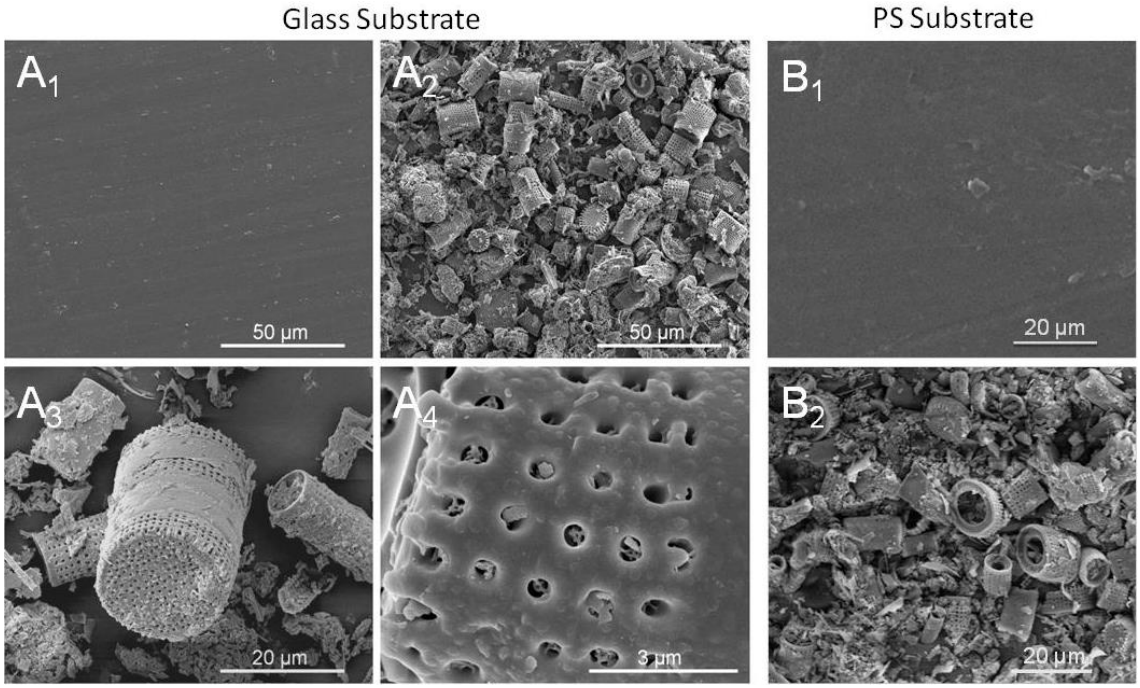

Figure 4.1: SEM images of glass substrate before (A_1) and after coating with DE (A_{2-4}). Magnification images from both diatomaceous silica microskeleton (A_3) and the nanotexture on their surface (A_4). SEM images of polystyrene substrate before (B_1) and after coating with DE (B_2).

After the cleaning process we obtained a glass with a sintered diatom layer on the surface – see Figure 4.1A_2. The DE layer provided roughness to the surface at the microscale level complemented with a nanotexture given by the diatom surface morphology – see Figure 4.1A_3 and 4.1A_4.

To characterize the changes on surface roughness, the surface topography was analyzed by optical profilometry – Figure 4.2. The glass surface is clearly smooth at the sub-micrometer level – see Figure 4.2A. After coating with DE we clearly see a roughness at the microscale level that seems homogenous throughout all the analyzed area – Figure 4.2B. Unmodified glass surface presented an average roughness (Ra) of 4.2 ± 0.5 nm and the DE coated glass surface exhibited a Ra of 3.0 ± 0.2 µm. On the Figure 4.2B, a representative profilometry of surface with a 1 mm^2 was presented. On this area, if smaller areas are selected and compared between them these areas present similar morphology. Therefore a homogenous DE coating on substrate surface was achieved at a sub-millimeter level.

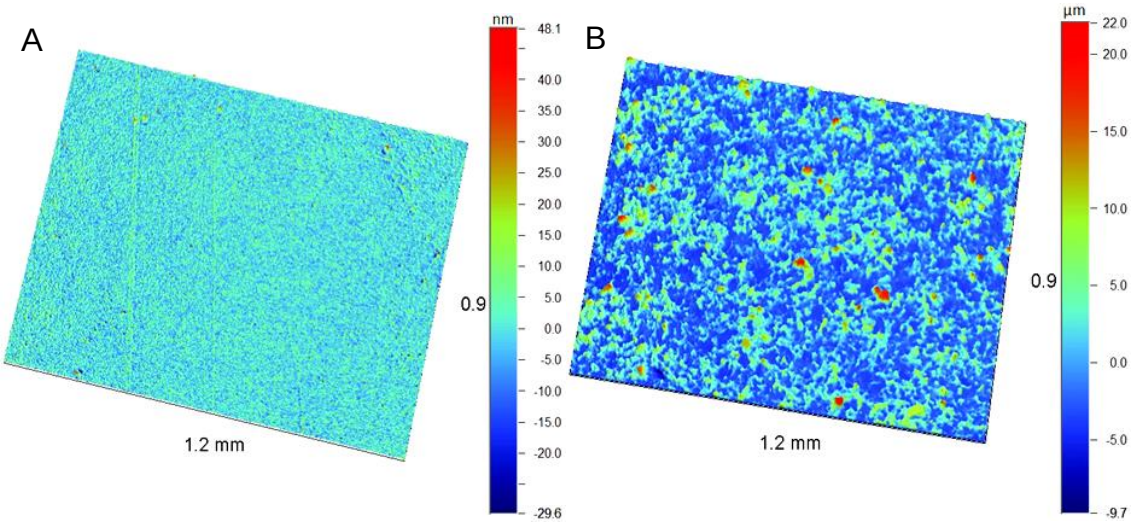

Figure 4.2: Optical profilometry images of the unmodified glass surface (A) and the glass substrate surface after the coating with DE (B). Images show an area of 0.9 mm × 1.2 mm (Magnification 5×).

The resulting modified surface has superhydrophilic properties – see Figure 4.3A_1. This behavior was the result of the combination between surface roughness and the hydrophilic nature of the

substrate.[19] In fact, the diatoms are hydrophilic due to the SiO_2 groups on their surface. To decrease the surface energy the substrate was subjected to fluorosilanization.[20] The chemical surface modification was confirmed by XPS analysis. As showed in Table 4.1 the surface with a DE layer (G2) is mostly constituted by oxygen and silica. The presence of carbon in unmodified glass (G1) and after DE coating (G2) is due to surface contamination.[21] Initially on the DE modified glass the fluorine content is almost inexistent and after the silanization process a peak indicating the presence of fluorine on the surface appears – compare Figure 4.3A_2 with Figure 4.3B_2.

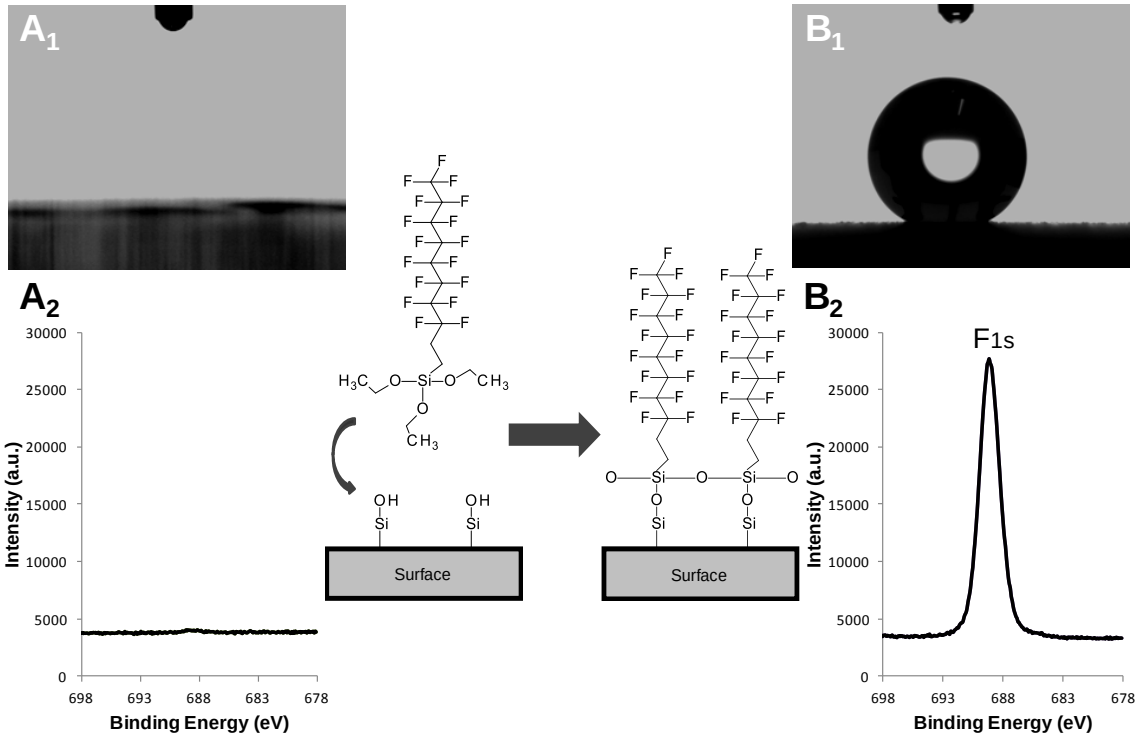

Figure 4.3: The chemical modification of the DE coated glass surface performed by a fluorosilane transform the initial superhydrophilic substrate (see water profile A_1) to superhydrophobic one (see water profile B_1). The chemical modification was confirmed by XPS analysis: the F_{1s} spectra of the two samples are presented in A_2 and B_2, respectively.

With the chemical modification the surface present a decrease on oxygen from 55.6% to 29.4% and a flour content of 31.8% - sample G3 in Table 4.1. Due to the changes on surface chemistry the initial superhydrophilic surface becomes superhydrophobic with a WCA of 151.0 ± 0.9˚ and a WCA hysteresis of 5.8 ± 1.4˚.

Table 4.1. Atomic composition of the studied substrates determined from XPS analysis. The present results are for unmodified glass (G1), glass substrate coated with DE (G2), DE coated glass chemically modified with PFDTS (G3) and DE/PFDTS modified glass after Argon plasma treatment (G4).

	Atomic Composition (%)			
Samples	C_{1s}	O_{1s}	Si_{2p}	F_{1s}
G1	19.3	48.9	22.4	0.5
G2	8.8	55.6	27.6	0.4
G3	18.9	29.4	16.7	31.8
G4	10.8	50.1	26.1	7.4

Two theories have been used to explain the occurrence of the SH behavior. The Wenzel model postulated that the hydrophobicity of a surface can be increased by providing roughness to the surface, if the initial smooth substrate is already hydrophobic. In this model, the surface is completely wet since water completely fills all the surface roughness to form a fully wetted interface.[22] The second model, called Cassie model, predicts that air can be trapped in the surface roughness, the air blocks water infiltration into the valleys of the rough surface and the water droplet is partially suspended by air pockets.[9, 23, 24] For this model, the relation between WCA of the rough surface (θ^*) and the WCA of the smooth surface (θ) is given by the Cassie–Baxter equation:

$$\cos\theta^* = f(1+\cos\theta) - 1 \quad (1)$$

where f is the area fraction of the liquid–solid contact. As the SH substrate obtained in this work showed a lower WCA hysteresis we will assume that the Cassie model could explain its wettability properties. As the WCA of the smooth glass surface modified by fluorosilane was 112.7 ± 2.4°, we can estimate that f = 0.2.

We hypothesis that it is possible to use the same strategy to produce superhydrophobic surfaces using other kind of substrates, such as polymers. Experiments were carried out in order to modify

a polystyrene (PS) substrate with DE. The PS was chosen due to be an amorphous material and when heated the PS undergoes a glass transition to a rubbery state at a relatively low temperature. One of the main vantages of PS is that it is both inexpensive and very accessible material, almost of labs use Petri dishes that are made of PS. The strategy is to melt superficially the substrate to bind DE to the surface – see Figure 4.1B$_2$. In the glass case, first the substrate was coated with DE and after that the coated surface was modified with a fluorosilane. However using PS as substrate, the chemical modification of DE was performed prior the deposition onto the PS that occurs at a temperature sufficiently low to maintain the properties of the fluorosilane. The binding process was carried out applying pressure over the surface with the DE layer to avoid PS substrate deformation due to temperature. As the PS has a glass transition temperature of 80-120 °C, using a temperature of 90 °C the PS exhibits a considerable viscoelastic behavior.[25] Appling pressure on the DE layer over the substrate, the DE particles penetrate on the PS surface. Then with the temperature decrease the PS becomes rigid and the hydrophobic particles stay trapped on PS surface. Initially the PS, obtained from the Petri dishes, presents a hydrophobic behavior. After the treatment with the hydrophobic DE particles the PS shows superhydrophobic properties – see Figure 4.4. The modified PS substrate with DE present a WCA of 153.6 ± 3.1˚ and a WCA hysteresis of 3.3 ± 1.1˚.

After the chemical modification of the DE particles with PFDTS the obtained hydrophobic particles were analyzed by EDS. The chemical characterization reveals that the fluorine amount on particles was 2.8 ± 0.3%.

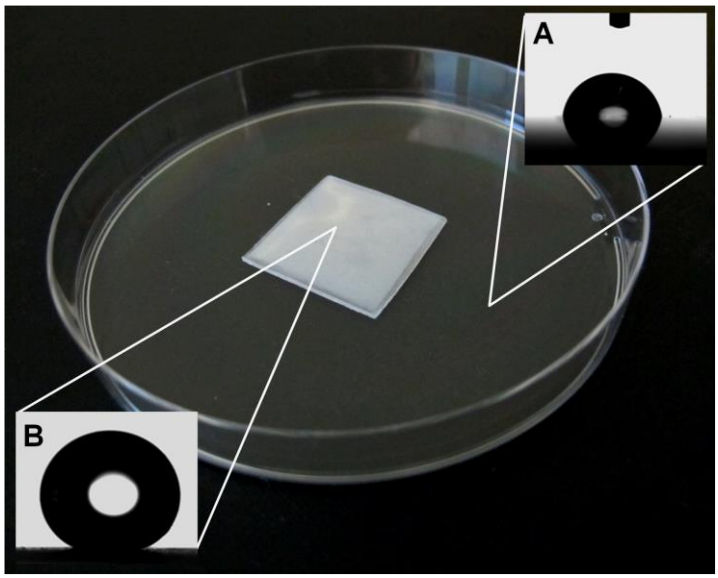

Figure 4.4: The polystyrene obtained from Petri dishes is a hydrophobic material (see the inset image A). After surface modification with hydrophobic DE particles the polystyrene becomes superhydrophobic (see the inset image B).

To modify the surface wettability of the obtained SH substrates we exposed the fluorinated glass surfaces to an Argon plasma treatment. By increasing the exposure time, the WCA of the SH surface decreased steadily down to the hydrophilic regime such phenomenon was previously observed in SH polymeric surfaces.[26] The relationship between plasma treatment time and the WCA on the glass substrate surface is showed in Figure 4.5.

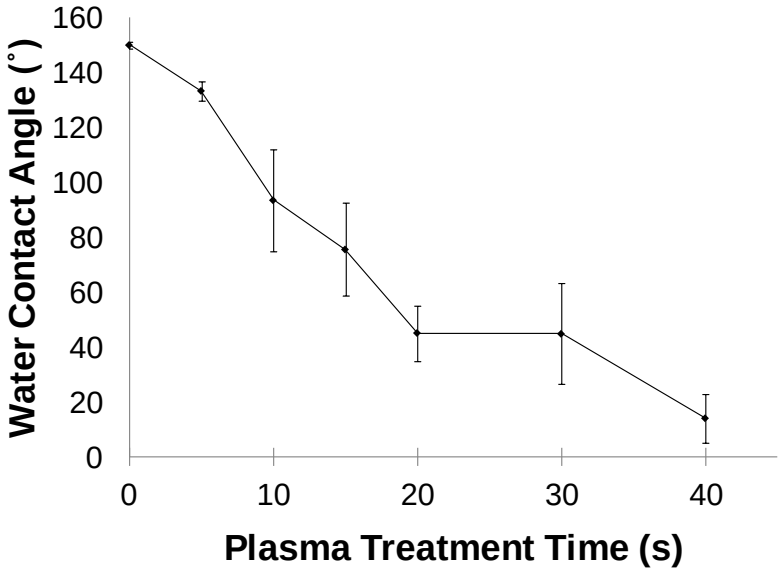

Figure 4.5: Influence of Argon plasma treatment time on the WCA of the initial SH surface using the glass substrate.

When a fluoropolymer is treated by plasma both surface defluorination and oxidation occurs, during which CF_2 carbons are changed by CF, CH_2, C=O and C–O carbons.[27, 28] We believe that the fluorinated SH surface experienced a similar process. The chemical state of carbon on the obtained surfaces was analyzed by XPS before and after plasma treatment (samples G3 and G4 respectively) and the collected results are presented in Table 4.2.

Table 4.2. Chemical state assessment of carbon functional groups on surface of DE coated glass chemical modified with PFDTS (G3) and DE/PFDTS modified glass after Argon plasma treatment (G4).

		C_{1s}				
		C-C, C-H	C-O	O=C-O	CF_2	CF_3
Binding Energy (eV)		285.0	286.5±0.3	289.0±0.2	291.5±0.3	293.8±0.3
Samples	G3	21.7%	10.5%	8.8%	48.3%	10.7%
	G4	61.1%	14.6%	10.1%	10.3%	3.8%

The relative content of CF_2 and CF_3 carbons decreases and C-H, C-O and O=C-O carbons increase with plasma treatment. With this treatment the fluorine content on the surface decreases strongly and a new specie in the F1s spectrum at energy 685.5 eV is observed, corresponding to the bond of type Si-F – see Figure 6. Due to defluotination combined with the surface oxidation the surface energy increases and consequently also the surface wettability. After plasma surface modification the surface WCA remains stable until at least 5 days.

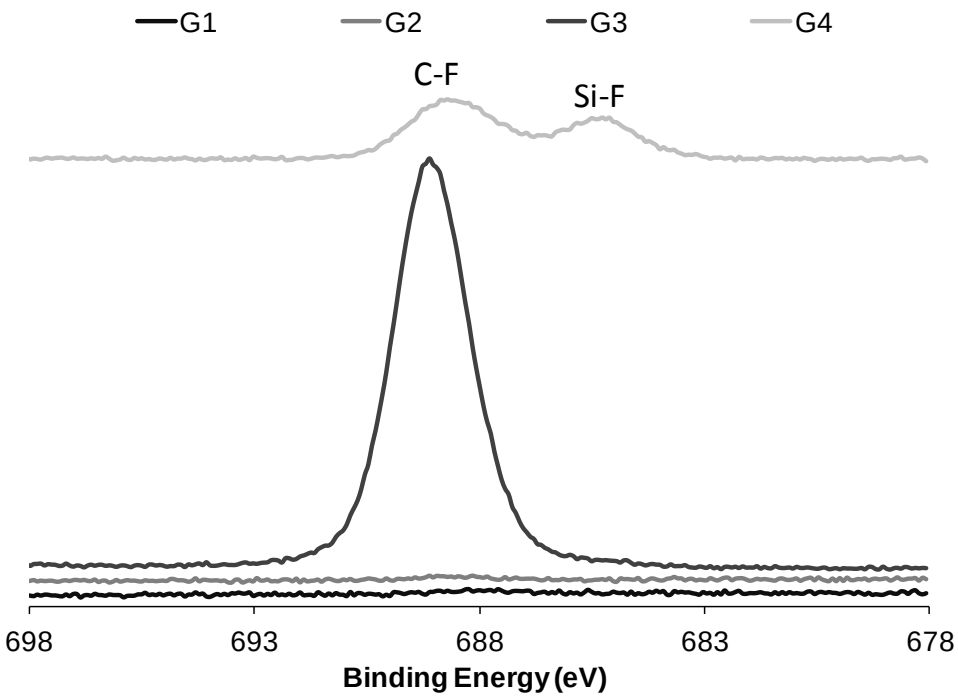

Figure 4.6: XPS F_{1s} spectra comparison between the different samples: unmodified glass (G1), glass substrate coated with DE (G2), DE coated glass chemical modified with PFDTS (G3) and DE/PFDTS modified glass after Argon plasma treatment (G4).

Surface modification can be performed in selected areas on the surface, so that patterns on the surface can be created. Using appropriate hollowed masks we can modify only specific areas on the surface. We used masks of plastic sheets in which different shapes were cut, namely squares, circles, lines or triangles. The masks were placed over the SH glass substrate and the ensemble was subjected to Argon plasma treatment. The exposed regions gave rise to hydrophilic features with the same geometry in the substrate. Such wettable regions can be wetted and support the confinement of liquids that will not transpose to the surrounding superhydrophobic regions due to the high contrast in surface tension. The patterning of wettable spots with three distinct geometries is shown in Figure 4.7A_1-A_3. Through this procedure we can produce platforms with imprinted patterns with potential to be used in high-throughput screening applications, open microfluidics and gel fabrication with different shapes, for example. The platform can also be used to generate gradients of different materials in an easy and fast way – see Figure 4.7A_4.

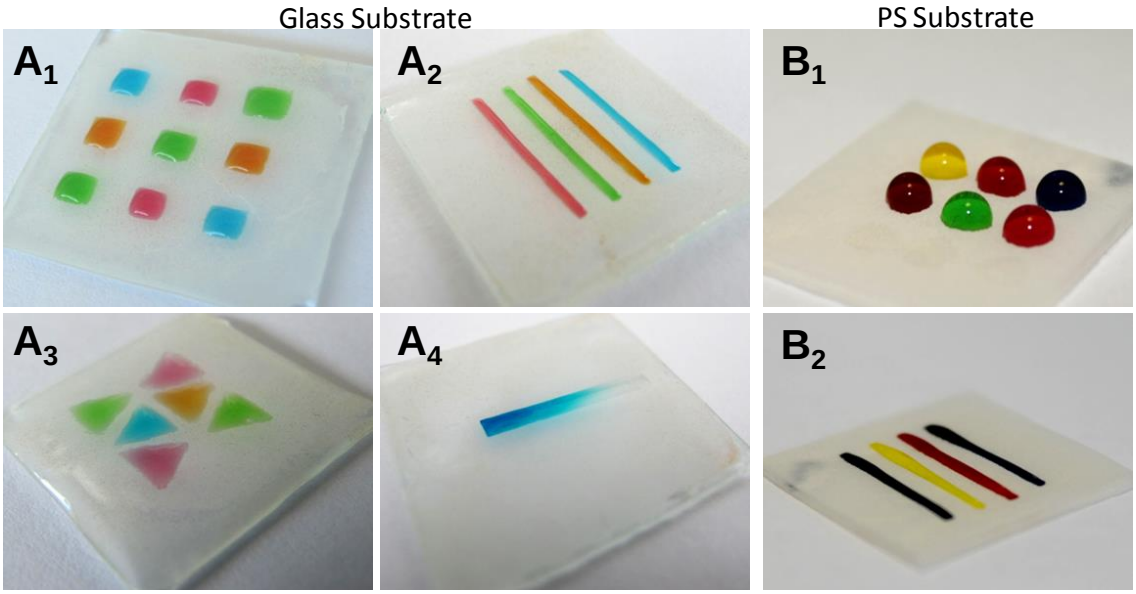

Figure 4.7: Hydrophilic patterns with different shapes and able to confine liquid volumes can be imprinted on the SH glass surfaces (A_1–A_3), suck as on the SH polystyrene surfaces (B_1-B_2). Surfaces with channel-like patterns can be used as platforms to produce material gradients (A_4). The patterns on surface was produced by Argon plasma treatment using masks with the desired shapes.

The hydrophilic stripe imprinted on surface should be prewetted with a solution A. Then using a pipette a solution B can be dropped at one end of the prewetted stripe. The solution B spreads along to the fluid stripe and by convection generates a gradient of material B on the material A. It was proposed that such surface-tension-driven centimeter scale gradients could be used in diagnostics, cell behavior studies or drug screening.[29] In a similar manner on the PS superhydrophobic surfaces wettable regions can also be patterned – see Figures 4.7B_1 and 4.7B_2. The surface modification was also performed by Argon plasma treatment. Due to the possibility of applying the strategy reported on this work in different kinds of substrates, we can envisage the fabrication of devices exhibiting SH surfaces with very distinct properties, aimed to use in different applications.

4.5. Conclusion

We showed here the possibility to produce superhydrophobic surfaces using diatomaceous earth. The natural nano/micro-structure of the silica objects provided the necessary rough topography for the surface. After coating a glass surface with diatomaceous earth the desired hierarchical structure on the surface was obtained due to the anatomic characteristics of the diatom exoskeleton. The wettability of the produced superhydrophobic surfaces can also be precisely controlled by exposing the substrates to plasma treatment for specific times. The control in space of the plasma treatment can be used to imprint hydrophilic patterns on the superhydrophobic surface with well-defined geometries. It was also showed that the proposed strategy could be applied in other substrates, such as polystyrene. This open the possibility to produce superhydrophobic surfaces for specific applications through the choice of the most convenient substrate.

4.6. Acknowledgments

This work was carried out under the scope of the EU 7th Framework Programme (FP7/2007-2013) under grant agreement no. FP7-KBBE-2010-4-266033 (SPECIAL). N. M. Oliveira acknowledges the financial support from Portuguese Foundation for Science and Technology – FCT (Grant SFRH/BD/73172/2010), from the financial program POPH/FSE from QREN.

4.7. References

1. Roach, P.; Shirtcliffe, N. J.; Newton, M. I., Progess in superhydrophobic surface development. *Soft Matter* **2008,** *4*, 224-240.

2. Zhang, X.; Shi, F.; Niu, J.; Jiang, Y. G.; Wang, Z. Q., Superhydrophobic surfaces: From structural control to functional application. *Journal of Materials Chemistry* **2008,** *18*, 621-633.

3. Oliveira, N. M.; Neto, A. I.; Song, W. L.; Mano, J. F., Two-dimensional open microfluidic devices by tuning the wettability on patterned superhydrophobic polymeric surface. *Applied Physics Express* **2010,** *3*.

4. Neto, A. I.; Custodio, C. A.; Song, W. L.; Mano, J. F., High-throughput evaluation of interactions between biomaterials, proteins and cells using patterned superhydrophobic substrates. *Soft Matter* **2011,** *7*, 4147-4151.

5. Bhushan, B.; Jung, Y. C., Natural and biomimetic artificial surfaces for superhydrophobicity, self-cleaning, low adhesion, and drag reduction. *Progress in Materials Science* **2011,** *56*, 1-108.

6. Guo, Z. G.; Liu, W. M.; Su, B. L., Superhydrophobic surfaces: From natural to biomimetic to functional. *Journal of Colloid and Interface Science* **2011,** *353*, 335-355.

7. Oliveira, M. B.; Salgado, C. L.; Song, W. L.; Mano, J. F., Combinatorial on-chip study of miniaturized 3d porous scaffolds using a patterned superhydrophobic platform. *Small* **2013,** *9*, 768-778.

8. Barthlott, W.; Neinhuis, C., Purity of the sacred lotus, or escape from contamination in biological surfaces. *Planta* **1997,** *202*, 1-8.

9. Cassie, A. B. D.; Baxter, S., Wettability of porous surfaces. *Transactions of the Faraday Society* **1944,** *40*, 0546-0550.

10. Chen, P. H.; Hsu, C. C.; Lee, P. S.; Lin, C. S., Fabrication of semi-transparent super-hydrophobic surface based on silica hierarchical structures. *Journal of Mechanical Science and Technology* **2011,** *25*, 43-47.

11. Tsai, P. S.; Yang, Y. M.; Lee, Y. L., Hierarchically structured superhydrophobic coatings fabricated by successive langmuir-blodgett deposition of micro-/nano-sized particles and surface silanization. *Nanotechnology* **2007,** *18*.

12. Sun, M. H.; Luo, C. X.; Xu, L. P.; Ji, H.; Qi, O. Y.; Yu, D. P.; Chen, Y., Artificial lotus leaf by nanocasting. *Langmuir* **2005,** *21*, 8978-8981.

13. Yuan, Z. Q.; Chen, H.; Tang, J. X.; Gong, H. F.; Liu, Y. J.; Wang, Z. X.; Shi, P.; Zhang, J. D.; Chen, X., A novel preparation of polystyrene film with a superhydrophobic surface using a template method. *Journal of Physics D-Applied Physics* **2007,** *40*, 3485-3489.

14. Rabosky, D. L.; Sorhannus, U., Diversity dynamics of marine planktonic diatoms across the cenozoic. *Nature* **2009,** *457*, 183-U73.

15. Yang, W. R.; Lopez, P. J.; Rosengarten, G., Diatoms: Self assembled silica nanostructures, and templates for bio/chemical sensors and biomimetic membranes. *Analyst* **2011,** *136*, 42-53.

16. Fei, B.; Hu, Z. G.; Lu, H. F.; Xin, J. H., Preparation of a panoscopic mimic diatom from a silicon compound. *Small* **2007,** *3*, 1921-1926.

17. Begum, G.; Rana, R. K.; Singh, S.; Satyanarayana, L., Bioinspired silicification of functional materials: Fluorescent monodisperse mesostructure silica nanospheres. *Chemistry of Materials* **2010,** *22*, 551-556.

18. Simpson, J. T.; D'Urso, B. R. July 10, 2012.

19. Koch, K.; Barthlott, W., Superhydrophobic and superhydrophilic plant surfaces: An inspiration for biomimetic materials. *Philosophical Transactions of the Royal Society a-Mathematical Physical and Engineering Sciences* **2009,** *367*, 1487-1509.

20. Shi, X. M.; Nguyen, T. A.; Suo, Z. Y.; Wu, J. L.; Gong, J.; Avci, R., Electrochemical and mechanical properties of superhydrophobic aluminum substrates modified with nano-silica and fluorosilane. *Surface & Coatings Technology* **2012,** *206*, 3700-3713.

21. Yu, Y.; Addai-Mensah, J.; Losic, D., Functionalized diatom silica microparticles for removal of mercury ions. *Science and Technology of Advanced Materials* **2012,** *13*, 015008.

22. Wenzel, R. N., Resistance of solid surfaces to wetting by water. *Industrial and Engineering Chemistry* **1936,** *28*, 988-994.

23. Marmur, A., The lotus effect: Superhydrophobicity and metastability. *Langmuir* **2004,** *20*, 3517-3519.

24. Wang, S.; Jiang, L., Definition of superhydrophobic states. *Advanced Materials* **2007,** *19*, 3423-3424.

25. Kim, H.; Vishniakou, S.; Faris, G. W., Petri dish pcr: Laser-heated reactions in nanoliter droplet arrays. *Lab on a Chip* **2009,** *9*, 1230-1235.

26. Song, W. L.; Veiga, D. D.; Custodio, C. A.; Mano, J. F., Bioinspired degradable substrates with extreme wettability properties. *Advanced Materials* **2009,** *21*, 1830-+.

27. Inagaki, N.; Narushima, K.; Yamamoto, T., Surface modification of tetrafluoroethylene-perfluoroalkyl vinylether copolymer (pfa) by plasmas for copper metallization. *Journal of Applied Polymer Science* **2002,** *85*, 1087-1097.

28. Hara, Y.; Ooka, K.; Zettsu, N.; Yamamura, K., Relationship between peroxide radical species on plasma-treated pfa surface and adhesion strength of pfa/electroless copper-plating film. *Current Applied Physics* **2012,** *12*, S38-S41.

29. Hancock, M. J.; He, J. K.; Mano, J. F.; Khademhosseini, A., Surface-tension-driven gradient generation in a fluid stripe for bench-top and microwell applications. *Small* **2011,** *7*, 892-901.

Chapter 5

Open Fluidics: A Cell Culture Flow System Developed Over Wettability Contrast-Based Chips

This chapter is based on the following publication:

Nuno M. Oliveira; Rui L. Reis; João F. Mano. Open Fluidics: A Cell Culture Flow System Developed Over Wettability Contrast-Based Chips. *Submitted.*

5.1. Abstract

Biological tissues are recurrently exposed to several dynamic mechanical forces that influence cell behavior. On this work, we focused particularly on shear stress forces induced by a fluid flow. The study of flow-induced effects on cells lead to important advances in cardiovascular, cancer, stem cell and bone biology understanding. These studies were performed using cell culture flow (CCF) systems, mainly parallel plate flow chambers (PPFC) and microfluidic systems. Here, we propose an original CCF system based on the open fluidics concept. The system was developed using a planar superhydrophobic (SH) platform of polystyrene with hydrophilic paths on its surface. The paths worked as channels to drive cell culture medium flows without using walls for liquid confinement. The liquid streams were controlled just based on the wettability contrast on top of the developed chip. To validate the proposed concept, we studied the effect of the shear stress stimulus in the osteogenic differentiation of C2C12 myoblast cells. Combining bone morphogenic protein (specifically BMP-2) stimulation with this mechanical stimulus, a synergistic effect of these stimuli combination was found on osteoblast differentiation of C2C12 cells. This synergistic effect was confirmed by the enhancement of alkaline phosphatase (ALP) activity, a well-known early marker of osteogenic differentiation, for the combined stimulation. The proposed CCF system showed to combine some characteristics and advantages of both PPFC and microfluidic systems. For these reasons, we believe that the presented chip has high potential to achieve widespread use in different biological studies.

5.2. Introduction

Biological tissues are often exposed to several dynamic mechanical forces, namely hydrostatic compression, fluid shear stress, mechanical tension, compression, and bending.[1] Wherein, the cellular response to specific mechanical stimuli is called of mechanotransduction.[2, 3] Studies in cell mechanobiology demonstrated that mechanical forces have important influence regulating cell decision events, such as cell proliferation and growth, cell migration, shape modulation, differentiation, and apoptosis.[1, 2, 4]

In particular, shear stresses result from the intermolecular friction forces of a fluid acting on a body in the path of that fluid. Fluid shear stress plays a significant role in regular physiology. An obvious example is what happens in the blood vessels. Increasing the blood flow rate, blood vessels are able to increase its diameter in order to ensure a constant blood pressure. This vasodilatation process depends on the response of endothelial cells (EC) to the shear stress inflicted by blood flow.[3] Studies of flow-induced effects on mammalian cells lead to important advances on the understanding of biological processes in cardiovascular biology,[5] cancer,[6-9] stem cell,[1, 10, 11] bone biology,[3, 12] and others.[2, 4]

There are basically two generations of cell culture flow (CCF) systems to study the shear stress effect on adherent cells. The first CCF systems present macroscale dimensions, whereas the second generation have moved to the miniaturization with the appearing of the microfabrication techniques.[5] At the macroscale, the parallel plate flow chamber (PPFC) and variations on its basic design are the most commonly used systems.[4] PPFC systems usually consist of two plates in which fluid flows between and with a silicon gasket separating the plates to determine the height of the flow path. Adherent cells are placed and cultured in one of the plates, usually over glass slides, and then placed into the chamber. Typically, the dimensions of PPFC are in the order of several centimeters for width and length and hundreds of micrometers for height.[13-16] Using

microfabrication techniques, namely soft lithography, distinct microscale-based CCF systems were developed for studying the shear stress influence on adherent cells.[2, 5] These microfluidic systems claim to offer higher versatility, possibility for high-throughput studies and precise control over all chemical and mechanical stimuli, among others advantages.[4, 5]

Here, we propose an innovative CCF system based on the open fluidics concept engineered over a planar superhydrophobic (SH) platform. Open fluidics consists in the use of small fluid volumes which are not enclosed in channels, presenting large air/liquid interfaces.[17] Some examples are a droplet on a flat surface,[18, 19] thin films,[20] ribbons of fluid,[21, 22] or flow in grooves.[23, 24] In our case, we can spatially confine liquid flows by patterning wettable strips on polymeric SH surfaces. Similar platforms, where individual liquid streams were guided only by the wettability contrast on a planar substrate, were previously reported.[25-27] However, to best of our knowledge, this is the first time that a fluidic platform based on the wettability contrast was developed to study the shear stress effect on adherent cells. A platform consisting of a polystyrene SH planar surface with hydrophilic parallel paths on top was used. On the paths, adhered cells were exposed to shear stress stimuli inflicted by the culture medium flowing over the cell layer. For proof of concept, we studied the effect of this mechanical stimuli in the osteoblast differentiation of C2C12 myoblasts, a mouse adherent myoblast cell line. We hypothesize that the developed platform has high potential to achieve widespread use in the biological laboratories, due to combine characteristics from both generations of CCF systems, such as we discuss forward.

5.3. Materials and Methods

5.3.1. Preparation of the superhydrophobic surfaces with wettable paths

Polystyrene (PS) superhydrophobic surfaces were prepared as previously reported.[25] PS (184K, Styrolution) was dissolved in tetrahydrofuran (THF; Sigma) at a concentration of 70 mg/mL. This solution was then mixed at a ratio of 2:1.3 (v:v) with absolute ethanol. The mixture was vigorously shaken, until it became transparent. Pristine PS substrates were protected with strips of stickers with 30 mm x 2 mm separated by 4 mm, based on a previously reported patterning protocol.[28] The PS solution prepared in THF and ethanol was dispensed in the substrates. The excess of solution was then removed and the PS substrates were immersed in absolute ethanol. After the drying of the substrates, the obtained PS superhydrophobic (PS-SH) surfaces were modified with 1H,1H,2H,2H-perfluorodecyltriethoxysilane (PFDTS, 97%; Sigma) by immersion for up to 48 hours in 1% (v/v) PFDTS solution in absolute ethanol, after air plasma treatment for 30 seconds at 30 W (Plasma Prep5, Gala Instruments).[29] Then the chemically modified substrates were washed with absolute ethanol to remove the unreacted PFDTS and fluorinated superhydrophobic (F-SH) surfaces were obtained. Finally, the stickers were removed using tweezers and the regions covered by the stickers remained untreated and transparent.

5.3.2. Surface Characterization

The morphology of the samples was analyzed using scanning electron microscopy (SEM; JSM-6010 LV, JEOL). To confirm the chemical modifications on the different substrate surfaces, energy dispersive spectroscopy (EDS; INCAx-Act, PentaFET Precision, Oxford Instruments) analysis were performed. The water contact angle (WCA) was also determined for the different surfaces produced over the PS substrates. The WCA was measured in a OCA 15+ goniometer (DataPhysics Corporation) at room temperature. The WCA was measured by a sessile drop method with a 6 μL water droplet. The WCA for the different surfaces (PS, SH-PS and F-SH) was also monitored during

48 hours that the samples were submerged on Dubbelco's modified essential medium (DMEM; Invitrogen) with 10% (v/v) of fetal bovine serum (FBS; Gibco).

5.3.3. Modification of the paths surface by plasma treatment

Surface treatment using a plasma reactor Plasma Prep 5 (Gala Instruments) was performed in order to increase paths hydophilicity. Air was used such as the operational gas and the pressure in the reactor chamber was controlled in the range of 0.1–0.2 mbar. The treatment was performed using a power of 30 W and different time periods of treatment were tested on pristine PS. Stencil masks were used to expose only the desired areas to the plasma treatment. For cell confluence assessment, cell number quantification and osteogenic differentiation experiments, chips with four hydrophilic paths (previously modified by a 30 seconds plasma treatment) were used.

5.3.4. Injection of dye on liquid stream to assess flow regime

Using as the base chips with hydrophilic paths (described before) and the fluid system described forward, a setup was developed to perform a dye injection to assess flow regime. Taking advantage from the direct access to the liquid stream on the paths on the chip, a small diameter needle (30 gauge syringe needle) was placed inside of the liquid rivulet. On the liquid stream, a dye of blue color was injected. We used a dye flow rate of 5 μL/s controlled by a syringe pump (NE-1000 Programmable Single Syringe Pump). A digital camera (Canon Powershot G12) was used to record by video the dye behavior for further analysis. Then, video frames where the dye profile was completely developed on the water stream were selected. The obtained images were analyzed in grayscale and the dye dispersion on the liquid flow was measured by the ImageJ software (NIH, USA). Dye dispersion profile in the interior of the liquid stream was analyzed for different liquid flow rates in the range 0.5–3 mL/min.

5.3.5. Fluidic system for feeding the chip with hydrophilic paths

The fluidic system consists in a peristaltic pump, four pulsation dampeners (one per channel), tubes and a SH platform with four paths. The liquid flow was used in a closed loop circulation for each channel and the used liquid volume per channel was 3 mL. To prevent the pulsatile flow generated by the peristaltic pump, a pulsation dampener was introduced on the fluidic system. The liquid flow rate was precisely controlled by a peristaltic pump of four channels (Ismatec REGLO Digital MS-4/6). Hydrophilic glass needles were used to feed and extract the liquid from each channel of the chip. To perform cell culture on the developed chip ensuring sterile conditions, a home-made incubation chamber was built that guaranteed a perfectly sealed environment and included an entrance for air circulation through a sterile syringe filter with a 0.22 μm pore size.

5.3.6. On-chip cell culture

A mouse myoblast cell line (C2C12 cells) was used, aiming to study the effect of the shear stress stimulus in its osteogenic differentiation. Cell expansion was carried out in DMEM with 10% (v/v) FBS and 1% (v/v) antibiotic/antimycotic (Gibco). Cell culture media were exchanged every 2 days. The wettability contrast-based chips were sterilized by immersion in ethanol 70% overnight. The SH platforms were then dried inside a laminar flow chamber before the cell culture. Chip paths were coated with fibronectin protein (EMD Millipore) by placing 35 μL per path of fibronectin solution at 25 μg/mL for 15 minutes. Cell suspensions at a density of $5x10^5$ cells/mL were dispensed in each wettable path of the chip with a volume of 35 μL. After overnight incubation for cell adhesion, on-chip cell culture was performed under static or dynamic conditions. In static conditions, cells were culture for 48 hours on the paths of the chip. The dynamic conditions consisted in 24 hours of initial static cell culture followed by 24 hours of cell culture under a constant flow of cell culture medium. In both conditions the cell culture medium was changed after 24 hour of culture. On the experiments to study the effect of shear stress stimulation on C2C12 osteoblast differentiation, the

cell culture medium was supplemented with 200 ng/mL of BMP-2 (Invitrogen). Different times of contact between cells and the supplemented medium were tested, namely 24 or 48 hours such as schematically represented on Figure 5.5.

5.3.7. Cellular characterization on the paths of the chip

The formation of cellular layers and respective morphology on the wettable paths was assessed after the fixation of the cells with 10% formalin. Cells' nuclei were stained with 4',6-diamidino-2-phenylindole (DAPI; Sigma, diluted 1000x). F-actin was stained with phalloidin-tetramethyl rhodamine isothiocyanate (Phalloidin; Sigma, diluted 1000x). Images of the cell layers were acquired using both reflected fluorescent light and visible light microscopy (Axio Imager Z1, Zeiss).

5.3.8. Quantification of alkaline phosphatase (ALP) activity

ALP is frequently used as an early biochemical marker of osteogenic differentiation. The cytochemical detection of ALP activity was performed using fast violet B salt (Sigma) in solution at 0.25 mg/mL diluted in naphthol AS-MX phosphate alkaline solution (Sigma), flowing the manufacturer assessment procedure. The ALP presence was revealed by the appearing of a violet staining on channels. Staining area for the different conditions was measured by ImageJ software and normalized with the respective control condition of reference.

5.3.9. Statistical analysis

All data are presented as means ± standard deviations. The data was analyzed using one way ANOVA with Tukey's post-hoc test and p values <0.05 were deliberated as statistically significant.

5.4. Results and Discussion

The initial SH platform was produced by a one-step procedure, being both surface hydrophobization and patterning performed simultaneously. Strips of stickers were used to protect the desired areas from being modified by the phase separation process that provide superhydrophobicity to the surface (Figure 5.1A). Then, a polystyrene superhydrophobic (PS-SH) surface was obtained and presenting a water contact angle (WCA) of 153 ± 2°. This feature was reached by conferring micro- and nanoroughness to the pristine polystyrene (PS) surface,[30, 31] such as is illustrated by the SEM images (Figure 5.1A). Then the surface oxidation was promoted by air-plasma treatment,[32] and the plasma-oxidized polystyrene was chemically modified by a fluorosilanization process. During this process, covalent binding occurred between the fluorosilane molecule and the –OH groups formed on the PS-SH surface by the plasma modification.[33, 34] The fluorinated superhydrophobic (F-SH) surface exhibited a high WCA of 163 ± 3°, due to the low surface free energy of the fluorosilane.[35] The chemical surface modification was confirmed by EDS analysis with the appearing of two peaks, indicating the presence of fluorine and silicon both from the fluorosilane molecule (Figure 5.1A). This chemical surface modification showed to be essential to increase the surface resistance to be wetted by the cell culture medium. Samples of PS, PS-SH and F-SH surfaces were submerged on cell culture medium with 10% of fetal bovine serum (FBS) for up to 48 hours, during which the WCA of the tested samples was monitored – see Figure 5.1B. The detected changes on WCA are attributed to protein adhesion on the surface, from the FBS present in the medium. Superhydrophobicity showed to be fundamental for preventing protein adhesion for at least 4 hours.[36, 37] Wherein the surface resistance to protein adsorption was attributed to the trapped-air effect,[36] one important characteristic from the SH surfaces used here. The higher resistance to protein adsorption of F-SH surface comparing to PS-SH surface can be attributed to the different chemistry of the surface, namely to the fluorine presence that showed

to reduce the adsorption of proteins.[37] In the end of this two steps (Figure 5.1 A), the stickers were removed and a SH platform was obtained with straight, transparent and wettable paths. Due to the superhydrophobicity surrounding the protected areas, the liquid on top of the developed platform remained confine to the channel-shaped paths.

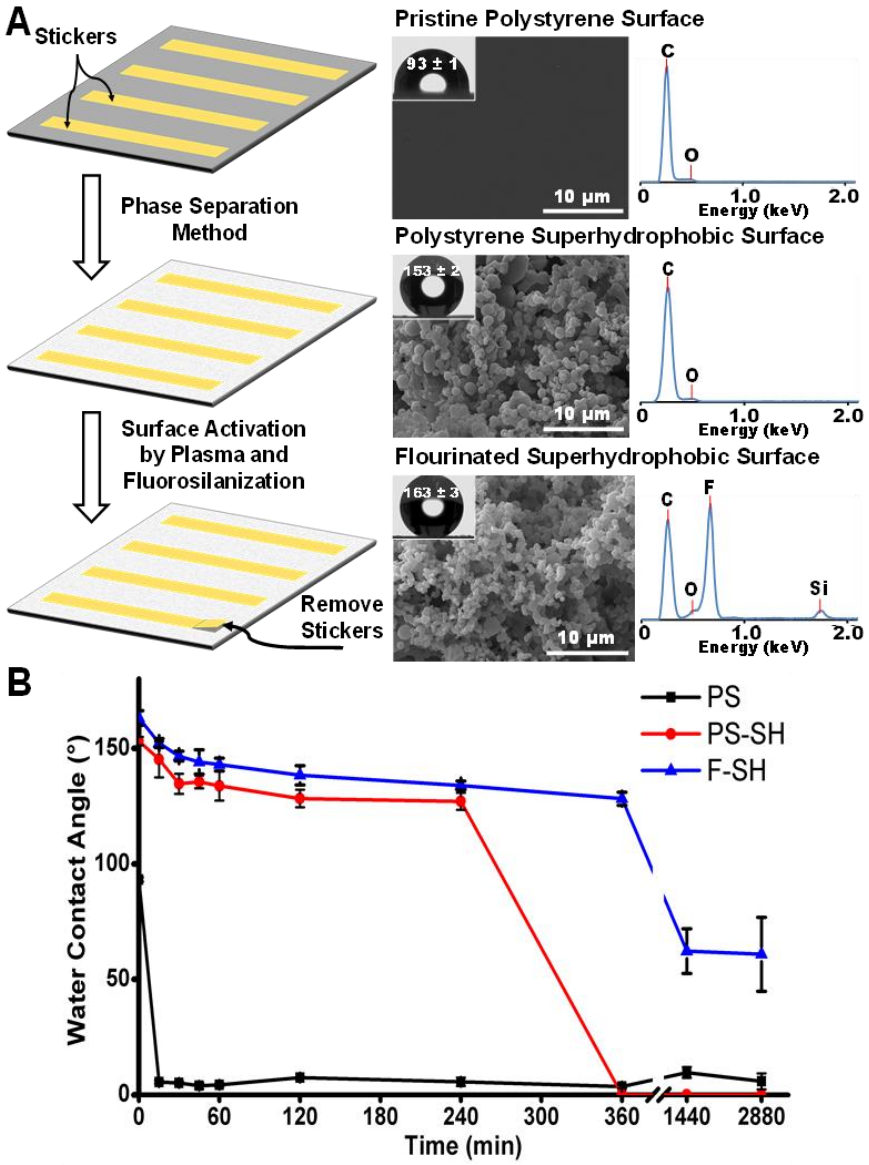

Figure 5.1: (A) Preparation of superhydrophobic (SH) platforms patterned with strips of wettable regions: first, several strips of stickers in a pristine polystyrene (PS) substrate were glued; second, the increase in roughness was achieved by a phase separation method such as illustrated by SEM images, and consequently inducing an increase of the surface hydrophobicity proven by the higher water contact angle showed on the images of the water droplets profiles; then the polystyrene superhydrophobic (PS-SH) surface was chemically modified through a fluorosilanization process

obtaining a fluorinated superhydrophobic (F-SH) surface, confirmed by EDS analysis with the appearing of both fluorine and silicon peaks, from the fluorosilane molecule; finally, wettable and transparent channel-shaped paths surrounded by a SH surface were obtained by removing the stickers. (B) Water contact angle monitoring over time of PS, PS-SH and F-SH surfaces submerged on cell culture medium with 10% of FBS for up to 48 hours.

The wettability contrast on the top of the SH platform made possible to control liquid fluid flows without using walls for the confinement. The flow rate of the liquid stream on the planar platform was controlled through a fluidic system powered by a peristaltic pump system. To classify the fluid flow concerning to flow regime – laminar or turbulent – the injection of dye was performed, by injecting a dye jet of low momentum.[38] If the dye forms a straight and smooth line this will be indicative of low flow velocities and a laminar regime. By contrast, if the dye forms turbidity on the fluid flow this will be a sign of a fully turbulent flow. In between of these two regimes, there is a transition regime that presents a mixed behavior. Taking advantage from the direct access to the flow stream allowed by this open fluidic chip, a home-made setup was constructed for the dye injection test (Figure 5.2A). A syringe pump was used to precisely control the dye injection rate on the flow stream and a digital camera was used to record by video the dye behavior for further analysis. Using water, several flow rates were tested in the range 0.5–3 mL/min (Figure 5.2B). After selecting video frames where the dye profile on the water stream was completely developed, the obtained images for each tested flow rate were analyzed. Analyzing images in grayscale, the dye dispersion on the liquid flow was measured at two distinct injection distances of the channel – lines (i) and (ii) in Figure 5.2B. Comparing the dye dispersion profile in both lines, similar profiles were obtained for the flow rates: 0.5, 1 and 2 mL/min. In the line (ii) in Figure 5.2B, the straight and smooth line formed by the dye on the liquid flow presented a larger width that can be attributed to the molecular diffusion of the dye between adjacent layers of the liquid.[39] For the flow rate of

3 mL/min, a diffuse line of the dye on the liquid flow was observed, being an indication that the transition regime was reached on this flow rate for the developed open fluidic system. We used fluid flow rates lower than 3 mL/min to perform the studies in laminar flow conditions. This choice was based on the fact that constant laminar flow is the most common situation used to study the effect of shear stress on cell behavior.[5, 6, 40]

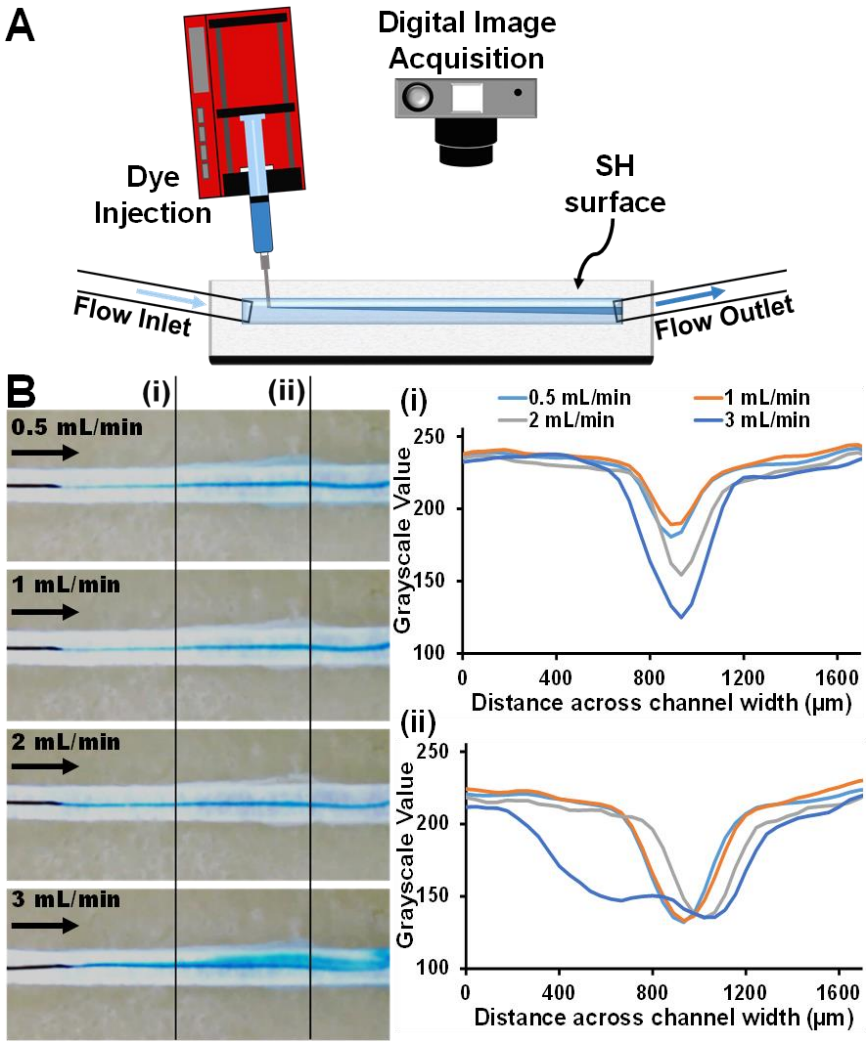

Figure 5.2: (A) Schematic representation of the home-made setup to perform the dye injection method to assess the flow regime – laminar, transition or turbulent flow. A syringe pump was used to control the dye injection rate and the results were recorded by video using a digital camera. (B) Representative video frame for each one of the water flow rates studied here and respective intensity profile of the dye dispersion in two distinct areas of the channel, represented by the lines (i) and (ii). Arrows on images indicate fluid flow direction.

Before, SH platforms with wettable patterns showed high versatility on biomedical applications,[41, 42] still this is the first time that these platforms are present as a CCF system. A simple CCF system was engineered that consist of a peristaltic pump, a pulsation dampener per channel, connection tubes and a SH platform (Figure 5.3A). The liquid flow in each channel was used in a closed loop circulation. Since the peristaltic pump generates a pulsatile flow, a pulsation dampener was introduced on the fluidic system to prevent the pulsatile flow. The air pocket trapped in the dampener had the role to absorb pulsations from the pump.[43] The SH platform was placed in a home-made incubation chamber perfectly sealed to perform cell culture studies, ensuring the sterility of the system out of the laminar flow chamber (Figure 5.3A).

As proof of concept, we present a system of four channels to show that the parallelization concept from microfluidics can also be applied here, using SH platforms. An advantage that second generation CCF systems claimed comparing with the PPFC systems, once parallelization allows to perform high-throughput studies increasing the efficiency of experimentation. Other advantage is that cross-contaminations between different conditions can be avoid by using separated channels. In our system, we used a few milliliters of cell culture medium, a midway volume if compared with microfluidics and PPFC systems. Once, in microfluidics is used a volume in the microliter range and in PPFC systems can be achieved hundreds of milliliters of cell culture medium. A general concern with the low volume of microfluidics is that sometimes it is not possible to detect some cellular metabolites using the conventional techniques and equipment available for biochemical analysis.[5] Our systems overcome this issue by using higher volumes than microfluidics. Simultaneously, comparing with the PPFC systems important cost savings can be archived by using lower volumes.

On the developed chips, the patterned paths were constructed with the dimensions of 30 mm of length and 2 mm width. Cell culture medium was fed and extracted to the chip by glass needles

(Figure 5.3B). The use of hydrophilic needles was crucial to maintain the liquid rivulet stable, by preventing the occurrence of the dewetting phenomenon.[44] Other important step on chip optimization it was to increase the paths hydrophilicity by air plasma treatment, using a stencil mask to expose only the channels area to plasma (Figure 5.3C). By controlling the exposure time to the plasma treatment, PS hydrophilicity was easily controlled (Figure 5.3D).

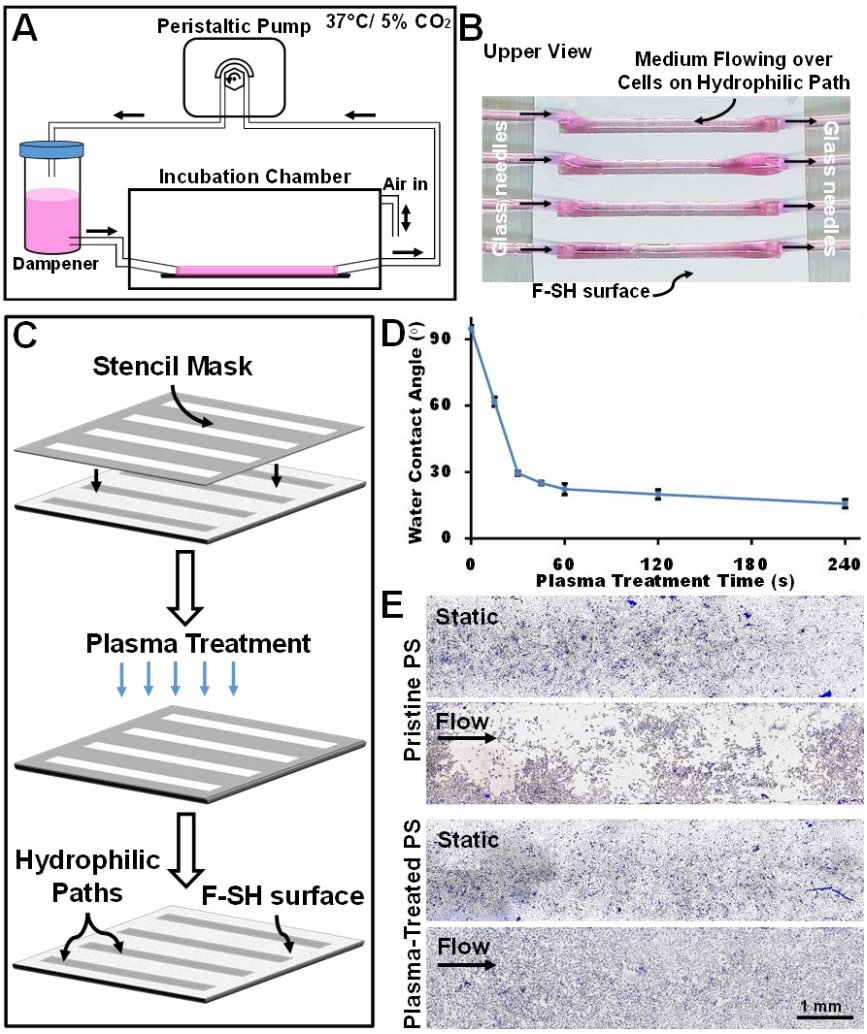

Figure 5.3: (A) Schematic representation of the home-made setup of a cell culture flow (CCF) systems based on planar superhydrophobic platforms with hydrophilic paths patterned on its surface. The CCF system comprised a peristaltic pump, a pulsation dampener for channel to prevent the pulsatile flow, tubes for connection and a SH platform of four parallel channels. The liquid flow in each independent channel was applied in a closed loop circulation. The SH platform was placed in a sealed incubation chamber to ensure the sterility of the system during the cell culture studies. (B) Using glass needles, cell culture medium was fed and extracted from each of the four independent

channels patterned on the chip. Cells were previously adhered to the hydrophilic paths and a continuous physical stimulus was applied by the continuous flow of cell culture medium over cells. (C) Paths hydrophilicity was increased by air plasma treatment, the selective exposure of the channels area to plasma was achieved using a stencil mask. (D) Paths hydrophilicity was precisely controlled by controlling the exposure time of pristine PS paths to the air plasma treatment. (E) Increasing paths hydrophilicity demonstrated to improve cell attachment that allowed cells to hold fluid flow conditions. Images comparing C2C12 adhered cells on both pristine PS and plasma-treated channels cultured in static conditions and under fluid flow conditions at low flow rate (0.5 mL/min) for up to 48 hours. Images are a combination of visible microscopy and fluorescence microscopy, where the fluorescent staining of cell nuclei (DAPI) is presented in blue. Arrows on images indicate fluid flow direction.

Increasing the wettability contrast between the channels and the superhydrophobic surrounding area, liquid rivulets more stable were reached.[45] To accomplish this requirement, pristine PS from the platform channels was treated by plasma for 30 seconds to reach a WCA of ~30°. Other important parameter to control was the liquid volume on the hydrophilic paths that should be less than 47 μL. This theoretical volume was calculated considering that the liquid rivulet on the paths presented a geometry similar to half cylinder and ensured that the apparent contact angle on the surface is less than 90°.[21, 46] Controlling these two parameter, hydrophilicity and liquid volume, stable and uniform rivulets were obtained in static conditions that remained stable also in the fluid flow conditions studied here.

The step of increasing paths hydrophilicity demonstrated also to be necessary for the improvement of cell attachment and to be able to endure fluid flow conditions (Figure 5.3E). C2C12 myoblast cells previously adhered on pristine PS showed to detach at a low flow rate of 0.5 mL/min. After plasma treatment of the PS, cells showed to remain attach at the flow rate of 0.5 mL/min and even higher, such as presented in Figure 5.4.

After optimizing the SH platform and the fluidic system, cellular cultures were performed under dynamic conditions provided by the fluid flow and three different flow rates were studied: 0.5, 1 and 2 mL/min. Tests were made using chips with pre-adhered C2C12 myoblast cells on the hydrophilic paths and chips under static conditions were used as control. On this step, the relationship between culture medium flow rate and both cell confluence and density was analyzed (Figure 5.4).

Both cell confluence and cell density exhibited a similar tendency with the culturing conditions - see Figures 5.4A and 5.4B. Under dynamic conditions the area covered by cells and the cell number significantly decreased comparing with the static condition. After 48 hours of cell culture, the flow rates of 0.5 and 1 mL/min presented equivalent values and for 2 mL/min a significant decrease on cell confluence and cell density was observed. For a cell culture medium flow of 2 mL/min, it seems that cells were washed-out from the open channels on the SH platform.

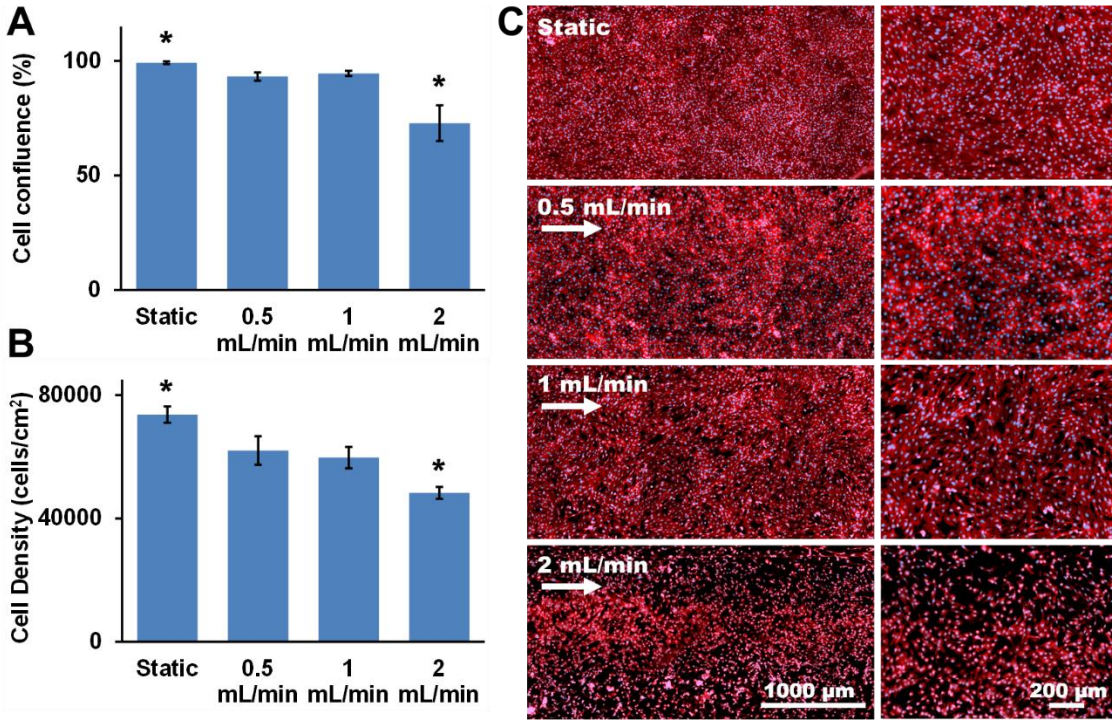

Figure 5.4: (A) Cell confluence determined by the percentage of area that was occupied by cells, upon 48h of culture under static conditions and using different fluid flow rates. (B) Cell densities for the different studied conditions. (C) Images illustrating confluence, density and morphology of C2C12 cells under static culture conditions and under shear

stress conditions provided by cell culture medium flow over the cells (48h of culture). Magnified images for each of the studied conditions are also showed. Cells were stained with DAPI on its nuclei and with Phalloidin on its filamentous actin. Arrows on images indicate fluid flow direction. Bars with * present values that are statistically different comparing with the other conditions for $p < 0.05$.

These differences on both cell confluence and density for the different tested conditions are illustrated by the images of Figure 5.4C. Cells presented a more elongated morphology when cultured under flow conditions. Shear stress stimuli were previously reported as the responsible for change the cell morphology, namely inducing cell alignment and cell elongation.[12, 40, 47, 48] To prove the concept that the developed SH platform can be used as the base for a CCF system, we chose C2C12 myoblast cells to study the influence of the shear stress stimuli on its osteoblastic differentiation. Previously, it was reported that C2C12 cells behavior was conditioned by both static and cyclic mechanical stretching.[49-52] In which, it was found a synergistic effect of mechanical stretching and bone morphogenic protein (specifically BMP-2) stimulation in the osteoblast differentiation of C2C12 myoblast cells.[51, 52] We hypothesize that a similar synergistic outcome can be observed by applying shear stress forces as mechanical stimulus, inflicted by cell culture medium flowing over the pre-adhered C2C12 cells. To determine the influence of this different stimulation on the osteoblast differentiation, ALP activity was assessed as a well-known early marker of osteogenic differentiation. ALP activity was detected directly on the chip by a colorimetric staining using an *in situ* detection procedure, performed after cell fixation on the open channels. The cytochemical detection of ALP was revealed with the appearing of a violet staining on channels. Several combinations between the mechanical stimulus (shear stress) and the biochemical stimulus (BMP-2) were studied – see Figure 5.5. Mechanical stimulus was performed by applying a cell culture medium flow of 1 mL/min and the biochemical stimulus by supplementing the cell

culture medium with 200 ng/mL of BMP-2. In all conditions cells were cultured by 48 hours, wherein the dynamic condition consisted in 24 hours of initial static cell culture followed by 24 hours of cell culture under a constant flow of cell culture medium. Different times of BMP-2 presence on the cell culture were also tested, namely 0, 24 and 48 hours.

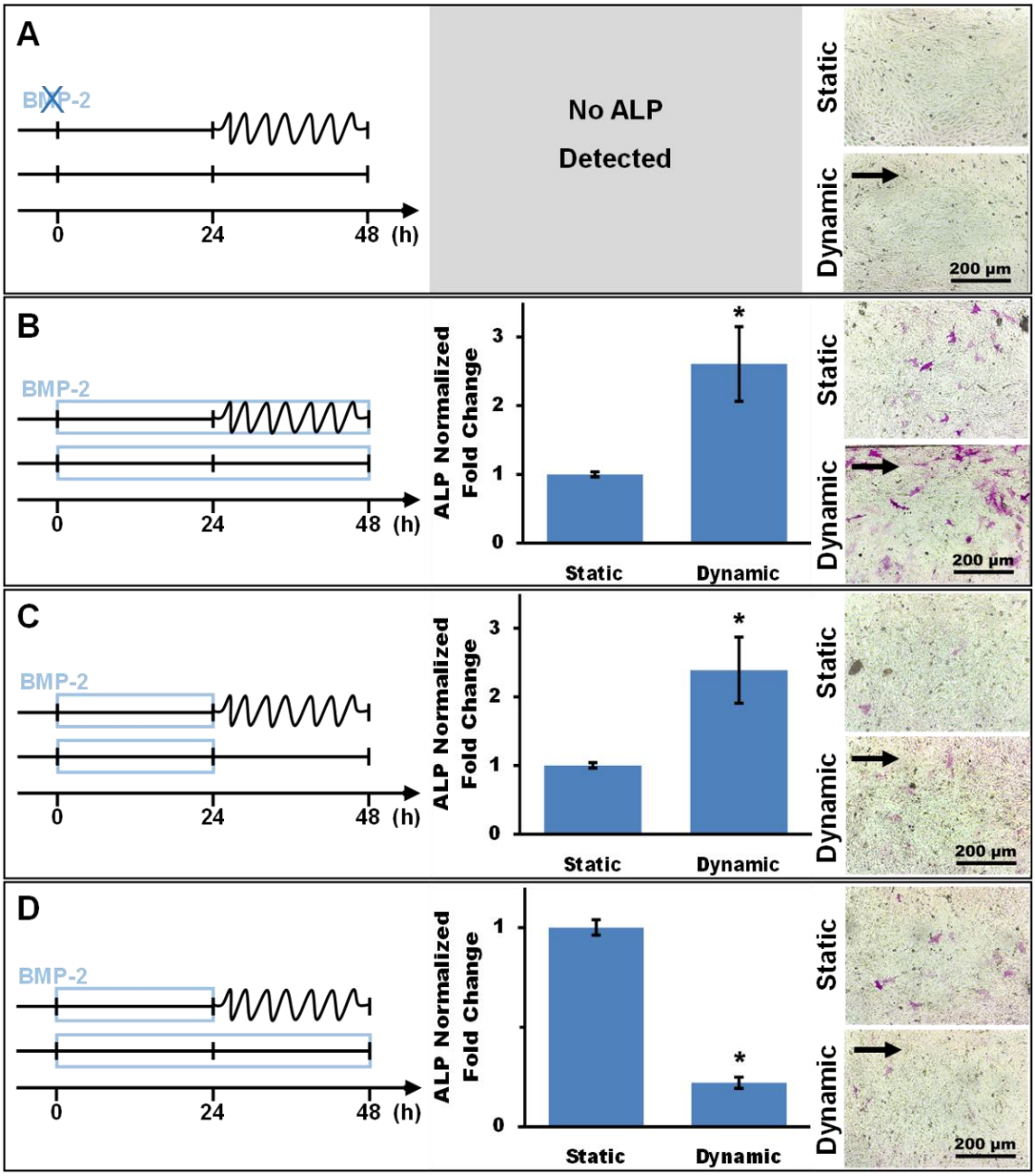

Figure 5.5: Different combinations between mechanical (shear stress) and biochemical (BMP-2) stimuli were tested for static and dynamic conditions. Static condition consisted in to perform cell culture on the open channels for 48 hours and dynamic conditions consisted in 24 hours of initial static cell culture followed by 24 hours of cell culture under a constant flow of cell culture medium. Schematic representation of the used experimental protocol, comparison

of the ALP activity levels between both static and dynamic conditions and representative imagens of microscopy are presented for each combination of stimuli. On images the violet staining indicates ALP activity. (A) Regular cell culture medium was used to study the isolated effect of the shear stress stimulus on the ALP activity of the C2C12 cells. (B) Supplemented medium with BMP-2 was used during the 48 hours of cell culture for both static and dynamic conditions. (C) Supplemented medium with BMP-2 was used only in the first 24 hours of cell culture for both conditions. (D) To compare the potency of the mechanical and biochemical stimuli on ALP activity levels, supplemented medium with BMP-2 was used in the first 24 hours of cell culture for the dynamic condition and during the 48 hours of cell culture for the static condition. Arrows on images indicate fluid flow direction. Bar values with * are statistically different comparing with the static conditions for $p < 0.05$.

For the conditions without BMP-2 stimulation, no violet staining was detected on the channels for both static and dynamic conditions (Figure 5.5A). Indicating that for the established conditions the mechanical stimulus alone did not encourage C2C12 differentiation into osteoblasts. Comparing the results of both static and dynamic conditions for cell cultured with BMP-2 for the 48 hours of culture, an enhancement in ALP activity was detected due to the mechanical stimulus (Figure 5.5B). Similar tendency was also detected by the same conditions but just using BMP-2 supplemented medium in the first 24 hours of culture (Figure 5.5C). The results clearly demonstrate that there was a synergistic effect by combining both stimuli, such as previously reported for the mechanical stretching stimulus.[51, 52] However comparing the dynamic condition using BMP-2 only in the first 24 hours of culture and the static condition using BMP-2 along all the culture time, less ALP activity was observed in cells exposed to mechanical stimulation versus those induced with BMP-2 alone for 48 hours (Figure 5.5D). Indicating that, such as previously reported, the mechanical stimuli (mechanical stretching and now shear stress) were less potent that a continued cell culture of C2C12 myoblast cells with BMP-2 to induce its osteogenic differentiation.[51, 52]

Using an open fluidic system for applications on cell culture under fluid flow conditions brings some important advantages. First, open fluidic chips allow direct and fully access to the culture channels before, during and after the application of flow. Such possibility makes easier to perform procedures such as cell seeding, cell fixation and permeabilization prior to immunostaining, protein extraction or culture media collection for molecular secretion measurements, for example. Then, due to the high air-liquid interface, there are no physical limitations to oxygen diffusion and allows also experiment with modified atmospheres where a precise control of the gas amount that reach cells is mandatory. Finally, the open fluidic chips are easy and cheap to produce, due to the proposed methodology but also to the used material, the PS. The PS offers the possibility to use the chips as disposable material for single use, ensuring simultaneously chemically resistance and optical transparency to aid visualization. In which may include real-time monitoring of live cells by designing a specific incubation camera to perform cell culture directly on a time-lapse video microscope. PS is also the most commonly used material in laboratory cultureware, because this material ensure their inertness to biological outcomes. In this work chips with four channels were produced for the proof-of-concept. However, we could envisage the production of supports with more channels permitting the independent monitoring of the effect of different culturing conditions, which would increase the throughput possibility of such technology.

5.5. Conclusion

In summary, we have reported a novel cell culture flow (CCF) system to study the shear stress effect on adherent cells, based on a planar superhydrophobic (SH) platform with hydrophilic paths patterned on its surface. On the paths, cells were pre-adhered and cultured under shear stress stimuli that was inflicted by the cell culture medium flowing over the cell layer. To show the pertinence of the proposed concept, we studied the influence of this mechanical stimuli in the

osteogenic differentiation of C2C12 myoblast cells. A synergistic effect between the mechanical and a biochemical stimuli on the osteoblast differentiation of C2C12 cells was found. Combining bone morphogenic protein (specifically BMP-2) stimulation with the shear stress, an enhancement on ALP activity was detected. On the optimization process of the developed system, the chemical surface modification of the SH platform with a fluorosilane and the increase of hydrophilicity of the channels revealed to be important for system robustness and flow stability. With the fluorosilanization process the surrounding area of the channel presented higher resistance to protein adhesion, which was crucial to maintain the liquid streams morphology and integrity along all the period of the dynamic culture. The increasing of the hydrophilicity of the paths combined with the glass needles, used to feed and extract the culture medium to the open chip, helped to increase liquid streams stability preventing the dewetting phenomena. A higher hydrophilicity of the cell culture channels showed to improve cell attachment and cells could hold higher cell culture medium flow rates. One characteristic of the developed chip was that until a flow rate of 2 mL/min the flow regime was laminar.

We believe that the presented work is a step forward on the potential applications of the patterned SH platform and on the CCF systems. SH platforms with wettable patterns on its surface have shown a high versatility on biomedical applications. Still, to best of our knowledge, this is the first time that this kind of platform was developed to study the shear stress effect on cell behavior. An interesting achievement of the proposed CCF system is that the SH platform with hydrophilic paths combined characteristics and advantages of both main systems used for cell culture under flow conditions, the parallel plate flow chambers and the microfluidic devices.

5.6. Acknowledgements

This work was financially supported by the European Research Council grant agreement ERC-2012-ADG 20120216-321266 for project ComplexiTE. N. M. Oliveira acknowledges the financial support from Portuguese Foundation for Science and Technology – FCT (Grant SFRH/BD/73172/2010), from the financial program POPH/FSE from QREN.

5.7. References

1. Hao, J.; Zhang, Y. L.; Jing, D.; Shen, Y.; Tang, G.; Huang, S. S.; Zhao, Z. H., Mechanobiology of mesenchymal stem cells: Perspective into mechanical induction of msc fate. *Acta Biomaterialia* **2015,** *20*, 1-9.

2. Polacheck, W. J.; Li, R.; Uzel, S. G. M.; Kamm, R. D., Microfluidic platforms for mechanobiology. *Lab on a Chip* **2013,** *13*, 2252-2267.

3. Mullender, M.; El Haj, A. J.; Yang, Y.; van Duin, M. A.; Burger, E. H.; Klein-Nulend, J., Mechanotransduction of bone cells in vitro: Mechanobiology of bone tissue. *Medical & Biological Engineering & Computing* **2004,** *42*, 14-21.

4. Shemesh, J.; Jalilian, I.; Shi, A.; Yeoh, G. H.; Tate, M. L. K.; Warkiani, M. E., Flow-induced stress on adherent cells in microfluidic devices. *Lab on a Chip* **2015,** *15*, 4114-4127.

5. Young, E. W. K.; Simmons, C. A., Macro- and microscale fluid flow systems for endothelial cell biology. *Lab on a Chip* **2010,** *10*, 143-160.

6. Rizvi, I.; Gurkan, U. A.; Tasoglu, S.; Alagic, N.; Celli, J. P.; Mensah, L. B.; Mai, Z. M.; Demirci, U.; Hasan, T., Flow induces epithelial-mesenchymal transition, cellular heterogeneity and biomarker modulation in 3d ovarian cancer nodules. *Proceedings of the National Academy of Sciences of the United States of America* **2013,** *110*, E1974-E1983.

7. Tong, Z. Q.; Cheung, L. S. L.; Stebe, K. J.; Konstantopoulos, K., Selectin-mediated adhesion in shear flow using micropatterned substrates: Multiple-bond interactions govern the critical length for cell binding. *Integrative Biology* **2012,** *4*, 847-856.

8. Kim, S.; Lee, H.; Chung, M.; Jeon, N. L., Engineering of functional, perfusable 3d microvascular networks on a chip. *Lab on a Chip* **2013,** *13*, 1489-1500.

9. Polacheck, W. J.; German, A. E.; Mammoto, A.; Ingber, D. E.; Kamm, R. D., Mechanotransduction of fluid stresses governs 3d cell migration. *Proceedings of the National Academy of Sciences of the United States of America* **2014,** *111*, 2447-2452.

10. Arnsdorf, E. J.; Tummala, P.; Kwon, R. Y.; Jacobs, C. R., Mechanically induced osteogenic differentiation - the role of rhoa, rockii and cytoskeletal dynamics. *Journal of Cell Science* **2009,** *122*, 546-553.

11. Bodle, J. C.; Hanson, A. D.; Loboa, E. G., Adipose-derived stem cells in functional bone tissue engineering: Lessons from bone mechanobiology. *Tissue Engineering Part B-Reviews* **2011,** *17*, 195-211.

12. Prodanov, L.; Semeins, C. M.; van Loon, J. J. W. A.; te Riet, J.; Jansen, J. A.; Klein-Nulend, J.; Walboomers, X. F., Influence of nanostructural environment and fluid flow on osteoblast-like cell behavior: A model for cell-mechanics studies. *Acta Biomaterialia* **2013,** *9*, 6653-6662.

13. Vankooten, T. G.; Schakenraad, J. M.; Vandermei, H. C.; Busscher, H. J., Development and use of a parallel-plate flow chamber for studying cellular adhesion to solid-surfaces. *Journal of Biomedical Materials Research* **1992,** *26*, 725-738.

14. Usami, S.; Chen, H. H.; Zhao, Y. H.; Chien, S.; Skalak, R., Design and construction of a linear shear-stress flow chamber. *Annals of Biomedical Engineering* **1993,** *21*, 77-83.

15. Xiao, Y.; Truskey, G. A., Effect of receptor-ligand affinity on the strength of endothelial cell adhesion. *Biophysical Journal* **1996,** *71*, 2869-2884.

16. Bos, R.; van der Mei, H. C.; Busscher, H. J., Physico-chemistry of initial microbial adhesive interactions - its mechanisms and methods for study. *Fems Microbiology Reviews* **1999,** *23*, 179-230.

17. Davey, N.; Neild, A., Pressure-driven flow in open fluidic channels. *Journal of Colloid and Interface Science* **2011,** *357*, 534-540.

18. Wixforth, A., Acoustically driven planar microfluidics. *Superlattices and Microstructures* **2003,** *33*, 389-396.

19. Oberti, S.; Neild, A.; Quach, R.; Dual, J., The use of acoustic radiation forces to position particles within fluid droplets. *Ultrasonics* **2009,** *49*, 47-52.

20. Burriel, P.; Ignes-Mullol, J.; Claret, J.; Sagues, F., Two-dimensional microfluidics using circuits of wettability contrast. *Langmuir* **2010,** *26*, 4613-4615.

21. Gau, H.; Herminghaus, S.; Lenz, P.; Lipowsky, R., Liquid morphologies on structured surfaces: From microchannels to microchips. *Science* **1999,** *283*, 46-49.

22. Darhuber, A. A.; Troian, S. M.; Miller, S. M.; Wagner, S., Morphology of liquid microstructures on chemically patterned surfaces. *Journal of Applied Physics* **2000,** *87*, 7768-7775.

23. McKnight, T. E.; Melechko, A. V.; Austin, D. W.; Sims, T.; Guillorn, M. A.; Simpson, M. L., Microarrays of vertically-aligned carbon nanofiber electrodes in an open fluidic channel. *Journal of Physical Chemistry B* **2004,** *108*, 7115-7125.

24. Wang, K. G.; Wang, L.; Li, J.; Xu, G. W.; Jin, A. Z.; Gu, C. Z.; Liu, W. Q.; Niu, H. B., The morphology of DNA solution in an open fluidic channel studied by non-contact afm. *Micron* **2008,** *39*, 481-485.

25. Oliveira, N. M.; Neto, A. I.; Song, W. L.; Mano, J. F., Two-dimensional open microfluidic devices by tuning the wettability on patterned superhydrophobic polymeric surface. *Applied Physics Express* **2010,** *3*.

26. Sousa, M. P.; Mano, J. F., Patterned superhydrophobic paper for microfluidic devices obtained by writing and printing. *Cellulose* **2013,** *20*, 2185-2190.

27. Dong, Z. C.; Wu, L.; Li, N.; Ma, J.; Jiang, L., Manipulating overflow separation directions by wettability boundary positions. *Acs Nano* **2015,** *9*, 6595-6602.

28. Oliveira, M. B.; Neto, A. I.; Correia, C. R.; Rial-Hermida, M. I.; Alvarez-Lorenzo, C.; Mano, J. F., Superhydrophobic chips for cell spheroids high-throughput generation and drug screening. *Acs Applied Materials & Interfaces* **2014,** *6*, 9488-9495.

29. Lima, A. C.; Puga, A. M.; Mano, J. F.; Concheiro, A.; Alvarez-Lorenzo, C., Free and copolymerized gamma-cyclodextrins regulate the performance of dexamethasone-loaded dextran microspheres for bone regeneration. *Journal of Materials Chemistry B* **2014,** *2*, 4943-4956.

30. Zhang, X.; Shi, F.; Niu, J.; Jiang, Y. G.; Wang, Z. Q., Superhydrophobic surfaces: From structural control to functional application. *Journal of Materials Chemistry* **2008,** *18*, 621-633.

31. Song, W. L.; Veiga, D. D.; Custodio, C. A.; Mano, J. F., Bioinspired degradable substrates with extreme wettability properties. *Advanced Materials* **2009,** *21*, 1830-+.

32. Johansson, B. L.; Larsson, A.; Ocklind, A.; Ohrlund, A., Characterization of air plasma-treated polymer surfaces by esca and contact angle measurements for optimization of surface stability and cell growth. *Journal of Applied Polymer Science* **2002,** *86*, 2618-2625.

33. North, S. H.; Lock, E. H.; Cooper, C. J.; Franek, J. B.; Taitt, C. R.; Walton, S. G., Plasma-based surface modification of polystyrene microtiter plates for covalent immobilization of biomolecules. *Acs Applied Materials & Interfaces* **2010,** *2*, 2884-2891.

34. Oliveira, N. M.; Reis, R. L.; Mano, J. F., Superhydrophobic surfaces engineered using diatomaceous earth. *Acs Applied Materials & Interfaces* **2013,** *5*, 4202-4208.

35. Isimjan, T. T.; Wang, T. Y.; Rohani, S., A novel method to prepare superhydrophobic, uv resistance and anti-corrosion steel surface. *Chemical Engineering Journal* **2012,** *210*, 182-187.

36. Leibner, E. S.; Barnthip, N.; Chen, W. N.; Baumrucker, C. R.; Badding, J. V.; Pishko, M.; Vogler, E. A., Superhydrophobic effect on the adsorption of human serum albumin. *Acta Biomaterialia* **2009,** *5*, 1389-1398.

37. Stallard, C. P.; McDonnell, K. A.; Onayemi, O. D.; O'Gara, J. P.; Dowling, D. P., Evaluation of protein adsorption on atmospheric plasma deposited coatings exhibiting superhydrophilic to superhydrophobic properties. *Biointerphases* **2012,** *7*.

38. Reynolds, O., An experimental investigation of the circumstances which determine whether the motion of water shall be direct or sinuous, and of the law of resistance in parallel channels. *Philosophical Transactions of the Royal Society of London* **1883,** *174*, 935-982.

39. Tan, J. N.; Neild, A., Microfluidic mixing in a y-junction open channel. *Aip Advances* **2012,** *2*.

40. Steward, R.; Tambe, D.; Hardin, C. C.; Krishnan, R.; Fredberg, J. J., Fluid shear, intercellular stress, and endothelial cell alignment. *American Journal of Physiology-Cell Physiology* **2015,** *308*, C657-C664.

41. Lima, A. C.; Mano, J. F., Micro/nano-structured superhydrophobic surfaces in the biomedical field: Part i: Basic concepts and biomimetic approaches. *Nanomedicine* **2015,** *10*, 103-119.

42. Lima, A. C.; Mano, J. F., Micro/nano-structured superhydrophobic surfaces in the biomedical field: Part ii: Applications overview. *Nanomedicine* **2015,** *10*, 271-297.

43. Ota, H.; Yamamoto, R.; Deguchi, K.; Tanaka, Y.; Kazoe, Y.; Sato, Y.; Miki, N., Three-dimensional spheroid-forming lab-on-a-chip using micro-rotational flow. *Sensors and Actuators B-Chemical* **2010,** *147*, 359-365.

44. Tan, J. N.; Alan, T.; Neild, A., Stability of flowing open fluidic channels. *Aip Advances* **2013,** *3*.

45. Matsui, H.; Noda, Y.; Hasegawa, T., Hybrid energy-minimization simulation of equilibrium droplet shapes on hydrophilic/hydrophobic patterned surfaces. *Langmuir* **2012,** *28*, 15450-15453.

46. Speth, R. L.; Lauga, E., Capillary instability on a hydrophilic stripe. *New Journal of Physics* **2009,** *11*.

47. Liu, X. L.; Zhang, X.; Lee, I., A quantitative study on morphological responses of osteoblastic cells to fluid shear stress. *Acta Biochimica Et Biophysica Sinica* **2010,** *42*, 195-201.

48. Ishibazawa, A.; Nagaoka, T.; Takahashi, T.; Yamamoto, K.; Kamiya, A.; Ando, J.; Yoshida, A., Effects of shear stress on the gene expressions of endothelial nitric oxide synthase, endothelin-1, and thrombomodulin in human retinal microvascular endothelial cells. *Investigative Ophthalmology & Visual Science* **2011,** *52*, 8496-8504.

49. Kook, S. H.; Lee, H. J.; Chung, W. T.; Hwang, I. H.; Lee, S. A.; Kim, B. S.; Lee, J. C., Cyclic mechanical stretch stimulates the proliferation of c2c12 myoblasts and inhibits their differentiation via prolonged activation of p38 mapk. *Molecules and Cells* **2008,** *25*, 479-486.

50. Chen, R.; Feng, L. Q.; Ruan, M.; Liu, X. H.; Adriouch, S.; Liao, H., Mechanical-stretch of c2c12 myoblasts inhibits expression of toll-like receptor 3 (tlr3) and of autoantigens associated with inflammatory myopathies. *Plos One* **2013,** *8*.

51. Kim, I. S.; Song, Y. M.; Cho, T. H.; Kim, J. Y.; Weber, F. E.; Hwang, S. J., Synergistic action of static stretching and bmp-2 stimulation in the osteoblast differentiation of c2c12 myoblasts. *Journal of Biomechanics* **2009,** *42*, 2721-2727.

52. Khayat, G.; Rosenzweig, D. H.; Khavandgar, Z.; Li, J.; Murshed, M.; Quinn, T. M., Low-frequency mechanical stimulation modulates osteogenic differentiation of c2c12 cells. *ISRN Stem Cells* **2013,** *2013*, 9.

Chapter 6

Hanging Drop Platform for Stem Cell 3D Spheroids Production and Characterization under Co-Culture Conditions

This chapter is based on the following publication:

Nuno M. Oliveira, Mariana B. Oliveira, Rui L. Reis, João F. Mano. Hanging Drop Platform for Stem Cell 3D Spheroids Production and Characterization under Co-Culture Conditions. *Submitted*.

6.1. Abstract

Cell spheroids are three-dimensional (3D) structures of living cells with high interest for biomedical research. One of the most promising spheroids applications is in tissue engineering, where they have been suggested for cell-based regenerative approaches and for organ/tissue bio-fabrication as building blocks. Especially, co-cultured spheroids are gaining momentum because they allow studying cellular interactions occurring in the native in vivo environment. Here, we propose a hanging drop system based on a superhydrophobic (SH) platform for the production and culturing of human adipose-derived stem cell (hASC) spheroids under co-culture conditions. hASC spheroids were formed in the SH surfaces in indirect co-cultures with L929 and Saos-2 cell lines, and human umbilical vein endothelial cells (HUVEC). The method allowed obtaining compact spheroids with uniform sizes. The co-culture with Saos-2 cells indicated that the spheroid production and hASC differentiation into an early osteogenic phenotype can be obtained in a one-step procedure. These SH platforms may be interesting systems for massive production of pre-differentiated spheroids to be used in bio-fabricated constructs for bone regeneration. The developed platform also showed versatility for cell analysis, as it permitted easily harvesting and transferring spheroids between platforms, and directly performing on-chip cell viability assessment.

6.2. Introduction

Cell spheroids are three-dimensional (3D) structures of living cells with high interest as models for basic science. Also, they are very important for cancer research, drug discovery and tissue engineering.[1] Spheroids are progressively finding application in tissue engineering strategies as building block units to be used in a multiplicity of approaches targeting the regeneration of different organs and tissues,[2-5] including bio-printing and bio-fabrication techniques.[6-8] The increasing importance assumed by spheroids on biomedical research is justified by their similarity to the native 3D biological niches present in *in vivo* tissues. In spheroids, cell-to-cell interactions are increased, reproducing better all functional and architectural characteristics of the native tissues, as compared to 2D cell culture.[9] Several methods for spheroid production have been reported, namely centrifugal pellet culture, spinner flask culture, use of non-adhesive substrates, rotating wall vessels and porous 3D scaffolds, external force cell aggregation enhancement (electric, acoustic or magnetic), microfluidics, micro-molded hydrogels and hanging drop culture.[1, 10]

With the goal to faithfully mimic the *in vivo* environment, complex systems combining simultaneously different cell types have been studied. Co-culture spheroid models were reported as valuable tools for gaining in-depth understanding of cancer biology and for oncology drug development and discovery. Generally, these models are a closer approximation of the *in vivo* environment as they are able to combine different cell types like those present in the body.[11, 12] For example, studying the interactions between different cells can be applied in cell- and antibody-based immunotherapies, by using cytokines to improve natural immune system against cancer cells.[13-15] Other of the most promising clinical applications of co-culture systems may be related to 'personalized tumor analyses', where after collecting the cells from patients, customized treatment strategy can be designed.[16]

In this work, we propose a hanging drop platform for spheroid production under indirect co-culture conditions. A platform consisting of a polystyrene (PS) superhydrophobic (SH) planar surface with wettable areas was used. In a first step, one cell type was left to adhere as a monolayer on the wettable patterns. Afterwards, droplets of suspended cells, of a second type, were placed over the formed cell layer. The SH platform was immediately turned upside-down, taking advantage of the high adhesiveness of the droplets to the spots. The cells, which were initially suspended in the droplets, assembled to form one spheroid per droplet due to the effect of gravity.

There are numerous systems for distinguished biomedical applications using SH-based platforms, showing its high versatility.[17] Reported applications include microfluidic devices,[18] production of smart drug delivery systems,[19] biocompatible polymeric microparticles with nearly 100% drug encapsulation yield,[20] bioactive spherical structures with shape memory capability[21] and high-throughput generation of shape-controlled microgels.[22] Other promising application of these platforms involves the easy *in-situ* analyzes of cellular response.[23, 24]

The use of a SH platform for spheroids production in mono-culture conditions was previously reported.[23, 25-28] Such technology allowed precisely controlling spheroids' size with very low size variability, by simply tailoring both cell number and droplet volume. Different superhydrophobic patterned platforms were previously developed for high-throughput spheroid generation for application in combinatorial drug screening[23, 25, 28] and for testing the therapeutic efficacy enhancement for angiogenesis and insulin secretion.[26, 27]

The high array of applications of SH platforms in the biomedical field, as well as their high versatility, inspired the design of a chip for a novel application, where both components of a co-culture - 3D spheroids and 2D monolayers - could be studied in each hanging droplet. The system was used for the production of human adipose-derived stem cell (hASC) spheroids under co-culture

conditions with a cell monolayer, in a setup that allowed their further growth and possible differentiation, as well as their on-chip analysis.

6.3. Materials and Methods

6.3.1. Preparation of the superhydrophobic surfaces with wettable regions

Polystyrene (PS) superhydrophobic surfaces were prepared as previously reported.[18] PS (184K, Styrolution) was dissolved in THF (Sigma) at a concentration of 70 mg/mL. This solution was then mixed at a ratio of 2 : 1.3 with absolute ethanol. The mixture was vigorously shaken, until it became transparent. PS of upper lids of petri dishes were protected in regions of 2 x 2 mm^2 separated by 2 mm with poly(vinyl) carbonate (PVC) stickers, similarly as reported by Oliveira *et al.*.[25] The PS solution prepared in THF and ethanol was dispensed in the petri dish lid, inducing polymeric phase separation. The solution was then removed and the lids were treated with absolute ethanol. After the drying of the lids, the stickers were removed using tweezers. The regions covered by the stickers remained untreated, showing a wettable behavior. The wettability contrast-based chips were sterilized by immersion in ethanol 70% overnight. The samples were then dried inside a laminar flow chamber.

6.3.2. Cell isolation and expansion

Human abdominal subcutaneous adipose tissue was used to isolate human stem cells derived from the adipose tissue (hASC). The samples were obtained from patients undergoing lipoaspiration procedure, after informed consent. The retrieval and transportation of the samples to the 3B's Research Group laboratorial facilities were performed under a protocol previously established with the Department of Plastic Surgery of Hospital da Prelada (Porto, Portugal) and approved by the local Ethical Committee. All samples were processed within 24 h after the surgical procedure, and isolation was carried out according to a protocol previously described.[29] The

undifferentiated cells were cultured and expanded under basal condition, using Minimum Essential alpha Medium (α-MEM, ThermoFisher Scientific), supplemented with 10% (v/v) fetal bovine serum (FBS, ThermoFisher Scientific) and 1% (v/v) penicillin-streptomycin (ATB), until passages 2 and 3. The cells were used in passages 3 to 5.

Immortalized cell lines L929 (mouse fibroblasts), Saos-2 (human osteoblast-like cells) and human umbilical venous endothelial cells (HUVEC) were purchased from Sigma. Their expansion was carried out in Dulbecco's Modified Essential Medium (DMEM, Invitrogen) with 10% FBS and 1% ATB, for L929 and Saos-2, and in medium 199 (M199) with 20% FBS, 1% ATB and 1% Glutamax, supplemented with heparin (100 μg/mL) and endothelial cell growth supplement (50 μg/mL; ECGS, Invitrogen), for HUVEC. Cell culture media were exchanged every 3 days.

6.3.3. Preparation of a cell layer on-chip

Cell suspensions at a density of $2.5x10^5$ cells/mL were dispensed in each wettable spot of the chips with a volume of 5 μL. Cells were either L929 or Saos-2 suspended in DMEM, or HUVEC in M199. All cell culture media had the same complete formulation presented previously.

The cell suspension droplets were left in contact with the wettable spots for 4 hours, promoting cellular adhesion, at 37 °C and 5% CO_2 environment. The excess medium and non-adhered cells were then removed using a micropipette in all spots. Fresh medium was then added to the wettable spots, in a volume of 5 μL. The cells were then cultured on chip overnight at 37 °C, 5% CO_2. The wettable spots later used for the formation of cell spheroids without co-culture were left empty during this step.

6.3.4. Preparation of hASC cell spheroids on-chip

The cell culture medium used to culture the cell lines previously adhered to the wettable spots overnight was removed from the spots using a micropipette. A 7.5 μL droplet of hASC cell suspension at a cell density of $3.33x10^5$ cells/mL was dispensed in the wettable spots of the chips,

which were rapidly turned 180°, acquiring a hanging drop configuration. hASC dispensed in the wettable spots containing adhered L929 or Saos-2 were suspended in α-MEM with 10% FBS. For the spots containing adhered HUVEC, the hASC were suspended in M199 with 10% FBS and 1% Glutamax, supplemented with heparin (100 μg/mL) and ECGS (50 μg/mL). The control spheroids, cultured as a monoculture (i.e., in cell-free wettable spots), were cultured in both α-MEM and M199 supplemented media. As such, we promoted a hanging drop configuration for the growth of hASC cells in the presence (or absence, in the case of control samples) of a 2D monolayer of cell lines. The lower lid of the petri dishes was filled with sterile PBS with 10% of α-MEM. The schematic representation of the co-culture setup can be found in Figure 6.1B. The chips were incubated at 37 °C, 5% CO_2 for 72 h. Medium replacement was performed every 24 hours, by adding 2 μL of medium to each spot.

6.3.5. Characterization of the cellular layers

The formation of cellular layers and respective morphology on the wettable spots was assessed after the fixation of the cells with 10% formalin. Cells' nuclei were stained with 4',6-diamidino-2-phenylindole (DAPI, Sigma, diluted 1000x). F-actin was stained with phalloidin-tetramethyl rhodamine isothiocyanate (Sigma, diluted 1000x). Images of the monolayers were acquired using a reflected fluorescent light microscope (Axio Imager Z1, Zeiss).

6.3.6. Measurement of spheroid diameter and roundness

Images of the produced spheroids were acquired using a regular microscope. Then, the diameter of spheroids for each tested condition was measured using the ImageJ software. The roundness parameter was also determined using the same software, based on the equation 1.

6.3.7. Quantification of total dsDNA in the spheroids

The total amount of double stranded DNA (dsDNA) in the spheroids was quantified to assess cellular proliferation. Quantification was performed using the Quant-iTt Pico-Green dsDNA Assay

Kit (Invitrogen, Molecular Probes, Oregon, U.S.A.), according to the instructions of the manufacturer. After rinsing twice with PBS, cells in the spheroids were lysed by osmotic and thermal shock. Briefly, the spheroids were collected in ultrapure water, stirred using a vortex for 1 minute (3x) and incubated at room temperature for 30 minutes. The samples were frozen at -20°C, until their use for quantifications. After thawing at room temperature, the samples were exposed to ultrasounds for 15 minutes. The freezing/thawing followed by ultrasound exposure process was repeated twice for all samples. All samples were submitted to centrifugation (1 minute, 300 g) before quantifications, and the supernatant was used for the dsDNA quantification assays. The fluorescence of the dye was measured at an excitation wavelength of 485/20 nm and at an emission wavelength of 528/20 nm, in a microplate reader (Synergie HT, Bio-Tek, USA). The dsDNA concentration for each sample was calculated using a standard curve (dsDNA concentration ranging from 0.0 to 1 µg/mL) relating the quantity of dsDNA and fluorescence intensity.

6.3.8. Quantification of alkaline phosphatase (ALP) activity

Alkaline Phosphatase (ALP) is frequently used as an early biochemical marker of osteogenic differentiation. The activity of this marker was evaluated using a commercially available Alkaline Phosphatase Detection Kit (Sigma, 245-325-0), following the protocol recommended by the manufacturer. The fluorescence was read at 360/440 nm excitation/emission on a plate reader (Synergie HT Izasa).

The presence of enzymatically active ALP in the spheroids was also corroborated by staining the enzyme with the substrate nitro-blue tetrazolium chloride / 5-bromo-4-chloro-3'-indolyphosphate p-toluidine salt (BCIP/NBT, Sigma) overnight. BCIP/NBT shows a purple color when in contact with ALP. The samples were then washed with a buffer and images acquired before and after staining using a stereomicroscope (Zeiss).

6.3.9. Spheroid transference

The ability of hASC spheroids to be transferred from the chip where they were formed (as part of a hanging drop system) to a clean cell-free chip allows performing on-chip assays where the spheroids were analyzed separately from the 2D cell monolayer. An on-chip protocol was developed to prove the suitability of this technique. Empty sterilized cell-free chips with the same disposition and size of wettable spots were aligned with the chips containing cell layers and 3D cell spheroids. The spheroids were passed to the new clean chips by contact established between the wettable spots through the cell culture medium droplet. A schematic representation of this step can be found in Figure 6.4A.

6.3.10. On-chip metabolic activity testing

The metabolic activity of the transferred spheroids was assessed on-chip by adapting the AlamarBlue protocol to the few microliter dimensions of the chips. The excess medium transferred to the clean wettable spots was removed using a micropipette. 4 μL of AlamarBlue reagent (AbDSerotec) diluted 100x (in α-MEM or M199) was added to each spot of the chips. The chips were incubated at 37 °C, 5% CO2 for 8 hours and, immediately after, pictures of the chips were acquired (Canon Powershot G12). Cell viability ratios were calculated by measuring the red color channel intensity in each spot. The images RGB channels were split using the ImageJ free software (NIH, USA), and the grey intensity corresponding to the red channel was quantified. Cell viability ratios of co-cultured samples were calculated using monocultured spheroids as a reference (with value 1). The tests were performed using at least 4 spots per condition.

6.3.11. Statistical analysis

All quantitative data are presented as means ± standard deviations. All data was analyzed using one way ANOVA with Tukey's post-hoc test and p values <0.05 were considered statistically significant.

6.4. Results and discussion

The SH platform used here was manufactured by a one-step patterning/hydrophobization process, using square shaped stickers to protect the desired areas from being reached by the phase-separation reagents that confer to the surface superhydrophobicity, resulting in water contact angles higher than 150°.[18] This property was achieved by the introduction of micro- and nanoroughness on the PS surface (Figure 6.1A), mimicking the extreme water repellency of lotus leaves. Due to the superhydrophobicity surrounding the untreated areas, cell suspensions remained restricted to these areas. In two steps, it is possible to produce an array of co-culture droplets – see Figure 6.1B. One type of cells (here called "cells 1") is first cultured in the surface of the wettable spots. Then, droplets of a suspension of cells 2 are added. By inverting the chip, cells 2 are forced to assemble into a spheroid shape, keeping the contact with cells 1 via paracrine signaling. Note that in each spot the nature and amount of cells 1 or cells 2 could be independently controlled, being thus possible to generate versatile chips for high-throughput analysis.

In this study, we analyzed the effect of preparing hASC spheroids in indirect contact with three different cell types – L929 fibroblast cell line, Saos-2 osteoblast-like cell line and human umbilical vein endothelial cells (HUVEC). In the chip's indirect co-culture setup, no physical barrier (such as the trans-well systems) was used and cells were only separated by the culture medium. Minimum essential alpha medium (α-MEM) was used for hASC co-culture with L929 and Saos-2 cells. However, the hASC/HUVEC co-culture was carried on a suitable cell culture medium for HUVEC cell survival/proliferation: medium 199 complemented with endothelial cell growth supplement and heparin (M199).

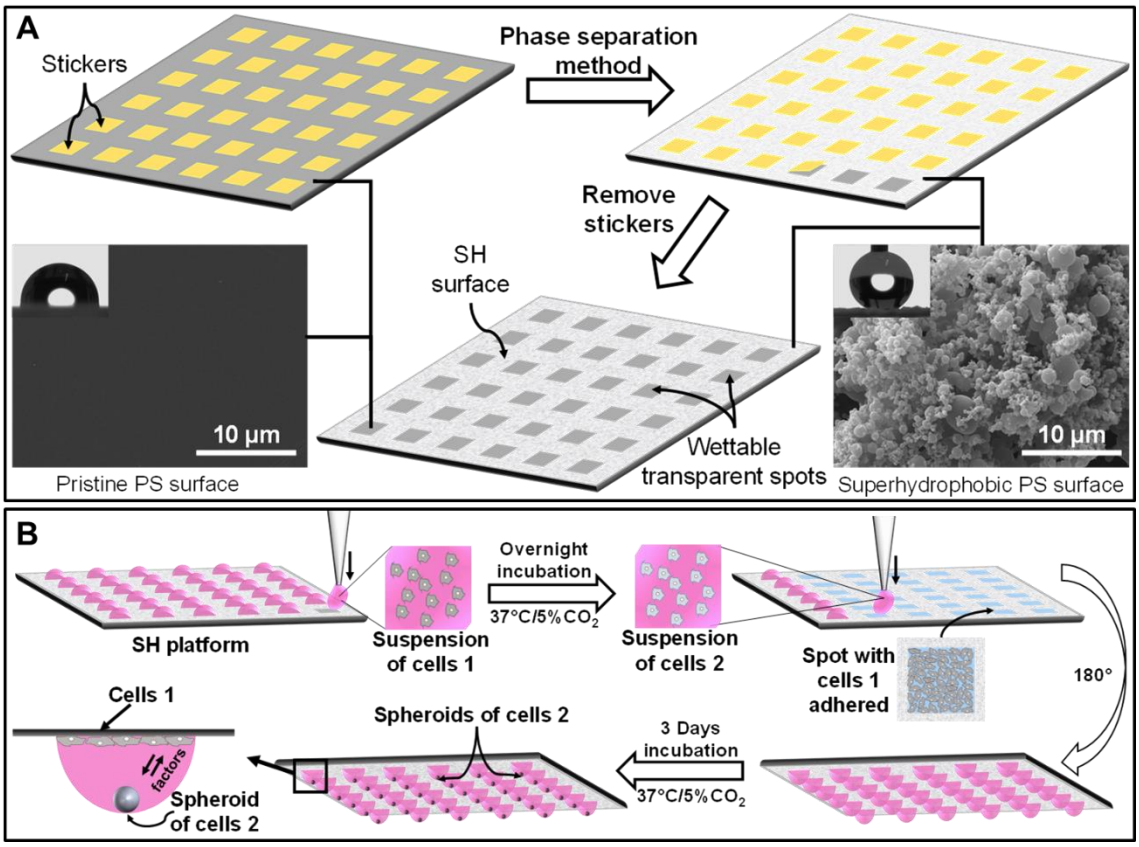

Figure 6.1: (A) Preparation of superhydrophobic (SH) platforms patterned with arrays of wettable regions: first, an array of stickers in a pristine polystyrene (PS) substrate was made; then, a roughness increasing was achieved by in situ deposition of PS such as illustrated by SEM images, and consequently inducing an increase of the surface hydrophobicity at the macroscopic level proven by the water contact angle images; finally, wettable transparent spots surrounded by a SH surface were obtained by removing the stickers. (B) Schematic representation of the procedure for the production of spheroids of cells 2 in co-culture conditions of cells 1 on the developed platform: addition of a suspension of cells 1 into the wettable spots by pipetting; after overnight incubation, during which cells 1 adhered onto the surface, a cell suspension of cells 2 was dispensed in each single spot over the previously adhered cells 1; then, the platform was rotated 180° to create a hanging-drop setup; finally, the spheroids of cells 2 were left to aggregate for 3 days in indirect co-culture contact with the adhered cells.

Taking advantage of the wettable areas transparency, spheroid formation was easily monitored over time using a regular microscope, as well as the proliferation of adhered cell layers. After 3 days of incubation for complete hASC spheroids formation, the obtained spheroids for all studied conditions presented a diameter size in the range 195-215 µm (Figure 6.2A). Spheroids developed

under co-culture conditions presented a similar diameter value comparing with the respective control, where spheroids were cultured only with α-MEM or M199 medium (Figure 6.2A). Equation 1 was used to calculate spheroids' roundness, which allowed characterizing and comparing the shape of the different spheroids.

$$Roundness = 4 \times \frac{[Area]}{\pi \times [Major\ axis]^2} \qquad \text{Equation 1}$$

Spheroids presented a roundness value in the range 0.75-0.95 (Figure 6.2B), and those cultured under co-culture conditions presented a roundness value in the same range of the respective controls. However, no significant differences on both measures were verified. Figure 6.2C shows images of spheroid profiles for each tested condition, and fluorescent images of the cell layer adhered on the PS above of the respective spheroid. These cell layers showed that cells were confluent and had spread morphology, showing a good adhesion to the PS substrate. The proposed technique would allow a pre-adsorption of an adhesive protein or other surface treatment to PS envisaging the enhancement of cell adhesion, which was not necessary in this case. Since, a low number of cells detaching from the monolayer and adhering to the spheroid was detected (Figure 6.S1). For a similar amount of hASC cells and droplet volume, spheroids presented diameter values in the same magnitude of the ones reported elsewhere.[26] Importantly, the obtained spheroids were compact and with a uniform size. Seo et al. and Lee et al. found that this hanging drop method using SH surfaces originated stem cell spheroids high higher quality than using both spinner flask and hanging drop culture on a petri dish.[26, 27] The explanation for the better results using SH platforms instead of petri dishes relies in the favorable internal hydrodynamic flow of the medium droplet during the spheroid formation. On a static hanging droplet, the droplet internal flow can be influenced by the surface and medium chemical properties, the surface geometry and evaporation rate of the liquid. Due to large contact angle and small contact area between the SH surface and medium droplet, the hydrodynamic forces on the interface

liquid/substrate generated by medium evaporation are weaker than that on the petri dish surface. For this reason, gravity forces are more prevalent over cell aggregates than internal hydrodynamic forces. Consequently, cell aggregates can more promptly accumulate at the drop apex, generating compact and functionally enhanced spheroids.[26]

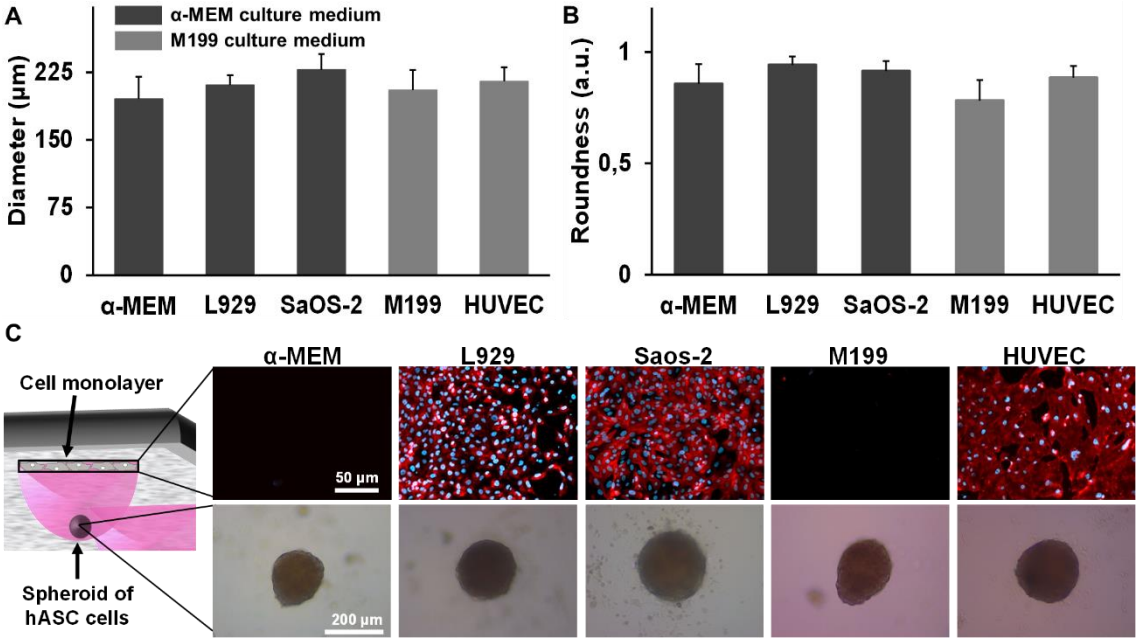

Figure 6.2: (A) Size distribution of the obtained hASC spheroids after 3 days of culture, either in single cell culture or co-culture, is shown for the tested conditions. (B) Shape characterization of spheroids taking in account the roundness parameter. (C) Transmitted light microscopy images of the spheroids acquired from the top of the developed platform, through the transparent spot. Nuclei (DAPI)/cytoskeleton F-actin (phalloidin-TRITC) staining was performed in the cells adhered to the pristine PS spot above the respective spheroid.

We hypothesized that the SH platforms previously used for spheroids production would also be compatible with hASC spheroids production under indirect co-culture conditions with other cell types. The use of this platform allows easily assessing the effect of preparing spheroids under different co-culture conditions on different biological features, including specific markers expression. As proof of concept, we investigated the effect of producing and culturing the spheroids in different co-cultures on their alkaline phosphatase (ALP) expression, which is a well-known earlier marker of osteogenic differentiation. The expression of ALP in mesenchymal stem cells, namely

hASC, is known to be affected by their crosstalk with osteoblast-like cells and HUVEC cells. Both are known to drive an increased expression of this marker in early time points.[30-35]

Double stranded DNA (dsDNA) quantification showed that the stem cell spheroids produced in different co-culturing procedures presented approximately three times more dsDNA than the control conditions (cultured as monocultures in either α-MEM or M199) (Figure 6.3A). Similar results were previously reported for other indirect co-culture methods, where stem cell proliferation was increased via co-culture with osteoblast cells[30][31] and HUVEC cells.[33, 34] However, these differences detected on dsDNA amount did not originate significant differences on spheroid diameters, suggesting that co-culture conditions promoted the formation of more compact spheroids.

ALP activity results showed that hASC spheroids produced in the presence of Saos-2 cell line presented twice more ALP activity, normalized by total sdDNA, as compared to the spheroids produced both under monoculture conditions in α-MEM or in co-culture with fibroblast cell line L929 (Figure 6.3B). Despite the observed trend, the difference was not statistically significant compared to spheroids cultured in α-MEM. However, the use of either L929 or Saos-2 cell lines showed a significant difference in the expression of ALP. Birmingham *et. al* described similar results for two-dimensional co-cultures, showing that osteogenic differentiation of mesenchymal stem cells can be directed by performing indirect co-culture with osteoblast-like cells in the absence of osteogenic media.[30] For the HUVEC co-culture case, the ALP activity was reduced for half of the value detected on the control condition (M199), as shown in Figure 6.3B. This results may be correlated with previous findings which showed that HUVEC cells inhibited mesenchymal bone marrow stem cells (BMSC) differentiation into mature osteoblasts when co-cultured in indirect contact,[33] even using osteogenic medium.[36] In contrast, direct co-culture of HUVEC cells with stem cells has been established as enhancing its osteoblastic phenotypic markers, resulting for

example in an increase of ALP expression.[34, 35] Villars and coworkers highlighted these differences by comparing direct and indirect co-cultures of HUEVC and BMSC cells.[33]

To corroborate the obtained results for ALP activity, and also to adapt the biochemical tests to rapid on-chip detection, a colorimetric detection method for ALP was used. In the employed method, an insoluble product is formed by a reaction with ALP and is easily observable with its purple color. Figure 6.3C shows ALP activity in all the studied conditions. hASC spheroids co-cultured with Saos-2 is distinguished from others by the intense purple staining of the spheroid, indicating an enhanced ALP activity.

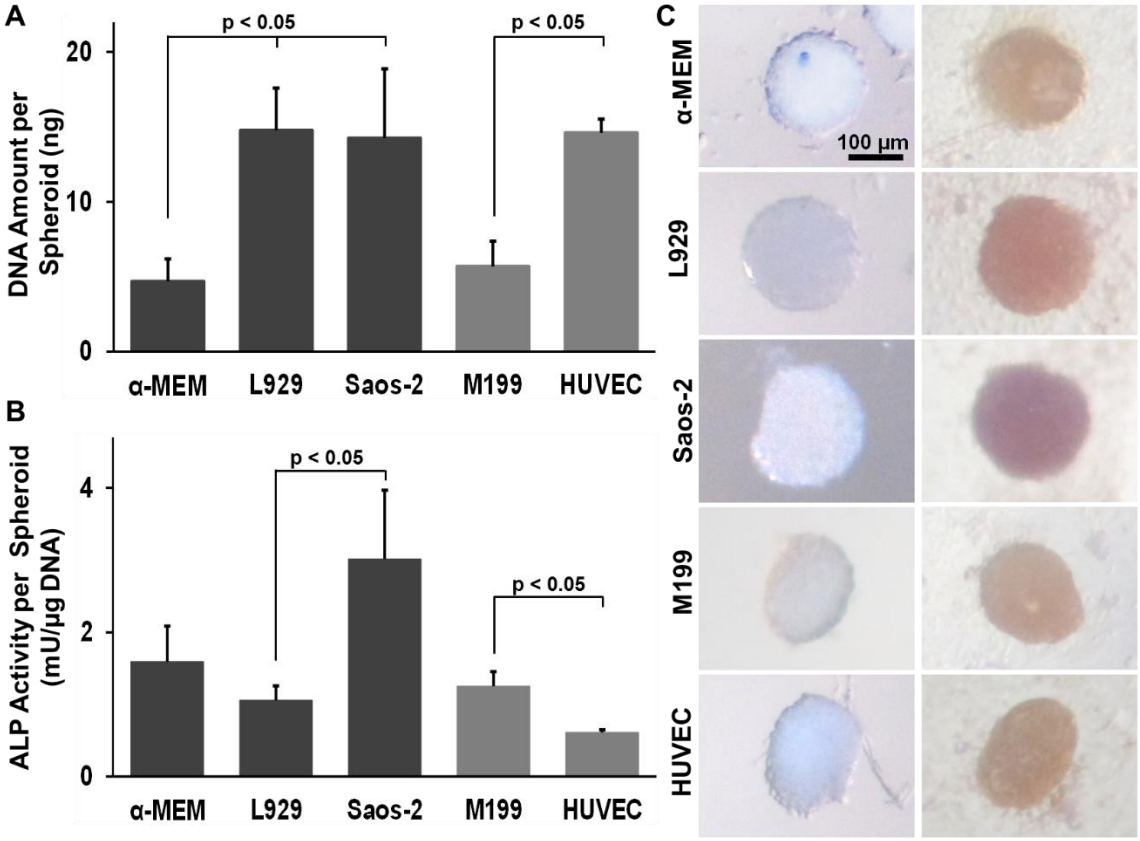

Figure 6.3: (A) Quantification of the DNA content per spheroid for each of the studied conditions at day 3. (B) Alkaline phosphatase (ALP) activity in each spheroid for the different tested conditions. (C) Images of spheroids obtained from the different co-cultures before and after ALP staining. More intense purple color indicates enhanced ALP activity.

Taking advantage of SH platform versatility, a technique for rapid and low handling cellular viability assessment directly on chip is here presented. Using an equivalent platform to the one employed on spheroid production, by aligning and touching with the spheroid production platform on the empty platform the spheroids were transferred for the new platform – see Figure 6.4A. With this simple step the spheroid can be easily separated from the cell layer adhered on the first platform. From that point on, both spheroids and cell layer can be analyzed separately. For example, the platform with the adhered cell layer can be processed in order to characterize cell morphology, as shown by the fluorescent images present in Figure 6.2C. However, other kind of assays can be easily performed on these platforms such as immunocytochemistry staining to study specific markers on cells.

The new platform containing harvested spheroids was used to perform AlamarBlue assay. The blue color of the AlamarBlue solution changes to red due to a reduction reaction promoted by viable cells. Through image analysis, the red channel intensity is amenable to be measured and this way metabolic activity on spheroids can be assessed (Figure 6.4A). By analyzing the image presented in Figure 6.4B, the relative cell viability could be determined, using as reference the respective control condition (α-MEM and M199). The cell viability for the co-cultured spheroid was very similar to the control conditions, where no significant differences were found (Figure 6.4B). By relating the previous results with the cell viability results, we conclude that even though co-cultured spheroids presented higher amount of DNA they showed the similar cell viability to controls. One possible explanation could be that the spheroid obtained in co-culture conditions showed a high level of compactness, and cells on spheroid core may be dead. For this reason the spheroids with higher DNA amount did not present a higher AlamarBlue reduction rate, as would be expected. Relating the conditions using α-MEM medium with the conditions using M199 medium, the last presented an intense red color comparing with the first conditions (Figure 6.4B). This evident difference may

be attributed to the composition of the medium 199 or its supplements. As such, controls with cell-free medium were established for both cell culture media used in this experiment.

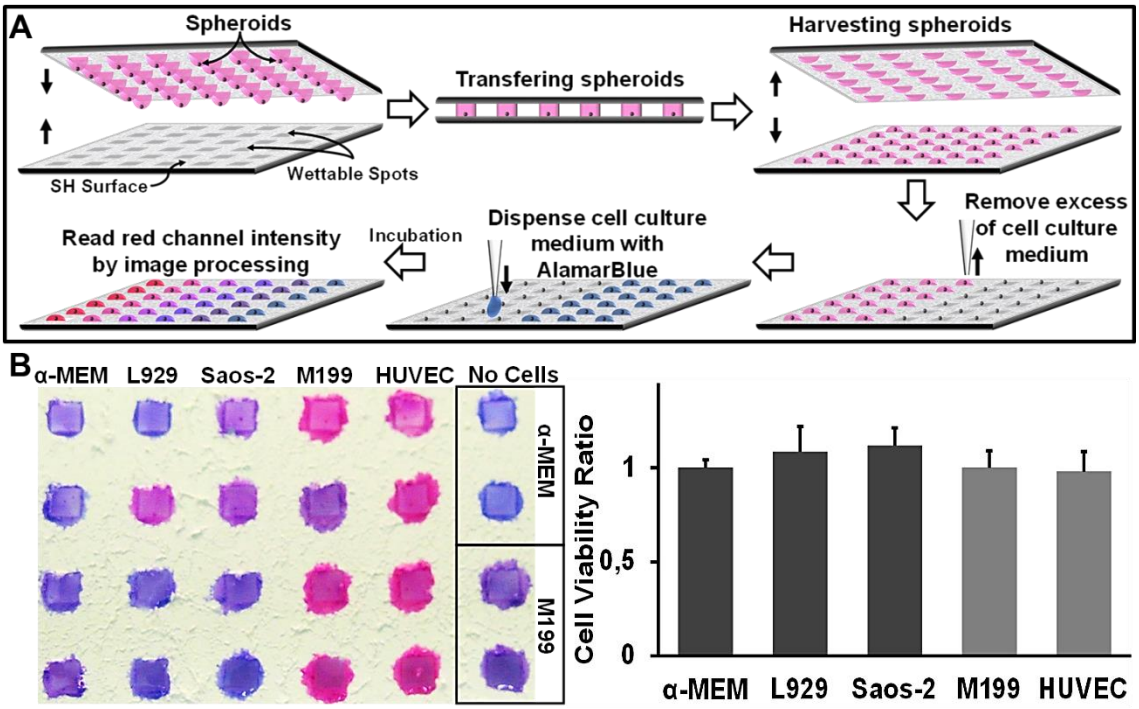

Figure 6.4: (A) Schematic representation of the procedure for the on-chip AlamarBlue assay using the developed platform: by touching with the medium droplets containing the spheroid on a second SH platform with empty wettable spots spheroids were transferred; on the harvesting step, spheroids and adhered cell layers were separated in two different chips allowing the independent processing of both; on the chip with spheroids, the excess of medium was removed from each spot and an AlamarBlue solution was dispensed, ensuring the same volume per spot; after incubation, an image from the chip was collected and processed to measure the red channel intensity, calculating this way the cell viability ratio. (B) After 8 hours of incubation, the obtained results for on-chip AlmarBlue assay for each of the tested conditions are present on the image, then after image processing the cell viability ratio was calculate taking as reference the respective control condition, α-MEM or M199.

We here present a simple and low cost platform for spheroid production and further culture under indirect co-culture conditions. To best of our knowledge, this is the first time a platform allows the formation of cell spheroids in the presence of a layer of other cell type. Recently, de Groot *et. al* reported an open microfluidic platform for hanging droplet culture that allows co-culture.[37]

Besides the complexity of both manufacturing process and spheroids harvesting, the co-culture was performed using polymeric scaffolds.[37] By using our platform, different co-culture conditions can be tested and compared on a single chip. Moreover, by improving the automatization of the platforms production and liquid dispensing, these SH platforms can also be used as part of a technique for massive spheroid production under the influence of a second cell type. The adaptation of the method to a high-throughput testing strategy would be easily achieved, considering that the platforms are compatible with automatic liquid dispensing equipment. The high-throughput screening of the results is assured by the proved compatibility of this system with image-based analysis of rapidly acquired data. This interest is increased by the fact that the hanging drop method based on SH surfaces originate spheroids with enhanced functionality.[26] As shown in this work, the produced spheroids were compact and with a uniform size, which are crucial characteristics for therapeutic applications in several fields, including biomedical engineering, cancer therapy development and production of microtissues for regeneration approaches.

6.5. Conclusion

We report a novel use for patterned superhydrophobic surfaces as affordable and easy-to-use chips for the production of 3D spheroids and their culture under co-culture conditions. As a proof of concept, we produced spheroid of hASC cells in indirect co-culture with L929, Saos-2 and HUVEC cells. After performing spheroid production under these conditioned conditions, increased ALP activity was detected on hASC spheroids cultured with the 2D monolayer of Saos-2 osteoblast-like cells. This result indicated that the hASC differentiation was amenable to be directed for an early osteogenic phenotype simultaneously with spheroid formation. These results open the path for the simultaneous production of 3D cellular structures and their differentiation promotion in a one-step procedure. Such spheroids pre-committed with the osteoblast linage may have high interest for

bone regeneration. The obtained 3D structures may be used as building blocks which, combined with the appropriate biomaterials, have potential to be used in the bio-fabrication of complex personalized constructions. The high versatility of these SH platform was also shown by the possibility of characterizing on-chip both types of cells involved in the co-culture by image-based analysis. We also developed a method to easily harvest the spheroids to new platforms and subsequently perform an on-chip cell viability assessment. As such, the developed methodology presents potential to be implanted in high-throughput strategies for biologically relevant studies in the biomedical field, namely in tissue regeneration, as well as in cancer biology and drug screening approaches.

6.6. Acknowledgments

This work was financially supported by the European Research Council grant agreement ERC-2012-ADG 20120216-321266 for project ComplexiTE. N. M. Oliveira acknowledges the financial support from Portuguese Foundation for Science and Technology – FCT (Grants SFRH/BD/73172/2010 and SFRH/BPD/111354/2015, respectively), from the program POPH/FSE from QREN.

6.7. References

1. Achilli, T. M.; Meyer, J.; Morgan, J. R., Advances in the formation, use and understanding of multi-cellular spheroids. *Expert Opinion on Biological Therapy* **2012,** *12*, 1347-1360.

2. Kelm, J. M.; Ehler, E.; Nielsen, L. K.; Schlatter, S.; Perriard, J. C.; Fussenegger, M., Design of artificial myocardial microtissues. *Tissue Engineering* **2004,** *10*, 201-214.

3. Abu-Absi, S. F.; Friend, J. R.; Hansen, L. K.; Hu, W. S., Structural polarity and functional bile canaliculi in rat hepatocyte spheroids. *Experimental Cell Research* **2002,** *274*, 56-67.

4. Lehnert, L.; Trost, H.; Schmiegel, W.; Roder, C.; Kalthoff, H., Hollow-spheres: A new model for analyses of differentiation of pancreatic duct epithelial cells. *Cell and Molecular Biology of Pancreatic Carcinoma: Recent Developments in Research and Experimental Therapy* **1999,** *880*, 83-93.

5. Rothermel, A.; Biedermann, T.; Weigel, W.; Kurz, R.; Ruffer, M.; Layer, P. G.; Robitzki, A. A., Artificial design of three-dimensional retina-like tissue from dissociated cells of the mammalian retina by rotation-mediated cell aggregation. *Tissue Engineering* **2005,** *11*, 1749-1756.

6. Kapur, S. K.; Wang, X.; Shang, H.; Yun, S.; Li, X.; Feng, G.; Khurgel, M.; Katz, A. J., Human adipose stem cells maintain proliferative, synthetic and multipotential properties when suspension cultured as self-assembling spheroids. *Biofabrication* **2012,** *4*.

7. Mironov, V.; Kasyanov, V.; Markwald, R. R., Organ printing: From bioprinter to organ biofabrication line. *Current Opinion in Biotechnology* **2011,** *22*, 667-673.

8. Jakab, K.; Norotte, C.; Marga, F.; Murphy, K.; Vunjak-Novakovic, G.; Forgacs, G., Tissue engineering by self-assembly and bio-printing of living cells. *Biofabrication* **2010,** *2*.

9. Pampaloni, F.; Reynaud, E. G.; Stelzer, E. H. K., The third dimension bridges the gap between cell culture and live tissue. *Nature Reviews Molecular Cell Biology* **2007,** *8*, 839-845.

10. Lin, R.-Z.; Chang, H.-Y., Recent advances in three-dimensional multicellular spheroid culture for biomedical research. *Biotechnology Journal* **2008,** *3*, 1172-1184.

11. Mehta, G.; Hsiao, A. Y.; Ingram, M.; Luker, G. D.; Takayama, S., Opportunities and challenges for use of tumor spheroids as models to test drug delivery and efficacy. *Journal of Controlled Release* **2012,** *164*, 192-204.

12. Benien, P.; Swami, A., 3d tumor models: History, advances and future perspectives. *Future Oncology* **2014,** *10*, 1311-1327.

13. Gottfried, E.; Kunz-Schughart, L. A.; Andreesen, R.; Kreutz, M., Brave little world - spheroids as an in vitro model to study tumor-immune-cell interactions. *Cell Cycle* **2006,** *5*, 691-695.

14. Grill, J.; Van Beusechem, V. W.; Van de Valk, P.; Dirven, C. M. F.; Leonhart, A.; Pherai, D. S.; Haisma, H. J.; Pinedo, H. M.; Curiel, D. T.; Gerritsen, W. R., Combined targeting of adenoviruses to integrins and epidermal growth factor receptors increases gene transfer into primary glioma cells and spheroids. *Clinical Cancer Research* **2001,** *7*, 641-650.

15. Muthana, M.; Scott, S. D.; Farrow, N.; Morrow, F.; Murdoch, C.; Grubb, S.; Brown, N.; Dobson, J.; Lewis, C. E., A novel magnetic approach to enhance the efficacy of cell-based gene therapies. *Gene Therapy* **2008,** *15*, 902-910.

16. van Moorst, M.; Dass, C. R., Methods for co-culturing tumour and endothelial cells: Systems and their applications. *Journal of Pharmacy and Pharmacology* **2011,** *63*, 1513-1521.

17. Lima, A. C.; Mano, J. F., Micro/nano-structured superhydrophobic surfaces in the biomedical field: Part ii: Applications overview. *Nanomedicine* **2015,** *10*, 271-297.

18. Oliveira, N. M.; Neto, A. I.; Song, W. L.; Mano, J. F., Two-dimensional open microfluidic devices by tuning the wettability on patterned superhydrophobic polymeric surface. *Applied Physics Express* **2010,** *3*.

19. Lima, A. C.; Song, W. L.; Blanco-Fernandez, B.; Alvarez-Lorenzo, C.; Mano, J. F., Synthesis of temperature-responsive dextran-ma/pnipaam particles for controlled drug delivery using superhydrophobic surfaces. *Pharmaceutical Research* **2011,** *28*, 1294-1305.

20. Costa, A. M. S.; Alatorre-Meda, M.; Oliveira, N. M.; Mano, J. F., Biocompatible polymeric microparticles produced by a simple biomimetic approach. *Langmuir* **2014,** *30*, 4535-4539.

21. Leite, A. J.; Caridade, S. G.; Mano, J. F., Synthesis and characterization of bioactive biodegradable chitosan composite spheres with shape memory capability. *Journal of Non-Crystalline Solids* **2016,** *432*, 158-166.

22. Neto, A. I.; Demir, K.; Popova, A. A.; Oliveira, M. B.; Mano, J. F.; Levkin, P. A., Fabrication of hydrogel particles of defined shapes using superhydrophobic-hydrophilic micropatterns. *Advanced Materials* **2016**, n/a-n/a.

23. Neto, A. I.; Correia, C. R.; Custodio, C. A.; Mano, J. F., Biomimetic miniaturized platform able to sustain arrays of liquid droplets for high-throughput combinatorial tests. *Advanced Functional Materials* **2014,** *24*, 5096-5103.

24. Oliveira, M. B.; Mano, J. F., On-chip assessment of the protein-release profile from 3d hydrogel arrays. *Analytical Chemistry* **2013,** *85*, 2391-2396.

25. Oliveira, M. B.; Neto, A. I.; Correia, C. R.; Rial-Hermida, M. I.; Alvarez-Lorenzo, C.; Mano, J. F., Superhydrophobic chips for cell spheroids high-throughput generation and drug screening. *Acs Applied Materials & Interfaces* **2014,** *6*, 9488-9495.

26. Seo, J.; Lee, J. S.; Lee, K.; Kim, D.; Yang, K.; Shin, S.; Mahata, C.; Jung, H. B.; Lee, W.; Cho, S. W.; Lee, T., Switchable water-adhesive, superhydrophobic palladium-layered silicon nanowires potentiate the angiogenic efficacy of human stem cell spheroids. *Advanced Materials* **2014,** *26*, 7043-+.

27. Lee, M.; Yang, K.; Hwang, Y. H.; Byun, Y.; Lee, D. Y.; Cho, S. W.; Lee, H., Spheroform: Therapeutic spheroid-forming nanotextured surfaces inspired by desert beetle physosterna cribripes. *Advanced Healthcare Materials* **2015,** *4*, 511-515.

28. Neto, A. I.; Correia, C. R.; Oliveira, M. B.; Rial-Hermida, M. I.; Alvarez-Lorenzo, C.; Reis, R. L.; Mano, J. F., A novel hanging spherical drop system for the generation of cellular spheroids and high throughput combinatorial drug screening. *Biomaterials Science* **2015,** *3*, 581-585.

29. Rada, T.; Reis, R. L.; Gomes, M. E., Distinct stem cells subpopulations isolated from human adipose tissue exhibit different chondrogenic and osteogenic differentiation potential. *Stem Cell Reviews and Reports* **2011,** *7*, 64-76.

30. Birmingham, E.; Niebur, G. L.; McHugh, P. E.; Shaw, G.; Barry, F. P.; McNamara, L. M., Osteogenic differentiation of mesenchymal stem cells is regulated by osteocyte and osteoblast cells in a simplified bone niche. *European Cells & Materials* **2012,** *23*, 13-27.

31. Ha, C. Z.; Chen, H. Y.; Wang, J.; Liu, W.; Zhang, Y. X.; Pan, L.; Wang, W. H.; Chen, S. F.; Wang, D. W.; Wang, L. X., Effect of diabetic osteoblasts on osteogenic differentiation of human umbilical cord mesenchymal stem cells. *Biomedical Papers-Olomouc* **2015,** *159*, 388-393.

32. Rozila, I.; Azari, P.; Munirah, S.; Safwani, W. K. Z. W.; Gan, S. N.; Azurah, A. G. N.; Jahendran, J.; Pingguan-Murphy, B.; Chua, K. H., Differential osteogenic potential of human adipose-derived stem cells co-cultured with human osteoblasts on polymeric microfiber scaffolds. *Journal of Biomedical Materials Research Part A* **2016,** *104*, 377-387.

33. Villars, F.; Bordenave, L.; Bareille, R.; Amedee, J., Effect of human endothelial cells on human bone marrow stromal cell phenotype: Role of vegf? *Journal of Cellular Biochemistry* **2000,** *79*, 672-685.

34. Inglis, S.; Christensen, D.; Wilson, D. I.; Kanczler, J. M.; Oreffo, R. O. C., Human endothelial and foetal femur-derived stem cell co-cultures modulate osteogenesis and angiogenesis. *Stem Cell Research & Therapy* **2016,** *7*.

35. Rouwkema, J.; De Boer, J.; Van Blitterswijk, C. A., Endothelial cells assemble into a 3-dimensional prevascular network in a bone tissue engineering construct. *Tissue Engineering* **2006,** *12*, 2685-2693.

36. Meury, T.; Verrier, S.; Alini, M., Human endothelial cells inhibit bmsc differentiation into mature osteoblasts in vitro by interfering with osterix expression. *Journal of Cellular Biochemistry* **2006,** *98*, 992-1006.

37. de Groot, T. E.; Veserat, K. S.; Berthier, E.; Beebe, D. J.; Theberge, A. B., Surface-tension driven open microfluidic platform for hanging droplet culture. *Lab on a Chip* **2016,** *16*, 334-344.

6.9. Supporting Information

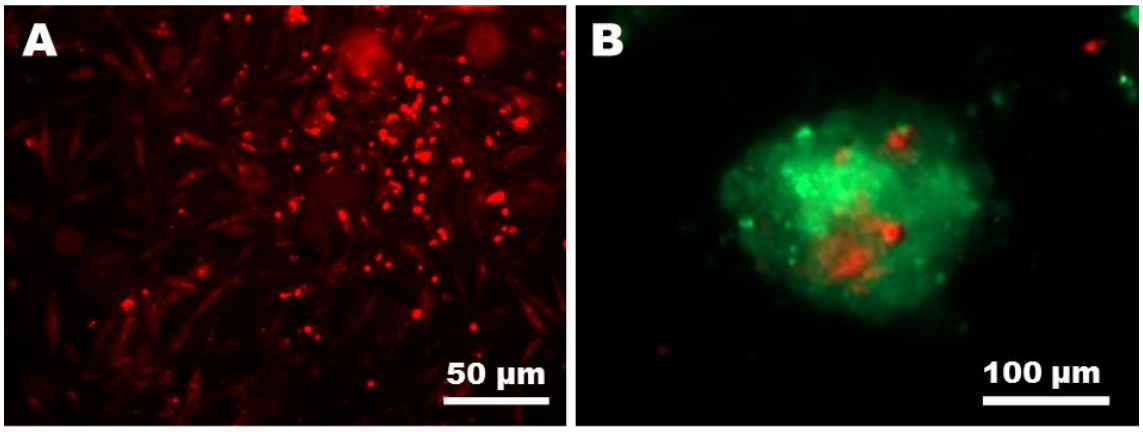

Figure 6.S1: Investigation of cell detachment from cell layer adhered to the PS above of the respective spheroid. (A) SaOs-2 cell layer adhered to the PS, being the SaOs-2 cells tagged with a red lipophilic staining before cell adhesion. (B) hASC spheroid formed in the SH surfaces in indirect co-cultures with Saos-2 cell line. hASC were tagged with a green lipophilic staining before the co-culture procedure. hASCs and the SaOs-2 cell line were pre-stained with 20mM 1,1′-Dioctadecyl-3,3,3′,3′-tetramethylindocarbocyanine perchlorate (DiI; Sigma, USA) and 3,3′-Dioctadecyloxacarbocyanine perchlorate (Dio; Sigma, USA), respectively. Cells were trypsinized and resuspended in 2 µM cell dye in serum-free medium for 10 min at 37 °C and washed with PBS prior to their seeding, performed such as described in experimental section. Images of the monolayer and spheroid were acquired using a reflected fluorescent light microscope (Axio Imager Z1, Zeiss).

Chapter 7

Liquid Marbles for High-Throughput Biological Screening of Anchorage-Dependent Cells

This chapter is based on the following publication:

Nuno M. Oliveira; Clara R. Correia; Rui L. Reis; João F. Mano; Liquid Marbles for High-Throughput Biological Screening of Anchorage-Dependent Cells. *Advanced Healthcare Materials* **2015**, 4, 264–270.

7.1. Abstract

Stable liquid marbles (LM) were produced by coating liquid droplets with a hydrophobic powder. The used hydrophobic powder was produced by fluorosilanization of diatomaceous earth, used before to produce superhydrophobic structures. Here, it is proposed LM use for high-throughput drug screening on anchorage-dependent cells. To provide the required cell adhesion sites inside the liquid environment of LM, surface modified poly(L-lactic acid) microparticles were used. A simple method that takes advantage from LM appealing features is presented, such as the ability to inject liquid on LM without disrupting (self-healing ability), and to monitor color changes inside of LM. After promoting cell adhesion, a cytotoxic screening test was performed as proof of concept. Fe^{3+} was used as a model cytotoxic agent and was injected on LM. After incubation, AlamarBlue reagent was injected and used to assess the presence of viable cells, by monitoring color change from blue to red. Color intensity was measured by image processing and analysis of pictures took using an ordinary digital camera. The proposed method was fully validated in counterpoint to a MTS (3- (4,5-dimethylthiazol-2-yl) -5- (3-carboxymethoxyphenyl) -2- (4-sulfophenyl) -2H- tetrazolium) colorimetric assay, a well-known method used for cytotoxicity assessment.

7.2. Introduction

Liquid marbles (LM) were first reported by Aussillous and Quéré.[1] LM were defined as liquid droplets covered with a hydrophobic powder. To manufacture the LM is only necessary to roll a liquid droplet over powder particles. The hydrophobic shell protects the encapsulated material by preventing any direct contact between the liquid and the external environment. However posteriorly, it was reported that LM can also be produced using hydrophilic particles, namely graphite and carbon black.[2, 3] LM make possible an easily manipulation of liquids, being good candidates to be used as micro-reactors, and sensors for water pollution detection, gas and pH.[4-9] Taking advantage of LM small dimensions, they can be used to miniaturize processes, reducing drastically the used amount of chemical/biological agents with high control over all the process conditions. LM are permeable to gases allowing their application for gas sensing.[6, 7] Since the required force to move LM on a surface is small, its manipulation can be easily done by using electrostatic, gravitational or magnetic fields, which make promising the LM usage on microfluidic applications.[10] Reports about LM applications on the biological field were published very recently. Arbatan T. and co-workers showed that LM could be used as a micro-bioreactor for rapid blood typing.[11] Using blood droplets to produce LM and by injection of specific antibodies it was possible to detect the blood type. The analysis was made by detecting differences on the LM color due to the haemagglutination reaction that occurs between the antibodies and the antigens on the surface of red blood cells. In another study, it was demonstrated that the LM could be used as micro-bioreactors for microorganisms culture by taking advantage of the LM permeability to gases.[12] On the biomedical and tissue engineering fields, LM were employed to produce cancer cell spheroids and embryoid bodies inside of LM.[13, 14] These works showed the applicability of LM to culture cells with ability to form aggregates by itself, such as the case of both cancer cell and embryonic stem cell lines.

Here, we propose a strategy to culture anchorage-dependent cells using the LM as cell culture reactors. The rational is based on the possibility of fast producing well designed LM in which high-throughput drug screening studies can be performed. To fabricate the LM, we propose to use a hydrophobic powder developed on a previous work that was produced by chemical surface modification of diatomaceous earth.[15] Diatomaceous are unicellular microalgae with a very peculiar silica micro-skeleton. After diatomaceous' dead, the exoskeletons remain and sediment on the bottom of lakes or sea, called diatomaceous earth. The exoskeletons of diatomaceous are microstructures with nanotextures on their surface – this could provide especial features to the particles, including increased water-repellency due to the well-known lotus effect – and are constituted mostly by amorphous silica. The dried diatomaceous earth can be easily hydrophobized by fluorosilanization to obtain hydrophobic particles.[15] Additionally, as the anchorage-dependent cells need to have a physical support to adhere and be able to proliferate, microparticles were dispersed on the LM core to be used as anchorage sites for the cells. This idea of using microparticles as supporting platforms for adherent cells was fully validated in previous works, in which functionalized poly(L-lactic acid) (PLLA) microparticles and cells were encapsulated within liquefied multilayered capsules.[16, 17] Taking advantage from the self-healing ability of the obtained LM it is possible to inject (or extract) controlled volumes of liquids without disrupting these structures. Color changes can be also visualized inside the LM. We hypothesize that such combination of characteristics could allow to develop a simple hierarchically organized device able to analyze the biological outcome of encapsulated cells in response to different agents, while maintaining the LM integrity. As proof of concept a cytotoxic study using iron (Fe^{3+}) was performed onto fibroblast-like cells using the proposed device.

Iron is a fundamental element for sustaining life. It is engaged in numerous biological processes and reactions, including DNA synthesis, erythropoiesis and both electron and oxygen transport.

However, iron is also potentially toxic, due it catalyses the generation of reactive oxygen species and highly reactive radicals (such as hydroxyl radicals) under aerobic conditions.[18]

7.3. Materials and Methods

7.3.1. Materials

Poly(L-lactic acid) (PLLA) with a molar mass Mw∼1600−2400 was purchased from Polysciences (Germany). Methylene chloride (CH_2Cl_2) was purchased from Fisher Chemical (U.K.). Diatomaceous earth (DE) commercially named Food-Grade Fossil Shell Fluor® was kindly supplied by Perma-Guard Europe (Switzerland). Iron (III) chloride hexahydrate ($FeCl_2.6H_2O$), 1H,1H,2H,2H-Perfluorodecyltriethoxysilane (PFDTS), polyvinyl alcohol (PVA), phosphate buffer saline (PBS), low glucose Dulbecco's Modified Eagle's Medium (DMEM) and sodium bicarbonate were purchased from Sigma-Aldrich (U.S.A). CellTiter 96 Aqueous One Solution Cell Proliferation Assay (MTS Assay) was purchased from Promega (U.S.A). AlamarBlue reagent was purchased from AbD Serotec (U.K). The immortalized mouse lung fibroblast cell line (L929) was purchased from the European Collection of Cell Cultures.

7.3.2. Hydrophobic powder production

The hydrophobic powder was prepared by chemical modification of DE with PFDTS, as already described before, with minor modifications.[15] To promote water desorption and expose more silanol groups on diatom surface the DE was heated at 190 °C under vacuum for 2 hour.[19] By mixing DE (1 g) with PFDTS solution (10 mL at 1% v/v) prepared in deionized water a DE suspension was prepared, the mixture was left to react overnight. By filtration it was separated the solid phase from the liquid. After dried in air, the obtained solid was heated at 220 ˚C for 5 minutes to promote silane hydrolysis and condensation, thereby producing a stable fluorosilanated layer on

the diatom surface. To remove any unreacted silane, the modified DE was washed with ethanol (20 mL) and dried on air before to use.

The modified DE morphology was analyzed using a Leica Cambridge S-360 (Leica, Germany) Scanning Electron Microscope (SEM) and the samples were pre-coated with a conductive gold layer.

7.3.3. PLLA microparticles production and characterization

Poly(L-lactic acid) (PLLA) microparticles were produced by emulsion solvent evaporation technique as elsewhere described.[17] Briefly, a 5% w/v solution composed by PLLA dissolved in CH_2Cl_2 was prepared. Under agitation, this solution was added to a 0.5% w/v PVA solution, and, ultimately, it was left to stir for 2 days at room temperature (RT) to evaporate the organic solvent. The produced PLLA microparticles were collected by centrifugation (300 g, 5 min) and washed several times with distilled water. Microparticles were subsequently frozen at −80 °C and freeze-dried (Cryodos, Telstar) for 3 days. Microparticles were stored at 4 °C until further use. The surface of PLLA microparticles was modified by air plasma treatment. The PLLA microparticles were placed inside a plasma reactor chamber (PlasmaPrep5, Gala Instrumente, Germany) fitted with a radio frequency generator. After the pressure of the chamber had stabilized to ∼0.2 mbar, a glow discharge plasma was created by controlling the electrical power at 30 V of electrical potential difference. Microparticles were treated for a total plasma reaction of 15 minutes with a gentle mixing every 5 minutes. PLLA plasma-treated microparticles (450 mg) were sterilized by UV radiation for 30 minutes and then immersed in acetic acid (30 mL at 0.02 M) containing collagen I (1200 μg) for 4 hours at RT. A mild shaking was employed every hour. Finally, microparticles were collected by centrifugation (300 g, 5 min) and washed three times with PBS.

The morphology of PLLA microparticles was visualized by optical microscopy (Axio Imager Z1m, Zeiss, Germany).

7.3.4. *In vitro* cell culture

The immortalized mouse lung fibroblast cell line (L929) was routinely cultured with low glucose DMEM supplemented with 3.7 $g \cdot L^{-1}$ sodium bicarbonate, 10% FBS, and 1% penicillin–streptomycin at pH 7.4. Cells were grown in 150 cm^2 tissue culture flasks and incubated at 37 °C in a humidified air atmosphere of 5% CO_2. Every 3–4 days, the medium was replaced with fresh medium.

7.3.5. Cytotoxicity test of the hydrophobic powder

The cytotoxicity test was accessed by an indirect contact method. The hydrophobic powder obtained from the DE was sterilized by autoclaving at 121 °C for 30 minutes. Hydrophobic powder (4 g) in DMEM culture medium (20 mL) were incubated at 37 °C and 60 rpm for 48 hours to extract possible leachable from the hydrophobic powder. After the extraction period, the extraction fluid was filtered using a 0.45 μm membrane filter. As negative and positive controls polystyrene cell tissue culture coverslips and latex rubber were used, respectively. On both cases the leachable extraction was performed under the same conditions of the samples. In a 6-well tissue culture plate L929 cell line suspension (2 mL) were dispensed per well in order to have a cell density of 10,000 cells per cm^2. Samples were incubated at 37 °C in a humidified air atmosphere of 5% CO_2. After 24 hours, in order to establish a 70-80% confluent cell monolayer, the cell culture medium was replaced by the different extraction fluids. Samples were incubated at 37 °C in a humidified air atmosphere of 5% CO_2 for more 48 hours. Then, a MTS colorimetric assay was performed to assess the cytotoxicity of the different materials.

7.3.6. Liquid Marble manufacture and PLLA microparticles effect assay on cell behavior

A uniform layer of hydrophobic powder was spread on a Petri dish. Over the hydrophobic powder layer droplets of the L929 cell suspension with or without PLLA microparticles on the suspension were dispensed one by one. Then, the liquid marbles by rolling the droplets over the hydrophobic

powder were produced. A cell concentration of 1×10^6 cells/mL and modified PLLA microparticles concentration of 50 mg/mL were used. 48-well plates were used to store the LM during the incubation period (n = 4 LM per well). To decrease water loss due to evaporation, only the wells on the center of the plate were used and a well of space between the LM and the plate border was left. The empty wells around the wells with LM were filled with water and plates with low evaporation lid were used. To access the PLLA microparticles effect over cell behavior, LM with or without PLLA microparticles were produced. Cell viability and proliferation assessment were performed by MTS colorimetric and DNA quantification assays, respectively.

The morphology of the adhered cells at the surface of the modified PLLA microparticles was analyzed by SEM. In a 96-well plate, modified PLLA microparticles and L929 cells were incubated at 37 °C in a humidified air atmosphere of 5% CO_2 for 24 hours. Then, culture medium was removed and 10% formalin was added to each well. After 1 hour at RT, formalin was removed and samples were dehydrated using sequential ethanol series (60, 70, 80, 90, 96, and 100%, 10 minutes each). For SEM (Cambridge S-360, Leica, Germany) visualization, the microparticles with cells were coated with gold.

7.3.7. Cytotoxicity screening assay on the developed device as proof of concept

A mixture of cells and PLLA microparticles was prepared and incubated at 37 °C in a humidified air atmosphere of 5% CO_2 for 3 hours. Then, the incubated mixture was used on the LM production with 20 µL of volume. After 24 hours of incubation, the $FeCl_3.6H_2O$ cytotoxic agent (4 µL) was injected on the LM. A range of concentrations from 6 to 18 mM (concentration inside the LM) was tested. The $FeCl_3.6H_2O$ solutions were prepared in PBS solution. After the agent injection, the LM were incubated. After 24 hours, MTS and DNA quantification assays were performed.

7.3.8. DNA Quantification Assay

For each condition 4 LM (with 20 μL each) per well were used to perform the DNA quantification assay. To compare between LM with or without PLLA microparticles, the measurements were performed at 0, 24, and 48 hours of incubation. On the $FeCl_3.6H_2O$ cytotoxicity test, the same procedure was used but the measurement was only performed in the end of the incubation period, namely 48 hours. After incubation, ultra-pure water (1 mL) was added to each well and LM were destroyed. After 1 hour of incubation, samples were transferred to eppendorf tubes and immediately stored at -80 °C, until quantification. The total amount of double-stranded DNA was quantified by using the Quant-iT PicoGreen dsDNA Assay Kit according to the manufacturer's instructions. The measurements were performed and using a multi-mode microplate reader (Synergy HT, BioTek, U.S.A). No background interference was detected due to the presence of hydrophobic powder or PLLA microparticles, as confirmed by a preliminary test using samples without cells (data not shown).

7.3.9. MTS viability assay

The cell viability was evaluated using the MTS colorimetric assay, according to the instructions of the manufacturer. On each well MTS medium (500 μL) were dropped and the LM were destroyed such as reported previously. LM without cells were also prepared to remove the background interference on the measurement. The MTS assays were performed after 48 hours of LM incubation. On the cytotoxicity assay, first it was determined the effective optical density (O.D.) value for each sample, by taking off the value of background interference to the O.D. measured at 490 nm. Then the relative cell viability (RCV) ratio was determined, by dividing the O.D. value of each sample by the O.D. value of the reference. The value of reference was the determined O.D. for the conditions that only PBS solution was injected in the LM.

7.3.10. AlamarBlue assay performed without destroying the liquid marbles

LM were produced such as reported previously using a cell suspension with PLLA microparticles. 96-well plates were used and a 40 µL LM were placed per well. As referred before to prevent water loss due to evaporation, only the wells on the center of the plate were used to store the LM, the empty wells around the LM were filled with water and plates with low evaporation lid were used. After the initial incubation of 24 hours, Fe^{3+} solution (8 µL) was injected on the LM in a concentration ranging from 6 to 18 mM. After more 24 hours of incubation, AlamarBlue reagent (4 µL) were injected in each LM and samples were incubated at 37 °C for 3 hours. After incubation, 24 bit color images were took from the 96-well plates using a 10 megapixel digital camera (Canon PowerShot G11). The pictures were taken with the camera fixed at 50 cm above the plates and with an optical zoom of 5×. Using the ImageJ software, the images were split in three channels: red, green and blue. On the 8 bit red channel, the red intensity was measured manually by defining on the image the area of interest for each LM. LM without cells were prepared to be used on background determination. By subtracting the red intensity value of background to the red intensity value for each condition, the effective red intensity (ERI) for each tested condition was determined. The red intensity value was measured using the ImageJ software. Then, by dividing the ERI value of each condition for the reference ERI value, the RCV ratio was determined. Such as before reference value was value for the conditions where only PBS solution was injected.

7.3.11. Statistical Analysis

At least two independent experiments in triplicate were performed. The results were present as mean ± standard deviation. To assess the level of significant differences on cytotoxicity test of hydrophobic powder, an one-way ANOVA followed by a Turkey's test was performed. Comparing LM with or without PLLA microparticles, the level of significant differences was performed by t-test or by two-way ANOVA for MTS or DNA assays, respectively. The difference between the proposed

method and the standard MTS assay was also analyzed by two-way ANOVA. All the statistical analysis was carried out using Graph Pad Prism 5.0 software for Windows.

7.4. Results and Discussion

On this work, we propose a method to use liquid marbles (LM) in high-throughput screening applications, involving cells compartmentalized in three-dimensional (3D) environments. The LM production is easy and enables to create individual micro-bioreactors where, for example, the effect of a chemical agent over cellular behavior can be study. To produce LM it is only necessary to roll a liquid droplet over a hydrophobic powder layer until complete coating of the droplet. The used hydrophobic powder was diatomaceous earth that was chemical modified with a fluorosilane. By the fluorosilanization process the surface energy of diatom decrease and the hydrophilic diatoms become hydrophobic. This modification process was reported and fully characterized in a previous work.[15] Taking advantage from the LM self-healing ability that allows to inject liquid without destroying its integrity, it is possible to inject different agents throughout time and study the biological outcome of encapsulated cells. By injecting an agent that changes its color against some specific cellular response, it is possible to observe and compare the tested conditions and correlate with cell response only by monitoring the color change of the LM. This is possible due to the fact that the LM are translucent. The color monitoring can be performed by simply taking pictures of the LM, and then measuring the color intensity by image processing. An overview of all steps involved in the proposed method is schematically represented in Figure 7.1.

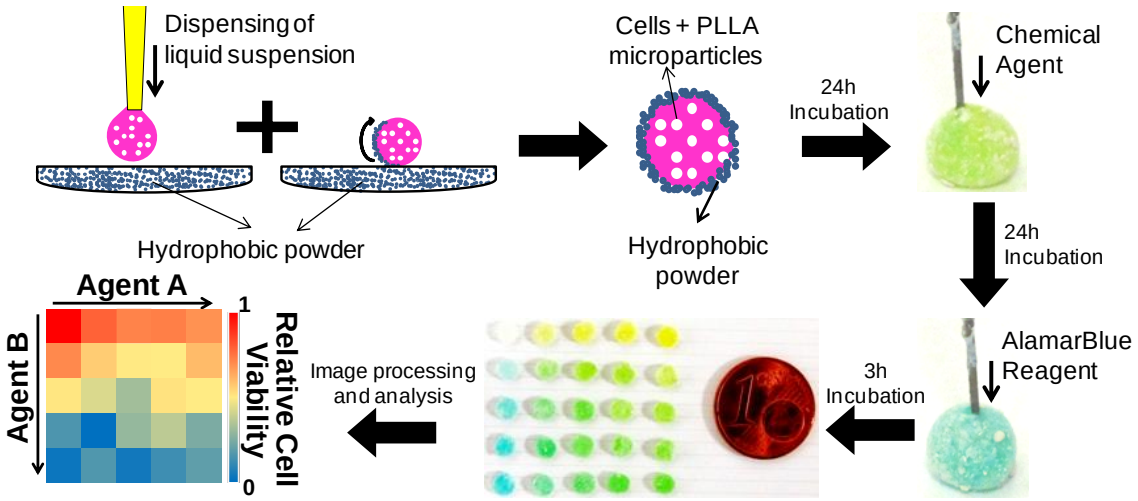

Figure 7.1: Schematic representation of the proposed method for liquid marbles usage on high-throughput drug screening. First, a defined volume of cell suspension with modified PLLA microparticles was dispensed over a hydrophobic powder bed. After to coat the liquid droplet with the hydrophobic powder, the produced liquid marbles were incubated for 24 hours. Then, taking advantage of the ability to inject liquids inside the liquid marbles maintaining its integrity, chemical agents (drugs) to be tested can be injected. After a new incubation period, AlmarBlue reagent can be injected to monitor cell viability by color change inside of the liquid marbles. The measurement of the color intensity was performed by image processing/analysis of pictures of the liquid marbles and a heat map with the results can be obtained.

The used diatomaceous to produce the hydrophobic powder present a cylindrical shape, as showed in Figure 7.2(A). To access the ability of LM to support living cell encapsulation using the proposed hydrophobic powder, we performed a cytotoxicity test. As showed on Figure 7.2(B), the hydrophobic powder does not present any cytotoxicity for cells compared with tissue culture polystyrene used as negative control. These results are due to the high hydrophobicity of the powder, in which the interaction with the water-based liquids, such as the medium culture, is low. Therefore, any toxic substances from hydrophobic powder are released to culture medium.

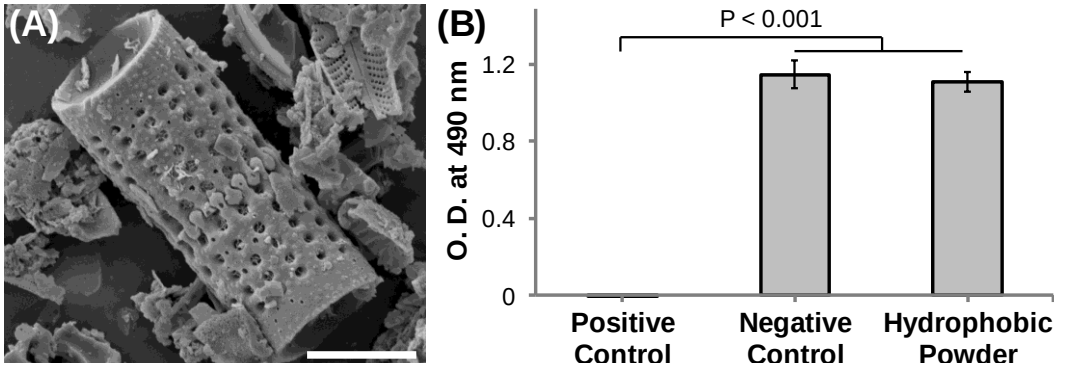

Figure 7.2: (A) SEM image of diatomaceous earth that was used to produce the hydrophobic powder. Scale bar is 5 µm. (B) Cytotoxicity test of the hydrophobic powder using the L929 cell line was accessed by MTS assay. As positive and negative controls latex rubber and tissue culture polystyrene coverslips were used, respectively.

Our main objective was to develop a screening system for anchorage-dependent cells culture using the LM. Previously similar systems were reported but for non adherent cells, namely for cell spheroids and embryoid bodies production.[13, 14] To achieve our goal cell anchorage sites for cell adhesion were introduced by incorporating solid microparticles in the liquid environment of the LM. We specifically used PLLA microparticles modified by plasma treatment with collagen.[16, 17] The produced PLLA microparticles present a size in the range of 20-100 µm, suitable to be used as cell carriers (Figure 7.3(B)). The surface of PLLA microparticles was modified to enhance cell adhesion by combining air plasma treatment and deposition of collagen I. Collagen is a natural biomacromolecule with domains that are known as specific binders to integrin on cellular membrane. To test the importance of the presence of PLLA microparticles on the proposed system, we produced LM with and without PLLA microparticles dispersed together with cells in the LM core. LM marbles with several controlled volumes can be easily produced such as illustrated in Figure 7.3(A).

Figure 7.3: (A) Liquid marbles with distinct sizes produced from liquid droplets with the following volumes: 5, 7.5, 10, 20, 30 and 40 µL. Scale bar is 1 mm. (B) Optical microscopy image of PLLA microparticles that were dispersed in the core of the liquid marbles to provide anchorage sites for cell adhesion. Scale bar is 100 µm.

The DNA quantification results showed on Figure 7.4(A) show a higher amount of DNA per LM after 48 hour of incubation on the LM with PLLA microparticles inside, suggesting that the cell proliferation was enhanced by PLLA microparticles presence.[17] These results were corroborated by the MTS (3- (4,5-dimethylthiazol-2-yl) -5- (3-carboxymethoxyphenyl) -2- (4-sulfophenyl) -2H-tetrazolium) assay results on Figure 7.4(B), that show a higher cell viability for LM with PLLA microparticles, also for an incubation period of 48 hours. The cell viability can be directly related with the optical density at 490 nm wavelength on the MTS assay. In both assays, cells encapsulated in LM without PLLA microparticles showed a cell proliferation and viability that were around 50% less of that obtained for LM with PLLA microparticles. The results clearly demonstrate the importance of introducing such particulate elements to provide anchorage points for adherent cells. By using the microparticles, an advantage is that a higher surface area for cell adhesion is provided comparing with two-dimensional (2D) cell culture in well plates. A 20 µL LM with PLLA microparticles offer 50-60% more area (assuming that particles density is 1 $Kg.dm^{-3}$ and average particle size is 60 µm) for cell adhesion than a well of the 96 well plate. This advantage is also associated with the necessity to use less volume of culture medium. Only 20 µL of culture medium were used on LM, when the recommended working volume for a 96 well plate is 75-200 µL per well. The cells-microparticles interactions were visualized by SEM. Figure 7.4(C) show that cells were adhered and spread across the modified PLLA microparticles surface, evidencing their

fibroblast-like elongated morphology. Based on the SEM image analysis, after 24 hours of incubation the PLLA microparticles aggregated by cell adhesion. We observed this phenomena in previous works, and attributed to the fact that the dorsal side of cells adhered to one particles can adhere to the surface of other particles, thus contributing for particle aggregation.[16, 17] Hereby, we believe that with the PLLA microparticles/cells aggregation a 3D structure was obtained inside of the LM.

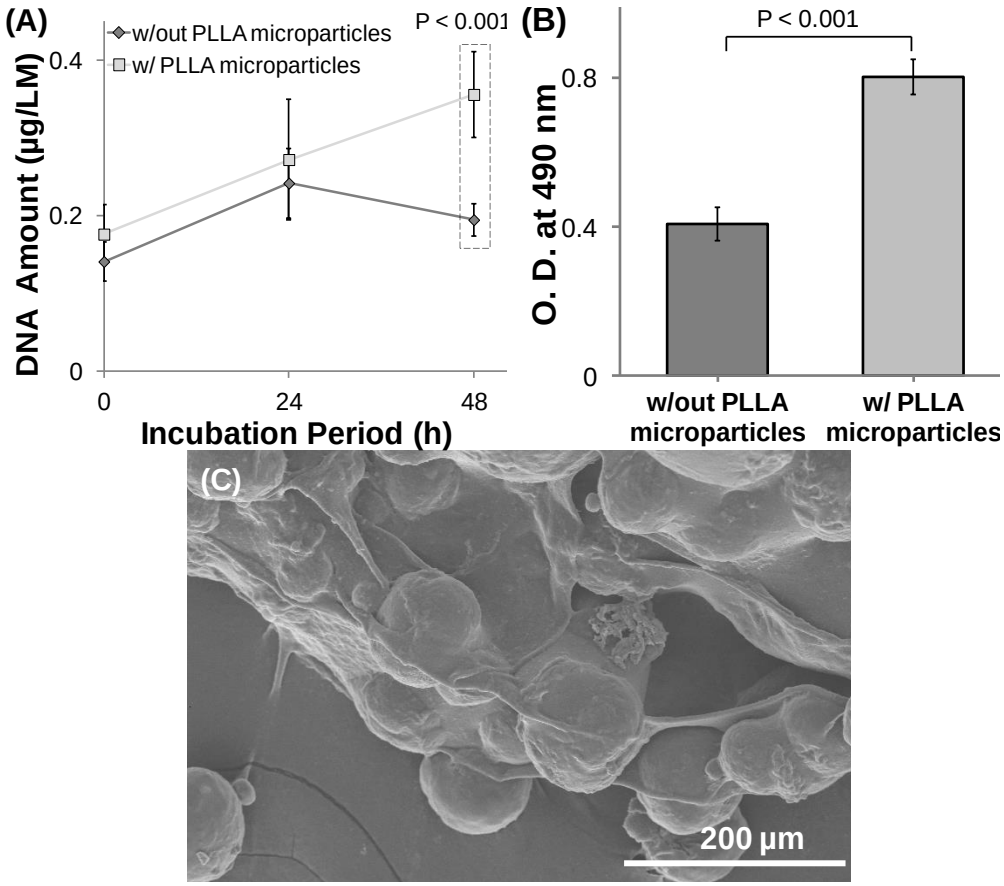

Figure 7.4: L929 cell response upon encapsulation in liquid marbles without (w/out) or with (w/) PLLA microparticles inside the core. (A) DNA quantification per liquid marble at different incubation periods, namely 0, 24 and 48 hours. (B) Optical density values of MTS assay at 490 nm for liquid marbles without (w/out) or with (w/) PLLA microparticles after 48 hours of incubation. (C) SEM image of modified PLLA microparticles with adhered L929 cells on surface after 24 hours of incubation.

After assessing the non-cytotoxicity of hydrophobic powder and the beneficial effect of encapsulating cells with PLLA microparticles within LM, cytotoxicity study with a chemical agent

was performed to validate the system as a drug-screening device. We propose to use LM with PLLA microparticles as a means to carry out high-throughput screening of drugs on anchorage-dependent cells. The ability of LM to handle the injection of small volumes (until around of 30% of the initial volume) and to take out liquid without disrupt the LM make the LM good candidates for the suggested application – see Figure 7.5 that illustrates this liquid transfer possibility.

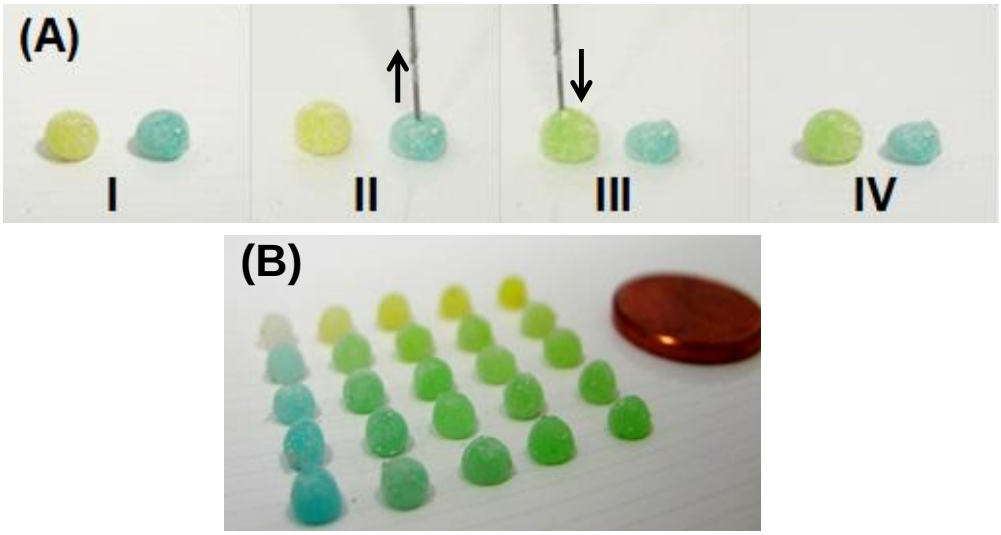

Figure 7.5: (A) An image sequence to show that it is possible to remove or inject liquid on liquid marbles without destroy its structure. I- Two liquid marbles with the same volume were produced. II- Partial volume of the blue liquid marble was withdrawn. III- The removed volume in the previous step was injected on the yellow liquid marble. IV- The liquid marble structures remain stable after manipulation. (B) Several liquid marbles can be produced to test different conditions during cell culture, showing their ability to be used as high-throughput drug screening devices.

The self-healing ability of LM can be explained by the fact that the hydrophobic powder coating possibly is multilayered. Bormashenko *et. al* reported a work where they studied the inflation and deflation (by evaporation) of LM.[20] Their results are explained below and we believe that our case fits in the described events. When a liquid is injected, the core volume increases and consequently the surface area of the LM also increases. To compensate this effect, the particles from the inner layer of the hydrophobic coating migrate to the LM surface, maintaining the integrity of the LM structure. On the other hand at the micrometer level, the particles of the coating are not

homogeneously distributed and some clearings can be found on the LM surface. When an amount of the liquid core is withdraw, the surface area of the clearings decreases.[20] This dynamic behavior of the LM shell gives them the great feature of self-healing properties after the injection step.

For the proof of concept, the Fe^{3+} was choose as the cytotoxic agent and was used on the concentrations ranging from 6 mM to 18 mM. After 24 hour of cell culture in the LM containing PLLA microparticles in contact with Fe^{3+}, cell proliferation for the different conditions was determined by DNA quantification. The DNA amount ratio was determined taking as the reference the LM in which PBS solution was injected. Figure 7.6 shows that the relative DNA amount ratio decreases with increasing of iron concentration. The same tendency was confirmed by MTS assay, as shown in Figure 7.7. As expected, with the increasing of Fe^{3+} concentration the cell viability decrease, showing that the iron toxicity is concentration-dependent. An iron excess on medium results in increasing of oxidative stress and damage in the DNA, lipids and proteins.[21]

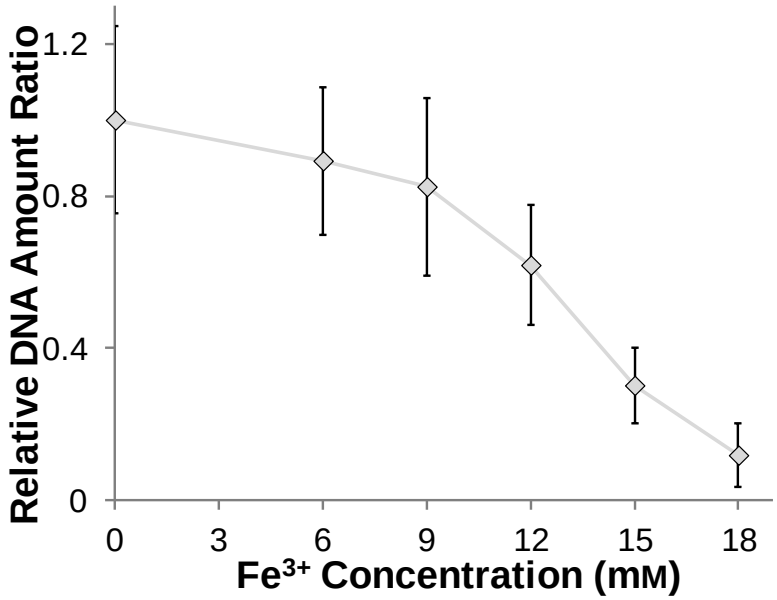

Figure 7.6: Relationship between Fe^{3+} concentration and the relative DNA amount ratio. LM injected only with PBS were used as the reference. The measurement was performed after 48 hours of cell culture, 24 hours without Fe^{3+} and more 24 hours of culture in contact with the cytotoxic agent.

We also aimed to develop a strategy to monitor the behavior of encapsulated cells within the LM, while the integrity of the LM is maintained. Taking advantage from the fact that it is possible to detect color changes on the core of LM, the cell monitoring inside the LM can be done, by using appropriate reagents that change its color in response to some cellular event. Both MTS and AlamarBlue reagents have this kind of characteristics and are used on conventional tests to access the cell viability. In the MTS assay, a tretrazolium salt is reduced into a formazan product and, subsequently, the color of MTS solution changes from yellow to brown. A similar process also occurs in the AlamarBlue assay, where a resazurin-based product is reduced to resofurin, and the color of the solution changes from blue to red in the presence of viable cells. In both assays, the mitochondrial enzymes of metabolically active cells promote a similar reduction reaction. Therefore, the two methods have comparable sensibility for the measurement of cell viability.[22, 23] Based on this evidence, we adapted the AlamarBlue assay to the developed LM and the results were compared with the standard MTS assay. The advantage in using the AlamarBlue reagent is that it can be added directly to the encapsulated cells, without the need of using a different solvent, as in the case of the MTS assay in which a serum free medium is required. Other advantage is the red color that appears in the presence of viable cells, that is specifically one of the three single channels that a digital camera can detect. For the adapted AlamarBlue assay, the reagent was injected on LM and the assay was performed without the need to destroy the LM, whereas for MTS assay, it was necessary to disrupt the LM. Comparing the measurement performed by the two methods, no significant differences were detected, as shown in Figure 7.7. However, the values obtained by image acquisition have a higher standard deviation compared to the standard MTS assay.

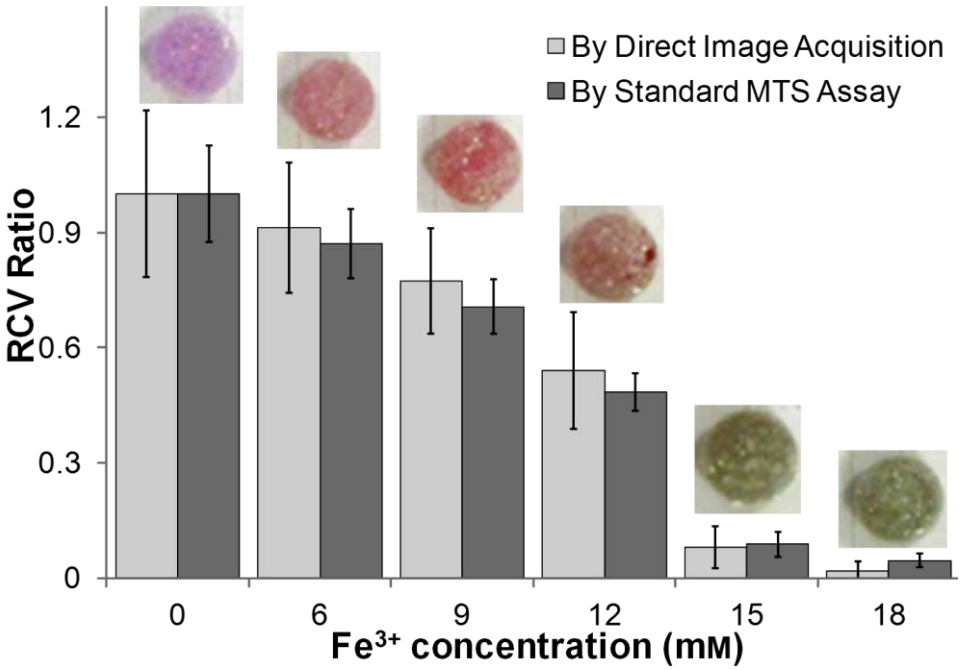

Figure 7.7: Relationship between Relative Cell Viability (RCV) ratio and Fe^{3+} concentration determined using two different methods. A non-destructive method by image processing of pictures from LM using a conventional digital camera is compared with a standard destructive MTS assay. A representative picture of LM is show for each condition. No significant differences were found between the two methods for all Fe^{3+} concentrations analyzed.

Although, some non-homogenous distribution of hydrophobic particles on LM surface at the micro-level was reported before on literature by Bormashenko *et. al.*[24] However, for the proposed method this fact does not show to be critical, because at the macro-level wherein we performed the color intensity measurements the obtained values are not so different between them, such as shown in Figure 7.S1 and Figure 7.S2 from supporting information. In other words, the non-homogenous particles distribution at micro-level does not interfere significantly on the proposed *in situ* colorimetric methodology.

To express the impact of the tested cytotoxic agent on the cell viability the IC_{50} factor (inhibitory concentration for 50% of viable cells) was determined. For MTS assay the obtained value was 11.49 mM and for the proposed non destructive method was 11.92 mM. For the same cytotoxic agent and cell line, the reported values on literature were 3.58 mM and 5.42 mM.[25, 26] Different

contact times between the cells and the cytotoxic agent, different cell densities and viable cell quantification methods were used on these three studies. However, the major difference is that the cytotoxicity test was performed in this study in a 3D cell culture microenvironment, while on previous reported studies, a 2D cell culture was employed. It has been reported that 3D cell culture environments have more resistance to cytotoxic agents as compared to 2D cell culture environments.[27, 28] This benefits the proposed assay platform as the cytotoxicity results from the 3D systems are considered to be more reliable to predict *in vivo* toxicity effects. In fact, cell behavior and both cell-cell and cell-matrix interactions on 3D models are more analogous to their native state.[27, 29] In this sense, several studies presenting strategies to culture cells on 3D environment were been reported, namely spheroid and scaffold-based strategies.[30-32]

For example, Ho *et al.* developed a high throughput screening method based on multicellular tumor spheroid culture from breast cancer cells.[31] However, spheroid-based high throughput screening methods are both reagent and time consumption, because after spheroid production they need to be harvest and translocated for multi-well plates for posterior drug testing. During drug testing with the medium exchange cell loss also occur. To solve these issues, Li *et al.* presented a method based on a micro-scaffold array chip for cell-based high-throughput drug testing.[28] A sponge-like micro-scaffolds were used as a means to prevent cell loss during medium exchange and for auto-loading of cells or drugs. However, special equipment is required to produce the reported chip such as a laser engraver machine. By our method only simple and regular lab equipments are required.

7.5. Conclusion

We showed the possibility to use hydrophobized diatomaceous earth to produce liquid marbles (LM). The LM can be easily produced with several controlled sizes. Injection or removal of liquid from the LM can be performed without destroy its structure. Color changes inside the developed LM are easily detected permitting to use such compartments in colorimetric-based non-destructive tests. Since the main goal was to culture anchorage-dependent cells, we proposed a novel strategy to culture these cells inside the LM using PLLA microparticles to provide sites for cell adhesion. The importance of adding PLLA microparticles to the liquid core of LM on cell proliferation was demonstrated. As the size of the microparticles is at least one order of magnitude lower than the size of the LM the system maintains its flexibility and handleability. The application of the developed hierarchical LM as a high-throughput drug screening device was assessed. It was shown to be possible to perform cytotoxicity tests using LM, by monitoring color changes *in situ*. The proposed alternative was fully validated by comparison with a well know (destructive) conventional method. We believe that the LM with encapsulated solid microparticles can be used on high-throughput drug screening with several benefits. As a 3D cell culture system, LM provide reliable results for predicting *in vivo* effects, and with low need of resources, namely in terms of medium volume, cell number, drug/reagent amount, equipment, and time. The versatility of the proposed system could be also easily adapted to other applications including as a platform to set-up disease model or for fabrication of 3D micro-tissues for tissue engineering.

7.6. Acknowledgments

This work was carried out under the scope the EU 7th Framework Programme (FP7/2007–2013) under grant agreement no. FP7KBBE-2010–4–266033 (SPECIAL). The work was also financially supported by the Portuguese Foundation for Science and Technology (FCT) project PTDC/CTM-BIO/1814/2012. N. M. Oliveira acknowledges the financial support from Portuguese Foundation for Science and Technology – FCT (Grant SFRH/BD/73172/2010), from the financial program POPH/FSE from QREN.

7.7. References

1. Aussillous, P.; Quere, D., Liquid marbles. *Nature* **2001,** *411*, 924-927.

2. Dandan, M.; Erbil, H. Y., Evaporation rate of graphite liquid marbles: Comparison with water droplets. *Langmuir* **2009,** *25*, 8362-8367.

3. Bormashenko, E.; Pogreb, R.; Musin, A.; Balter, R.; Whyman, G.; Aurbach, D., Interfacial and conductive properties of liquid marbles coated with carbon black. *Powder Technology* **2010,** *203*, 529-533.

4. Xue, Y. H.; Wang, H. X.; Zhao, Y.; Dai, L. M.; Feng, L. F.; Wang, X. G.; Lin, T., Magnetic liquid marbles: A "precise" miniature reactor. *Advanced Materials* **2010,** *22*, 4814-+.

5. Bormashenko, E.; Musin, A., Revealing of water surface pollution with liquid marbles. *Applied Surface Science* **2009,** *255*, 6429-6431.

6. Tian, J. F.; Arbatan, T.; Li, X.; Shen, W., Liquid marble for gas sensing. *Chemical Communications* **2010,** *46*, 4734-4736.

7. Tian, J. F.; Arbatan, T.; Li, X.; Shen, W., Porous liquid marble shell offers possibilities for gas detection and gas reactions. *Chemical Engineering Journal* **2010,** *165*, 347-353.

8. Dupin, D.; Armes, S. P.; Fujii, S., Stimulus-responsive liquid marbles. *Journal of the American Chemical Society* **2009,** *131*, 5386-+.

9. Bormashenko, E.; Balter, R.; Aurbach, D., Use of liquid marbles as micro-reactors. *International Journal of Chemical Reactor Engineering* **2011,** *9*.

10. Bormashenko, E., Liquid marbles: Properties and applications. *Current Opinion in Colloid & Interface Science* **2011,** *16*, 266-271.

11. Arbatan, T.; Li, L. Z.; Tian, J. F.; Shen, W., Liquid marbles as micro-bioreactors for rapid blood typing. *Advanced Healthcare Materials* **2012,** *1*, 80-83.

12. Tian, J. F.; Fu, N.; Chen, X. D.; Shen, W., Respirable liquid marble for the cultivation of microorganisms. *Colloids and Surfaces B-Biointerfaces* **2013,** *106*, 187-190.

13. Arbatan, T.; Al-Abboodi, A.; Sarvi, F.; Chan, P. P. Y.; Shen, W., Tumor inside a pearl drop. *Advanced Healthcare Materials* **2012,** *1*, 467-469.

14. Sarvi, F.; Arbatan, T.; Chan, P. P. Y.; Shen, W., A novel technique for the formation of embryoid bodies inside liquid marbles. *Rsc Advances* **2013,** *3*, 14501-14508.

15. Oliveira, N. M.; Reis, R. L.; Mano, J. F., Superhydrophobic surfaces engineered using diatomaceous earth. *Acs Applied Materials & Interfaces* **2013,** *5*, 4202-4208.

16. Correia, C. R.; Sher, P.; Reis, R. L.; Mano, J. F., Liquified chitosan-alginate multilayer capsules incorporating poly(l-lactic acid) microparticles as cell carriers. *Soft Matter* **2013,** *9*, 2125-2130.

17. Correia, C. R.; Reis, R. L.; Mano, J. F., Multilayered hierarchical capsules providing cell adhesion sites. *Biomacromolecules* **2013,** *14*, 743-751.

18. Wang, J. A.; Pantopoulos, K., Regulation of cellular iron metabolism. *Biochemical Journal* **2011,** *434*, 365-381.

19. Zhuravlev, L. T., The surface chemistry of amorphous silica. Zhuravlev model. *Colloids and Surfaces a-Physicochemical and Engineering Aspects* **2000,** *173*, 1-38.

20. Bormashenko, E.; Musin, A.; Whyman, G.; Barkay, Z.; Starostin, A.; Valtsifer, V.; Strelnikov, V., Revisiting the surface tension of liquid marbles: Measurement of the effective surface tension of liquid marbles with the pendant marble method. *Colloids and Surfaces a-Physicochemical and Engineering Aspects* **2013,** *425*, 15-23.

21. Marques, O.; da Silva, B. M.; Porto, G.; Lopes, C., Iron homeostasis in breast cancer. *Cancer Letters* **2014,** *347*, 1-14.

22. Nakayama, G. R.; Caton, M. C.; Nova, M. P.; Parandoosh, Z., Assessment of the alamar blue assay for cellular growth and viability in vitro. *Journal of Immunological Methods* **1997,** *204*, 205-208.

23. Pranczk, J.; Jacewicz, D.; Wyrzykowski, D.; Chmurzynski, L., Platinum(ii) and palladium(ii) complex compounds as anti-cancer drugs. Methods of cytotoxicity determination. *Current Pharmaceutical Analysis* **2014,** *10*, 2-9.

24. Bormashenko, E.; Bormashenko, Y.; Musin, A.; Barkay, Z., On the mechanism of floating and sliding of liquid marbles. *Chemphyschem* **2009,** *10*, 654-656.

25. Okazaki, Y.; Rao, S.; Asao, S.; Tateishi, T., Effects of metallic concentrations other than ti, al and v on cell viability. *Materials Transactions Jim* **1998,** *39*, 1070-1079.

26. Yamamoto, A.; Honma, R.; Sumita, M., Cytotoxicity evaluation of 43 metal salts using murine fibroblasts and osteoblastic cells. *Journal of Biomedical Materials Research* **1998,** *39*, 331-340.

27. Lee, J.; Lilly, G. D.; Doty, R. C.; Podsiadlo, P.; Kotov, N. A., In vitro toxicity testing of nanoparticles in 3d cell culture. *Small* **2009,** *5*, 1213-1221.

28. Li, X. K.; Zhang, X. Y.; Zhao, S.; Wang, J. Y.; Liu, G.; Du, Y. N., Micro-scaffold array chip for upgrading cell-based high-throughput drug testing to 3d using benchtop equipment. *Lab on a Chip* **2014,** *14*, 471-481.

29. Breslin, S.; O'Driscoll, L., Three-dimensional cell culture: The missing link in drug discovery. *Drug Discovery Today* **2013,** *18*, 240-249.

30. Friedrich, J.; Seidel, C.; Ebner, R.; Kunz-Schughart, L. A., Spheroid-based drug screen: Considerations and practical approach. *Nature Protocols* **2009,** *4*, 309-324.

31. Ho, W. Y.; Yeap, S. K.; Ho, C. L.; Rahim, R. A.; Alitheen, N. B., Development of multicellular tumor spheroid (mcts) culture from breast cancer cell and a high throughput screening method using the mtt assay. *Plos One* **2012,** *7*.

32. Fischbach, C.; Chen, R.; Matsumoto, T.; Schmelzle, T.; Brugge, J. S.; Polverini, P. J.; Mooney, D. J., Engineering tumors with 3d scaffolds. *Nature Methods* **2007,** *4*, 855-860.

7.8. Supporting Information

Average value of blue color intensity for each LM						Mean ± standard deviation
212.215	213.106	208.312	211.046	209.590	211.668	210.98 ± 1.62

Figure 7.S1: Liquid marbles (LM) with distinct sizes produced from liquid droplets with the following volumes: 5, 7.5, 10, 20, 30 and 40 µL. The average value of blue color intensity was determined by ImageJ for each LM, the whole area of each LM was used for the determination. The mean value of all six values was calculated as well as the respective standard deviation.

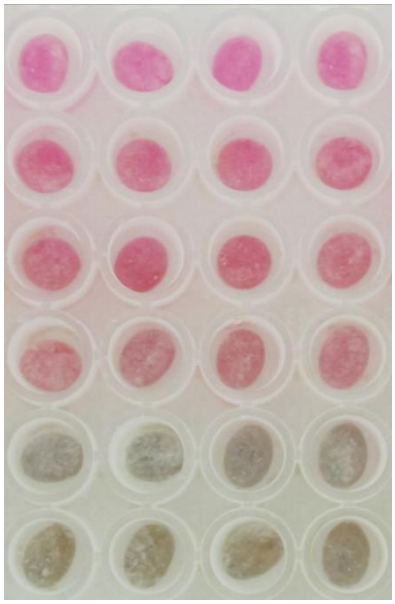

Average value of red color intensity for each LM				Mean ± standard deviation
211.413	211.734	211.679	211.268	211.52 ± 0.19
203.092	202.673	204.202	203.900	203.47 ± 0.61
194.577	192.821	194.221	195.192	194.20 ± 0.87
191.215	183.170	185.208	187.031	186.66 ± 2.97
156.172	156.984	152.214	160.006	156.34 ± 2.78
152.881	151.579	152.648	149.539	151.66 ± 1.32

Figure 7.S2: LM corresponding to the different studied concentrations are present in four replicates. The average value of red color intensity was determined by ImageJ for each LM, the whole area of each LM was used for the determination. The mean value of the four values of each condition was calculated as well as the respective standard deviation.

Chapter 8

Hydrophobic Hydrogels: Toward Construction of Floating (Bio)microdevices

This chapter is based on the following publication:

Nuno M. Oliveira; Yu S. Zhang; Jie Ju; Ai-Zheng Chen; Yu Chen; Sameer R. Sonkusale; Mehmet R. Dokmeci; Rui L. Reis; João F. Mano; Ali Khademhosseini; Hydrophobic Hydrogels: Toward Construction of Floating (Bio)microdevices. *Chemistry of Materials* **2016,** 28, 3641–3648.

8.1. Abstract

Hydrogels, formed through cross-linking of hydrophilic polymer chains, represent a class of materials that are capable of holding large volumes of water. Here we report a novel class of hydrophobic hydrogels that can free-float on the surface of different aqueous media by coating conventional hydrogels with a layer of hydrophobic microparticles. We further demonstrate that these floating hydrogel-based devices can be used for sensing applications on liquid surfaces such as the construction of floating pH meters. Moreover, we demonstrate that the floating hydrogels present high mobility with excellent self-assembling property on the surface of water. Importantly, the floating systems reserved the intrinsic biocompatibility of the core hydrogels, enabling microengineering of floating tissue constructs. It is expected that these floating hydrophobic hydrogel-based devices will likely find widespread applications including but not limited to sensing, tissue engineering, and biomedicine.

8.2. Introduction

Hydrogels, formed through cross-linking of hydrophilic polymer chains, represent a class of materials that are capable of holding large volumes of water.[1, 2] The dilute network of the polymers in the hydrogels can be created by a variety of techniques including physical, ionic, and covalent cross-linking via chemical-, light-, or pH-induced reactions.[1, 2] The water-rich nature of the hydrogel systems has found widespread applications in numerous fields such as sensing[3, 4] and biomedicine.[5-7] However, pristine hydrogels are often insufficient to achieve extended use due to the limited functionality that the unmodified networks possess, therefore necessitating the functionalization of the hydrogels for particular applications. For example, moieties such as RGD peptide and fibronectin have been incorporated into the hydrogels to promote cell adhesion;[8] vehicles for delivering bioactive molecules (e.g., growth factors) can be loaded into the hydrogels to promote tissue responses;[9] and conjugation of enzyme-sensitive peptide linkers with the polymer networks will induce cell-mediated remodeling of the hydrogels.[9-12] While all these conventional modifications of such water-rich systems largely retain their hydrophilic properties, the ability to maintain these bulk properties but at the same time altering their surface properties is important.

It has been demonstrated that free-standing, nonsticky liquid droplets can be coated with a layer of hydrophobic micro/nanoparticles on their outer surfaces.[13, 14] These particles adhere stably at the liquid/air interface, rendering these liquid droplets hydrophobic as individual nonwetting soft objects, while the hydrophilicity in their interiors is well maintained.[13, 14] The liquidity of these "liquid marbles" upon contact with a solid substrate is converted to a solid–solid contact as mediated by the hydrophobic microparticles at the interfaces.[15] The unique properties of these "liquid marbles" have made them suitable for a range of applications including sensing (e.g.

temperature, pH, UV, and gas),[16-18] and use as microreactors,[19, 20] as well as for high-throughput screening.[21-26]

Inspired by "liquid marbles", here we propose a novel concept termed "hydrophobic hydrogels". By coating the surfaces of solid, cross-linked hydrophilic polymer networks (i.e., hydrogels) with hydrophobic microparticles, it rendered these hydrogels with hydrophobic exteriors while maintaining the hydrophilic microenvironment in the interiors. Interestingly, it was found that these hydrophobic hydrogels could not only free-stand but also float on the surface of aqueous media, presumably due to the water repellency incurred by the presence of a layer of scattered air gaps trapped within the hydrophobic shell.[13, 14, 27, 28] These hydrophobic hydrogel units can therefore be processed into floating microdevices for uses in many unconventional applications. We further illustrated three unique applications of the hydrophobic hydrogels including the construction of floating optical pH sensors, microengineering of self-assembling floating hydrogels, and fabrication of engineered biological tissues, which could not be achieved with the conventional "liquid marble".

8.3. Materials and Methods

8.3.1. Preparation of hydrophobic microparticles

The hydrophobic microparticles were prepared by chemical modification of the pristine diatomaceous earth (DE) with 1H,1H,2H,2H-perfluorodecyltriethoxysilane (PFDTS). To promote water desorption, the DE was first dried at 190 °C under vacuum for at least 2 h before use. DE suspension was then prepared by mixing 1 g of DE with 10 mL of PFDTS solution at 1 vol% in deionized water. The reaction was allowed to take place overnight. The solid phase was subsequently separated from the liquid by filtration. The dried solid was heated at 220 °C for 5 min to stabilize the fluorosilanated layer on the DE surface. The unreacted silane was removed

by washing the modified DE with 20 mL of ethanol and the PFDTS-DE microparticles were finally dried in air. The morphology of the microparticles was analyzed using SEM (Ultra 55, Carl Zeiss). The surface chemical compositions of the pristine and coated DE microparticles were analyzed by X-ray photoelectron spectroscopy (XPS) (K-Alpha ESCA, Thermo Fisher Scientific).

8.3.2. Gelatin methacryloyl (GelMA) synthesis

GelMA was synthesized by following our established protocol. Briefly, gelatin type A was dissolved at 10 w/v% in phosphate buffered saline (PBS) at 60 °C under vigorous stirring. Methacrylic anhydride was then slowly added under constant stirring at 50 °C until a concentration of 8 vol% was reached and allowed to react for 2 h. Following a 2X dilution with warm PBS (40 °C) to stop the reaction, the solution was immediately dialyzed against deionized water using 12-14 kDa cutoff dialysis membrane at 40 °C for 1 week to remove salts, side products, and unreacted chemicals. After lyophilizing the dialyzed solution, a white porous foam of GelMA was obtained and stored at –80 °C for further use.

8.3.3. Fabrication of hydrophobic hydrogels

GelMA solutions at 4, 6, and 8 w/v% in PBS containing photoinitiator Irgacure (Ciba Specialty Chemicals) at 0.25 w/v% were prepared. Photo-cross-linking was conducted by exposing the prepolymer solution coated with a uniform layer of PFDTS-DE microparticles under UV light (OmniCure S2000, Excelitas Technologies) at a power of 800 mW and a distance of 8 cm between the UV output and the samples. Different UV exposure times for the photo-cross-linking process were tested: 15, 30, 45, and 60 s. Then, by rolling the cross-linked hydrogels over the PFDTS-DE microparticles, hydrogels coated with a uniform layer of hydrophobic microparticles were produced. The rolling process was performed until complete saturation of the hydrogel surface with the PFDTS-DE microparticles was reached (Figure 8.S1). Hydrogels with different shapes were obtained by

using in-house made poly(methyl methacrylate) (PMMA) stencil masks to control the initial shape of GelMA solution exposed to UV light.

To prepare pH-sensing microbeads, 22.5 mg of Bromothymol Blue (Sigma-Aldrich) was dissolved in 5 mL deionized water. The dye solution was then added with 256 mg of anion exchange resin microbeads (Dowexs chloride form, 200–400 mesh, Sigma-Aldrich), and the mixture was stirred for 2 h to allow uniform adsorption of the dye onto the resin microbeads (Figure 8.S2). To construct floating pH-sensing microdevices, pH-sensing microbeads were uniformly dispensed in GelMA prepolymer solution at a concentration of 10 w/v%. Then, spherical hydrophobic hydrogels were produced as described above, where a UV exposure time of 60 s was used to achieve complete cross-linking of the hydrogels. To better visualize the hydrophobic hydrogels that were used for studying the self-assembly process, colored polystyrene microbeads at 0.1 vol% were encapsulated into hydrogels.

8.3.4. Cell culture and cell encapsulation in the floating hydrogels

Human dermal fibroblasts (ATCC) were maintained in DMEM supplemented with 10 vol% FBS and 1 vol% penicillin-streptomycin (P-S, all from Life Technologies). Pristine human umbilical vein endothelial cells (HUVECs) were obtained from ATCC whereas GFP-positive HUVECs were obtained in-lab, both of which were cultured in Endothelial Cell Growth Medium (ECGM, Lonza). For both cell types, a concentration of 1×10^6 cells mL^{-1} in GelMA prepolymer solution in PBS was used to produce the hydrophobic hydrogels as described before, where photo-cross-linking was performed for 60 s. These floating hydrogels encapsulating fibroblasts or HUVECs were cultured in their respective medium for up to 10 days. Cell viability was analyzed by staining them with the Live/Dead kit (Lift Technologies) at days 0, 3, 7, and 10 according to the manufacturer's instructions. To better visualize the cells in the floating tissue assembly experiment, fibroblasts were prestained with CellTracker Red CMTPX Dye (Life Technologies) prior to encapsulation, while GFP-HUVECs were

used. After coating the hydrogels with the PFDTS-DE microparticles, different blocks were immediately placed in a Petri dish on the surface of a mixture of DMEM and ECGM (1:1 volume ratio) and allowed to assemble. Fluorescence images were taken using an inverted microscope (Axio Observer.D1, Carl Zeiss).

8.4. Results and discussion

8.4.1. Hydrophobic hydrogel produced by coating with hydrophobic microparticles

In the first step of our study, we performed a chemical modification to produce hydrophobic microparticles based on DE, using the same procedure reported in previous works.[25, 29] DE microparticles are extracted from the fossilized remains of diatoms, which are characterized by their micro- and nanoscale hierarchical structures (Figure 8.1a). These hierarchical structures have provided large specific surface areas than nonporous microparticles to potentially facilitate the functionalization and interaction with other materials. Since DE is mainly composed of silica, it is intrinsically hydrophilic. By modifying the surface with PFDTS (Figure 8.1b), we were able to render these microparticles hydrophobic. Figure 8.1c shows XPS analysis of the DE microparticles before and after treatment by PFDTS. Successful modification of the surface was shown by the appearance of the binding energy peak at around 689 eV. Importantly, the PFDTS treatment of DE microparticles did not alter their size distribution (8.54 ± 4.34 μm for PFDTS-DE *versus* 7.83 ± 3.80 μm for DE) nor caused aggregation of the microparticles (Figure 8.S3).

In this work we chose GelMA, a type of chemically modified gelatin that is photo-cross-linkable and strongly biocompatible,[6] to demonstrate our concept of hydrophobic hydrogel. As shown in Figure 8.1d, the uncoated GelMA hydrogel was hydrophilic with a water contact angle of 71°. After coating with a layer of pristine DE microparticles, the surface of the GelMA hydrogel block became superhydrophilic with a water contact angle approaching 0° (Figure 8.1e). However, when the

hydrogel block had been coated with hydrophobic PFDTS-DE microparticles (Figure 8.S1), a large water contact angle of 145° almost approaching superhydrophobicity (150°) could be achieved on its surface (Figure 8.1f), which we refer to as "hydrophobic hydrogels".

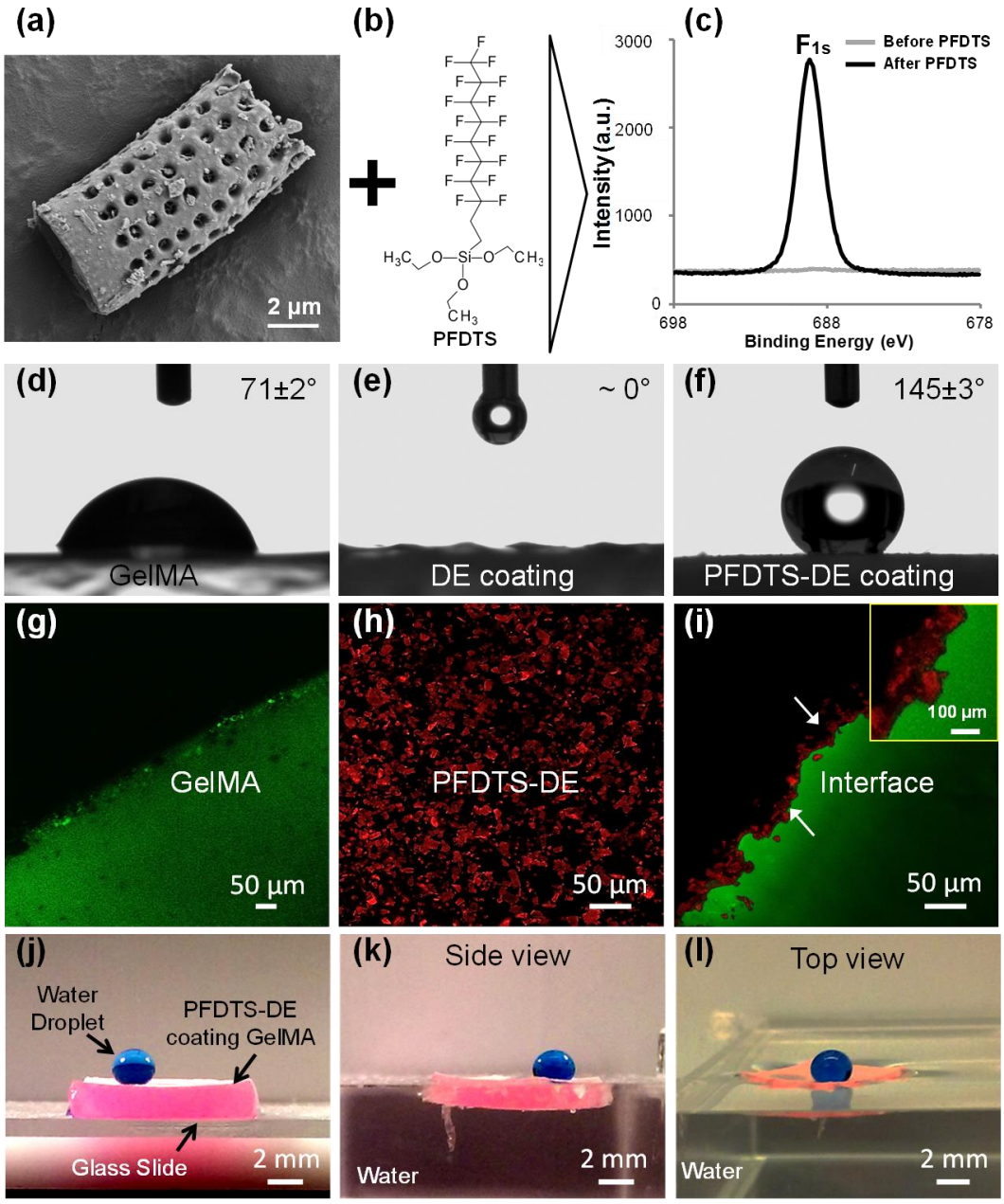

Figure 8.1: (a) SEM image of DE microparticles. (b) Formula of PFDTS used for hydrophobic treatment of DE. (c) XPS analysis of the pristine DE and PFDTS-DE microparticles. (d-f) Water contact angle measurements of cross-linked GelMA, GelMA coated with pristine DE microparticles, and GelMA coated with hydrophobic PFDTS-DE microparticles. (g-i) Confocal fluorescence micrographs showing the GelMA, PFDTS-DE microparticles, and GelMA coated with PFDTS-DE microparticles. GelMA was stained in green with fluorescein, and the PFDTS-DE microparticles were stained in red

with rhodamine. (j-l), Photographs showing a water droplet (dyed in blue) on top of a hydrophobic GelMA hydrogel block. The GelMA structure was placed on (j) a glass slide and (k, l) a pool of water.

We then used confocal microscopy to confirm the adhesion of the PFDTS-DE microparticles onto the surface of the GelMA hydrogel block. Prior to fabrication of the hydrophobic hydrogels, GelMA and the PFDTS-DE microparticles were first stained with fluorescein (green) and rhodamine (red), respectively (Figure 8.1g, h). After the coating process, it was clear that the outer surface of GelMA was completely covered by a thin layer of PFDTS-DE microparticles, at a thickness of approximately 15-20 μm (Figure 8.1i). Notably, due to the capillary force arising from the thin layer of water on the outer surface of the cross-linked hydrogel, PFDTS-DE microparticles adhered tightly, a phenomenon well observed with the classical "liquid marbles".[13, 14] Additionally, the hydrogel coated with the hydrophobic PFDTS-DE microparticles exhibited a unique water-repelling capacity, as demonstrated by the appearances of the convex meniscus formed by the surrounding water when it was placed at a water-air interface (Figure 8.S4).

Gently placing a droplet of water on a rectangular hydrophobic hydrogel resulted in free-standing of the droplet in an almost spherical shape, indicating the hydrophobicity of the hydrogel surface (Figure 8.1j). More interestingly, when we transferred the rectangular hydrophobic hydrogel into a pool of water, the hydrogel could easily float at the water/air interface without sinking as indicated in the side and top views in Figure 8.1, k and l. On the contrary, an ordinary hydrogel block without hydrophobic coating would sink to the bottom of a water tank (Figure 8.S5), due to the slightly higher density of the GelMA block (approximately 1.088 g cm^{-3}) than water. The contact of the hydrophobic hydrogel with water did not lead to dissociation of all surface-bond PFDTS-DE microparticles, but only those loosely attached (Figure 8.S6). Such excellent water repellency of the hydrophobic hydrogels might be attributed to an intermediate wetting state that is between the classical Wenzel and Cassie-Baxter states.[30, 31] In a typical Wenzel state, water will penetrate

into all the minute structures of a surface resulting in an enlarged solid-liquid contact area. On the other hand in a Cassie-Baxter state, air will be trapped in the structures and water is prevented from entering the structures, leading to a reduced solid-liquid contact area. For the peculiar intermediate wetting state formed here, water could partially enter the microstructures formed by the PFDTS-DE microparticles on the surface of the hydrogel while keeping a certain amount of air sealed in between the cavities. This explanation is consistent with the observation by Bormashenko *et al.*, who used microscopic images to determine the air layer separating the bulk liquid outside from that in the liquid marbles.[32] Similarly, we have also observed a partial mirror-like effect when a piece of hydrophobic hydrogel was immersed in water (Figure 8.S7, note the difference between the portions above and below water). The mirror-like effect arose from the presence of trapped air inside the porous structure (mean size: 5.37 ± 1.71 μm) formed on the surface of GelMA during the packing process. Such intermediate wetting state not only ensures the floating capacity of the hydrophobic hydrogels, but further potentially allows for liquid exchange between the hydrogels and the surrounding aqueous environment at the molecular level enabled by capillary force,[33] critical for their applications demonstrated later on. Importantly, the hydrogel block floating on top of water maintained its hydrophobicity on the upper side noncontact with liquid, verified by the ability to hold the spherical water droplet (Figure 8.1, k and l).

8.4.2. Floatability assessment of the hydrophobic hydrogels

To probe the factors influencing the floating capacity of the hydrophobic hydrogels, they were prepared with different concentrations (4, 6, and 8 w/v%) of GelMA and extent of cross-linking under various UV exposure time (15, 30, 45, and 60 s). For easy visualization, spherical hydrophobic hydrogel particles with a diameter of approximately 5 mm were fabricated. The as-prepared hydrophobic GelMA hydrogels were then placed in a water pool for up to 5 days, and their floating capabilities as a function of time were recorded. Specifically, we have defined the

parameters involved in the floating capability of the hydrophobic hydrogels. For a spherical hydrophobic hydrogel placed on the surface of water after equilibrium, height of the portion outside the water (i.e., exposed in the air) is denoted as d1, and height of the portion submerged in the water is denoted as d2 (Figure 8.2c). For example in extreme cases when the hydrogel entirely floats on the surface (Figure 8.2c-i) or sinks under water (Figure 8.2c-iii), d1/d2 approaches infinity and 0, respectively, where d1/d2 = 1 when exactly a half was exposed/submerged (Figure 8.2c-ii). Figure 8.2a, b shows the representative images at time 0 and 5 days after the hydrophobic GelMA hydrogel spheres were subjected to the floating assay. At the beginning, the spheres prepared under all conditions could float on the water/air interface, which exhibited a slight increase in d1 over d2 with longer UV cross-linking time. There was also a trend of improved floatability when the concentration of GelMA was increased. After 5 days of experiment, all the hydrophobic hydrogels prepared with 4% GelMA sank below the water/air interface; for the hydrogels prepared with 6% GelMA, those endured 15 and 30 s of UV exposure sank, while others were still floating; and for the hydrogels at a concentration of 8% GelMA, only the one with 15 s of UV exposure sank.

We also quantified and compared the floating performance of the hydrophobic hydrogels with different formulations at a range of time points (Figure 8.2, d-f). Well correlating with the photographs, both prolonging the UV cross-linking time and increasing the GelMA concentration resulted in stronger floating ability of the hydrophobic hydrogel spheres. It is presumed that the reduced floating ability of the hydrophobic hydrogels over time could be attributed to the decreased density of the PFDTS-DE microparticles upon the swelling of the hydrogels. To validate the assumption, we further quantitatively measured the swelling behavior (Figure 8.2g-i) and retention ability of the microparticles (Figure 8.2j-l) for the hydrophobic hydrogels. Indeed, the swelling behavior of the hydrophobic hydrogels exhibited a trend dependent on the concentration of GelMA

and UV exposure time, i.e., swelling was decreased with increasing cross-linking density of the hydrogels (Figure 8.2g-i).

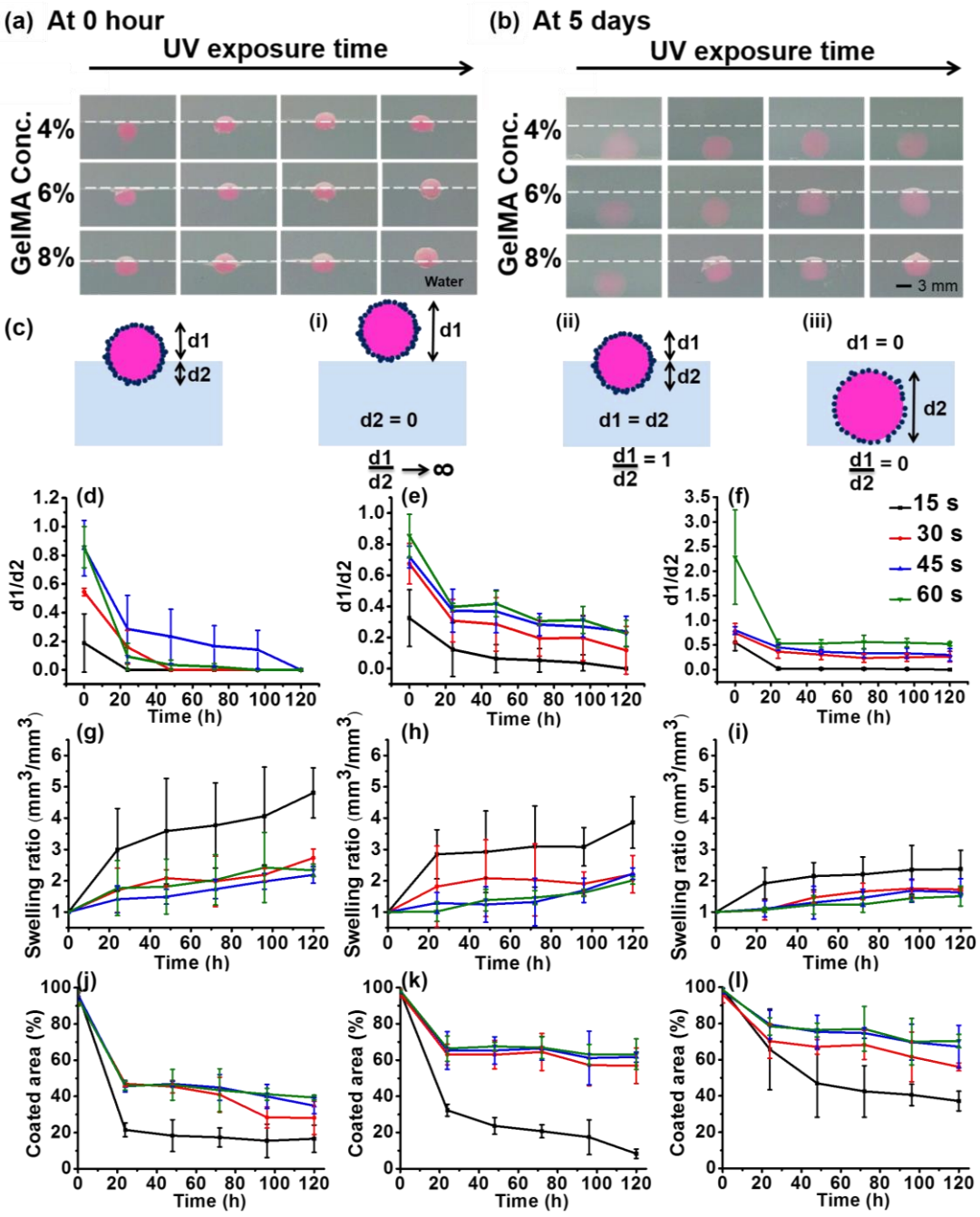

Figure 8.2: (a-b) Representative images of the floating performance of hydrophobic GelMA hydrogel spheres prepared under different conditions at time 0 and after 5 days in water. (c) Definition of the portion exposed in the air, d1, the portion submerged under water, d2, and the ratios of d1/d2 in three particular cases. (d-f) Plots of d1/d2 ratios versus floating time in water for hydrophobic hydrogels obtained under different UV cross-linking conditions for 4%, 6%, and 8% GelMA, respectively. (g-i) Plots of the swelling ratio of the hydrophobic hydrogels obtained under different UV cross-

linking conditions for 4%, 6%, and 8% GelMA, respectively. (j-l) Plots of the percentage of PFDTS-DE coating area on the hydrophobic hydrogels obtained under different UV cross-linking conditions for 4%, 6%, and 8% GelMA, respectively.

In comparison, with the swelling behavior of the pristine hydrogels (Figure 8.S8), the hydrophobic hydrogels exhibited slightly less swelling ratios due to the presence of the PFDTS-DE microparticles on their surfaces. The retention ability of the microparticles showed a reverse trend, where the hydrophobic hydrogels with less swelling resulted in better retention of the PFDTS-DE microparticles (Figure 8.2j-l). Therefore, as the initially densely packed layer of the microparticles became more sparsely distributed when the volumes of the hydrogel spheres expanded, the simultaneously diminishing microstructures formed by microparticles resulted in decreasing collective water repellency but increasing resemblance with pristine hydrogels, eventually leading to sinking of the spheres. Furthermore, the retention ability of the hydrophobic hydrogels for the PFDTS-DE microparticles showed a pH dependence. Lower pH resulted in reduced retention of the microparticles, while higher pH led to improved coating stability (Figure 8.S9). Experiments were also performed where Dulbecco's Modified Eagle Medium (DMEM) and DMEM supplemented with 10 vol% fetal bovine serum (FBS) were used as the aqueous environment (Figure 8.S10). In both cases, similar trends were observed, but the addition of salt and serum seemed to have slightly improved the floatability of the hydrophobic hydrogel spheres, which might be attributed to increased surface tension endowed by these molecules.[34, 35]

8.4.3. Construction of floating optical pH sensors

We next demonstrated the potential application of these hydrophobic hydrogels in the construction of floating microdevices such as pH sensors. Specifically, we introduced pH-sensitive beads (Figure 8.S2) into the GelMA hydrogels prior to coating with the hydrophobic PFDTS-DE microparticles (Figure 8.3a). As expected, incorporation of the pH-sensitive beads inside the GelMA did not affect the floating capacity of the hydrophobic hydrogels (Figure 8.3b). The slight increase in the volumes

submerged below the water surface was due to the higher density (≈1.2 g cm^{-3}) of the encapsulated pH-sensitive beads. Interestingly, when the pH of the surrounding water was increased from 5 to 9, the color of the floating devices, collectively reflecting that of the pH-sensing beads encapsulated inside, changed from vivid red to dark brown (Figure 8.3b). Such a process was reversible, where the color of the devices would change back to bright red upon decreasing the pH to 5. This observation clearly demonstrated that despite the hydrophobic nature of the coating resulted in floating of the microdevices, it still allowed for medium diffusion in/out of the hydrogels presumably due to the capillary force enabled by the porous PFDTS-DE microparticles. To be noted, such change in the color of the floating pH-sensors was quantifiable. By plotting the color intensity of the red channel of the captured photos, we were able to obtain a linear calibration curve against pH values (Figure 8.3b).

After validating the capability of the hydrophobic hydrogels as a floating device to sense the environmental pH, we further demonstrated the possibility to use such a device for real-time pH monitoring. A hydrophobic hydrogel piece with a shape of rectangular slab was fabricated and allowed to float in a water reservoir adjusted at pH of 5. Upon reaching equilibrium, a pellet of sodium hydroxide was dropped at the left end of the container, where the color of the pH-sensing floating hydrogel was then continuously monitored. As the dissolving sodium hydroxide diffused toward the right side, the color of the device gradually turned dark from the left, forming a color gradient along the long axis indicating the gradient of the pH below in the medium and eventually reaching a steady state where it became uniformly dark brown (Figure 8.3c). According to the correlation between pH values and the red channel color intensities, we could predict the pH values along the device at different time points (Figure 8.3c).

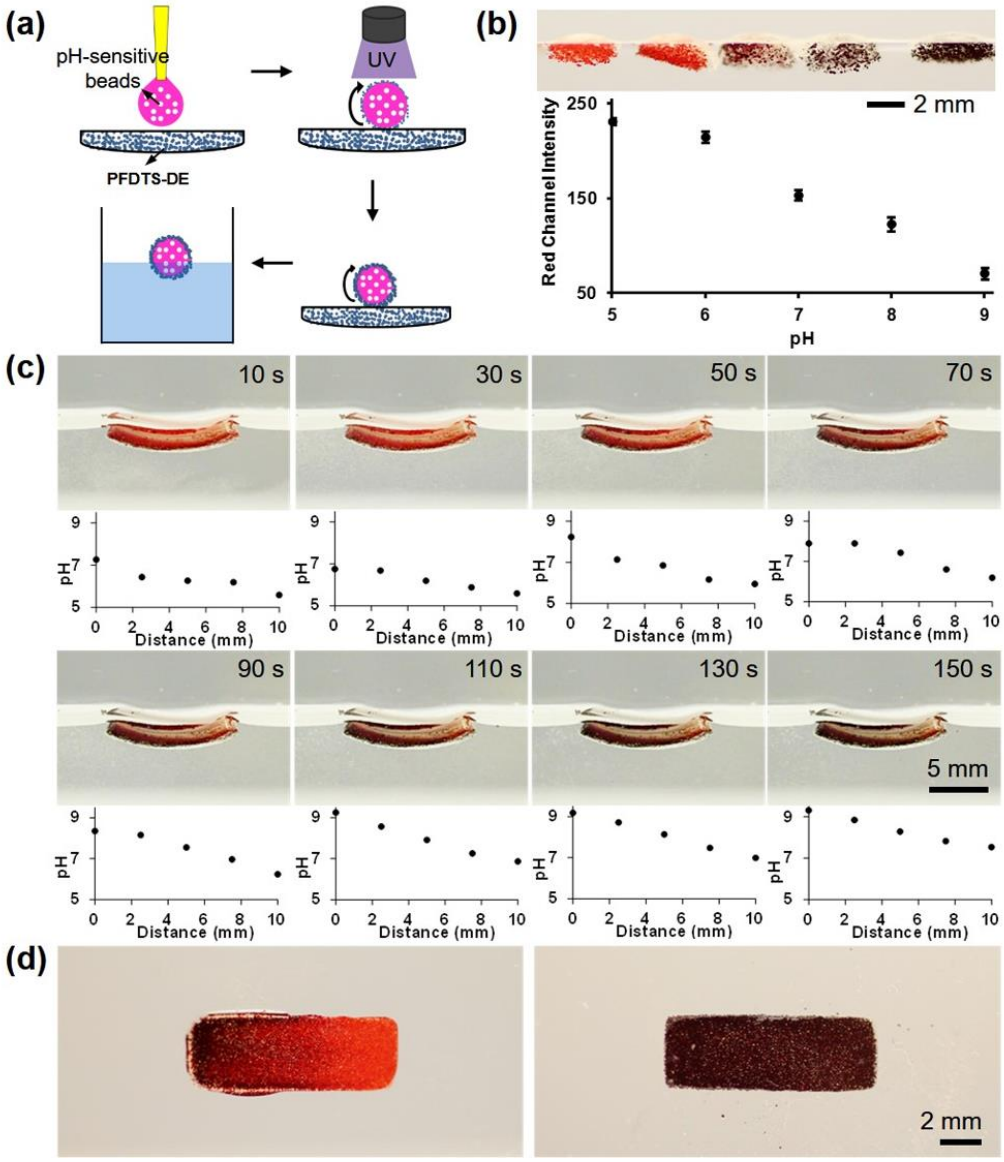

Figure 8.3: (a) Schematic representation of the method to produce the hydrophobic hydrogels encapsulation pH-sensing microbeads. (b) Side views of the floating pH meters at pH 5-9, where the red channel intensities of the devices were plotted against pH values. (c) Time-lapse photographs showing the color change of a slab of floating pH meter when a pellet of sodium hydroxide was dropped at the left side of the water container. The progressive pH increase along the long axis of the device was quantified from the standard curve. (d) Bottom view of the floating device at 1 min post addition of sodium hydroxide and when the pH of the medium became homogenous.

Figure 8.3d contains bottom views showing the color of the floating device at 1 min upon sodium hydroxide addition (Figure 8.3d, left) and at the end of the equilibrium (Figure 8.3d, right), where graded sensing capability of the device was well observed. While a pH sensor was used as a proof-

of-concept demonstration, microbeads sensing other molecules such as carbon dioxide[36-38] and ammonia[37-39] may also be readily encapsulated inside the hydrophobic hydrogels to construct other different types of floating sensors. Although conventional sensing materials and probes are widely available, there have rarely been reports on floating sensors that can be conveniently applied to measure desired parameters at liquid-air interfaces. This new class of floating sensing devices has opened up many potential future applications where environmental or biomedical monitoring at interfaces are required.

8.4.4. Microengineering of self-assembling floating hydrogels

Additionally, it was found that the floating devices engineered in this work revealed high mobility and could be manipulated to move directionally by using weak forces, such as electrostatic forces. Specifically, using a plastic pen that was positively charged by friction, we were able to drive a floating hydrogel sphere around in a Petri dish filled with water (Figure 8.4a). During this process, the hydrophobic PFDTS-DE microparticles coated on the outer surface of the hydrogel were induced to polarize when the charged pen approached them due to the pronounced electret characteristic of silica,[40, 41] the major constituent of DE. The polarization then rendered the side closer to the positively charged plastic rich in negative charges, and it is this electrostatic attraction force between the pen and the PFDTS-DE microparticles that drove the directional motion of the floating device on the surface of water.

Interesting enough, the floating devices constructed with complementary shapes could self-assemble on the surface of water (Figure 8.4b). The underlying driving forces for this spontaneous assembly are believed to arise from the capillary interactions between the floating hydrophobic hydrogels.[42, 43] It is well known that the surface free energy of a system is proportional to the overall surface area of the interface. When two convex or concave menisci are formed and brought together within the range of the capillary length of a liquid, they become instable and prone to

attract each other to assemble automatically.[44, 45] The as-formed menisci decrease the surface area of the interface and minimize the surface free energy of the system accordingly.[44, 45] Specifically to the convex menisci of water generated by the floating hydrophobic hydrogels, they were subject to the same capillary interactions, and the assembly of the hydrogels could thus be formed spontaneously when they approach each other to a distance within the capillary length of water (approximately 2 mm).

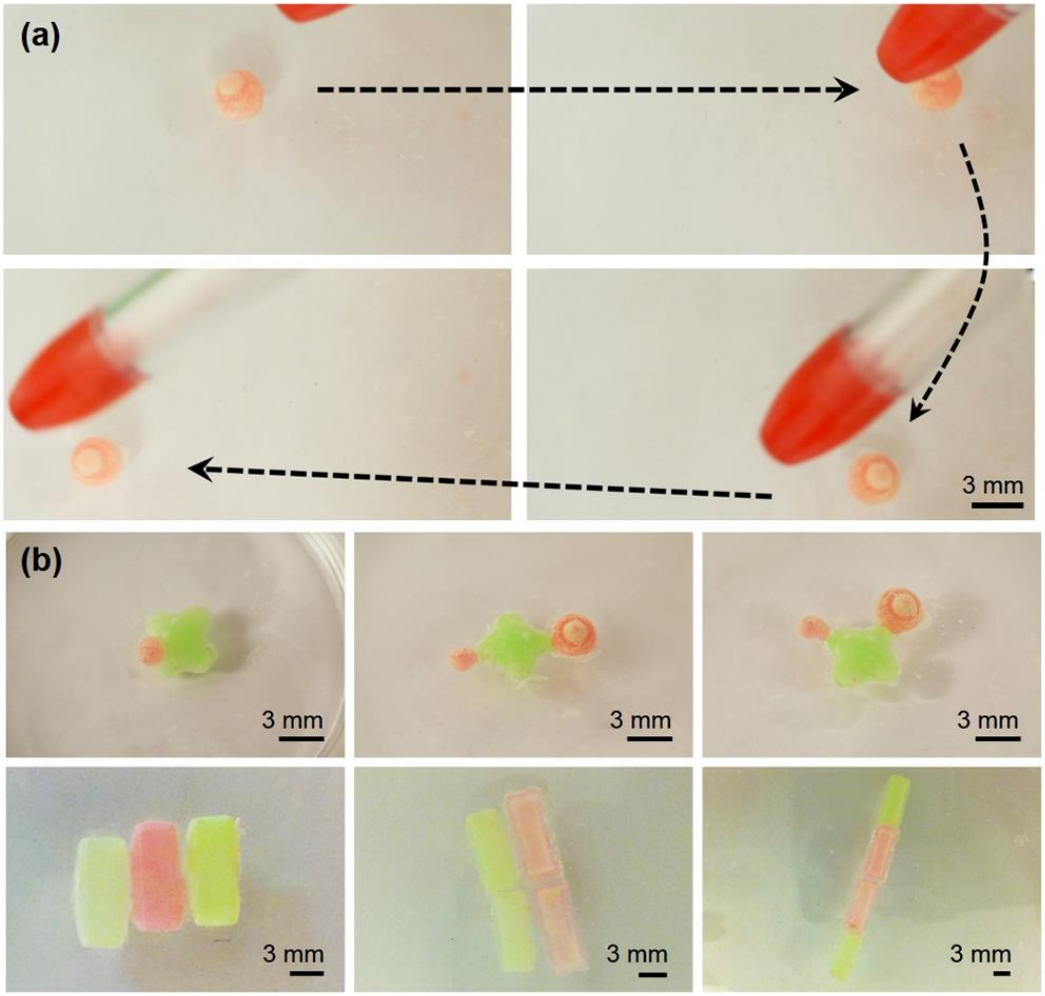

Figure 8.4: (a) The floating hydrogels could be directed to move on the surface of water using electrostatic forces, for example a charged plastic pen. (b) The floating hydrogels with different shapes could be manipulated and self-assemble in different configurations on the surface of water.

Of note, the assembled hydrogels were stable and could withstand strain; they could be manipulated together without disrupting their integral structures, until the strain reached a certain

amount; once separated, the devices would quickly reassemble again when coming back to proximity.

8.4.5. Engineering floating biological tissues

The self-assembly feature among complementarily shaped floating hydrogels demonstrated above supplies a potential strategy to engineer tissue constructs, particularly for those tissue types preferring the air-liquid interface.[46-48] Such a method of self-assembly would also be easily scaled up in fabricating large pieces of interconnected tissues.[49-51] To demonstrate this concept, we first encapsulated fibroblasts into the floating hydrogels and investigated their viability and spreading for up to 10 days. Live/dead analyses were performed at days 0, 3, 7, and 10 postseeding.

As shown in Figure 8.5a-h, the percentages of live cells (in green) on the side exposed to the air remained high at all the time points tested. The viability of the encapsulated cells on the side submerged in the medium, and the side exposed to the air did not differ much. The cell spreading over the entire period was also pronounced, during which we did not observe significant degradation of the hydrogel blocks. Such high viability of the encapsulated cells is critical to sustain the longterm functionality of assembled floating tissues and would not be possible using conventional “liquid marbles” containing liquid cores. We also demonstrated before that hydrogel building blocks could also self-assemble into larger pieces of tissues when they were allowed to float on the surface of high-density, hydrophobic liquids.[52] Nonetheless, the nonaqueous environment reported in this work was not able to support the viability of embedded cells over extended periods due to the lack of nutrient delivery. In contrast, the high viability observed here indicated a benign microenvironment for the encapsulated cells inside the floating hydrophobic hydrogels, proving that the nutrient exchange between the floating hydrogels and the surrounding aqueous medium was

sufficient. By further combining the cell encapsulation capacity with the self-assembly capability of the floating hydrogels, biomimetic 3D multitissue constructs could be produced.

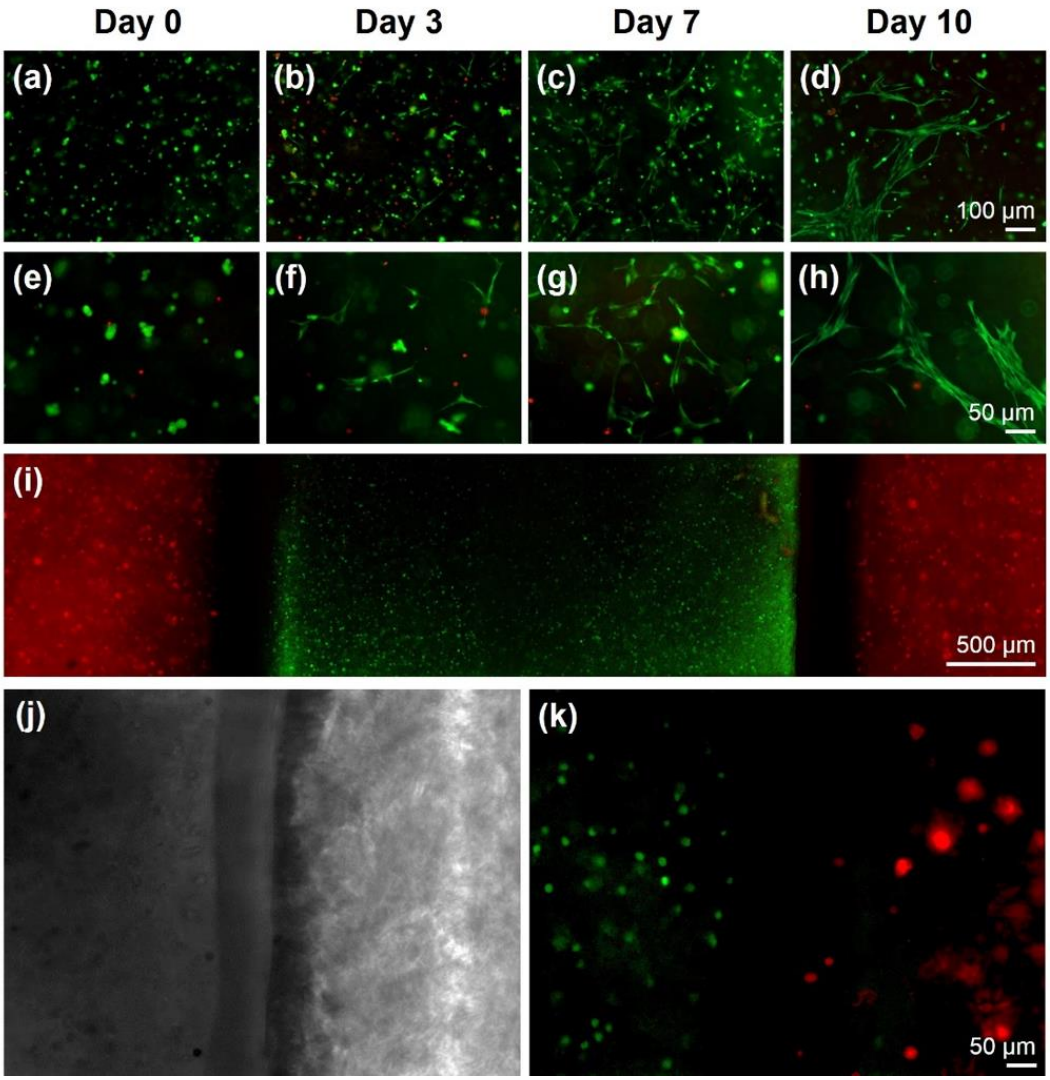

Figure 8.5: (a-h) Live/dead analysis of fibroblasts encapsulated inside the floating hydrophobic hydrogel blocks at days 0, 3, 7, and 10. Live cells are indicated in green and dead cells in red. (i) Fluorescence micrograph showing floating assembly of three hydrogel blocks encapsulating fibroblasts (red) on the sides and endothelial cells (green) in the center. (j, k) Magnified views showing the interface between the two adjacent blocks encapsulating the two cell populations.

As a proof of concept, two blocks encapsulating fibroblasts labeled in red and one block with encapsulated HUVECs expressing green fluorescent proteins (GFPs) were allowed to float in the same reservoir. These blocks could then be easily manipulated to assemble in a structure where

the endothelial block was flanked by the two hydrogels containing fibroblasts (Figure 8.5i-k), mimicking a vascularized skin construct floating at the air-liquid interface.

8.5. Conclusion

In summary, we have reported a novel class of hydrophobic hydrogels that could float on the surface of different types of aqueous liquids by coating conventional hydrogels with a layer of hydrophobic PFDTS-DE microparticles. We further demonstrated the potential of these floating hydrogel-based devices for the construction of floating pH meters and have inferred their potential for other different sensing applications. Moreover, we demonstrated that the floating hydrogels presented high mobility with excellent self-assembly property. Importantly, the floating systems reserved the intrinsic biocompatibility of the core hydrogels, as indicated by the high viability of cells encapsulated in the interior. We believe that these floating hydrophobic hydrogel-based devices will find widespread applications including but not limited to sensing, tissue engineering, and biomedicine.

8.6. Acknowledgments

This work was financially supported by the Office of Naval Research Young National Investigator Award, the National Institutes of Health (EB012597, AR057837, DE021468, HL099073, R56AI105024), and the Presidential Early Career Award for Scientists and Engineers (PECASE). N. M. Oliveira acknowledges the financial support from Portuguese Foundation for Science and Technology – FCT (Grant SFRH/BD/73172/2010), from the financial program POPH/FSE from QREN.

8.7. References

1. Drury, J. L.; Mooney, D. J., Hydrogels for tissue engineering: Scaffold design variables and applications. *Biomaterials* **2003,** *24*, 4337-51.

2. Hoffman, A. S., Hydrogels for biomedical applications. *Adv Drug Deliv Rev* **2002,** *54*, 3-12.

3. Guenther, M.; Gerlach, G., *Hydrogels for chemical sensors. In hydrogel sensors and actuators*. Springer: 2010; p 165-195.

4. Buengera, D.; Topuza, F.; Grollb, J., Hydrogels in sensing applications. *Progress in Polymer Science* **2012,** *37*, 1678-1719.

5. Augst, A. D.; Kong, H. J.; Mooney, D. J., Alginate hydrogels as biomaterials. *Macromolecular Bioscience* **2006,** *6*.

6. Nichol, J. W.; Koshy, S. T.; Bae, H.; Hwang, C. M.; Yamanlar, S.; Khademhosseini, A., Cell-laden microengineered gelatin methacrylate hydrogels. *Biomaterials* **2010,** *31*, 5536-5544.

7. Burdick, J. A.; Prestwich, G. D., Hyaluronic acid hydrogels for biomedical applications. *Adv Mater* **2011,** *23*, H41-56.

8. Hersel, U.; Dahmen, C.; Kessler, H., Rgd modified polymers: Biomaterials for stimulated cell adhesion and beyond. *Biomaterials* **2003,** *24*, 4385-415.

9. Martino, M. M.; Briquez, P. S.; Ranga, A.; Lutolf, M. P.; Hubbell, J. A., Heparin-binding domain of fibrin(ogen) binds growth factors and promotes tissue repair when incorporated within a synthetic matrix. *Proc Natl Acad Sci U S A* **2013,** *110*, 4563-8.

10. Sakiyama-Elbert, S. E.; Hubbell, J. A., Development of fibrin derivatives for controlled release of heparin-binding growth factors. *J Control Release* **2000,** *65*, 389-402.

11. Lutolf, M. P.; Lauer-Fields, J. L.; Schmoekel, H. G.; Metters, A. T.; Weber, F. E.; Fields, G. B.; Hubbell, J. A., Synthetic matrix metalloproteinase-sensitive hydrogels for the conduction of tissue regeneration: Engineering cell-invasion characteristics. *Proc Natl Acad Sci U S A* **2003,** *100*, 5413-8.

12. Purcell, B. P.; Lobb, D.; Charati, M. B.; Dorsey, S. M.; Wade, R. J.; Zellars, K. N.; Doviak, H.; Pettaway, S.; Logdon, C. B.; Shuman, J. A.; Freels, P. D.; Gorman, J. H., 3rd; Gorman, R. C.; Spinale, F. G.; Burdick, J. A., Injectable and bioresponsive hydrogels for on-demand matrix metalloproteinase inhibition. *Nat Mater* **2014,** *13*, 653-61.

13. Bormashenko, E.; Bormashenko, Y.; Musin, A.; Barkay, Z., On the mechanism of floating and sliding of liquid marbles. *Chemphyschem* **2009,** *10*, 654-6.

14. Aussillous, P.; Quere, D., Liquid marbles. *Nature* **2001,** *411*, 924-7.

15. McHale, G.; Newton, M. I., Liquid marbles: Topical context within soft matter and recent progress. *Soft Matter* **2015,** *11*, 2530-46.

16. Xu, Z.; Zhao, Y.; Dai, L.; Lin, T., Multi-responsive janus liquid marbles: The effect of temperature and acidic/basic vapors. *Particle & Particle Systems Characterization* **2014,** *31*, 839-842.

17. Zhang, L.; Cha, D.; Wang, P., Remotely controllable liquid marbles. *Adv Mater* **2012,** *24*, 4756-60.

18. Matsubara, K.; Danno, M.; Inoue, M.; Nishizawa, H.; Honda, Y.; Abe, T., Surface fluorination of polystyrene particles via cf_4 plasma irradiation using a barrel-plasma-treatment system. *Surface and Coatings Technology* **2013,** *236*, 269-273.

19. Gao, W.; Lee, H. K.; Hobley, J.; Liu, T.; Phang, I. Y.; Ling, X. Y., Graphene liquid marbles as photothermal miniature reactors for reaction kinetics modulation. *Angew Chem Int Ed Engl* **2015,** *54*, 3993-6.

20. Sheng, Y.; Sun, G.; Wu, J.; Ma, G., Silica-based liquid marbles as microreactors for the silver mirror reaction. *Angewandte Chemie International Edition* **2015,** *54*, 7012–7017.

21. Tian, J.; Fu, N.; Chen, X. D.; Shen, W., Respirable liquid marble for the cultivation of microorganisms. *Colloids Surf B Biointerfaces* **2013,** *106*, 187-90.

22. Arbatan, T.; Al-Abboodi, A.; Sarvi, F.; Chan, P. P.; Shen, W., Tumor inside a pearl drop. *Adv Healthc Mater* **2012,** *1*, 467-9.

23. Sarvi, F.; Arbatan, T.; Chan, P. P. Y.; Shen, W., A novel technique for the formation of embryoid bodies inside liquid marbles. *RSC Advances* **2013,** *3*, 14501-14508.

24. Sarvi, F.; Jain, K.; Arbatan, T.; Verma, P. J.; Hourigan, K.; Thompson, M. C.; Shen, W.; Chan, P. P., Cardiogenesis of embryonic stem cells with liquid marble micro-bioreactor. *Adv Healthc Mater* **2015,** *4*, 77-86.

25. Oliveira, N. M.; Correia, C. R.; Reis, R. L.; Mano, J. F., Liquid marbles for high-throughput biological screening of anchorage-dependent cells. *Adv Healthc Mater* **2015,** *4*, 264-70.

26. Serrano, M. C.; Nardecchia, S.; Gutierrez, M. C.; Ferrer, M. L.; del Monte, F., Mammalian cell cryopreservation by using liquid marbles. *ACS Appl Mater Interfaces* **2015,** *7*, 3854-60.

27. Sun, G.; Sheng, Y.; Wu, J.; Ma, G.; Ngai, T., Liquid marbles stabilized by charged polymer latexes: How does the drying of the latex particles affect the properties of liquid marbles? *Langmuir* **2014,** *30*, 12503-8.

28. Ooi, C. H.; Vadivelu, R. K.; St John, J.; Dao, D. V.; Nguyen, N. T., Deformation of a floating liquid marble. *Soft Matter* **2015,** *11*, 4576-83.

29. Oliveira, N. M.; Reis, R. L.; Mano, J. F., Superhydrophobic surfaces engineered using diatomaceous earth. *ACS Appl Mater Interfaces* **2013,** *5*, 4202-8.

30. Wang, S.; Jiang, L., Definition of superhydrophobic states. *Advanced Materials* **2007,** *19*, 3423-3424.

31. Xia, F.; Jiang, L., Bio-inspired, smart, multiscale interfacial materials. *Advanced Materials* **2008,** *20*, 2842–2858.

32. Bormashenko, E., New insights into liquid marbles. *Soft Matter* **2012,** *8*, 11018-11021.

33. Hensel, R.; Braun, H.-G., Free-floating hydrogel-based rafts supporting a microarray of functional entities at fluid interfaces. *Soft Matter* **2012,** *8*, 5293-5300.

34. Pegram, L. M.; Record, M. T., Jr., Hofmeister salt effects on surface tension arise from partitioning of anions and cations between bulk water and the air-water interface. *J Phys Chem B* **2007,** *111*, 5411-7.

35. Hill, M. J.; Wilson, T. A.; Lambert, R. K., Effects of surface tension and intraluminal fluid on mechanics of small airways. *J Appl Physiol (1985)* **1997,** *82*, 233-9.

36. Zilberman, Y.; Ameri, S. K.; Sonkusale, S. R., Microfluidic optoelectronic sensor based on a composite halochromic material for dissolved carbon dioxide detection. *Sensors and Actuators B: Chemical* **2014,** *194*, 404–409.

37. Chen, Y.; Zilberman, Y.; Mostafalu, P.; Sonkusale, S. R., Paper based platform for colorimetric sensing of dissolved nh3 and co2. *Biosens Bioelectron* **2015,** *67*, 477-84.

38. Zilberman, Y.; Sonkusale, S. R., Microfluidic optoelectronic sensor for salivary diagnostics of stomach cancer. *Biosens Bioelectron* **2015,** *67*, 465-71.

39. Zilberman, Y.; Chen, Y.; Sonkusale, S. R., Dissolved ammonia sensing in complex mixtures using metalloporphyrin-based optoelectronic sensor and spectroscopic detection. *Sensors and Actuators B: Chemical* **2014,** *202*, 976-983.

40. Sprenkels, A. J.; Twente Univ., E., Netherlands; Olthuis, W. B., P., *The application of silicon dioxide as an electret material*. IEEE: 1988; p 165-169.

41. Kressmann, R.; Sessler, G. M.; Gunther, P., *Space-charge electrets. Dielectrics and electrical insulation*. IEEE Transactions on 1996; p 607 - 623.

42. Blokzijl, W.; Engberts, J. B. F. N., Hydrophobic effects. Opinions and facts. *Angewandte Chemie International Edition in English* **1993,** *32*, 1545–1579.

43. Sanchez-Iglesias, A.; Grzelczak, M.; Altantzis, T.; Goris, B.; Perez-Juste, J.; Bals, S.; Van Tendeloo, G.; Donaldson, S. H., Jr.; Chmelka, B. F.; Israelachvili, J. N.; Liz-Marzan, L. M., Hydrophobic interactions modulate self-assembly of nanoparticles. *ACS Nano* **2012,** *6*, 11059-65.

44. Grzybowski, B. A.; Bowden, N.; Arias, F.; Yang, H.; Whitesides, G. M., Modeling of menisci and capillary forces from the millimeter to the micrometer size range. *J. Phys. Chem. B* **2001,** *105*, 404-412.

45. Bowden, N. B.; Weck, M.; Chol, I. S.; Whitesides, G. M., Molecule-mimetic chemistry and mesoscale self-assembly. *Acc. Chem. Res* **2001,** *34*, 231-238.

46. Zhao, X.; Lang, Q.; Yildirimer, L.; Lin, Z. Y.; Cui, W.; Annabi, N.; Ng, K. W.; Dokmeci, M. R.; Ghaemmaghami, A. M.; Khademhosseini, A., Photocrosslinkable gelatin hydrogel for epidermal tissue engineering. *Adv Healthc Mater* **2016,** *5*, 108-18.

47. Huh, D.; Matthews, B. D.; Mammoto, A.; Montoya-Zavala, M.; Hsin, H. Y.; Ingber, D. E., Reconstituting organ-level lung functions on a chip. *Science* **2010,** *328*, 1662-8.

48. Huh, D.; Fujioka, H.; Tung, Y. C.; Futai, N.; Paine, R., 3rd; Grotberg, J. B.; Takayama, S., Acoustically detectable cellular-level lung injury induced by fluid mechanical stresses in microfluidic airway systems. *Proc Natl Acad Sci U S A* **2007,** *104*, 18886-91.

49. Khademhosseini, A.; Langer, R., Microengineered hydrogels for tissue engineering. *Biomaterials* **2007,** *28*, 5087-92.

50. Du, Y.; Lo, E.; Ali, S.; Khademhosseini, A., Directed assembly of cell-laden microgels for fabrication of 3d tissue constructs. *Proc Natl Acad Sci U S A* **2008,** *105*, 9522-7.

51. Nichol, J. W.; Khademhosseini, A., Modular tissue engineering: Engineering biological tissues from the bottom up. *Soft Matter* **2009,** *5*, 1312-1319.

52. Zamanian, B.; Masaeli, M.; Nichol, J. W.; Khabiry, M.; Hancock, M. J.; Bae, H.; Khademhosseini, A., Interface-directed self-assembly of cell-laden microgels. *Small* **2010,** *6*, 937-44.

8.8. Supporting Information

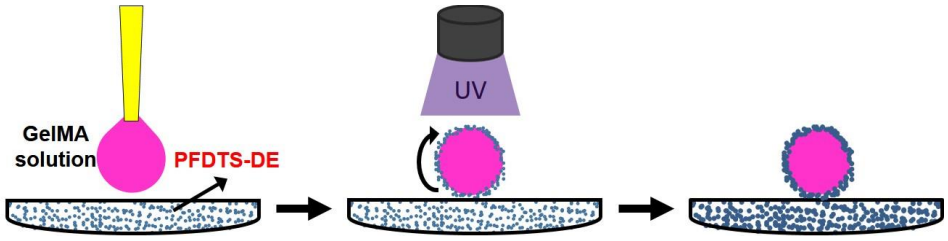

Figure 8.S1: Schematic diagram showing the preparation procedure of hydrophobic GelMA hydrogels.

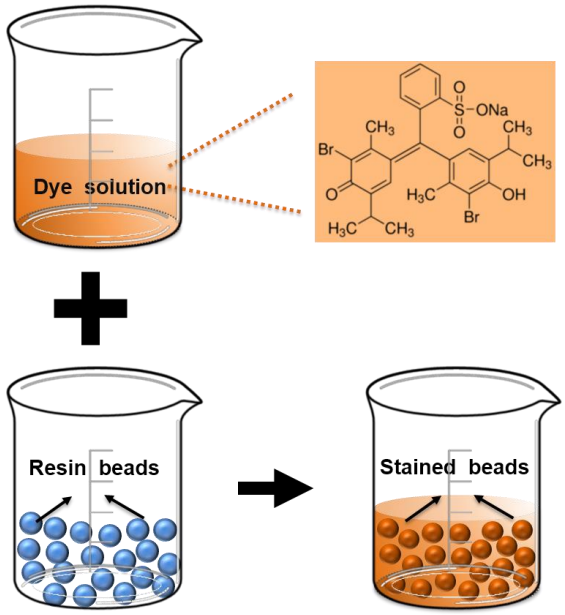

Figure 8.S2: Schematic showing fabrication process of pH-sensing resin microbeads. First a pH-sensitive dye, Bromothymol Blue, was dissolved in deionized water; then the dye solution was added into a beaker containing anion exchange resin microbeads; after stirring for 2 h for dye adsorption, pH-sensing microbeads could be obtained.

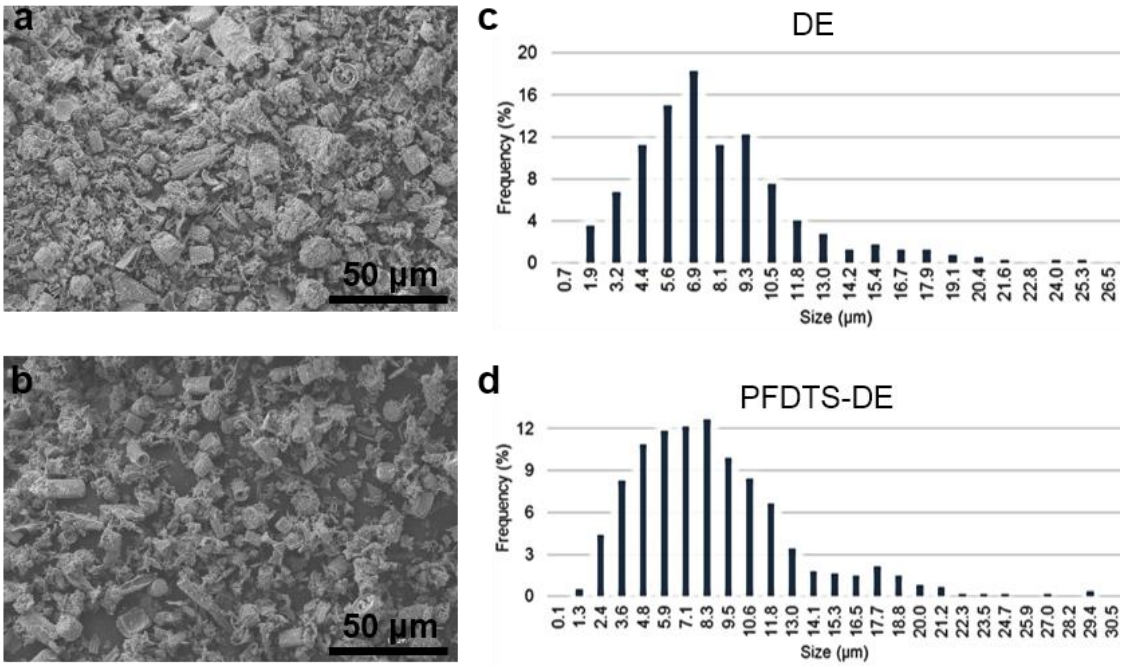

Figure 8.S3: (a, b) SEM images and (c, d) size distributions of the DE particles (a, c) before and (b, d) after PFDTS modification. Most DE particles were in the size range of 3.2-10.5 µm, while most PFDTS-DE particles fell in the size range of 3.6-10.6 µm.

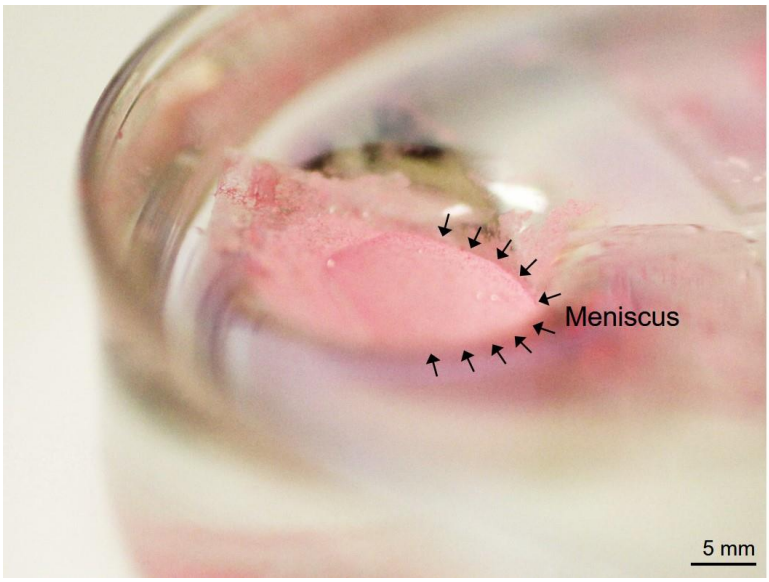

Figure 8.S4: Photograph showing the repellency of the hydrophobic hydrogel following slow insertion into a pool of water, indicated by the convex meniscus. The PFDTS-DE microparticles were dyed with rhodamine in red for better visualization.

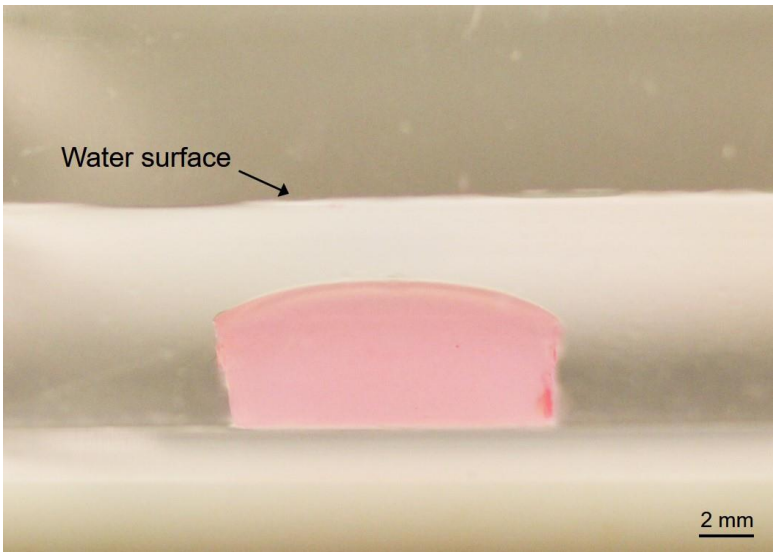

Figure 8.S5: Photograph showing a GelMA hydrogel block without coating of PFDTS-DE microparticles sank to the bottom of a water container.

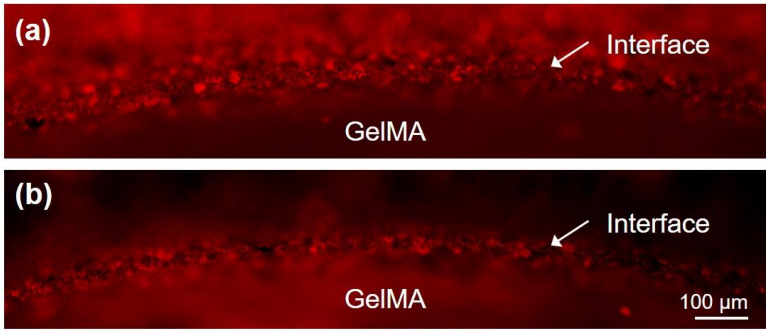

Figure 8.S6: Fluorescence micrographs showing the PFDTS-DE microparticles on the surface of the GelMA hydrogel (a) before and (b) after immersion in water.

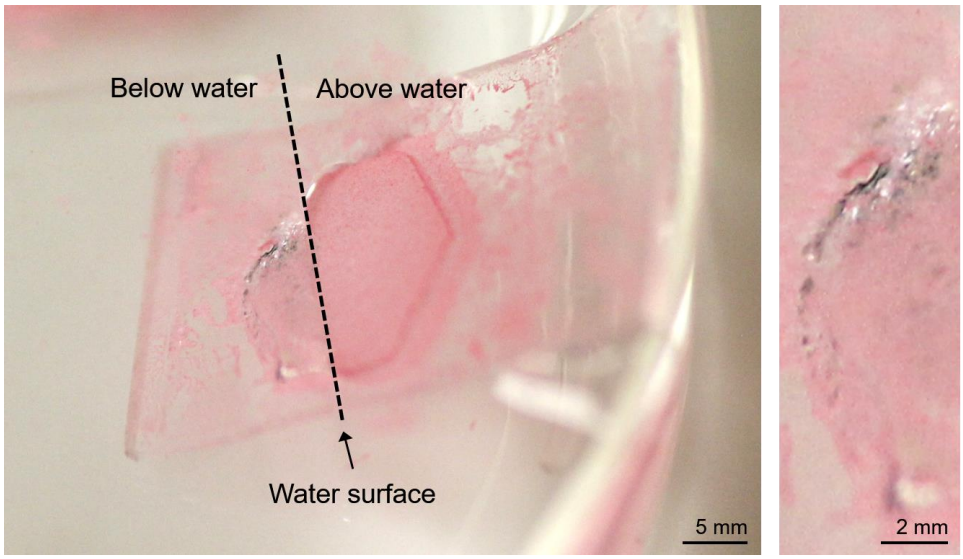

Figure 8.S7: Photograph showing the mirror-like effect of the hydrophobic hydrogel partially submerged in water. The PFDTS-DE microparticles were dyed with rhodamine in red for better visualization.

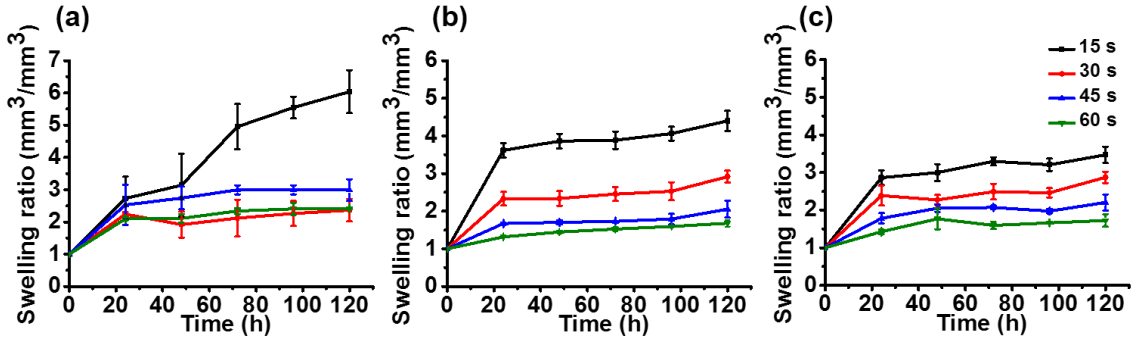

Figure 8.S8: Swelling behavior of pristine GelMA blocks at different time points. (a)-(c) are corresponding to the GelMA blocks prepared with 4%, 6%, and 8% of the GelMA solution. The different colored curves represent GelMA blocks with different UV crosslinking time.

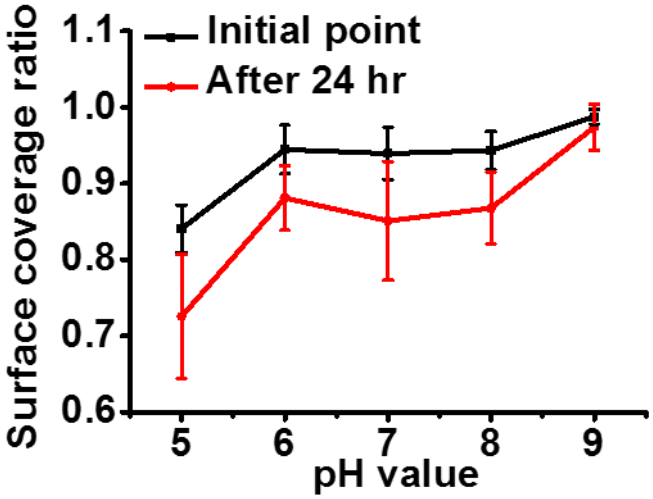

Figure 8.S9: Stability of the hydrophobic particles on the GelMA blocks in different pH solutions. The hydrophobic particles show increased retention ability on the GelMA surface with increasing pH values in the whole.

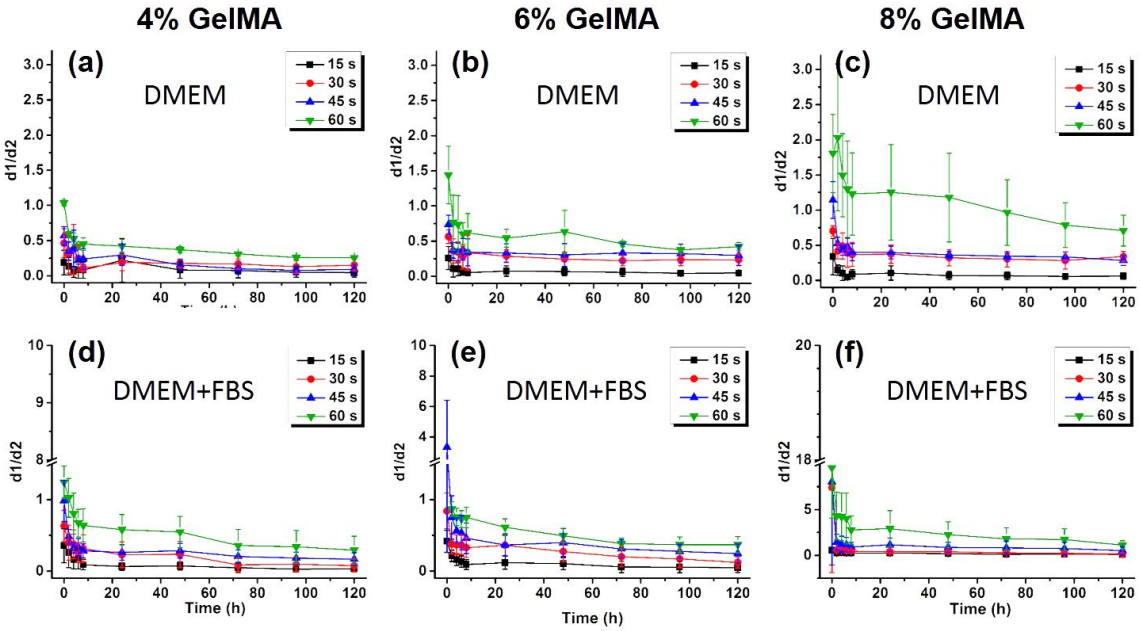

Figure 8.S10: Quantitative analysis of the floating ability of the hydrophobic GelMA hydrogels prepared under different conditions *versus* time in (a-c) DMEM and (d-f) DMEM supplemented with FBS.

SECTION IV. CONCLUDING REMARKS

Chapter 9. Conclusions and Future Perspectives

Chapter 9

Conclusions and Future Perspectives

The control of the surface wettability has been showed as an important parameter for several systems and applications on the biomedical field. The wettability is a relevant characteristic on the development of scaffolds or prosthesis, for example. Once the surface wettability can decisively affect the protein adsorption, and both bacteria and mammalian cell adhesion. On this thesis, the motivation was on the development of devices for biomedical applications based on the advanced control of wettability in surfaces, tuning directly the surface characteristics or modifying surfaces by coating with a hydrophobic microparticles.

Surfaces with ability to completely repel water, named superhydrophobic (SH) surfaces, can be achieved combining both low surface energy and hierarchical topography at nano/microscale. Here, it was showed the possibility to produce SH surfaces using diatomaceous earth (DE), which is a natural, accessible and cheap material constituted by silica micro-skeletons of unicellular algae – called diatomaceous or diatoms. The natural nano/microstructure of these silica objects provided the necessary rough topography for the surface. This desired hierarchical structure was created on a smooth surface of glass by coating, using directly these natural structure. The binding between DE and surface was performed by melting superficially the substrate, obtaining a layer of DE entrapped on its surface. On this step, superhydrophilic surfaces were obtained that became SH surfaces by further fluorosilanization of surfaces that decreased the surface energy. The possibility to change in a precise way the wettability of the produced SH surfaces was also explored, by exposing the substrates to plasma treatment for specific times. Using stencil masks, the control in

space of the plasma treatment was also performed, allowing to perform hydrophilic/superhydrophobic patterning on surfaces with well-defined geometries. Additionally, it was showed that the proposed strategy could be applied in other substrates, such as polystyrene. This open the possibility to produce SH surfaces for specific applications through the choice of the most suitable substrate.

Then, two different devices for cellular studies were engineered, but using other surfaces patterned with hydrophilic paths or square spots and fully constituted of polystyrene (PS). Once PS is the most commonly used material in laboratory cultureware, because this material ensure their inertness to biological outcomes. These SH platforms were manufactured by a one-step patterning/hydrophobization process, using stripe or square shaped stickers to protect the desired areas from being reached by the phase-separation reagents that confer the superhydrophobicity to the surface. The patterned paths on the surfaces worked such as channels to drive cell culture medium flows without using physical walls for liquid confinement. Controlling liquid flows on planar surfaces, a novel cell culture flow (CCF) system to study the shear stress effect on adherent cells was created, based on the open fluidics concept. On the paths, cells were pre-adhered and cultured under shear stress stimuli that was inflicted by the cell culture medium flowing over the cell layer. As proof of concept, it was studied the influence of this mechanical stimuli combined with bone morphogenic protein (specifically BMP-2) stimulation in the osteogenic differentiation of C2C12 myoblast cells. A synergistic effect between the mechanical and a biochemical stimuli on the osteoblast differentiation of C2C12 cells was observed, through the detection of an enhancement in the ALP activity – a well-known early marker of osteogenic differentiation. On the optimization process of the developed device, several procedures revealed to be crucial for the system robustness and flow stability such as the fluorosilanization of the SH surface, the increasing of channel hydrophilicity, and the use of glass needles to feed and extract the culture medium to the

open chip. These procedures helped to maintain both morphology and integrity of the liquid streams and preventing the dewetting of channels along all the period of culture. Additionally, an increased hydrophilicity of the cell culture channels showed to improve cell attachment and cells could hold higher cell culture medium flow rates, always in a laminar flow regime. Still, to best of our knowledge, this is the first time that this kind of platform was developed to study the shear stress effect on cell behavior.

The second application proposed for the patterned superhydrophobic surfaces was for the production of 3D spheroids and their culture under co-culture conditions. As a proof of concept, human adipose-derived stem cell (hASC) spheroids were produced and cultured in indirect co-culture with L929, Saos-2 and HUVEC cells. Performing spheroid production under these conditioned conditions, the co-culture with a 2D monolayer of Saos-2 osteoblast-like cells indicated that the simultaneous production of 3D cellular structures and their differentiation promotion can be obtained in a one-step procedure. The hASC differentiation into an early osteogenic phenotype was confirmed by the detection of an increased ALP activity. These pre-committed spheroids may have high interest for bone regeneration, such as building blocks that combined with the appropriate biomaterials may be used in the bio-fabrication of complex personalized constructions. These SH platforms with wettable patterns on its surface showed a high versatility on biomedical applications, namely in tissue regeneration, cancer biology or drug screening approaches.

As an alternative approach to conventional superhydrophobicity, it was arose the liquid marbles (LM). The LM production was performed using hydrophobized DE to coating liquid droplets. Taking advantage of the possibility to inject or remove liquid from the LM without destroy its structure, the use of LM for high-throughput drug screening on anchorage-dependent cells was presented. To provide the required cell adhesion sites inside the liquid environment, a novel strategy to culture these cells was developed adding poly(L-lactic acid) microparticles to the liquid core of LM. The

crucial importance of these microparticles for cell proliferation was demonstrated. By monitoring color changes *in situ*, cytotoxic screening tests were performed using LM. This innovative alternative was fully validated by directly comparing with a well-know (destructive) standardized method used for cytotoxicity assessment. As the LM provide a 3D cell culture environment, the assessed results should be more reliable for predicting *in vivo* effects and with low need of resources, namely in terms of medium volume, cell number, drug/reagent amount, equipment, and time. The versatility of the proposed system could be also easily adapted to other applications including as a platform to set-up disease model or for fabrication of 3D micro-tissues for tissue engineering.

Inspired by LM, a novel class of hydrophobic hydrogels was created by coating conventional hydrogels with a layer of hydrophobized DE microparticles. These hydrophobic hydrogels showed to be able free-floating on the surface of different aqueous media. It was demonstrated that floating hydrogel-based devices could be developed with applicability for pH sensing on liquid surfaces, showing also potential for other different sensing applications. Additionally, it was verified that the floating hydrogels presented high mobility with excellent self-assembly property. The floating systems preserved the intrinsic biocompatibility of the core hydrogels, as indicated by the high viability of cells encapsulated in the floating tissue constructs that were microengineered.

On this thesis, different biomedical devices were engineered just based on the advanced control of the wettability of different surfaces. These devices have high potential to achieve widespread use, namely for applications in sensing, drug screening, fabrication of 3D microtissues for tissue engineering, and biomedicine.